AD NUMBER

AD373321

LIMITATION CHANGES

TO:

Approved for public release; distribution is unlimited.

FROM:

Distribution authorized to U.S. Gov't. agencies only; Administrative/Operational Use; JAN 1955. Other requests shall be referred to Director, Defense Atomic Support Agency, Washington, DC 20301.

AUTHORITY

DSWA/OPSSI ltr dtd 8 May 1998

AD NUMBER
AD373321
CLASSIFICATION CHANGES
TO: **UNCLASSIFIED**
FROM: **CONFIDENTIAL**
LIMITATION CHANGES
TO: **Distribution authorized to U.S. Gov't. agencies only; Administrative/Operational Use; JAN 1955. Other requests shall be referred to Director, Defense Atomic Support Agency, Washington, DC 20301.**
FROM: **Distribution authorized to DoD only; Administrative/Operational Use; JAN 1955. Other requests shall be referred to Director, Defense Atomic Support Agency, Washington, DC 20301. Restricted Data.**
AUTHORITY
DNA ltr dtd 11 Mar 1994; DNA ltr dtd 11 Mar 1994

AD NUMBER
AD373321
CLASSIFICATION CHANGES
TO: **CONFIDENTIAL**
FROM: **SECRET**
AUTHORITY
9 Feb 1961, per document marking

WT-711

Copy No. [redacted] A

Operation UPSHOT-KNOTHOLE

NEVADA PROVING GROUNDS

March - June 1953

Project 1.1b

AIR PRESSURE AND GROUND SHOCK MEASUREMENTS

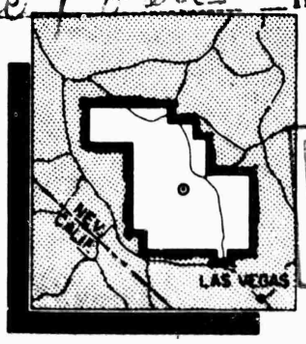

~~RESTRICTED DATA~~

HEADQUARTERS FIELD COMMAND, ARMED FORCES SPECIAL WEAPONS PROJECT
SANDIA BASE, ALBUQUERQUE, NEW MEXICO

~~SECRET~~ CONFIDENTIAL

WT-711

This ~~document consists of 222 pages~~

No. ~~[illegible] of 225 copies, Series A~~

OPERATION UPSHOT-KNOTHOLE

Project 1.1b

AIR PRESSURE AND GROUND SHOCK MEASUREMENTS

~~REPORT TO THE TEST DIRECTOR~~

~~by~~

L. M. Swift
D. C. Sachs

January 1955

Stanford Research Institute
Stanford, California

CONFIDENTIAL ~~SECRET~~

ABSTRACT

The specific objectives of Project 1.1b included the determination of pressure vs time variations with ground range, at and near the ground surface, for five nuclear shots detonated at very high, intermediate, and relatively low heights of burst, as well as a limited study of the near-surface underground accelerations produced by air burst explosions. Using these data, the report discusses air blast scaling laws, Mach reflection (path of the triple point), precursor characteristics, the empirical height of burst chart, and earth accelerations. The results of some experiments on instrumentation are included as Appendix B. appendix.

The performance was highly satisfactory except on Shot 10, during which cables were broken when several towers blew down. The gage records are reproduced (in reduced form) in Appendix A. Data from the records have been tabulated in two ways -- as-read, and A-scaled (normalized to one KT radiochemical yield with gage at sea level conditions). These data are tabulated and appear in numerous graphs, together with composite curves to emphasize certain comparisons.

In terms of fulfillment of the objectives of the tests, the following statements may be made. For convenience, the statements are rather positive; the qualifications and assumptions which accompany them are detailed in the text.

1. On the basis of the comparisons of A-scaled maximum pressures, phase durations and impulses, the total air blast phenomena of U-K Shot 9 and TUMBLER Shot 1 scale very well. The yield ratio for these two shots was about 26:1 and both were detonated over the same surface at an A-scaled burst height of 750 ft.

2. Shot 9 data indicate that the theoretical analysis of Mach triple point trajectory near the ground surface is not applicable for this intermediate height of burst. Thermal effects are such that Mach reflection appears to begin at very short ground ranges and the rise of the triple point shows two plateaus below the 10 ft level.

3. The precursor pressure waves observed on Shots 10 and 11 indicate that precursor effects are increased when the A-scaled burst height is decreased from 300 to 200 ft. Previous observations of the depression of maximum measured surface air

pressures in the precursor region were confirmed.

4. Precursor wave front orientations obtained from arrival time data seem to confirm the heated-layer theory of precursor formation.

5. Additional data for a composite height of burst chart were obtained for a number of scaled burst heights. Correspondence with previous data is good in the low pressure region, but not so in the 10-50 psi region.

6. A single measurement of dynamic pressure on Shot 11 indicates that in a region of thermal disturbance the Pitot-tube q gage measures a peak dynamic pressure which is significantly higher than the value one would compute using the measured side-on pressure and the classical Rankine-Hugoniot relations.

7. The earth acceleration data confirm results obtained on Operation TUMBLER and yield some information on the effect of gage depth upon observations.

Recommendations for directions of future studies are included.

FOREWORD

This report is one of the reports presenting the results of the 78 projects participating in the Military Effects Tests Program of Operation UPSHOT-KNOTHOLE, which included 11 test detonations. For readers interested in other pertinent test information, reference is made to WT-782, Summary Report of the Technical Director, Military Effects Program. This summary report includes the following information of possible general interest.

a. An over-all description of each detonation, including yield, height of burst, ground zero location, time of detonation, ambient atmospheric conditions at detonation, etc., for the 11 shots.

b. Compilation and correlation of all project results on the basic measurements of blast and shock, thermal radiation, and nuclear radiation.

c. Compilation and correlation of the various project results on weapons effects.

d. A summary of each project, including objectives and results.

e. A complete listing of all reports covering the Military Effects Tests Program.

ACKNOWLEDGMENTS

The planning and execution of Project 1.1b, Operation UPSHOT-KNOTHOLE, were under the direction of Mr. L. M. Swift, with Mr. L. H. Inman serving as Field Party Chief. Mr. S. C. Ashton was responsible for all logistics, as well as certain aspects of engineering design. Other members of the field party included C. C. Hughes, V. E. Krakow, R. V. Ohler, G. C. Pippin, C. T. Vincent, and C. M. Westbrook.

The authors are grateful to Mrs. S. R. Hornig and Mrs. J. C. Simons for their help in data reduction and report preparation.

The excellent cooperation of LCDR W. L. Carlson, USN, Director of Program 1, Field Command DNWT, and his staff, is gratefully acknowledged.

CONTENTS

ILLUSTRATIONS

TABLES

CHAPTER 1

INTRODUCTION

1.1 HISTORY

Los Alamos Report LA-743R,[1]* published in 1949, included what was then known concerning the optimum height of burst for maximizing the area of peak air blast overpressure at ground level. This information was based upon the theory governing the reflection of plane uniform shocks from a perfectly reflecting plane surface, together with limited nuclear explosion data from the Bikini-Able air drop and from a few tower shots. The Operation BUSTER shots in the fall of 1951 revealed considerable discrepancy, both in magnitude and in wave form, between the predicted and observed ground level pressures.[2] The BUSTER shots were the first well-instrumented nuclear bursts using operational heights of burst. The discrepancies encountered were attributed to instrumentation difficulties, thermal effects, dust, induction signals, etc. The Operation TUMBLER shots in the spring of 1952 were planned to resolve these differences.

The results of the TUMBLER shots confirmed the fact that, at relatively low scaled heights of burst, the form of the pressure wave departs considerably from the conventional form expected from theoretical considerations and small-scale HE experiments.[3] These unexpected results were shown to be associated with the thermal radiation acting jointly on the earth's surface and on the clouds of surface dust, which combined to produce a thermal layer. This layer was shown to be qualitatively capable of affecting the blast wave by lowering the peak pressure, increasing the rise time of the shock, and increasing the velocity of propagation of the initial air pressure wave. The last of these effects of the thermal layer sometimes resulted in an anticipatory pressure wave called a "precursor." In addition, the TUMBLER data indicated marked deviation from the theory of irregular (Mach) reflection.

Not enough quantitative data were obtained from TUMBLER to permit the development of analytical techniques for predicting the magnitude of the effects of the thermal disturbances under a known set of conditions. Factors such as the thermal absorption coefficient of the

* Superscript numbers denote references listed in the Bibliography at the end of this report.

surface, the moisture content of the surface, and the thermal absorption coefficient of the dust cloud, almost certainly enter into the total effects. The problem is further complicated by turbulence in the thermal layer so that single measurements of air pressure, temperature, velocity, or other quantities do not necessarily represent the macroscopic conditions in the vicinity of the point of measurement. It was hoped that some of these unsolved matters could be clarified using the results of Operation UPSHOT-KNOTHOLE.

The original plans for UPSHOT-KNOTHOLE included a total of 10 shots, the first eight developmental shots to be fired in Yucca Flat, and the last two, for military effects, to be fired in Frenchman Flat. Toward the end of the operation another developmental shot was added to the test series.

1.2 OBJECTIVES

The general objectives of Program 1 were (1) to add additional knowledge to blast phenomenology, particularly with respect to air blast scaling laws, Mach reflection, and precursor characteristics, and (2) to obtain for other effects programs definitive data on blast phenomena resulting from the two military effects shots (Shots 9 and 10). This report covers a portion of Program 1 (Project 1.1b) as directed toward these objectives.

The specific objective of Project 1.1b was to determine the pressure vs time variations with distance from ground zero at and near the ground surface, for five nuclear shots at very high, intermediate, and relatively low heights of burst. Three of the shots were to be detonated at a low scaled height; however, the spread in radiochemical yields of the three shots was 350:1.

A secondary specific objective was to determine the near-surface underground accelerations produced by air burst explosions for the purposes of (1) supplementing similar data obtained on TUMBLER, and (2) supplying support measurements to the effects projects dealing with buried targets, foxholes, field fortifications, and the like.

1.3 THEORETICAL CONSIDERATIONS

This section presents some of the theoretical considerations concerning the phenomena involved in the air burst of a nuclear weapon. These considerations, although not original, should aid in clarifying the analysis of the data obtained on UPSHOT-KNOTHOLE.

Three topics are discussed in this section: Mach stem phenomena, precursor phenomena, and earth acceleration. The small amount of analysis presented for other problems will be introduced in the appropriate portion of the discussion (Chapter 5).

As used in this report, the term "pressure" denotes overpressure, i.e., gage pressure. The "side-on pressure" is the difference between the pressure at any point within the blast wave and the pressure in front of the shock.

1.3.1 Mach Stem Phenomena

It is well known, in oblique shock reflection theory, that for a shock wave in a gas striking a rigid boundary conditions may exist in which regular reflection is not possible.[4] It is possible to define an incident angle, called the extreme angle, beyond which no regular reflection occurs. This extreme angle is a function of the incident shock pressure, as shown in Fig. 1.1. It is clear that as the shock strength is decreased, the acoustic limit is approached and thus the limiting angle must approach 90 degrees.

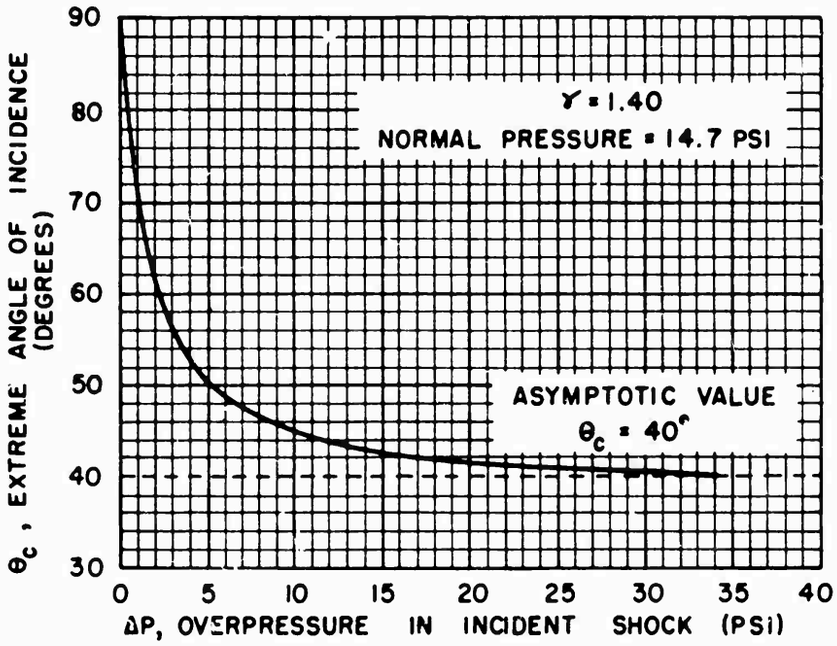

Fig. 1.1 Extreme Angle vs Shock Pressure

It has been found experimentally that, depending on the shock strength of the oblique shock wave impinging upon a rigid boundary, there is a critical incident angle at which the reflected shock will barely be capable of deflecting the stream so that it becomes parallel to the boundary plane. Beyond these critical conditions, the signal propagates back from the reflected shock into the region between the shocks and causes a fusion (Mach reflection) of the incident and reflected shocks.

This process of Mach reflection originates at the boundary and gradually spreads into the volume of the gas. As it spreads the two shocks merge and form a "Y" pattern standing on the boundary. In Mach reflection, it is as if reflection were no longer caused directly by the boundary but rather by a cushion of air resting on the boundary. It should be pointed out that the preceding analysis of reflection assumes that the air has no velocity component normal to the boundary before the arrival of the incident shock.

The qualitative picture of Mach reflection is quite simple for the case of a plane shock incident on a boundary. The problem is more complicated in the case of air blast pressure from a bomb. First, the angle of incidence and shock strength change as the blast wave proceeds outward from ground zero. In addition, the spherical character of the wave makes a quantitative difference where Mach reflection occurs, while it introduces no additional features in the case of regular reflection. This is true because regular reflection takes place entirely in the neighborhood of a single point on the boundary and, therefore, only local conditions at that point enter. The Mach "Y" type reflection, on the other hand, extends over a finite area and the properties of the shock in a larger area now become relevant.

It may be profitable to look at the assumptions associated with shock reflection theory in the light of effects from an air burst nuclear bomb:

(1) It is assumed that the earth's surface presents a perfect reflector to the oncoming incident blast wave. In this regard, it is possible to define a reflection coefficient, which is a ratio of the apparent bomb tonnage as indicated by the reflected and incident pressure vs distance curves. That is:

$$K = \left[\frac{R_r}{R_f}\right]^3 \qquad (p \text{ constant}), \qquad (1.1)$$

where R_r is the radial distance corresponding to a reflected pressure and R_f is the radial distance corresponding to the same pressure magnitude on an incident pressure vs distance curve. According to regular reflection theory, for weak shocks at large incident angles (large ground ranges) this reflection factor should be equal to 2, which corresponds to the effect from the bomb and its image at larger radii. The data available are for reflections from smooth concrete.[17] In this case, it was found that $K \simeq 1.5$, showing that even for this fairly ideal case there is a loss of some energy upon reflection. This energy loss may be significantly greater at the air-earth boundary of UPSHOT-KNOTHOLE, which could, in turn, alter somewhat the curve shown in Fig. 1.1.

(2) The assumption is made that the incident shock wave travels through undisturbed air. It is known that the thermal radiation from a nuclear bomb is appreciable. For a 20 KT weapon approximately 35 per cent of the energy is emitted as thermal radiation. This radiation precedes the blast wave and heats the earth and sometimes the air before the arrival of the air blast shock at any radius. In view of this, it would seem that the theoretical assumption that the incident wave is traveling through an undisturbed medium is not entirely valid. One would expect that the effects of thermal radiation would be particularly pronounced for large nuclear bombs exploded at relatively low burst heights (scaled heights of burst less than 400 ft). For these cases, heating can be so intense that spontaneous boiling up of the earth's water of hydration ("popcorning") can occur. The popcorning gives rise to a layer of dust-laden air near the ground surface, which may provide

an effective medium for heat transfer between the incident thermal radiation and the air.

At present, there exists only fragmentary experimental evidence of what occurs when a shock wave impinges upon a thermal boundary layer. One piece of evidence is the result of an experiment performed in the Princeton University shock tube.[5] The interferograms show that the incident shock disappears in the thermal layer, a slow pressure rise precedes the main shock near this layer, and something resembling a reflected shock is present. There is no evidence on the interferograms of a shock being transmitted in the thermal layer above the heated plate. If this same phenomenon were experienced in full-scale effects testing, the observed incident and reflected pressures at aboveground gages would indicate the presence of a Mach "Y" reflection with the height of the "stem" approximately equal to the thickness of the thermal layer. However, one should call this type of reflection a "thermal-Mach reflection," because it does not represent irregular reflection in the same sense as does the Mach reflection described previously.

In addition to the formation of the thermal-Mach reflection, the thermal layer will probably affect the more conventional Mach phenomena, the theory of which assumes no preshock velocity components perpendicular to the boundary plane. Probably the thermal layer will act to "smear out" the critical angle value corresponding to a particular shock strength. The reasoning here is that there will undoubtedly be a good deal of turbulence in the thermal layer which would give rise to complicated air and dust velocity gradients before the arrival of the incident shock. Since the Mach-type reflection extends over a finite area, it is likely that these disturbances would affect the formation and trajectory of the Mach triple point. If the effects due to the thermal absorption persist out to the range (for a given burst height) which corresponds to the critical angle, then it would be difficult to define in any simple manner the ground range at which the incident and reflected shocks should merge to form a Mach "Y."

Throughout this discussion it has been necessary to apply the theory for plane shock reflection to a case which involves spherical waves. There are necessarily limitations inherent in this procedure, but the lack of known theoretical analysis of the spherical case leaves no choice.

The increase in the angle of incidence of the expanding spherical shock results in an increase in the rate of rise of the triple point. Halverson has made extensive studies of the experimental data on the Mach effect for spherical waves.[6] Despite the lack of a satisfactory theory, the use of available experimental data together with the $W^{1/3}$ scaling law enables one to predict the main features of the behavior of a reflected spherical blast wave. Figure 1.2 presents the theoretical curve for the onset of Mach reflection as given in the TUMBLER Summary Report.[7] The figure shows the variation of the critical angle for regular reflection as a function of range and height of burst; this curve is probably of more value for prediction than is the curve of Fig. 1.1.

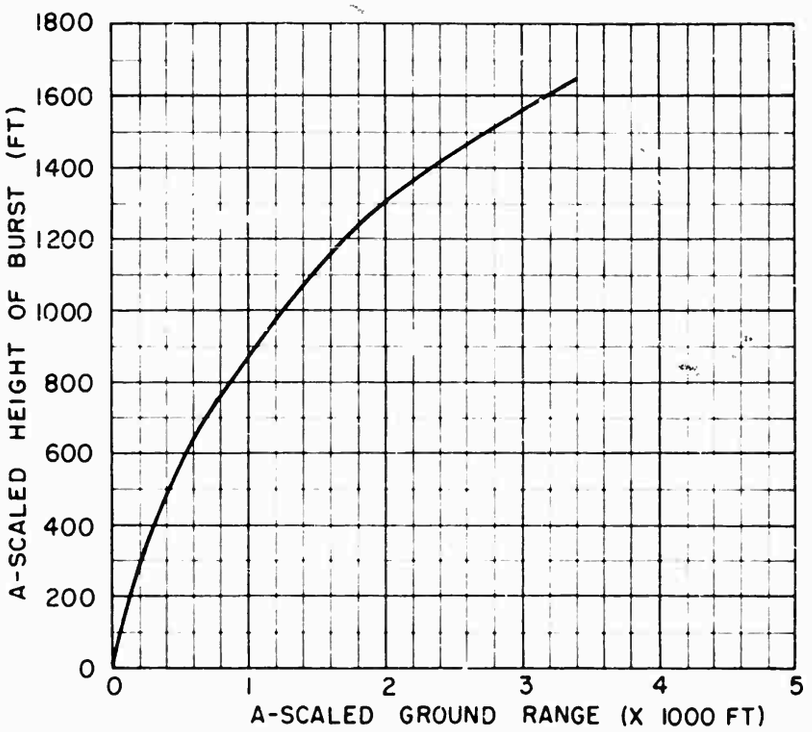

Fig. 1.2 Theoretical Curve for Onset of Mach Reflection

1.3.2 Precursor Phenomena

On TUMBLER Shot 4 the pressure records and high-speed photography clearly demonstrated the existence of a pressure wave, out to a distance of about 2000 ft, which developed around ground zero in advance of the incident shock wave from the bomb.[3] This wave, because it arrives at a station before the wave associated with the incident shock, is referred to as the precursor pressure wave. Re-analysis of the photograpny and pressure records from BUSTER indicated the previously unobserved existence of such a pressure wave. Present theory indicates that the formation of the precursor is due to the refraction of the incident shock wave by a layer of heated air near the ground surface. At a certain ground range, the incident wave is refracted so that the wave travels parallel to the ground. If the temperature of the heated layer is sufficiently high with respect to the ambient air above it, the velocity of this refracted shock wave is increased so that it reaches subsequent ground radii sooner than the incident shock wave. The refracted wave, as it propagates through the heated air layer, also sends another shock wave into the ambient air.[7]

This phenomenon can better be explained by reference to Fig.1.3, which is a schematic diagram of the sequence of events leading to precursor formation in the acoustic wave case. The boundary represents the separation of two media possessing very different sonic velocities.

In this case, the velocity C_2 in the lower medium is larger than velocity C_1. When the incident wave of the figure is at I_1, the reflected wave is at R_1, and the transmitted wave is at T_1. However, it will be noted that the wave at T_1 is not hemispherical, since its velocity in the lower medium is greater. For this acoustic case, the directions of wave fronts I_1 and T_1 at the boundary are derived from Snell's Law,

$$\frac{\text{Sin } \alpha_1}{\text{Sin } \alpha_2} = \frac{C_1}{C_2} \quad . \qquad (1.2)$$

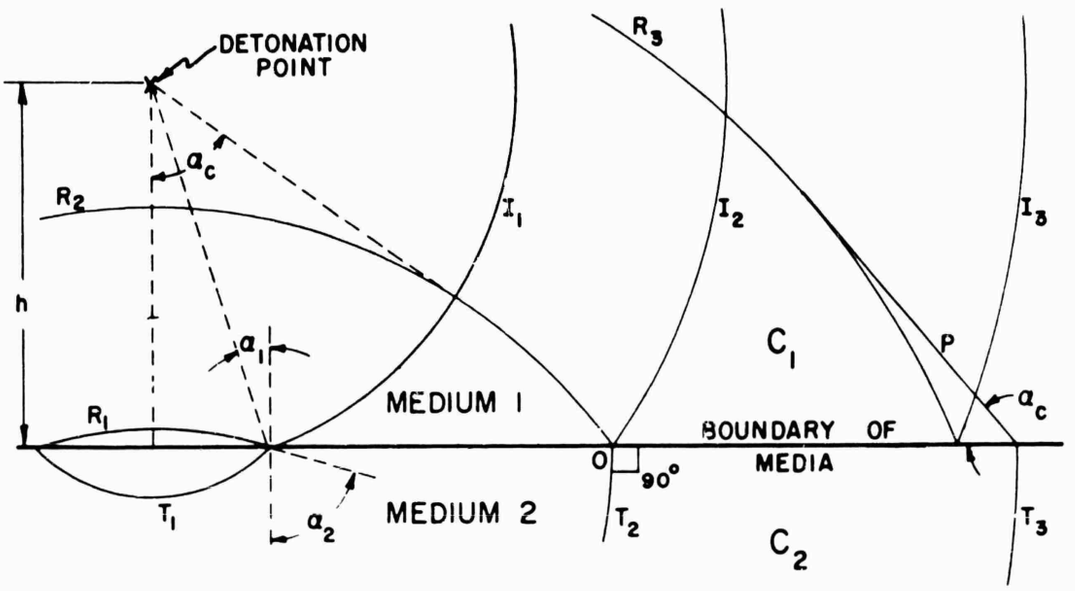

Fig. 1.3 Schematic Diagram of Precursor Formation (Acoustic Case)

Therefore, when angle α_2 increases to 90 degrees (at point O of Fig. 1.3),

$$\text{Sin } \alpha_c = \frac{C_1}{C_2} \quad , \qquad (1.3)$$

the transmitted wave, T_2, travels in such a direction that its front is normal to the boundary and continues to propagate in this direction. When the incident wave has reached I_3, the transmitted wave, T_2, will have arrived at T_3. However, since there can be no shock wave discontinuity at the boundary, this transmitted wave sends into the upper medium a new wave, P, the precursor. This same condition prevails at all greater distances from the detonation until the incident and transmitted waves decay to zero. The critical angle, α_c, at which the precursor forms is defined by Equation 1.3; moreover, the angle of intersection of the precursor wave with the boundary between the two media is also α_c.

It is unlikely that anything approaching a sharp demarcation between the heated and unheated media actually exists in practice.

However, it is possible that the temperature gradient will be quite steep and the reflecting surface of the ground may add reflected adiabatic waves. It is almost certain that the popcorning effect referred to previously will also influence the development of the thermal layer. The contribution of popcorning is probably closely related to the soil and general terrain characteristics near the surface of the ground. It is well known that the soil conditions at the Nevada Proving Ground are particularly conducive to the creation of a thermal layer.

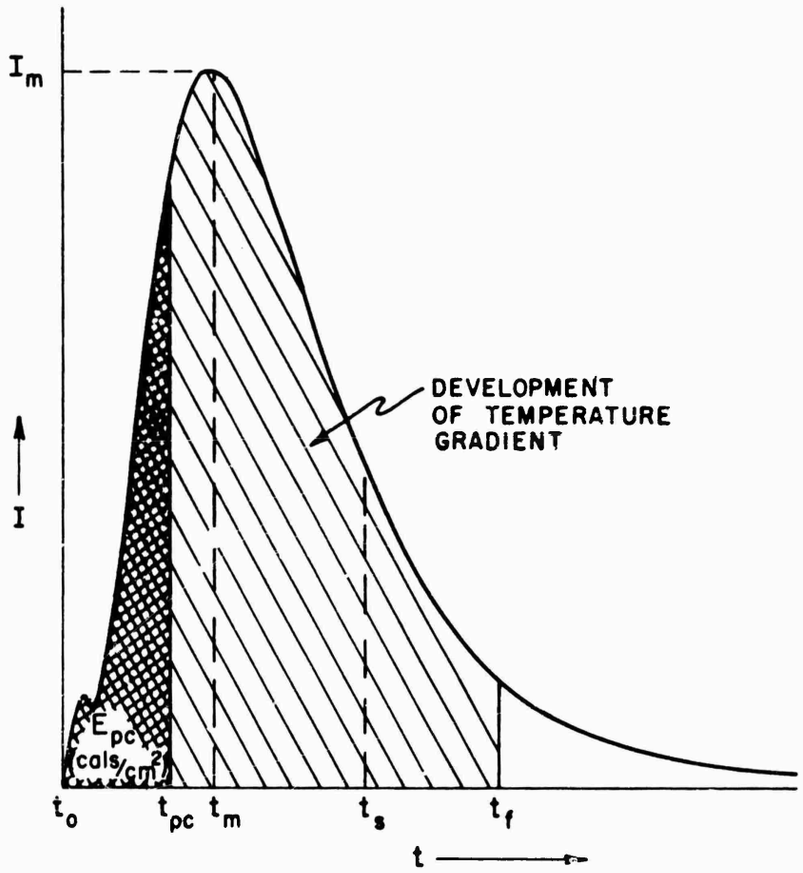

Fig. 1.4 Schematic Diagram of Thermal Intensity Wave Shape

Figure 1.4 is a schematic diagram of the manner in which the intensity (energy per unit area per unit time) of thermal radiation from a nuclear burst varies with time. The shape of this curve is a function of charge size only; however, for a particular charge weight, the maximum intensity, I_m, will decrease with increasing slant range. Laboratory irradiation of Nevada soil has shown that a minimum incident intensity ($cal/cm^2/sec$) will produce popcorning.[8] However, it should be mentioned that these irradiation experiments employed a square-wave

thermal intensity pulse of comparatively long duration (about 0.5 secs). For nominal nuclear weapons, the thermal intensity rises to a peak (I_m) in 0.1 to 0.2 sec and then decays rapidly as shown in Fig. 1.4. These facts suggest that the laboratory experiments[8] only established that there exists a minimum energy density, E_{pc} (cals/cm^2), for the popcorning phenomenon. This threshold energy density (time integral of intensity) is denoted schematically by the crosshatched area of Fig. 1.4. The popcorning probably continues for some finite time, ending when the dust layer produced by the effect no longer allows appreciable thermal energy to reach the ground surface.

Considering the diffusivity of a medium as the measure of the rate of rise of temperature at one point due to thermal input at another point, it is possible to assign a thermal time constant to earth. In Fig. 1.4, the time, t_m, for the thermal intensity to rise to its maximum value, I_m, is in most cases much shorter than this thermal time constant of the earth. Thus, this energy will be absorbed effectively in only a thin surface sheet of earth, little being transmitted to larger depths. However, after the initial radiation and popcorning, a dense air-dust layer is presented to all subsequent thermal energy coming from the detonation. This layer, unlike the earth medium, has a short thermal time constant, which means that radiation heats the dust layer fairly uniformly rather than a large part being absorbed by the topmost portions.

The shaded area under the curve of Fig. 1.4 is that portion of the radiation which is most effective in creating the temperature layer. The time, t_f, denotes the end of the development of this gradient; after time t_f, the radiation is sufficient to maintain the gradient for only a very short time, after which the temperature gradient will decay rapidly to some equilibrium condition.

At some time, t_s, the free air incident shock wave will arrive at the thermal layer. This time will depend upon the shock strength of the wave and the slant range. When considering the development of the thermal layer and subsequent precursor formation, the arrival time of the incident shock wave with respect to the thermal pulse becomes quite significant. It is evident, from the foregoing discussion, that no precursor is observed if the incident shock wave arrives "too soon" (no effective thermal layer exists) or "too late" (the layer has dissipated).

Using the experimental data available on precursor waves from nuclear detonations, Shelton[9] has constructed a comprehensive picture of the criteria for precursor formation. The results of his analysis are presented in Fig. 1.5, where the region of precursor formation is shown on a height of burst chart. The shaded area surrounding the computed curve represents the estimated uncertainty in the analysis.

The points corresponding to previous nuclear tests are also plotted in this figure. It is evident that the analysis presents a consistent picture of past performance; that is, precursors were observed on all shots whose data points fall in the precursor region of the figure, whereas, for the shots whose points fall in the "no precursor" region, no definite precursor pressure wave was observed. There are three points in the shaded "uncertain" area, corresponding to the Nagasaki, GREENHOUSE Easy, and UPSHOT-KNOTHOLE Shot 1 detonations. There are no definitive data on the Nagasaki burst; however, the GREENHOUSE Easy

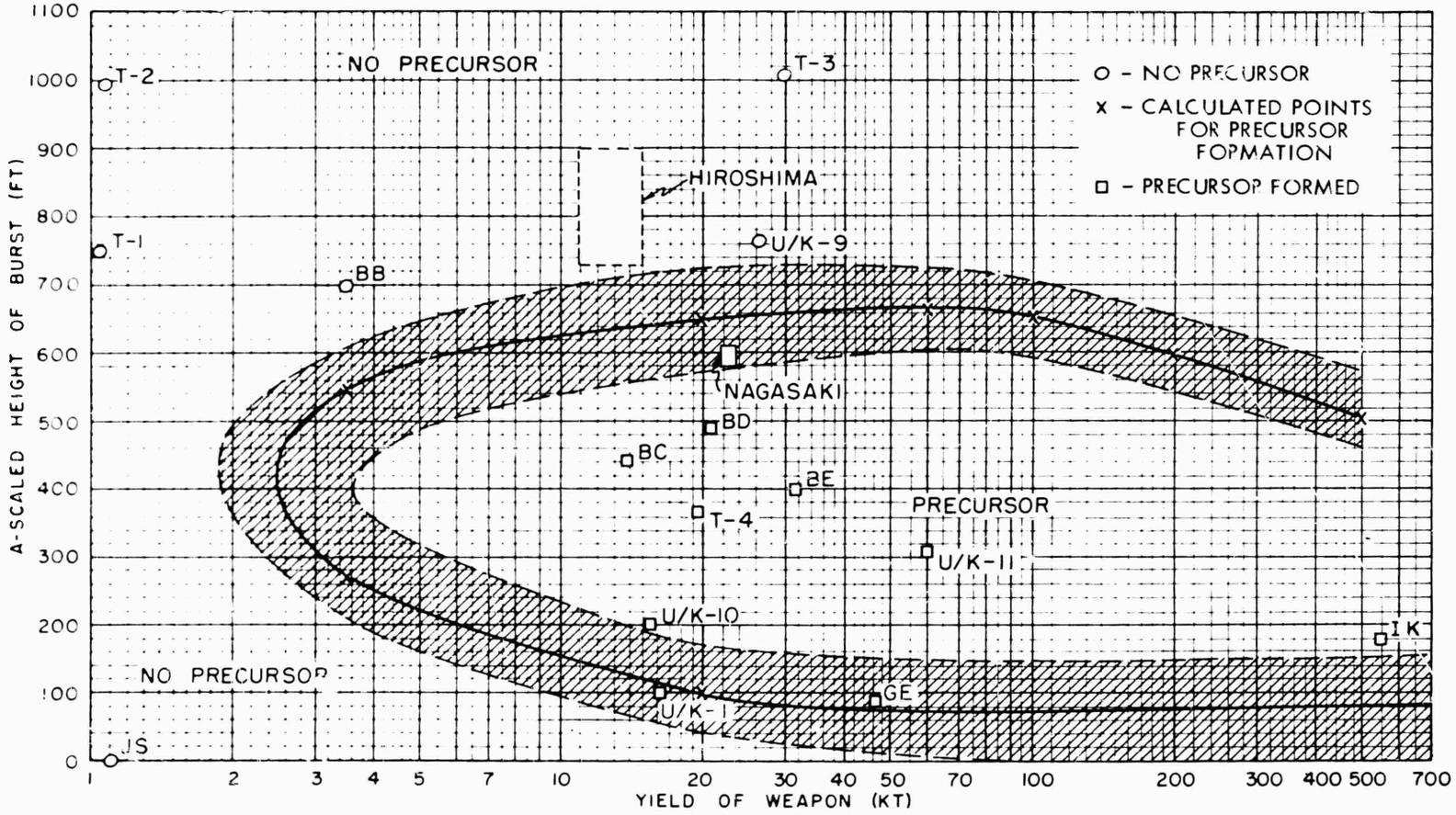

Fig. 1.5 Precursor Formation as a Function of Height of Burst and Yield of Weapon

data and that from Shot 1 of UPSHOT-KNOTHOLE indicate the presence of a precursor pressure wave at some of the gage stations.

Shelton bases his construction of Fig. 1.5 upon the consideration of three main variables: (1) the fraction of the radiochemical yield emitted as thermal radiation; (2) the time during which the weapon radiates prior to shock arrival; (3) the fraction of the total thermal energy emitted during this time. Thus, one arrives at a quantitative result based upon an analysis similar to that described schematically in Fig. 1.4.

This discussion of precursor formation has considered soils in which a dust layer is created very early in the thermal pulse. It is possible, although not confirmed by experiment, that a thermal layer may result when a large amplitude radiation pulse is incident upon a dust-free, opaque boundary. In this case, there would be need to account for the thermal layer on the basis of complex convection and conduction of heat from the surface to the air layer. Such an analysis is outside the scope of this report.

1.3.3 Earth Acceleration and Particle Velocity

The most important theoretical considerations concerning earth acceleration and particle velocity are included in the TUMBLER Project 1.7 report.[10] It is necessary here only to review briefly the conclusions contained in that report to establish a basis for analysis of results.

The manner in which the air blast excites the earth may be explained with reference to the wave front pictured in Fig. 1.6 and the time of arrival diagram of Fig. 1.7. As the incident air blast sweeps along, its apparent horizontal velocity, c', along the earth surface is given by

$$c' = U/\sin\theta \quad , \qquad (1.4)$$

where U is the shock velocity and θ is the angle of incidence. However, the impulse given the earth will eventually outrun this apparent velocity, c'. This may result from a near-surface seismic velocity that is greater than c', or from earth transmission along a curved path which dips into the higher velocity lower earth strata. In the two diagrams this out-running is shown to occur at ground range R_2. Beyond R_2, the first information received by a near-surface accelerometer will be that from the earth wave running ahead.

Consider what happens in an amplitude sense at ground range R_3, beyond R_2 (see Fig. 1.6). Information received at some time intermediate between earth and air arrivals will have suffered attenuation in both earth and air paths. Because of the much smaller attenuation in the air path, the largest amplitudes will occur when the earth path is a minimum. This corresponds to the air blast passing over the gages. Hence, it may be expected that for gages beyond the outrunning limit R_2, the envelope of the measured wave train should tend to increase and reach a maximum when the air blast passes over the gage. This direct local effect of the air blast is termed the "slap," because of the sudden increase in earth motion which is observed.

When the earth wave outruns the air blast, it might be expected that information would be fed back into the air to form a precursor wave. However, it has been shown that for TUMBLER Shot 4 the "round-trip" pressure ratio was about 1/1400.[10] Thus it is unlikely that any significant fraction of the precursor pressure is due to this type of energy transfer.

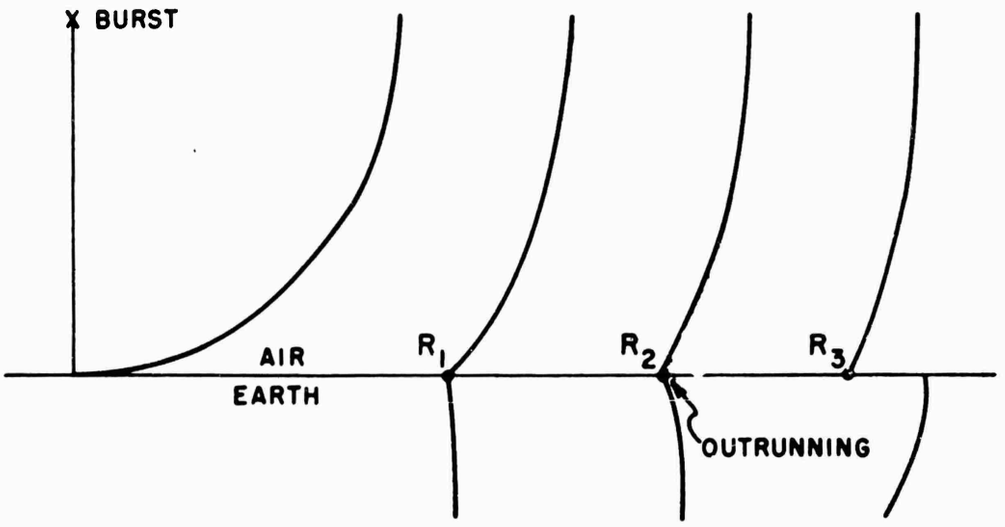

Fig. 1.6 Incident and Refracted Wave Fronts for Air Burst

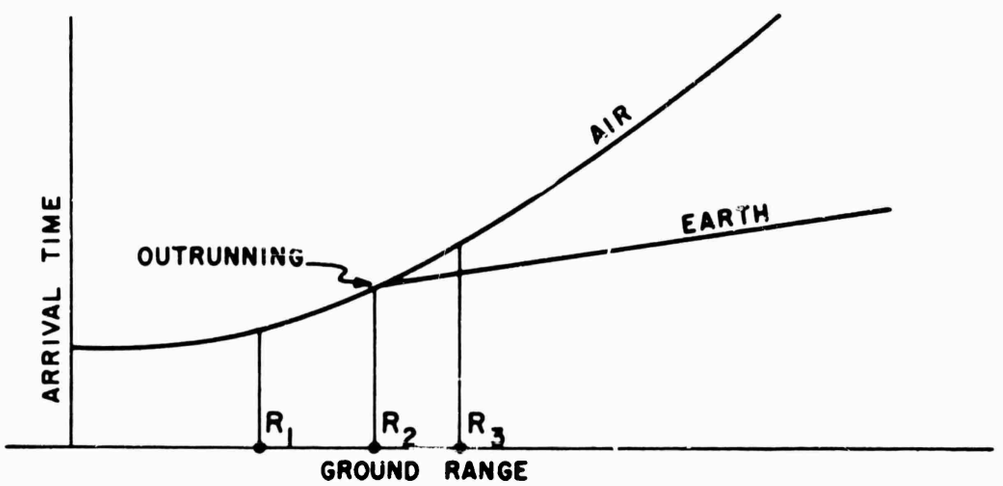

Fig. 1.7 Time of Arrival Diagram for Information Received by Surface Gage

CHAPTER 2

INSTRUMENTATION

2.1 GENERAL SYSTEM

The basic instrumentation system consisted of Wiancko variable-reluctance air pressure gages with associated terminal equipment, used in conjunction with William Miller Model J recording oscillographs. The details of this system have been reported elsewhere.[11,12] The following discussion will therefore be confined to information essential to an understanding of the data and to an explanation of changes made since previous reports.

The prime power supply for all instruments during actual shots was a bank of storage batteries. Suitable converters were used to produce 115 volts AC for such components as required this type of source. An individual converter was used for each rectifier power supply, thus minimizing the probability of gross failure due to converter failure.

Instruments were powered at suitable times before zero time by Edgerton, Germeshausen, and Grier (EG&G) relay circuits, with lock-in relays controlled by a time delay circuit to continue operation for approximately 1 minute after zero time, in spite of the fact that the EG&G relays drop out sooner. Utmost attention was paid to circuitry and procedures to insure maximum reliability of operation.

2.2 GAGE MOUNTING

All air pressure gages were mounted with their inlets at the center of a 17 in. diameter cast aluminum baffle. If the gage was to be at ground level, this baffle was cemented flush with the earth's surface, and was held in place with a buried anchor. If it was to be above the surface, the baffle was oriented so that a vertical plane through instrument ground zero formed a positive angle of 5 degrees with the surface of the baffle. The positive angle is defined as permitting slightly "face-on" incidence for a shock wave originating from instrument ground zero. This orientation was chosen for all pressure gages in Program 1 as a result of wind tunnel studies analyzed by Dr. J. D. Shreve of Sandia Corporation.[13] These studies indicated that, as the angle of impact was varied in both directions from zero, the accuracy

of the pressure gage readings was relatively unaffected by angles between minus 1 degree and plus 12 degrees. The 5-degree orientation was therefore chosen in the middle of this range so that bombing errors would have a minimum effect on accuracy. As a convention, all baffles were oriented so that the gage inlet opening faced to the right when viewed by an observer facing ground zero, except in the case of secondary gages on Shot 10, such as 16B50A. In this case, the gages were mounted with opposite orientation to help define the true pressure if true ground zero did not coincide with instrument ground zero. These gage baffle mountings were identical to those used by several other agencies in these and previous tests. Experience has shown excellent correlation between the results obtained by different agencies and between different tests. Other techniques of measurement also substantiate the accuracy of the gage readings. Typical gage installations are shown in Fig. 2.1.

Each accelerometer was mounted in a canister to protect the buried instrument (see Fig. 2.2). The canister was cemented into a hole about 4 in. in diameter and the hole was refilled and tamped to present a smooth surface.

One Pitot tube q-gage assembly was incorporated into the instrumentation for Shot 11. The mounting details for this gage are included in a Sandia report.[14]

2.3 GAGE RESPONSE

The response time of the pressure gage recording system was determined by the characteristics of the recording galvanometer used. These galvanometers had an undamped natural frequency of 315-340 cps and were damped to have an overshoot of approximately 7.5 per cent. This corresponds to a nominal rise time (to 90 per cent of final amplitude for a square wave) of 1.3 msec, or to a total rise time (to peak deflection) of 2.1 msec.

The undamped natural frequency of the gages themselves varied from about 1400 cps to about 2000 cps. Since the damping of these gages tended to be nonlinear, each gage was adjusted prior to the test to have a total rise time of less than 1 msec. The resultant overshoot and ringing were at a frequency above that to which the galvanometer and other parts of the system would respond, so that they do not appear on the final record. This procedure avoided the possibility that nonlinear damping effects could increase the rise time in the latter portions of the rise -- an effect noted in some previous tests.

2.4 CALIBRATION

Each pressure gage was calibrated in the field by the application of several values of static pressure, after the gage had been installed in its final location and connected to its associated equipment for the shot. After each shot, a post-shot calibration was performed to check the stability of the system.

In the calibration procedure, several pressures ranging from zero to well above the expected peaks were applied to each gage in sequence. For each pressure, the galvanometer deflection was recorded.

Surface Level Baffle

10 Ft Level Baffles

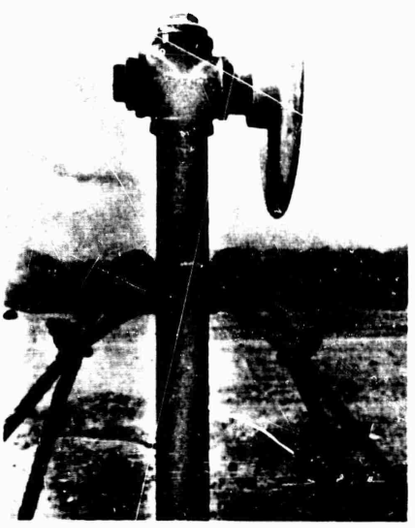

Close-up of Aboveground Baffle

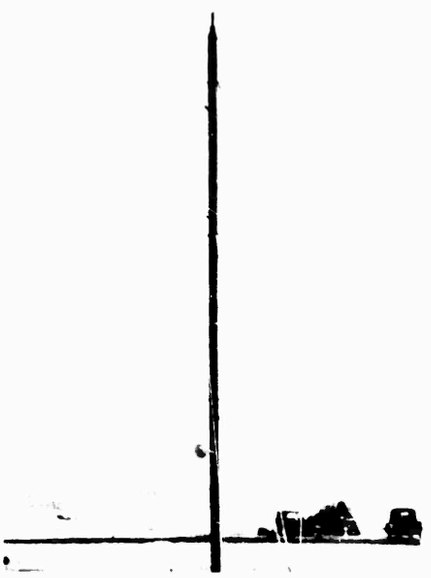

Gage Tower

Fig. 2.1 Typical Gage Installations

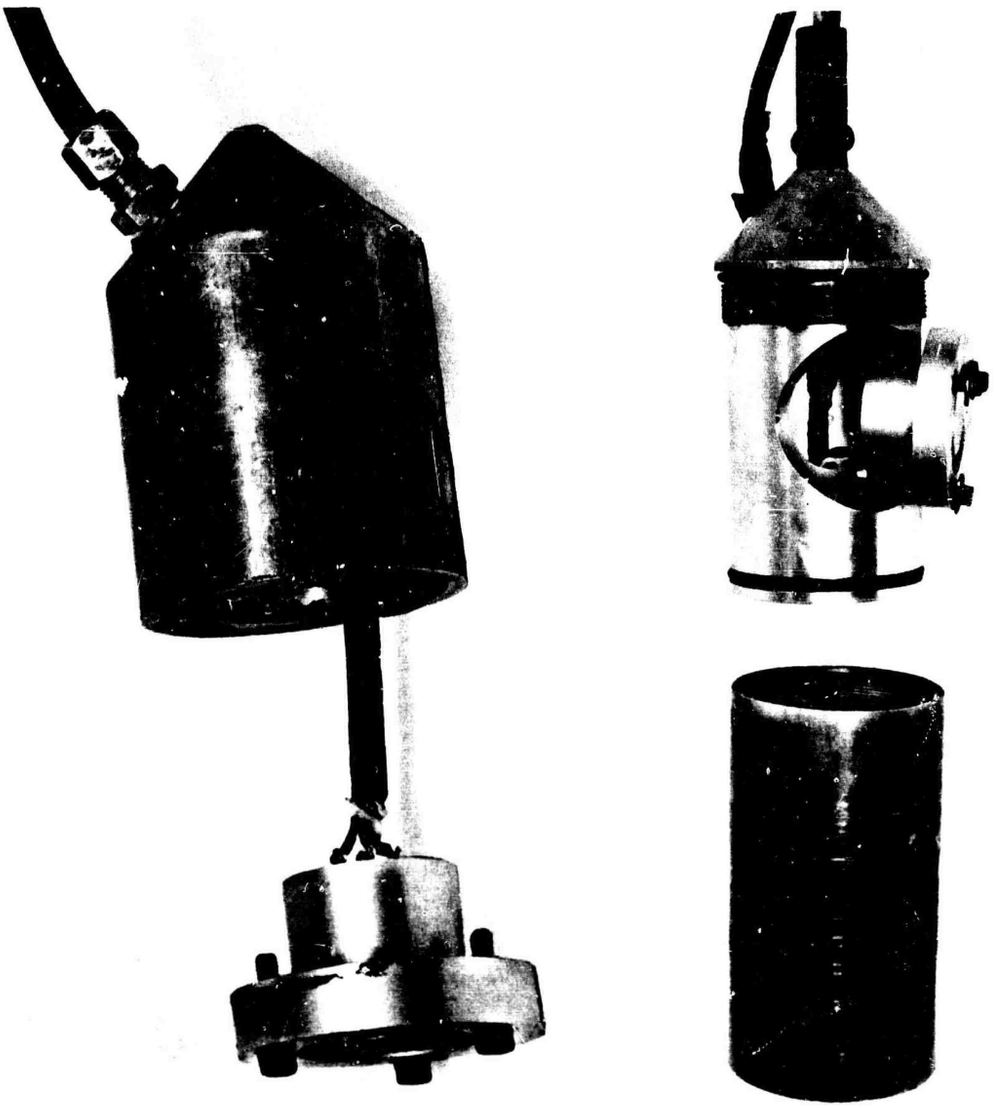

Vertical Horizontal

Fig. 2.2 Accelerometers Mounted in Canister

Using these data, a calibration curve showing deflection vs pressure was constructed. In addition, the deflection caused by an artificial signal injected into the gage circuit was recorded. This information provided a check on any changes of sensitivity of the recording system between calibration and the final test, since an identical signal was automatically injected on the final record about 10 sec before zero time.

Each accelerometer was calibrated in the field under operating conditions, before being planted, while it was connected to the cable and channel to be used. Two methods of calibration were used. Whenever the expected peak was low, the accelerometer, mounted in its canister, was turned in the earth's field, thus applying a known acceleration to the element. The corresponding deflection was noted. A synthetic "calibration" signal was also applied, as described above for the pressure gages. The linearity of these accelerometers had been established to be excellent in these ranges, and this calibration procedure was used where expected peaks were under 4 G.

When higher peaks were expected, the accelerometer was mounted on a spin table of known radius, driven at a speed measured with a stroboscope (accuracy better than 0.5 per cent) and the normal calibration procedure was followed. Accelerations up to 100 G were possible with this arrangement.

2.5 INDUCTION SIGNAL PROTECTION

On some tests, particularly on TUMBLER Shot 4, considerable interference with the performance of the system was experienced from the so-called "induction signal." This electromagnetic disturbance is coincident with the explosion of the bomb and is picked up by the gage cable and/or the gages themselves. Normally this signal is of such an amplitude as to cause only a short disturbance at zero time on each recording channel, with recovery occurring in less than 5 msec. However, when a large nuclear device is detonated at a relatively low altitude and when gage cables of considerable length run to a point relatively near ground zero, the magnitude of this induction signal is sufficient to damage the instruments. In the case of SRI instrumentation, the major part of the damage experienced from this phenomenon has been restricted to unbalance of the ring modulators in the Wiancko coupling units. Apparently the currents induced in the line are of sufficient magnitude to overload the varistors comprising the ring modulators. In the Wiancko system these ring modulators are not isolated from the line by any circuit components other than a transformer and a condenser. Neither of the latter has been known to suffer damage from electromagnetic shock.

In pretest planning, consideration was given to the introduction of low pass filters into each line for the elimination of these disturbing signals. Unfortunately, little information was available as to the frequency range of the electromagnetic disturbance and practically none as to the frequency range and magnitude of the disturbing signal picked up by the gage channels. As a consequence, it was decided that it was not possible to design a filter which would give reasonable assurance of satisfactory operation. As a possible alternative, consideration was given to grounding or shielding systems which would prevent or

reduce the pickup of the electromagnetic signal on the cables themselves.

Examination of the TUMBLER records verifies the fact that the disturbing signal usually caused an unbalance in the ring demodulator circuit without damaging the gages themselves. In addition, the disturbing signals appeared to be of equivalent magnitudes on channels connected to gages at the top of 50 ft towers, gages at surface level, and gages (accelerometers) buried beneath the surface. In other words, the shielding of the earth apparently caused no reduction in induction signal amplitude. Under these conditions further shielding would be ineffective and the grounding system already used (all grounds at the central recording station) was decided to be the most effective possible.

In view of the improbability of improvement by other means, a "brute force" method of protection was decided upon as providing the best likelihood of success. The signal lead of each gage channel at the point of entrance to the recording shelter was grounded through a separate contact on a multicontact relay. Provisions were incorporated for applying this ground by actuating the relay at approximately minus 5 sec, and releasing this ground by de-energization of the relay by a "blue box," thus restoring the circuit to normal at about plus 5 msec. In practice two blue boxes were used in parallel to provide greater assurance of operation. By this means the disturbing signal was shunted to ground at zero time, but the signal channel was in normal condition both for the auto-calibration operation which occurred at minus 15 sec and at the time of all gage signal arrivals. This protection was applied to from 12 to 24 channels on Shots 9, 10, and 11. Only such channels as were within 2000 or 3000 ft of ground zero were so protected.

The results were entirely satisfactory; the only damage which may have been due to the electromagnetic disturbance occurred for one air pressure gage on Shot 9.

2.6 TIME RECORDING

In order to provide highly accurate timing of all events and to provide time correlation between separate recorders, a new auxiliary timing circuit was designed after TUMBLER-SNAPPER. A Hewlett-Packard 300D low frequency standard was used as a primary source time standard; 100 cps and 1000 cps output from this instrument were applied to galvanometers on each recording oscillograph. The timing lines provided by the local fork in each recorder were retained as a convenient measure of approximate time, but accurate time readings were possible from the master time recorder. The induction signal disturbance provided an accurate indication of zero time on several channels of each recorder.

It is estimated that the use of this timing system permits the measurement of relative time of events to plus or minus 0.25 msec and the measurement of absolute time of events with reference to zero time with an accuracy of plus or minus 0.001 per cent plus 0.25 msec. This relative time accuracy is particularly important in calculating triple point trajectory and wave front shape by arrival times at various gages.

It was considered desirable to provide means for clinical post-test analysis of any major failure which might occur in the instrumental system. For this purpose a Foxboro 810 Operational Time Recorder was installed with the various pins actuated by the major operational

functions including the EG&G relays, blue box, and certain other critical relay operations in the system. The time recorder provided a record of the time of operation of each of these functions. Since no such failures occurred during the UPSHOT-KNOTHOLE tests, this provision is not of special interest. Its operation was entirely satisfactory, however, and full records were obtained on each shot.

2.7 ACCELEROMETER INSTRUMENTATION

The channels used for vertical acceleration measurements differed from those used for air blast in that amplification was introduced by means of Consolidated Model D-11 amplifiers used in place of the Wiancko station equipment. This permitted the use of Wiancko accelerometers having a higher undamped natural frequency than would otherwise have been possible. Wiancko 150G accelerometers were used for this purpose, having an undamped natural frequency of approximately 450 cps, while the recording galvanometers had an undamped natural frequency of approximately 460 cps. The response time of the acceleration recording system was thus limited about equally by the accelerometers and the recording galvanometers. The results obtained on TUMBLER indicate a need for this increase in the range of frequency response. Records from 1- and 5-ft deep vertical accelerometers show frequencies which approach the damped natural frequencies of the gage-galvanometer system, thereby introducing errors in calibration. The range of frequency response was increased for UPSHOT-KNOTHOLE so that more accurate data could be obtained. Special provisions were incorporated in the Consolidated amplifiers for the automatic recording of the calibration signal on each channel immediately prior to the shot.

Since the several channels of horizontal acceleration recording were added to the plan late in the operation, they could not be provided with amplifiers. Consequently, standard Wiancko channels were used, employing 300 cps galvanometers with Wiancko 30G accelerometers (190 cps natural frequency) or Wiancko 5G accelerometers (85 cps natural frequency).

2.8 ACCURACY

Except for pressures far below nominal gage rating, it is believed that the calibration procedure assures that the measurements were reliable to within plus or minus 5 per cent of the actual pressures. Low pressure measurements, particularly on Shot 3, may be somewhat less accurate.

Because the frequency response errors were reduced to a minimum in the case of the gages measuring vertical acceleration, it is estimated that these measurements are reliable to plus or minus 5 per cent. For this test, no vertical acceleration records exhibit frequencies which are close to the natural frequencies of the accelerometer-galvanometer system (see Table 5.11). For the horizontal accelerations, Table 5.11 shows that in many cases the recorded frequencies are close to the natural frequency of the gage-galvanometer system so that greater errors may be introduced.

In general, however, an accuracy of plus or minus 5 per cent is considered valid.

CHAPTER 3

OPERATIONS

3.1 TEST DESCRIPTION

The five nuclear explosions of UPSHOT-KNOTHOLE with which this report is concerned were detonated at the Nevada Proving Ground of the Atomic Energy Commission during the spring of 1953. Table 3.1 presents the pertinent data for the shots included in Project 1.1b. With the exception of Shot 3, which was a tower shot, all of the nuclear explosions were detonated using air-dropped, air-burst weapons.

TABLE 3.1 - Shot Descriptions

	Shot 3	Shot 4	Shot 9	Shot 10	Shot 11
Date (1953)	31 March	6 April	8 May	25 May	4 June
Location (area)	T-7-5a	T-7-3	FF	FF	T-7-3
Yield (KT)	0.20	11.0	26	14.9	60.8
Height of burst (ft)	300	6020	2423	524	1334
Ground zero relative to aiming point (ft)		80N 560E	837S 15W	139S 86W	232N 172W
Atmospheric pressure (mb) at ground zero at burst height	 873 863	 861 686	 900 825	 901 884	 867 824
Air Temperature (°C) at ground zero at burst height	 4.4 8.2	 15.5 -0.6	 16.7 8.0	 14.8 13.1	 13.3 12.2

As originally planned, Shot 3 was not to be instrumented as a part of this project. Its effects were measured at gage stations designed for Shot 4 on Yucca Flat and the gage layout was by no means optimum for the yield and height of burst. The closest gage station to ground zero for Shot 3 was at a distance of nearly 1100 ft. Shot 4 was detonated at a higher scaled height of burst than any previous nuclear weapons.

The Frenchman Flat site, used for Shots 9 and 10, presents a smooth, dusty, dry-lake bed surface. Because the scaled height of burst of Shot 9 would be comparable to that of TUMBLER Shot 1, (also detonated at Frenchman Flat), it was hoped that more information concerning thermal effects on blast and the validity of scaling laws could be obtained. Shot 10, with its relatively low scaled burst height, was expected to produce effects similar to those which were observed on Shot 4 of TUMBLER. Since TUMBLER Shot 4 was detonated at the Yucca Flat site, it was thought Shot 10 (at Frenchman Flat) might yield data concerning effects of terrain upon thermal phenomena. It was hoped that the Shot 10 explosion would give rise to precursor effects so that these effects might be studied in more detail.

Shot 11 was added late in the operation and was air-dropped over the Yucca Flat area. The terrain in this area differs greatly from Frenchman Flat in that it is covered with an extremely dry and powdery sand. The scaled height of burst of Shot 11 was expected to be closer to that of TUMBLER Shot 4 than was Shot 10. It was hoped that more information concerning the effect of terrain and height of burst upon precursor formation and development could be obtained.

In addition, it should be pointed out that some limited comparisons can be made between the BUSTER tests of autumn 1951, and those of UPSHOT-KNOTHOLE; the BUSTER shots were detonated at the Yucca Flat Site.

3.2 INSTRUMENTATION PLAN

Table 3.2 summarizes the number of air pressure and earth acceleration measurements made on each shot of Project 1.1, UPSHOT-KNOTHOLE. The experimental gages measured air pressure and are described in Appendix B of this report.

3.2.1 Shots 3 and 4

The general gage line layout in the T-7 area of Yucca Flat for Shots 3 and 4 is shown in Fig. 3.1. The gage layout was designed to secure the maximum information obtainable from Shot 4 with the available number (24) of gage channels. The height of burst was so great that simple considerations of geometry showed that ground ranges out to at least 15,000 ft would be desirable. Physical limitations, including feasible cable length and interference with the work of other agencies, limited this range to 13,000 ft. Nevertheless, even at this range, the expected pressure was 1 psi, which was below the optimum level for maximum signal-to-noise ratio with available instrumentation. A study of previous data (notably Fig. 1.2 of this report) and Mach stem theory showed that it was highly improbable that a Mach stem would form within this 13,000 ft range. It appeared that thermal effects would be so

TABLE 3.2 - Instrument Performance

Air Pressure			
Shot	Gages	Recording Channels	Satisfactory Gage Records
3	24	32	24
4	24	32	24
9	51	71	49
10	52	72	45
11	24	32	24
Totals	175	239	166
Acceleration			
Shot	Gages	Recording Channels	Satisfactory Gage Records
3	None	---	---
4	None	---	---
9	14	14	14
10	13	13	10
11	None	---	---
Totals	27	27	24
Experimental Gages			
Shot	Gages	Recording Channels	Satisfactory Gage Records
3	None	---	---
4	None	---	---
9	6	6	4
10	6	6	4
11	None	---	---
Totals	12	12	8

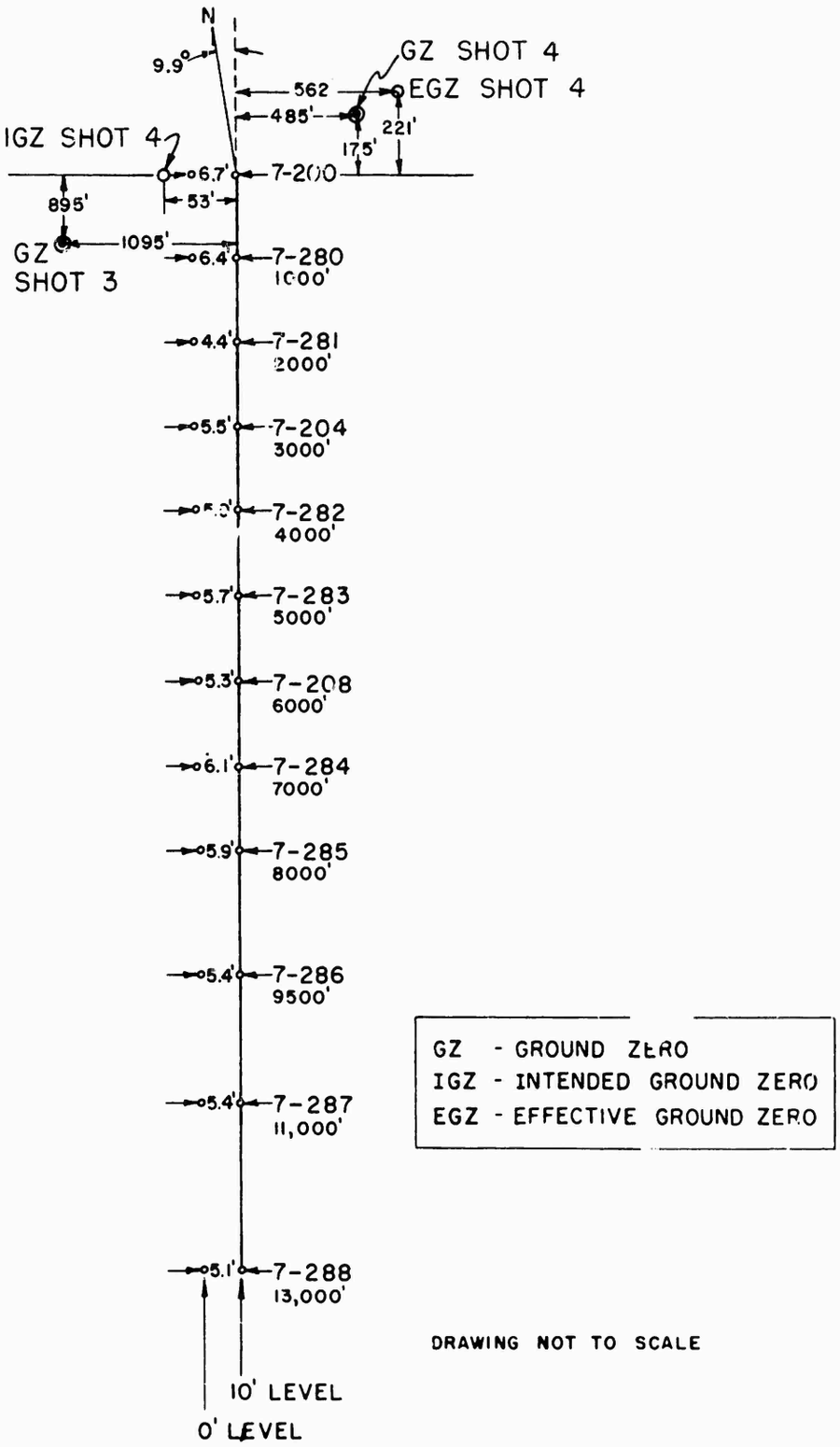

Fig. 3.1 Gage Line Layout, Shots 3 and 4

small as to preclude their interference with the blast wave at any range. These facts limited interest to measurements of incident and reflected air pressures at incident angles up to a maximum of approximately 65 degrees and at slant ranges out to 14,300 ft.

It was decided that these functions could be served by gages at surface level and at one other height, chosen as 10 ft for convenience. The gages at the 10 ft height were located in a line displaced 53 ft east of the nominal blast line. The nominal blast line was the same as used for the TUMBLER shots at this site; it passed through target ground zero. The surface level gages were mounted approximately 6 ft west of the 10 ft gages. The more accurate dimensions are shown in Fig. 3.1.

For Shot 3, the gage layout for Shot 4 was used with no change other than the minimum necessary gage range changes and such attenuator changes as were necessary. Since ground zero for this shot was 1095 ft west of the instrument blast line, the minimum ground range was 1100 ft and the maximum was 12,154 ft.

3.2.2 Shots 9 and 10

The gage layout for Shots 9 and 10 in the F area of Frenchman Flat is shown in Fig. 3.2. This layout was designed to obtain the maximum information from Shot 9. A maximum ground range of 7500 ft was established to provide measurements at pressure levels above 3 psi (another project instrumented the lower pressure region). Surface level gages were located at ground ranges between 7500 ft and ground zero, at intervals chosen to obtain maximum utilization of existing facilities (gage towers, etc.). For the measurement of incident pressures, gages at 50 ft heights were included at all stations out to 5000 ft ground range. Predictions for Shot 9 indicated that the Mach stem triple point would pass the 50 ft height before this 5000 ft range was reached. For the maximum detail in tracing Mach stem formation, and for documenting any precursor or thermal effects, gages at 10 ft height were also included out to 5000 ft, at 30 ft height out to 4000 ft, and at 40 ft height at four stations between 3000 and 4500 ft. Gages at 10 and 35 ft heights at a ground range of 6500 ft were included to supplement the data needed by Program 3 (Project 3.19, forest stand) at that range.

Accelerometers, buried 1 foot deep and mounted to measure the vertical component of earth acceleration near the surface, were located at stations out to 3500 ft. In addition, horizontal accelerometers were located at a depth of 5 ft at six of these stations (see Fig. 3.2). Since the latter were incorporated into the plan at the last moment, their locations were partially determined by available cables and other physical factors.

For Shot 10, all gages at ground zero and the aboveground gages at 500 ft ground range were eliminated, in view of the experience on TUMBLER Shot 4, where close-in gages and gage towers were destroyed. Secondary gages, located at 10 and 50 ft heights at the next two stations, were mounted with baffles facing opposite to the primary gage baffles to aid in the interpretation of the results in case of a serious difference between instrument ground zero and true ground zero. It was recognized that a real possibility remained that the aboveground gages at the first station (1000 ft ground range) would be destroyed, but the

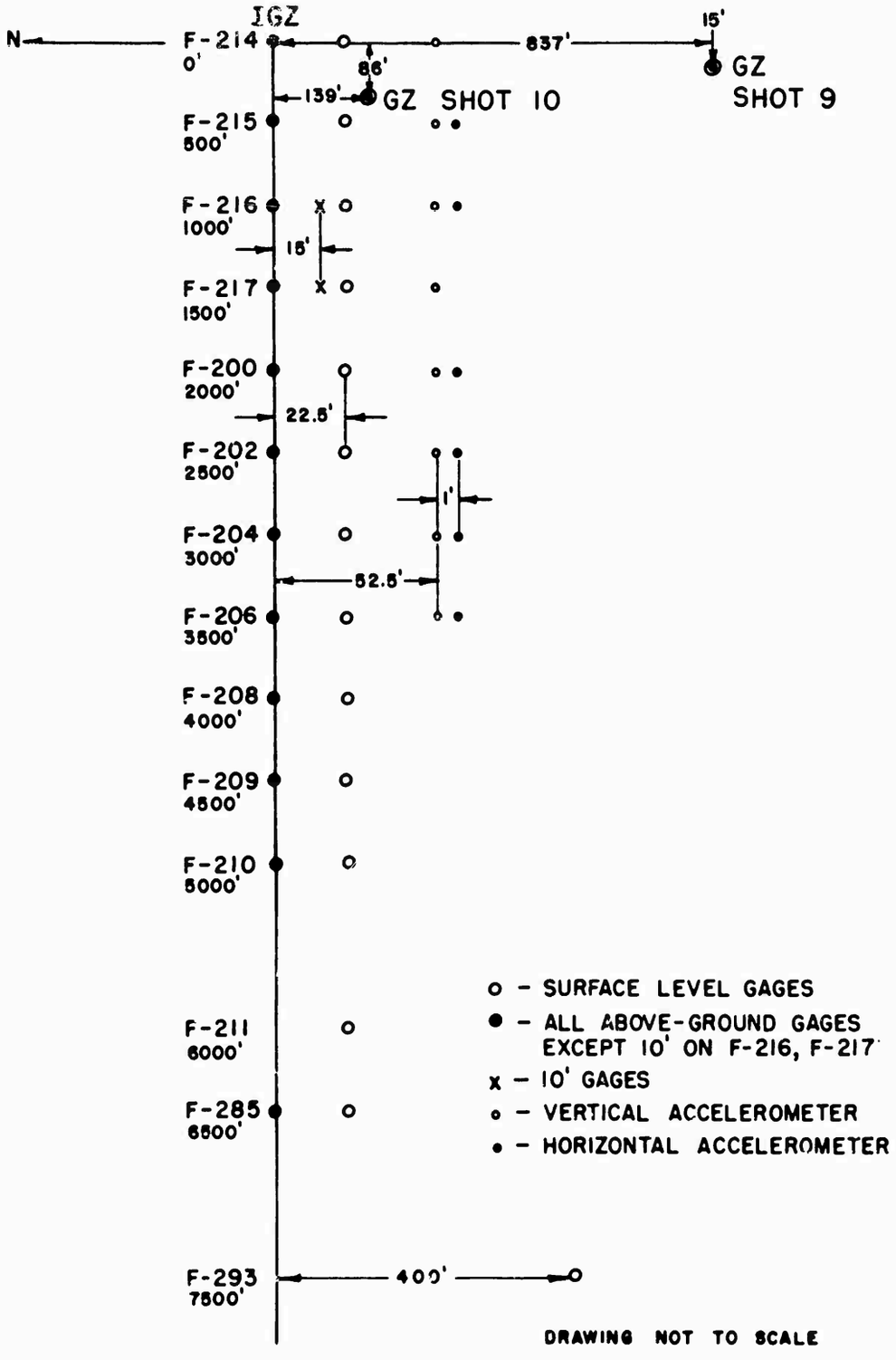

Fig. 3.2 Gage Line Layout, Shots 9 and 10

desirability of obtaining close-in data outweighed this hazard.

On this shot, in order to obtain some data as to the symmetry of the blast wave and in order to offer more detailed information to Projects 3.7 and 3.8, four zero-level blast gages were installed in the vicinity of these project structures at a ground range of about 900 ft. In addition, some auxiliary experimental gages employing magnetic recording techniques were installed for both Shots 9 and 10. The locations of these special gages are shown in Fig. 3.3.

3.2.3 Shot 11

The gage layout in the T-7 area of Yucca Flat for Shot 11 is shown in Fig. 3.4. Shot 11 was added very late in the operation and the blast line used for this shot was that available from Shot 4, with minor modifications. In view of the extreme over-damage results obtained in the precursor region of Shot 10 and because incomplete dynamic pressure measurements were obtained in this region on Shot 10, a Pitot tube (q-gage) was added at Station 7-204 for Shot 11. To accomplish this, it was necessary to eliminate the two conventional air pressure gages at this station; however, one channel of the q-gage gives a record of the side-on pressure and this, coupled with the mechanical gages of Project 3.30 at this station, could be depended upon to give sufficient air pressure information at this station. The q-gage for this installation was borrowed from the Sandia Corporation. The location of Station 7-204 (3000 ft from originally planned ground zero) was chosen as representative of the critical over-damage region for the precursor wave assumed to be generated by Shot 11. The q-gage was mounted at a height of 5 ft above the ground surface and oriented to point toward the expected ground zero. It should be noted that before the detonation of this shot, ground zero was changed as indicated in Fig. 3.4; this change, coupled with the bombing error, increased the ground range of Station 7-204 to 3445 ft.

3.2.4 Gage Coding

For identification of channels and recorded traces with their proper gages, a systematic coding was adopted. Station numbers were assigned by the Test Director for each gage station. Typical numbers were F-204 and 7-286; F designated the Frenchman Flat site and 7 the T-7 area of Yucca Flat. For convenience, only the last pertinent numbers (4 and 86 respectively) of these station numbers were used as the first part of the gage code. The second part of the gage code was a letter indicating the nature of the measurement. In this project, "B" for air blast, "V" for vertical acceleration, and "H" for horizontal acceleration were used. The third part of the code indicated the height of a gage above the surface or its depth below the surface, in feet. Typical gage code numbers then would be:

4B, a blast gage at Station 204, zero level;
86B10, a blast gage at Station 286, 10 ft height;
0V1, an accelerometer measuring vertical acceleration at Station 200, 1 ft depth.

On Shot 10, secondary dual gages were installed at some stations; these received the suffix "A," for example, 16B50A.

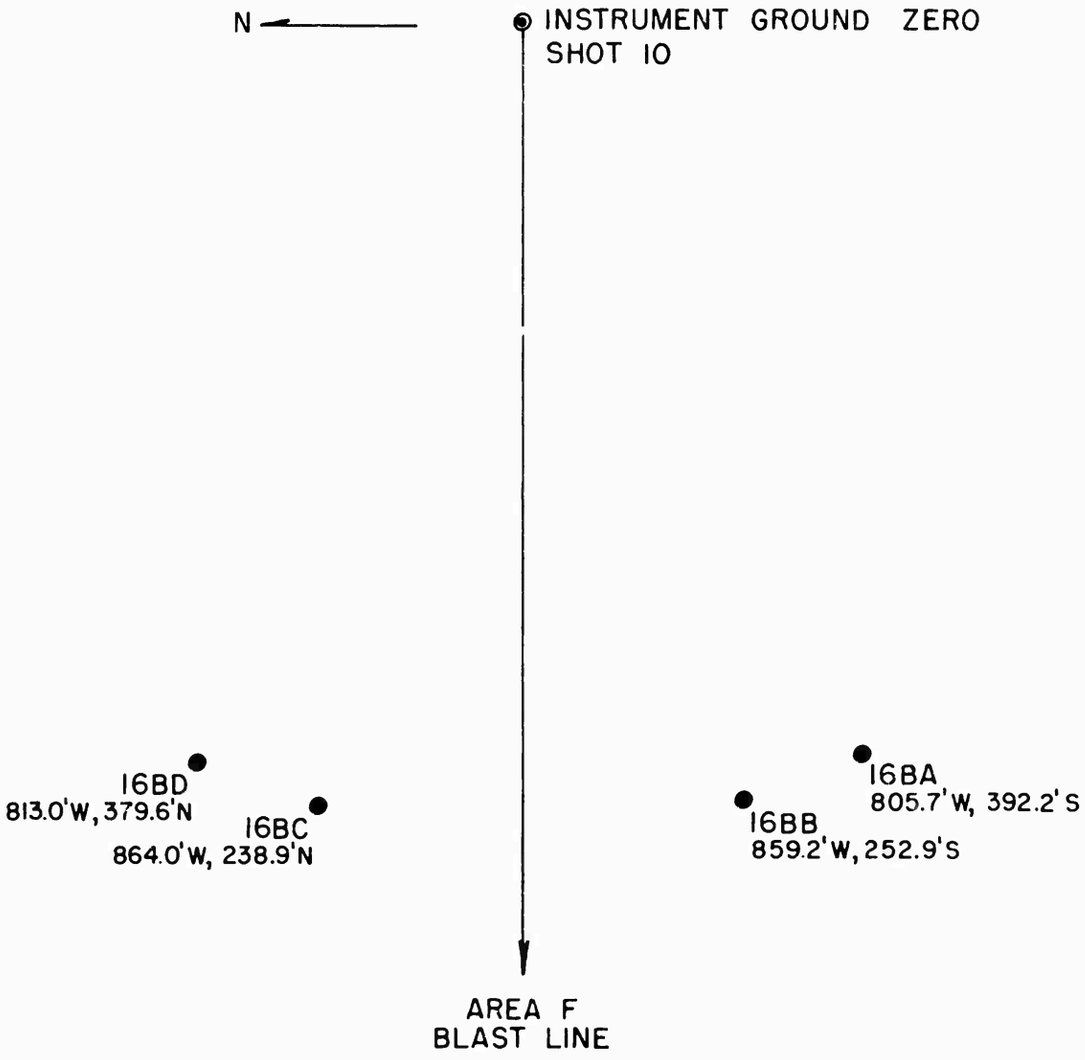

Fig. 3.3 Additional Gages (16BA, BB, BC, BD, Shot 10)

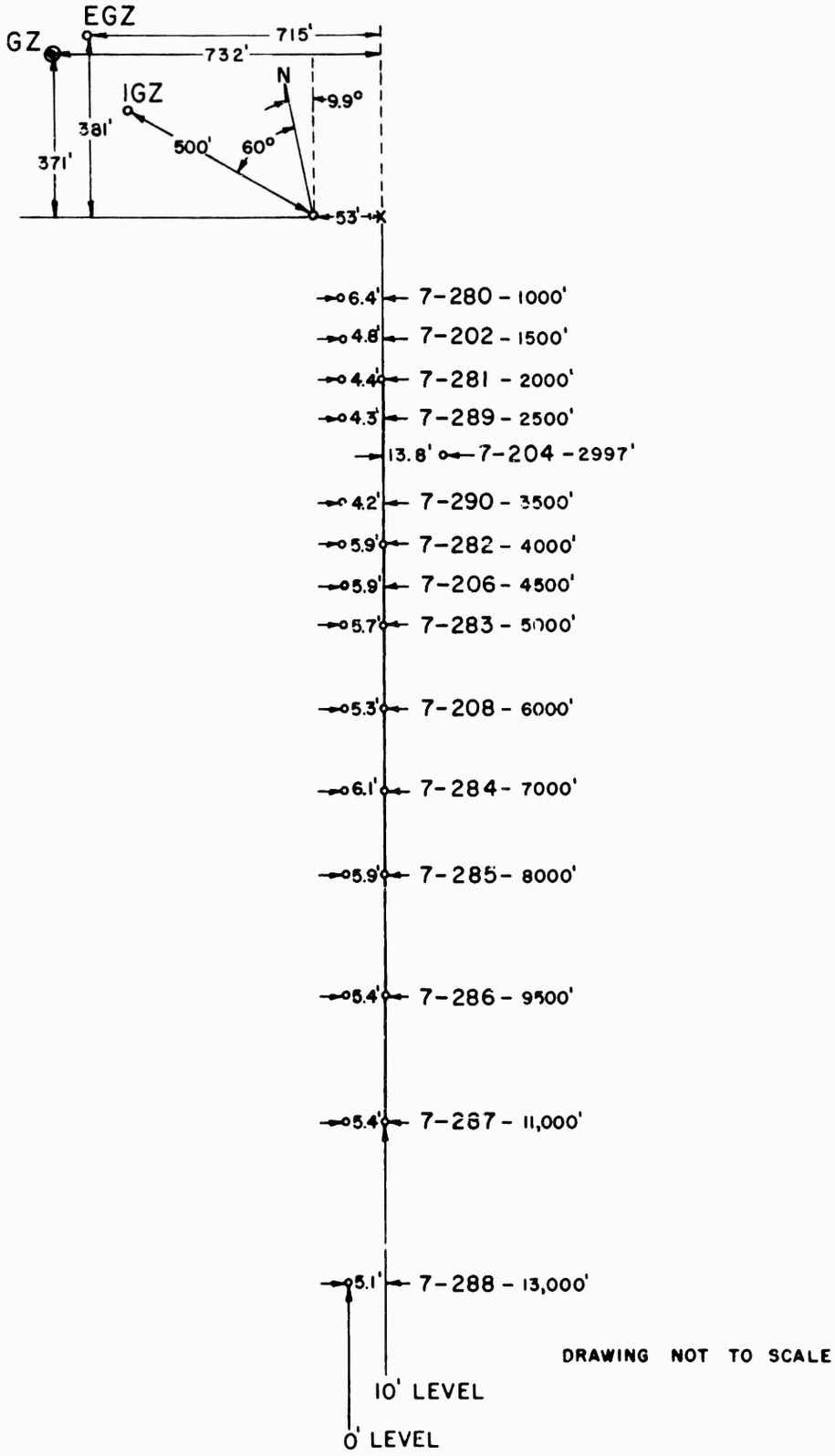

Fig. 3.4 Gage Line Layout, Shot 11

CHAPTER 4

RESULTS

4.1 INSTRUMENT PERFORMANCE

During the five shots, 175 air blast gage channels were connected which gave a total of 239 gage records. On 64 channels the electrical output was fed to two recording galvanometers in different oscillograph cameras, for the purpose of making partial compensation in case of recorder failure. Table 3.2, in addition to presenting a summary of the distribution of gages, lists the number of satisfactory gage records obtained on each shot. For Shots 3, 4, and 11, satisfactory records were obtained from all channels connected. On Shot 9, two of the air pressure gage channels failed to produce records, one because of a late cable failure and the other because of gage damage, possibly from the induction signal. On Shot 10 one of the four recording oscillograph cameras failed during the data recording period, breaking its paper at approximately H-2 sec. This resulted in the loss of records from 11 gage channels, 3 of which were acceleration measurements and 8 of which were air pressure measurements. Of the latter, however, one was a secondary gage mounted in a baffle adjacent to the primary gage for backup purposes. The resultant net loss consisted of records from 7 air pressure gages and 3 accelerometers. In addition, gage towers were destroyed at Stations F216, F217, and F200 on Shot 10, breaking their gage cables at times varying from 60 to 400 msec after the arrival of the shock wave. On some of these records all pertinent data had been recorded before the cable breaks occurred. Of the six auxiliary experimental gages on Shots 9 and 10, four gave usable records on each shot (Appendix B).

Because the yield from Shot 3 was considerably less than the estimates from which preshot predictions were made, the deflections on the records from this shot were in general quite low. This low yield detracted appreciably from the accuracy of the measurements but, with a few exceptions, quite satisfactory results were obtained. An outstanding deviation from the experimental plan was experienced in the location of ground zero for Shot 9. The true ground zero turned out to be over 800 ft south of the blast line (see Fig. 3.2), which ran east-west; this bombing error resulted in increasing the minimum ground range at which

measurements were taken and, more seriously, gave rise to a "true" blast line which differed significantly from the instrument blast line. This latter effect resulted in orientation angles at the aboveground gage baffles of from 20 to 12 degrees, instead of the desired 5 degrees (plus or minus 5 degrees) orientation. For completeness it should be noted that on Shot 11, although one gage cable broke at approximately 200 msec after blast arrival, the record from this 10 ft high gage was sufficiently long so that most of the pertinent data were obtained. The records from the Pitot tube q-gage on this shot were excellent.

4.2 PRESENTATION AND REDUCTION OF DATA

The primary data are the gage records. Reductions (about 5 to 1) of tracings of all usable records form Appendix A of this report. The portion shown includes all features displaying significant departures from normal behavior. If the whole positive phase had been portrayed, the necessary reduction would have resulted in excessive loss of resolution of phenomena occurring at the outset of the blast. Samples of these tracings are reproduced in this chapter to illustrate the variety of wave forms obtained. In addition, idealizations of the various types of wave forms are used to indicate which quantities have been tabulated.

In most air shock waves it is possible to observe certain features for which the time-space history may be traced more or less continuously over the entire air blast phenomena. These comprise various times and pressures as, for example, duration of the positive phase and peak pressure. These as-read values appear in the tables of this chapter. In order to compare the phenomena on a common basis, most of these as-read data have been normalized to 1 KT radiochemical yield at sea level and tabulated along with the as-read data. The term "A-scaled" has been adopted as shorthand for "reduced to a radiochemical yield of 1 KT with the gage at sea level conditions." The A-scaling factors applicable to these tests are given in Chapter 5 (Table 5.1).

4.2.1 Effective Ground Zero

The first efforts to plot a time-distance curve of first arrivals against slant range for Shot 4 resulted in curves which were slightly anomalous. This difficulty was resolved when it was recognized that the blast line is not level in the T-7 area of Yucca Flat, where this shot was detonated. The slope of the terrain is such that the most remote gage was some 120 ft lower than ground zero. For purposes of calculating true ranges it was found convenient to determine the location of a point designated on Figs. 3.1 and 3.4 as EGZ (effective ground zero). This point represents an intercept of a perpendicular drawn from the point of burst to the average terrain as shown in Fig. 4.1. Because complete survey data were not available, the data for computing this point were obtained from the AMS Series V 796 topographical maps. A schematic drawing of the pertinent section of the map used is shown in the figure, where the line "A" describes the average terrain most accurately. It should be clearly understood that this change in the point used as ground zero does not indicate that the data furnished as to the location of ground zero are incorrect, but only that a modification is

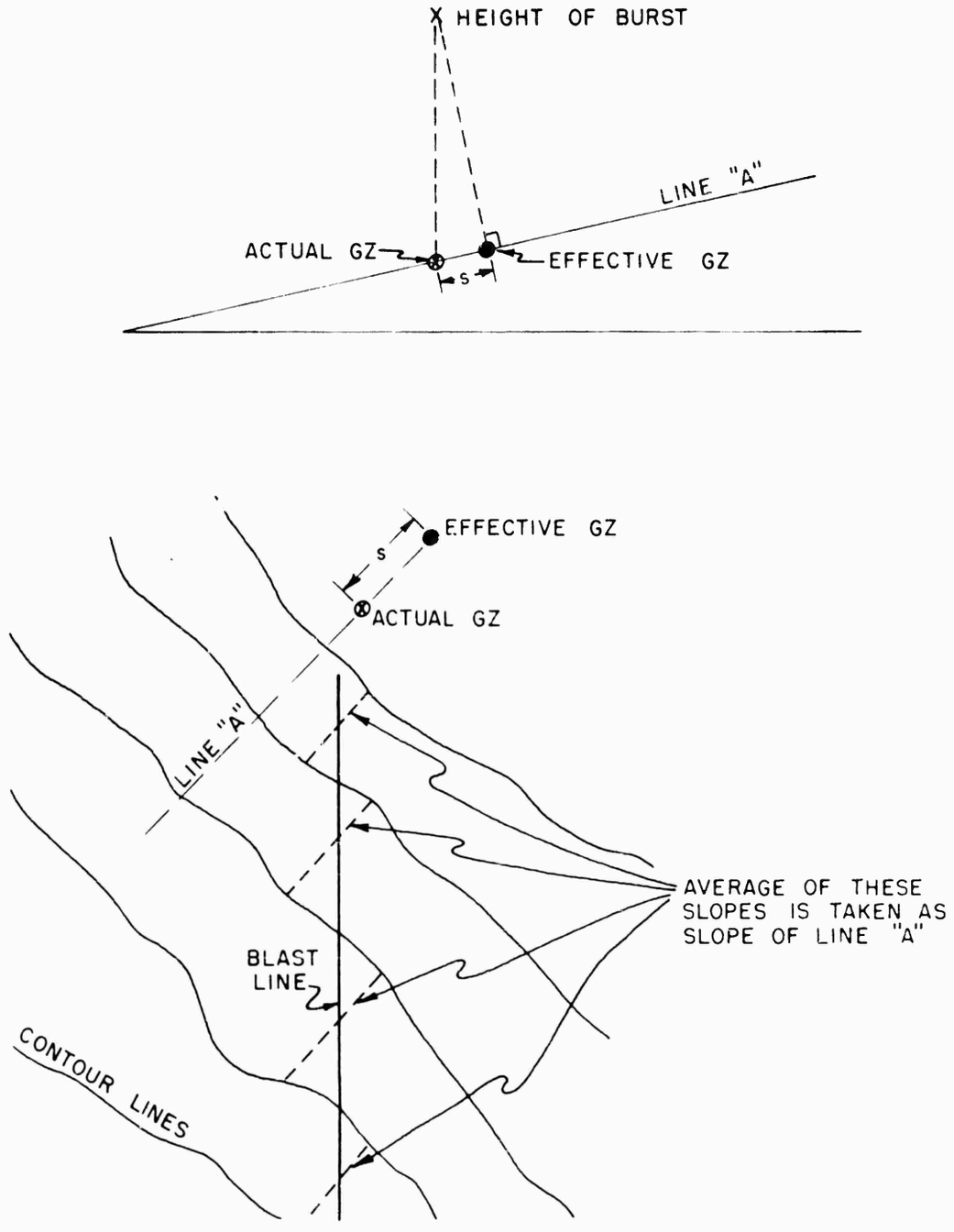

Fig. 4.1 Effective Ground Zero Diagram

necessary owing to the terrain slope. All calculations of ground range and slant range for Shot 4 are based on this effective ground zero. A similar effective ground zero was used in the case of Shot 11; however, since the height of burst was much lower than that of Shot 4, the correction was small.

4.2.2 Quantities Measured

Figures 4.2 and 4.3 illustrate some typical wave forms of pressure vs time labeled with the quantities that are read and recorded in tabular form in this chapter. In Fig. 4.2, examples of a sharp and rounded peaked pressure record are shown on the same sketch; in each case, a measure of the positive impulse (I_+) is the total shaded area defined by the pressure vs time positive pulse. Figure 4.4 shows an earth acceleration vs time record with the appropriate labels. This figure also illustrates the integration of the acceleration record to obtain maximum particle velocity associated with the air blast slap. For the purposes of this report only the maximum vertical and horizontal particle velocity associated with the air blast slap are recorded in tabular form.

4.3 WAVE FORMS

Figures 4.5 through 4.13 show some of the typical air blast wave forms obtained on Project 1.1b.

4.3.1 Shot 3

The records from Shot 3 (see Fig. 4.5) were typical of those to be expected in the Mach region. The only unusual characteristic noted was the building up of a secondary shock beginning at a ground range of about 3000 ft. This effect was perceptible at shorter radii as a rounded pulse with a slow rise time. At greater distances this shock persisted at essentially constant pressure.

4.3.2 Shot 4

The records from Shot 4 (see Fig. 4.6) were normal in every respect. All aboveground gages showed separate arrivals of incident and reflected pressures, indicating essentially regular reflection, with no evidence of a Mach stem. No secondary shocks were noted.

4.3.3 Shot 9

In general, the records from Shot 9 were normal, although a few peculiarities should be mentioned. In Fig. 4.7 it will be observed that the records of Gages 14B and 0B (the surface level gages at ground ranges of 820 and 2148 ft) show rise times of 3 to 4 msec, which are significantly longer than those recorded by other gages at similar ground ranges. Minor disturbances are notable immediately after the shock arrival on several gages.

Figure 4.8 shows typical aboveground gage records in the regular reflection region. The disturbances observed on the surface level gages

P_s = Shock pressure

P_m = Maximum pressure ($P_s = P_m$ for sharp-peaked shock record)

P_i = Incident pressure

P_{i2} = Final incident pressure

P_r = Reflected pressure

P_n = Maximum negative pressure

P_b = Pressure of secondary shock (blip)

t_s = Arrival time of shock wave

t_m = Time of maximum pressure

t_i = Arrival time of incident wave

t_r = Arrival time of reflected wave

t_x = Crossover time

t_{x2} = Second crossover time

t_n = Time of maximum negative pressure

t_b = Arrival time of secondary shock (blip)

Δt_s = Rise time to shock pressure

Δt_i = Rise time to incident pressure

Δt_r = Rise time to reflected pressure

Δt_{ir} = Duration of incident pressure

Δt_+ = Duration of positive phase

Δt_- = Duration of negative phase

I_+ = Positive phase impulse

I_- = Negative phase impulse

Labeled Quantities of Fig. 4.2

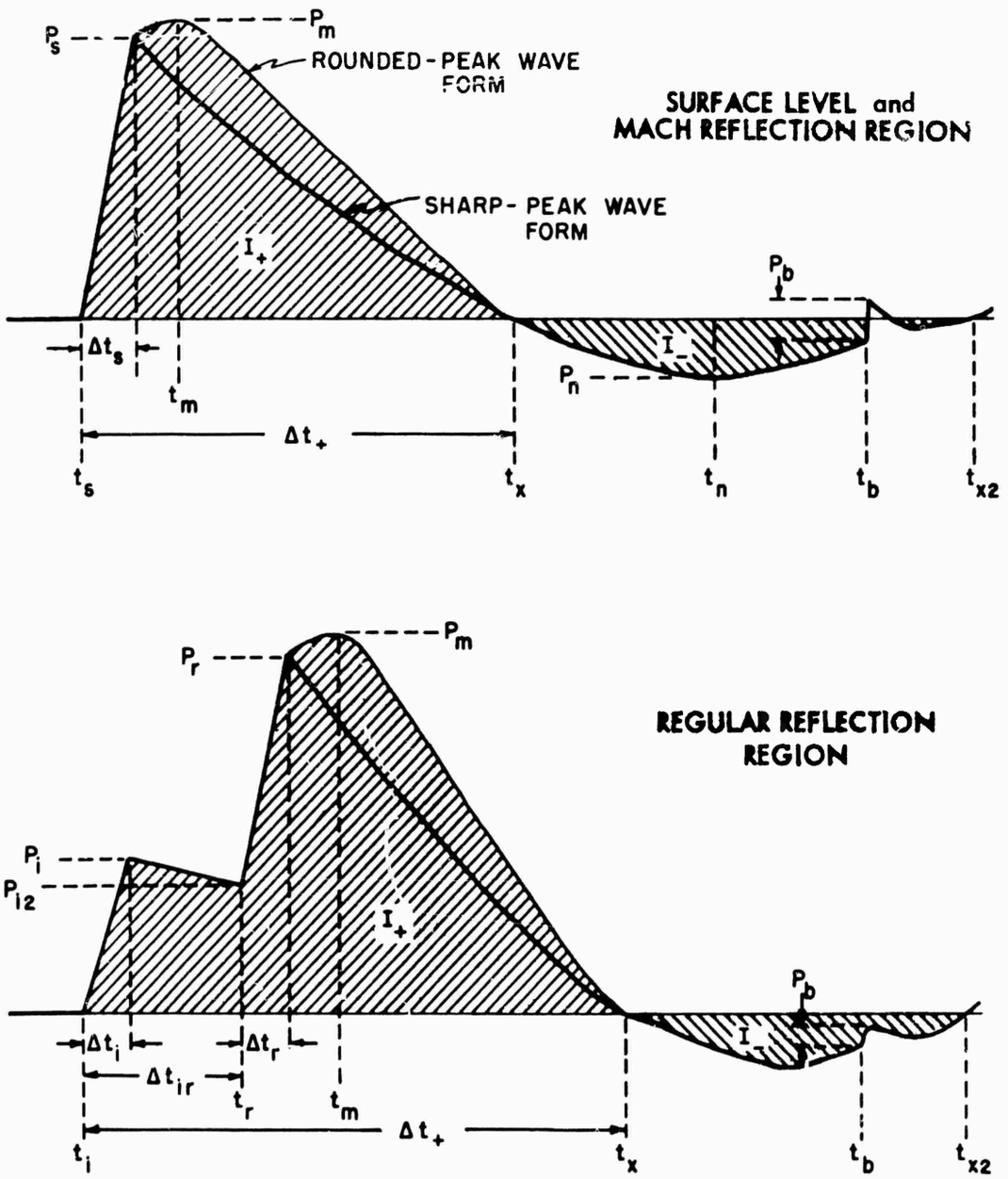

Fig. 4.2 Simplified Air Pressure Records, Surface Level and Aboveground
(See Facing Page for Labels)

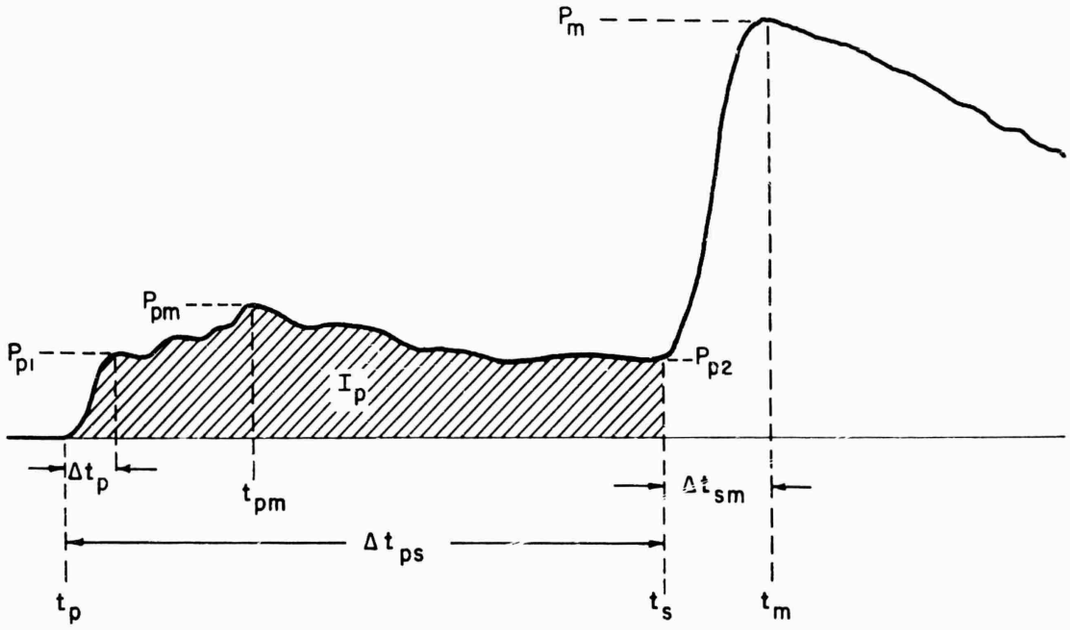

P_{p1} = Initial precursor pressure

P_{pm} = Maximum precursor pressure

P_{p2} = Final precursor pressure

P_m = Maximum pressure

t_p = Arrival time of precursor

t_{pm} = Time of maximum precursor pressure

t_s = Arrival time of main wave

t_m = Time of maximum pressure

Δt_p = Rise time to initial precursor pressure

Δt_{ps} = Duration of precursor

Δt_{sm} = Rise time to maximum pressure

I_p = Precursor impulse

Note: Positive impulse includes precursor impulse; positive phase duration includes precursor duration.

Fig. 4.3 Simplified Air Pressure Record, Precursor Region

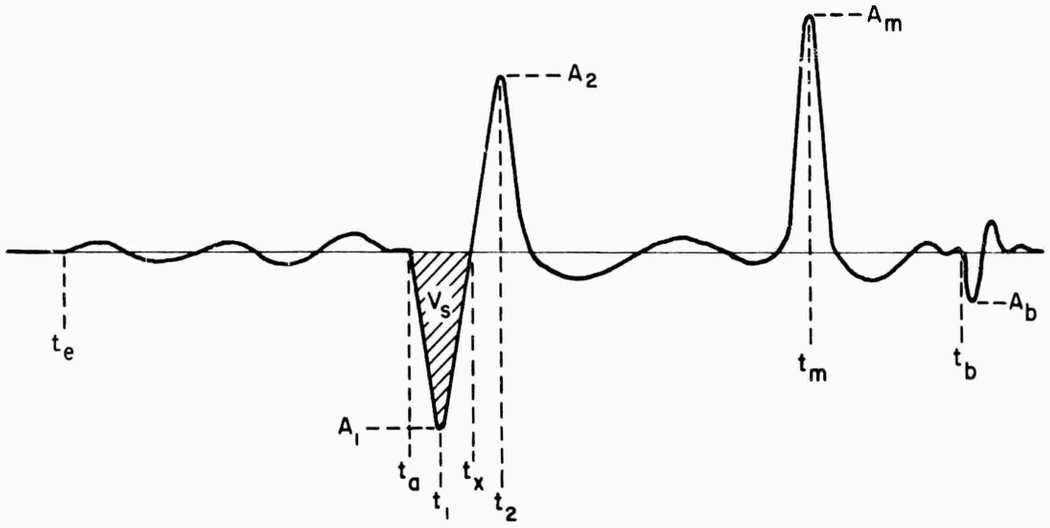

A_1 = First maximum acceleration

A_2 = Second maximum acceleration

A_m = Maximum acceleration (read only if greater than A_1 or A_2)

A_b = Acceleration of secondary shock (blip)

t_e = Arrival time of earth-transmitted wave

t_a = Arrival time of air blast slap

t_1 = Time of first maximum acceleration

t_x = Crossover time

t_2 = Time of second maximum acceleration

t_m = Time of maximum acceleration (read only if A_m is read)

t_b = Arrival time of secondary shock (blip)

V_s = Maximum slap velocity

Fig. 4.4 Simplified Earth Acceleration Record

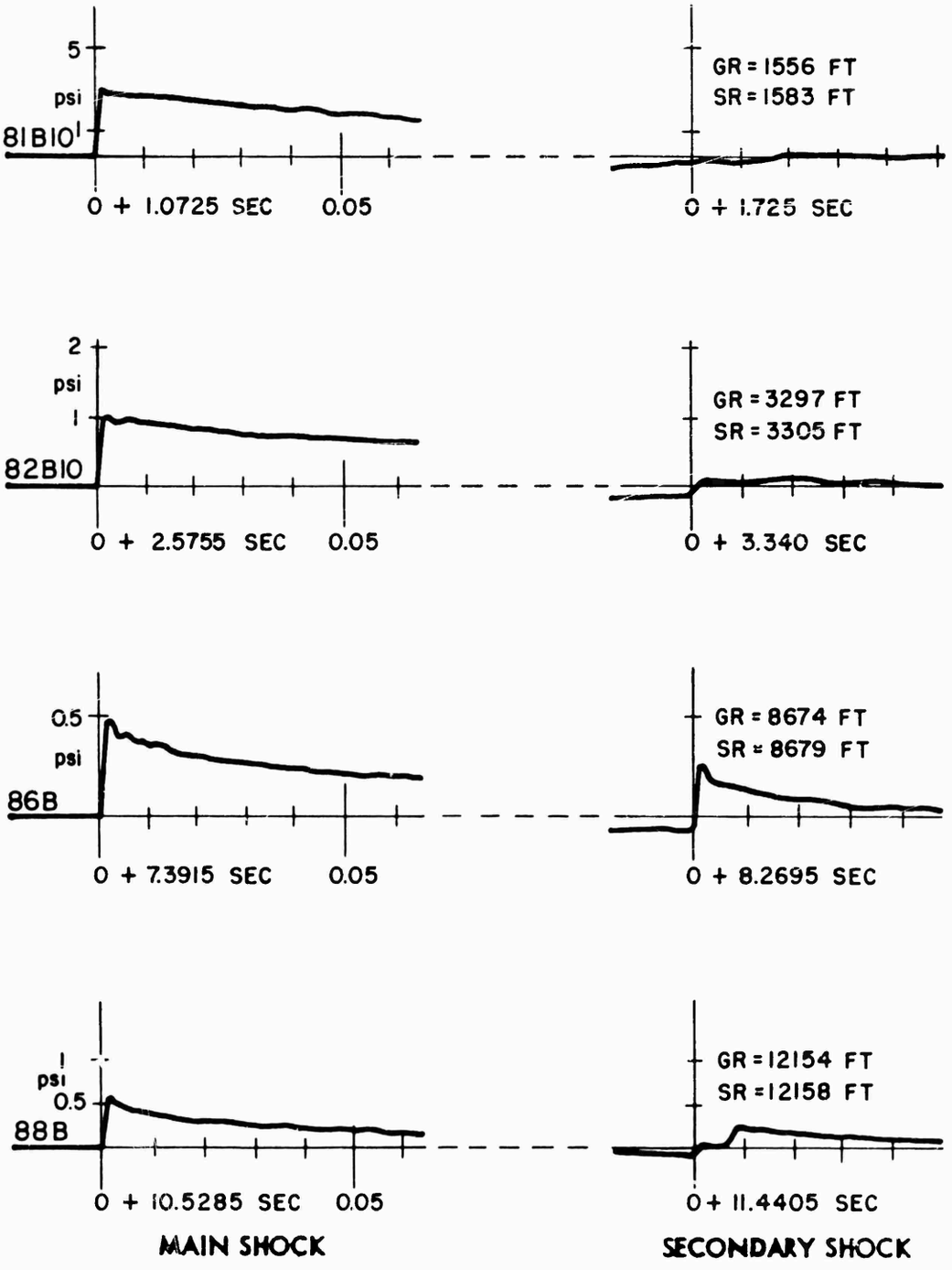

Fig. 4.5 Representative Air Pressure Gage Records, Shot 3
(Original Size)

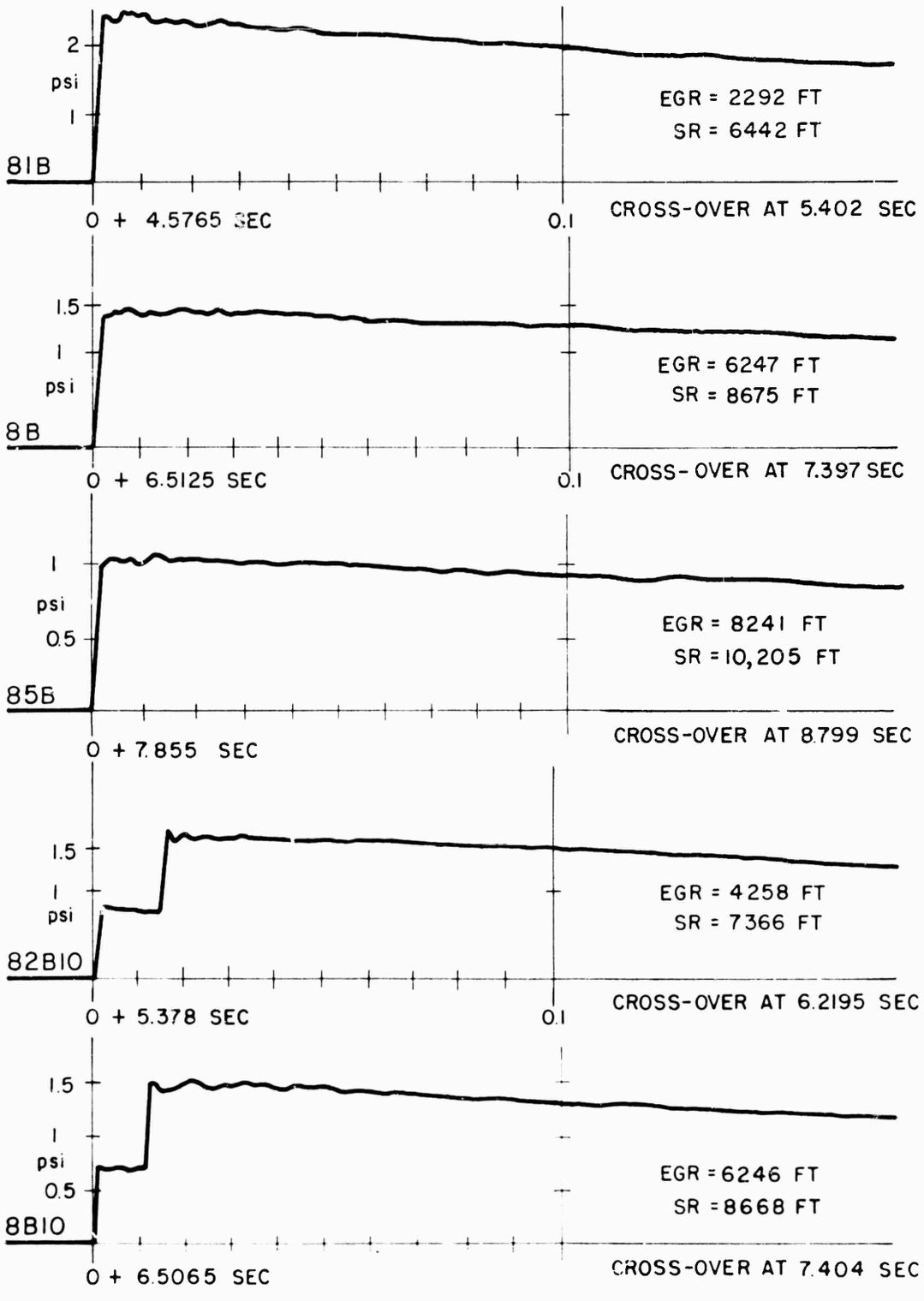

Fig. 4.6 Representative Air Pressure Gage Records, Shot 4
(Original Size)

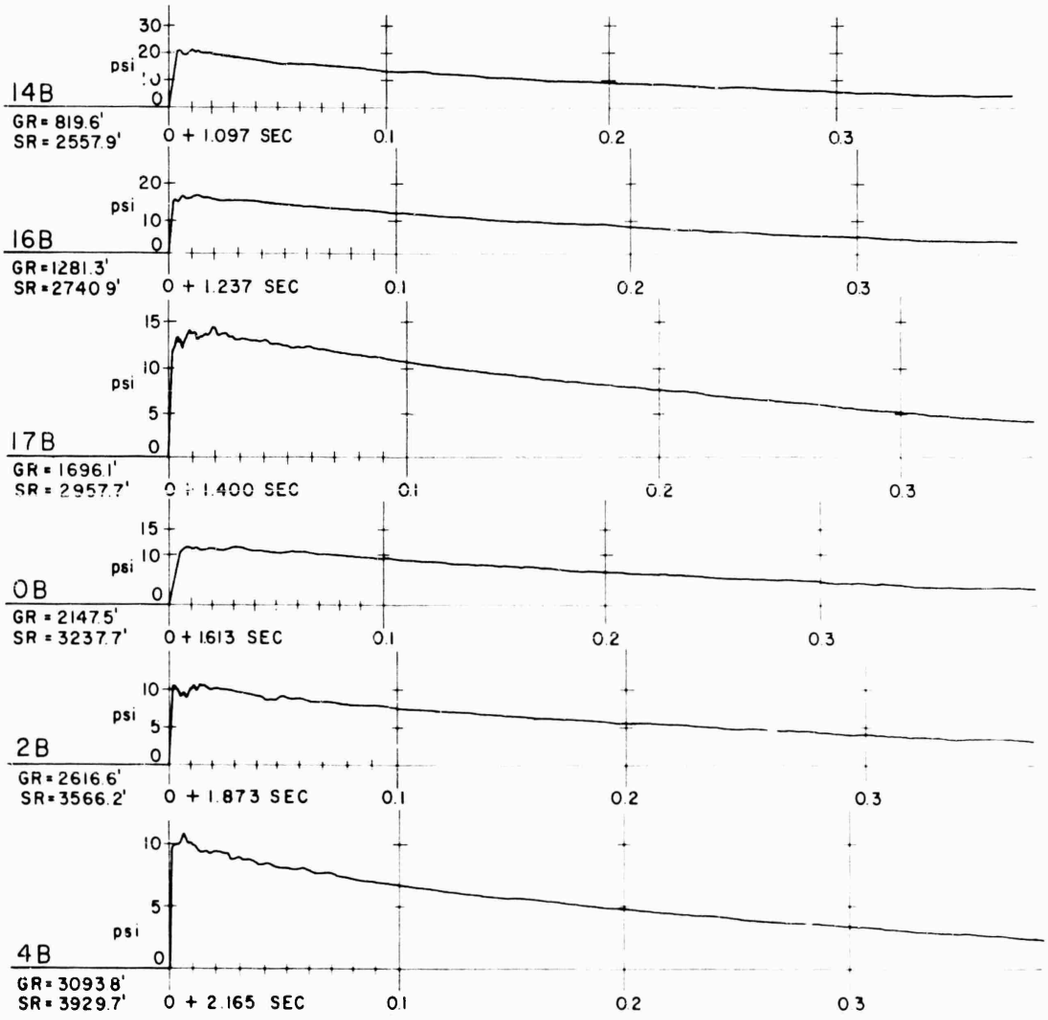

Fig. 4.7 Representative Air Pressure Gage Records, Shot 9, Surface Level

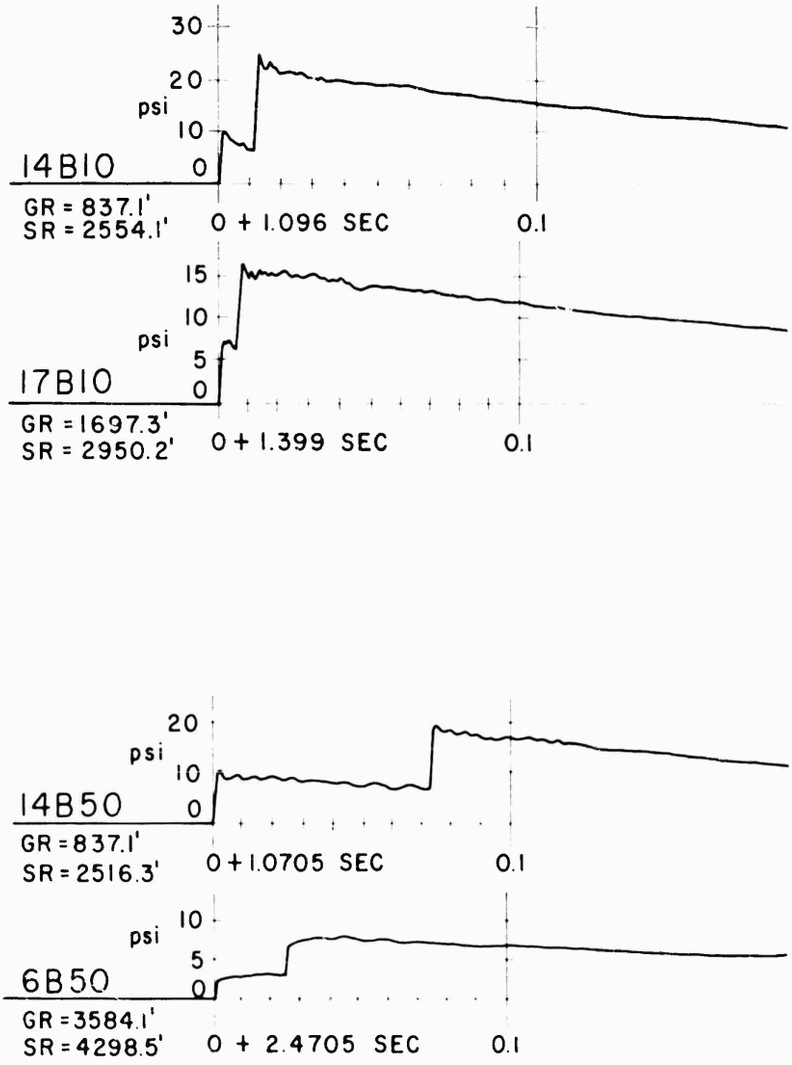

Fig. 4.8 Representative Air Pressure Gage Records, Shot 9, Aboveground Levels

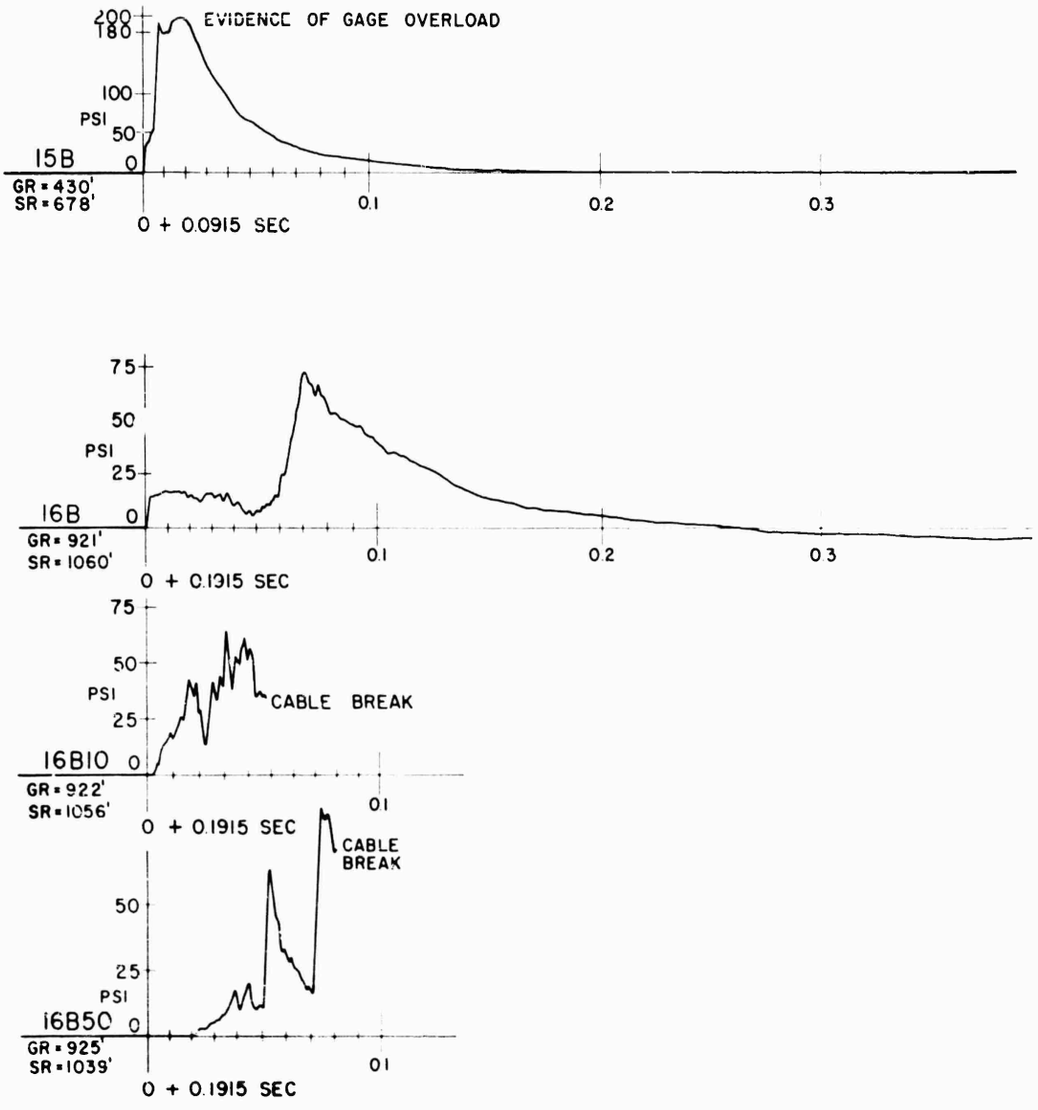

Fig. 4.9 Air Pressure Gage Records, Shot 10, Stations 215 and 216

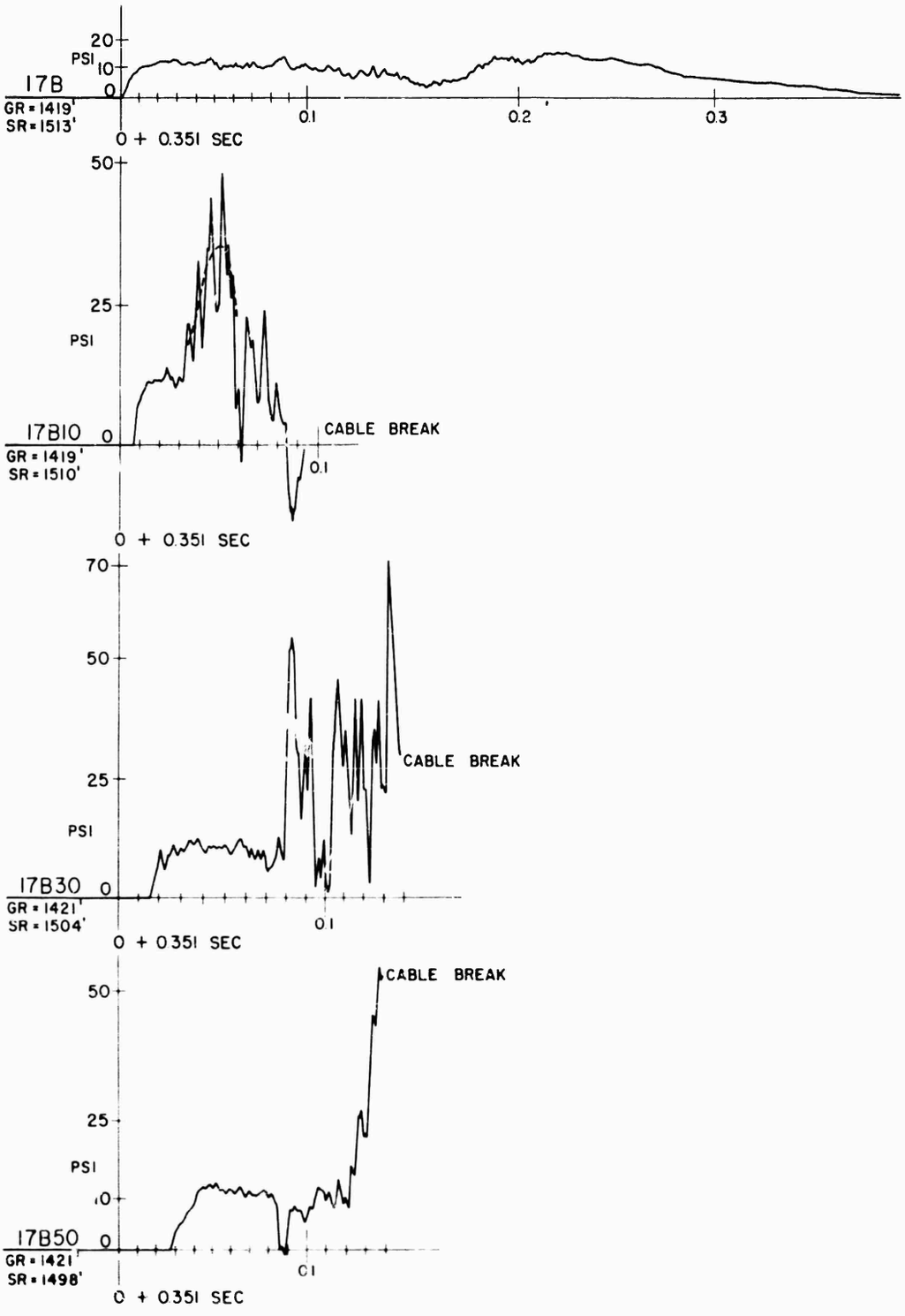

Fig. 4.10 Air Pressure Gage Records, Shot 10, Station 217

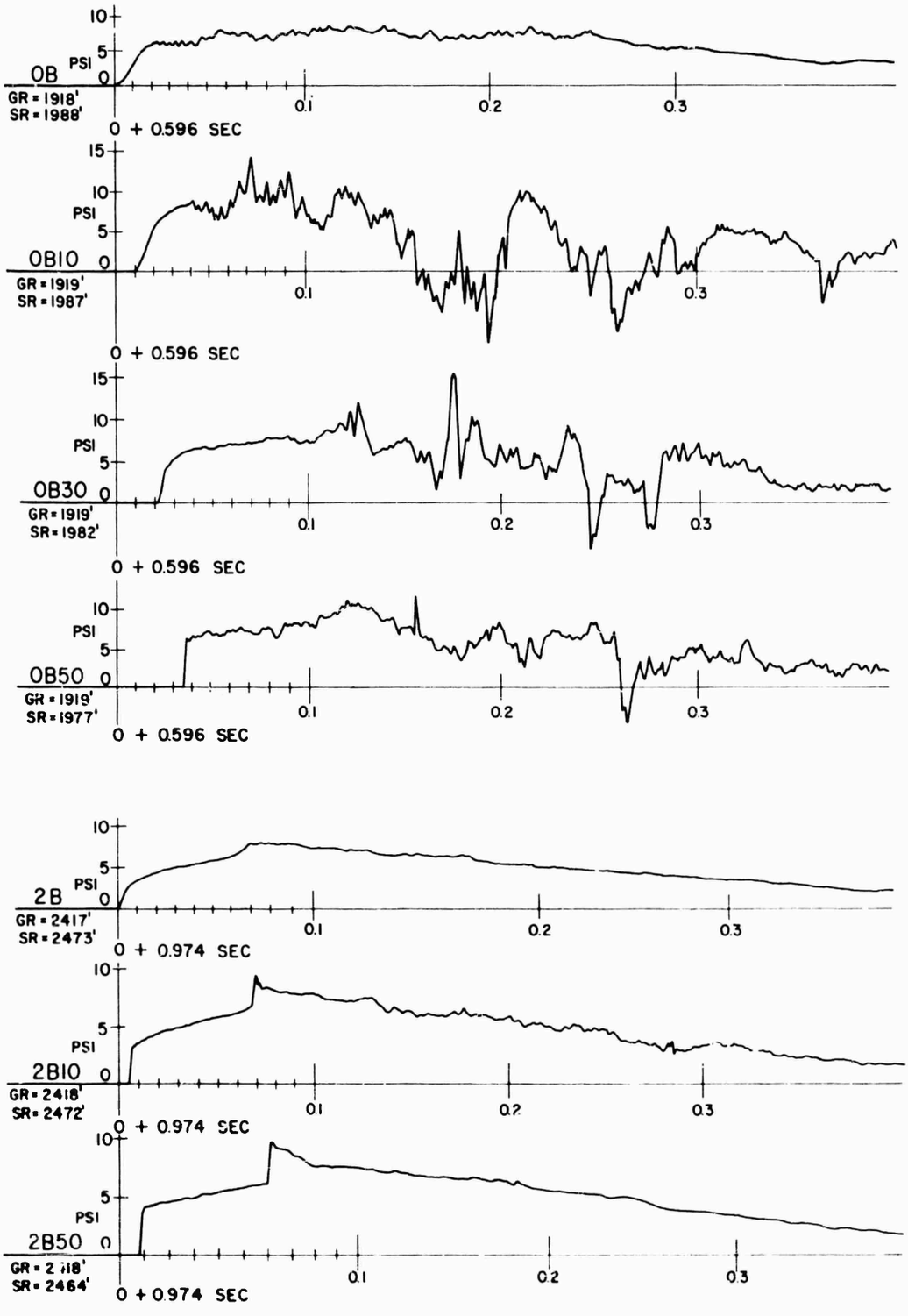

Fig. 4.11 Air Pressure Gage Records, Shot 10, Stations 200 and 202

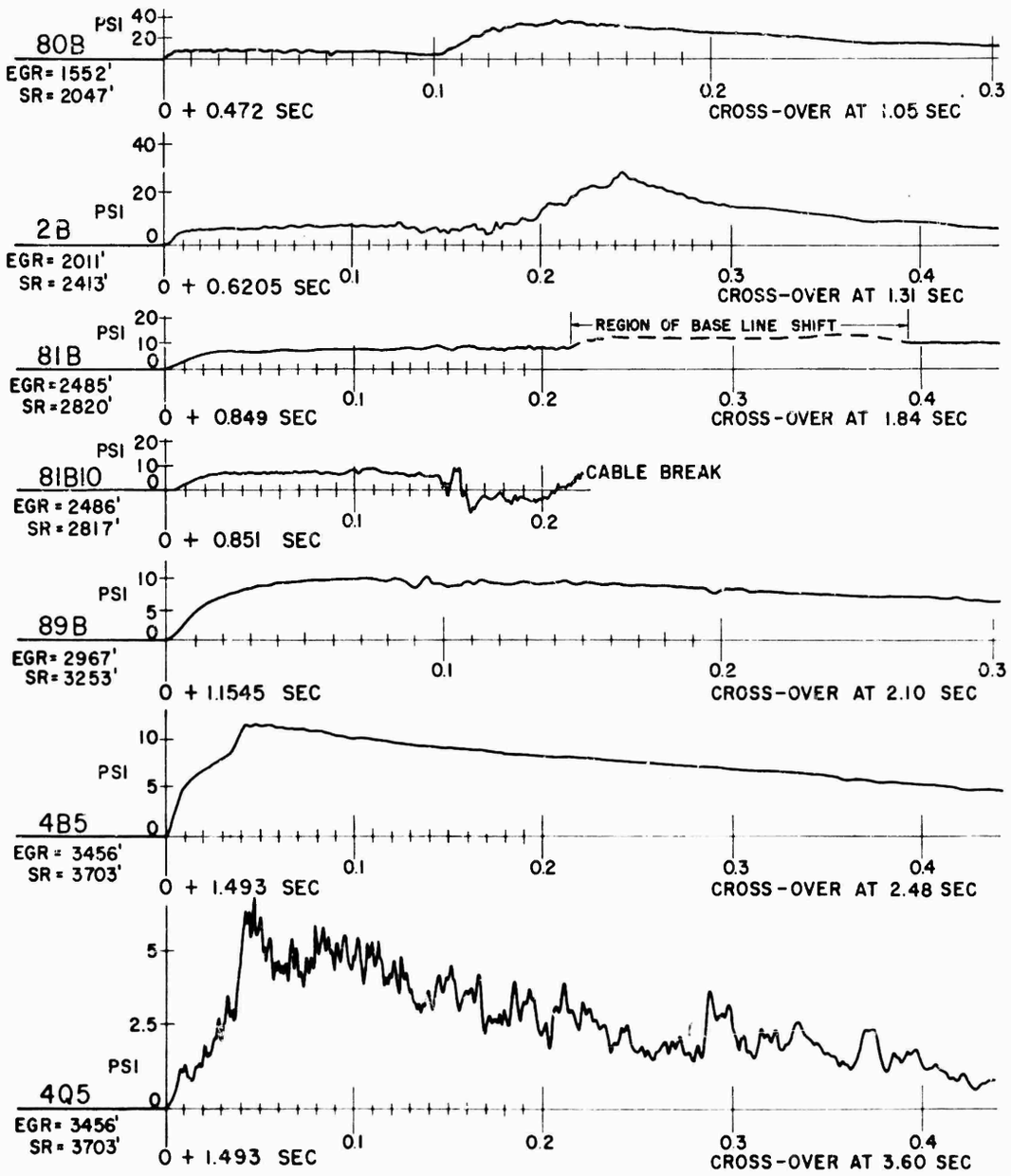

Fig. 4.12 Air Pressure Gage Records, Shot 11, Stations 280 through 204

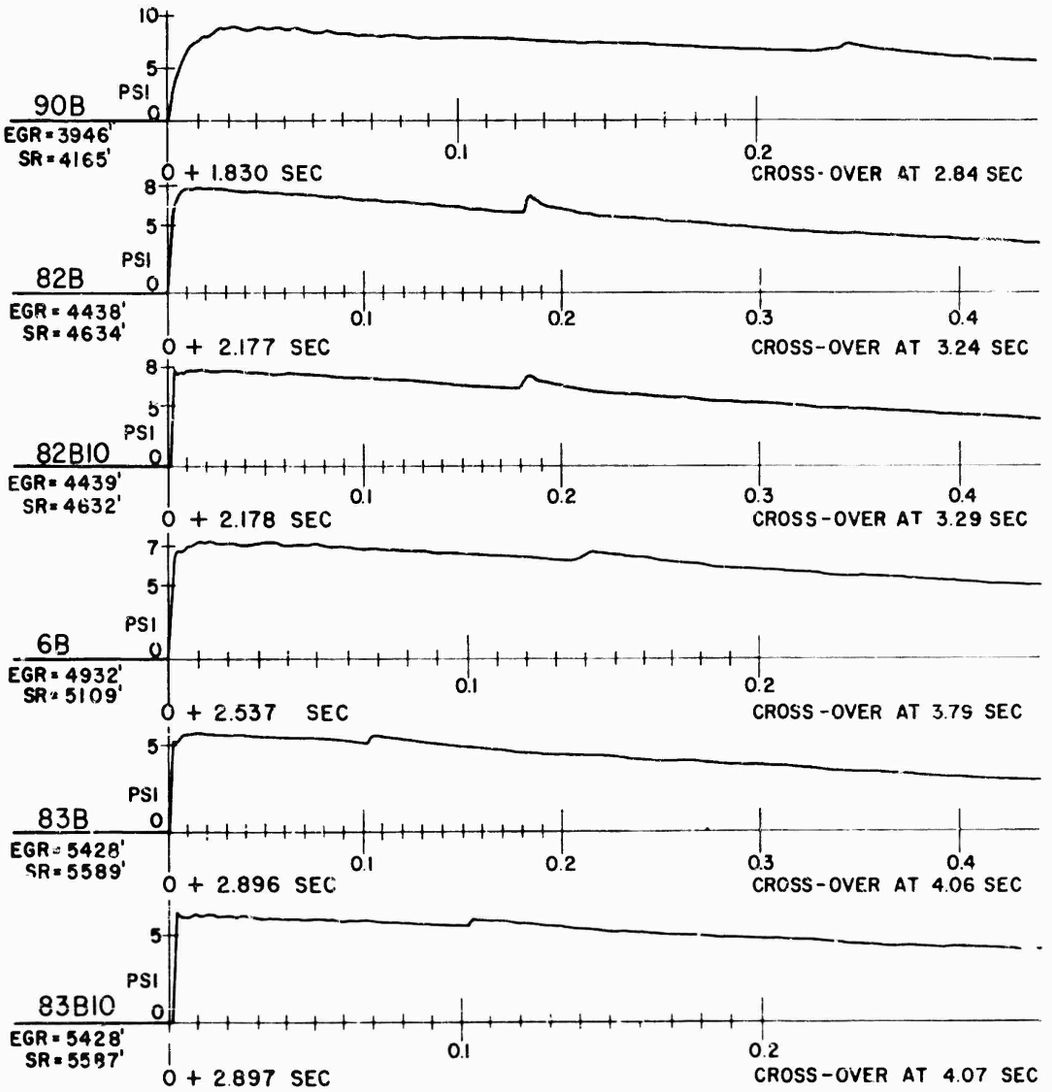

Fig. 4.13 Air Pressure Gage Records, Shot 11, Stations 290 through 283

are still present but less noticeable. At greater ground ranges, single arrivals were observed, indicating the formation of a Mach stem, with wave forms entirely similar to those observed from surface level gages.

4.3.4 Shot 10

The wave forms of the pressure-time records from UPSHOT-KNOTHOLE Shot 10 (14.9 KT at 524 ft burst height) are similar to those to be expected in view of the results of TUMBLER Shot 4 (19.6 KT at 1040 ft burst height). At all gage stations within 2500 ft of ground zero, the gage records show marked deviations from the classic shock wave. The significant portions of all primary records showing wave form distortion are reproduced in Figs. 4.9 through 4.11. A study of these records shows the development and subsequent decay of the precursor wave. The precursor pressure wave may be seen as a phenomenon separate from the main blast wave at Stations F216 and F202 (921 ft and 2417 ft ground range) and possibly at Station F215 (430 ft ground range).

The closest gage record, 15B (430 ft), as shown in Fig. 4.9 registers a short duration pressure rise to about 50 psi followed by a sharp increase in overpressure. The pressure then appears to remain essentially constant until another peak becomes evident. The rounded appearance of this later peak is probably due to gage overload (gage rating was 100 psi) and any estimation of the peak pressure would be highly speculative. As would be expected in this strong shock region, the 15B pressure record decays to zero overpressure quite rapidly and only a short negative pressure phase is observed.

At the next gage station, F216 (921 ft ground range), the surface level gage, 16B, shows a sharp rise to a broad jagged plateau, followed by a blast wave of essentially normal characteristics, except that the rise time does not indicate a true shock front. In the aboveground records at this location, 16B10 and 16B50, the later phases are lost owing to the destruction of the gage tower and subsequent cable breakage. The first pressure rise is less sharp and occurs later than at the surface level, and the plateau is much rougher. On 16B50 two subsequent sharp arrivals are noted, which appears to be compatible with the conventional incident and reflected arrivals, but the decay of pressure after the first of these arrivals is abnormally rapid.

Referring to Fig. 4.10, the records from Station F217 (1419 ft ground range) show the full development of the precursor. The surface level gage, 17B, shows a slow rise to a broad, rough plateau of very long duration with no marked pressure peaks. At aboveground gages at this station there is a similar slow first rise followed by a sustained violent oscillation which is later obscured by cable breakage. A tendency toward this oscillation effect was noticeable on the gages of Station F216 but it had not developed fully. It is particularly interesting to note that the onset of this oscillation is progressively later at higher elevations. Obviously it is impossible to discern any definite incident or reflected shock wave arrival at this station.

At Station F200 (1918 ft ground range) the record OB (see Fig. 4.11) retains the same characteristics as 17B, while the oscillation on the aboveground gages is reduced but still noticeable. At this station no cable breakage occurred, so the full pressure-time history

is available, but it is still impossible to perceive any late arrivals which could be attributed to the arrival of the main blast wave. At this station, a sharp initial rise is observed on the 50 ft gage, with slower rises on the surface and other gages. This is in contrast to the opposite tendency of station F216. The tendency for all correlatable events to occur later at the higher gages is still evident.

At Station F202 (2417 ft ground range), the later characteristics of the precursor effect are seen; the roughness and oscillation have disappeared and the sharp initial rise is observed on both aboveground gages. Following the initial rise the pressure increases gradually until the main blast wave arrives. This second arrival is most noticeable on the aboveground gages but is entirely perceptible at the surface level. The tendency for progressively later arrivals at the aboveground gages is still present but less pronounced. This is indicative that at this station the precursor front is becoming more nearly vertical, possibly due to the toe slowing up. The precursor apparently disappeared entirely before the next station (F204, 2916 ft ground range) was reached. Here the records were conventional, as they were at subsequent stations.

4.3.5 Shot 11

The tracings of the important oscillograph records obtained on Shot 11 are presented in Figs. 4.12 and 4.13. Figure 4.12 shows typical records from the precursor region and their resemblance to the records from Shot 10 is evident. Few aboveground gages were installed in this region for this shot, but 81B10 (ground range 2471 ft) shows some of the characteristics observed on aboveground gages in Fig. 4.11. On none of these records can a sharp blast wave arrival be observed, but on a few records the arrival of the main blast wave can be detected with some degree of certainty. In the 80B record (surface level at Station 7-280, 1529 ft ground range) the precursor pressure shows signs of decaying before the arrival of the main shock. For this reason it is not difficult to identify the arrival of the main shock; however, this identification becomes more vague as subsequent gage records are studied. At Station 7-204, (3445 ft ground range), the main shock arrival is observable on the record from Gage 4B5. The resemblance of this record to that from Gage 2B on Shot 10 is noticeable. Referring to Fig. 4.13, gage record 70B (3936 ft ground range) still shows strong evidence of a thermal effect, manifested by the slow rise time. This effect is still perceptible at the surface level gage of Station 7-282 (4430 ft ground range) but is not evident at the 10 ft gage, 82B10, or at subsequent gages at greater ground ranges.

The 4B5 and 4Q5 records of Shot 11 shown in Fig. 4.12 are from the Pitot tube gages. The 4B5 trace is a record of the conventional side-on static pressure at the gage station, while the 4Q5 record gives the drag pressure behind the shock wave. The record of this differential gage, 4Q5, exhibits a ringing effect which is not readily explained. However, these gages displayed similar effects when used on other shots by the Sandia Corporation (Project 1.1d).[15] Except for this ringing effect, the general wave form of this record is qualitatively similar to that obtained from Gage 4B5.

4.3.6 Earth Acceleration

Some record tracings of acceleration vs time from Shots 9 and 10 are shown in Figs. 4.14 and 4.15 respectively. The tracings are arranged so that the records of horizontal acceleration (indicated by the letter H in the code number) appear above those of vertical acceleration. According to the convention observed, an upward deflection indicates a positive acceleration, defined as a horizontal acceleration away from ground zero, or a vertical acceleration upward. The markers labeled t_p and t_s are used to indicate the time of arrival of the precursor air pressure wave and the main shock wave, respectively, at each gage station. Where the prior arrival of an earth-transmitted wave, t_e, is observable on the original record, this arrival time is noted on the tracings, but no effort was made to show these early arrivals, since they were not usually of sufficient amplitude to be meaningfully reproduced.

In Fig. 4.14, the Shot 9 horizontal acceleration record from the 16H5 gage (range 1260 ft, buried 5 ft deep) exhibits a slap-type wave form. The actual acceleration onset occurs about 4 or 5 msec after the air blast arrival, which would correspond to a velocity through the earth of about 1000 fps. This velocity is not unreasonable and is in the same range as that observed for the TUMBLER acceleration measurements.[10] From the gage record at the next station (2134 ft), it is obvious that the earth disturbance is experienced by the gage before the arrival of the blast wave slap. This indicates that the earth-transmitted wave has already outrun the air-transmitted wave at this radius as explained in Section 1.3.3. The vertical acceleration records shown in Fig. 4.14 exhibit much larger and sharper peaks associated with the air blast slap than do those of the horizontal acceleration.

Looking at Fig. 4.15 and the Shot 10 horizontal earth acceleration tracings, it becomes obvious that the precursor has a decided effect upon the wave forms. At Station F216 (16H5), the precursor gives rise to a measurable horizontal acceleration which arrives at the gage at a time (about 6 msec after t_p) corresponding to a near-surface earth velocity of about 1000 fps. The 0H5 record at Station F200 (1916 ft ground range) exhibits an outrunning characteristic similar to that observed on Shot 9. The vertical earth accelerations from Shot 10 as shown in Fig. 4.15, similar to the Shot 9 case, exhibit higher and sharper slap acceleration peaks than do the horizontal records. In the precursor region, the earth acceleration disturbances begin when the precursor wave arrives at the gage station and the rise time is much longer than that associated with a conventional shock wave.

4.4 TABLES

The primary as-read air pressure data for the surface and above-ground levels for all five shots are contained in Tables 4.1 through 4.22, which list the station, gage designation, ground range, slant range, positive pressure at the end of the shock rise, maximum positive pressure, maximum negative pressure, time of arrival of incident and reflected shocks, positive and negative phase duration, positive and negative impulse, initial and final incident pressure, reflected pressure,

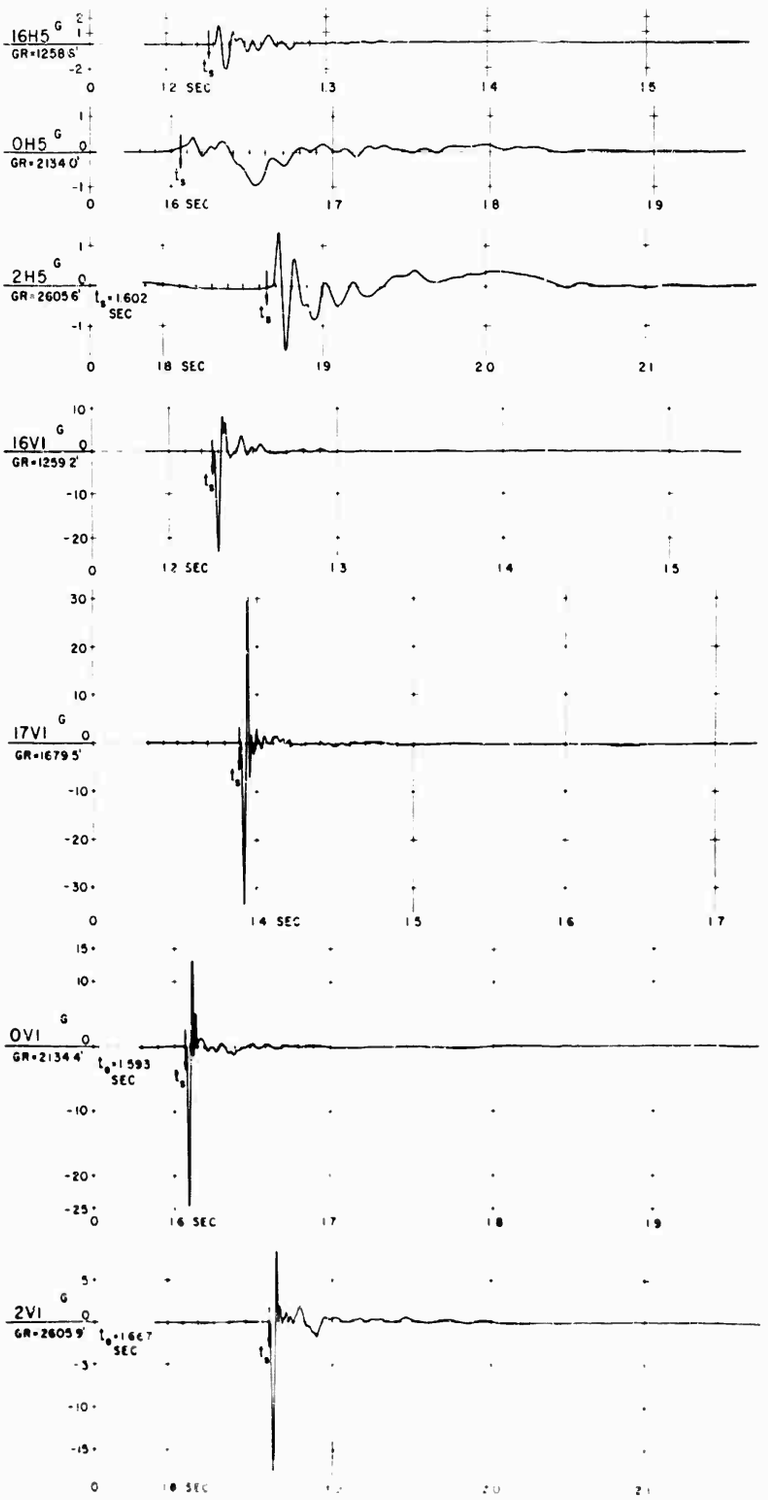

Fig. 4.14 Representative Earth Acceleration Gage Records, Shot 9

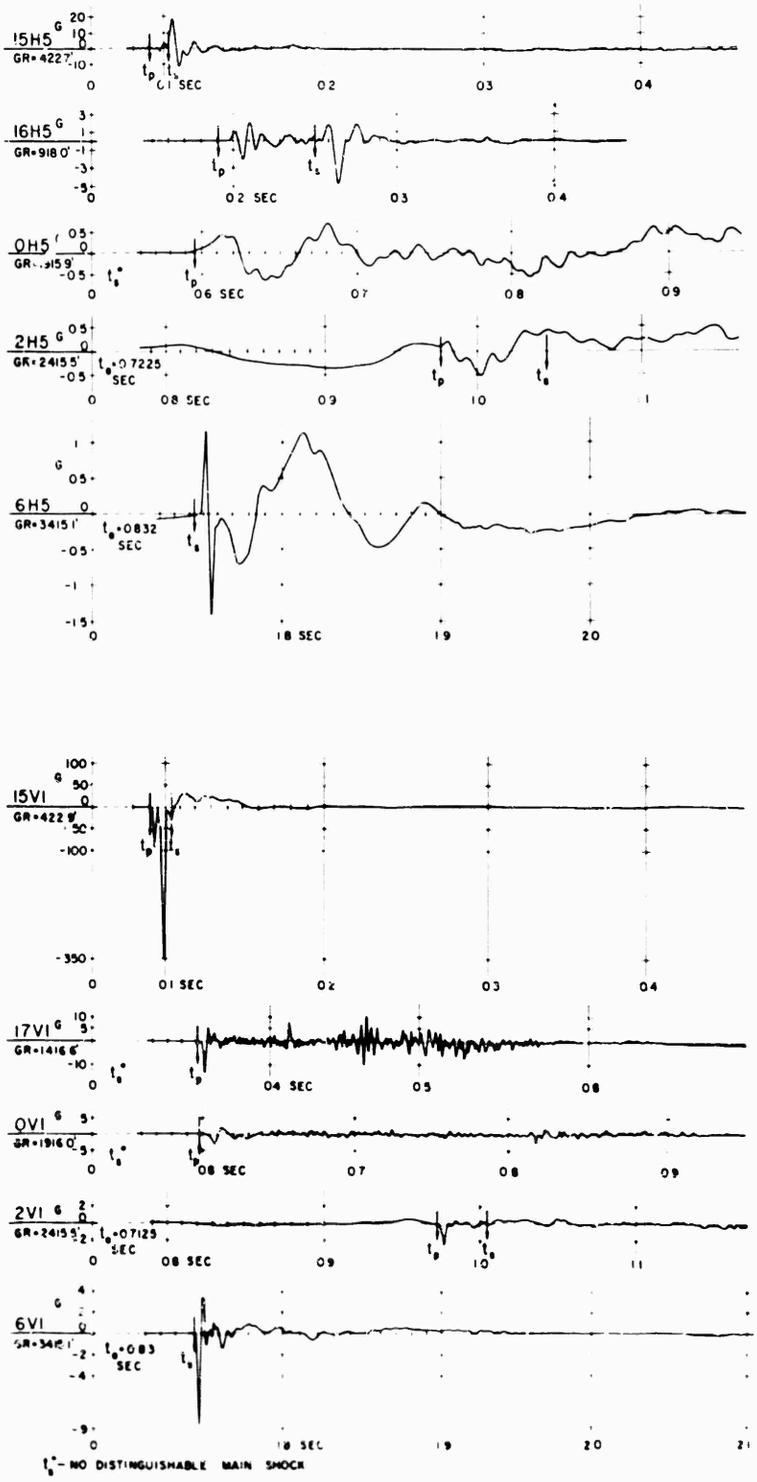

Fig. 4.15 Earth Acceleration Gage Records, Shot 10

and precursor pressure. In addition, these data are A-scaled and are presented in tables of normalized values. It should be noted that because of the pressure "blips" occurring in the negative phase on Shots 3, 10, and 11, it was not possible to determine correctly the duration of the negative phase or the negative impulse. For this reason, these quantities are omitted from the tables for these shots. In the case of Shot 9, although a "blip" was present, it was possible to estimate with reasonable accuracy the duration and impulse associated with the negative phase. Tables 4.23 and 4.24 present the earth acceleration and particle velocity data derived therefrom.

In the use of all tables, the reader may refer to Table 3.1 for pertinent data regarding shot conditions, Table 5.1 for scaling factors, and to Figs. 4.2, 4.3, and 4.4 for the meaning of certain notations. In addition, Figs. 3.1 through 3.4 are useful for the visualization of individual station locations and other data for each shot.

These tables constitute the bulk of the data presentation for this project. In many cases, data are included which are not discussed in this report, but which may be pertinent to further study by the reader. All graphs and presentations in this report are constructed from or derived from these tables.

4.5 GRAPHS OF PRIMARY AS-READ DATA

The primary as-read data are presented in graphical form in Figs. 4.16 through 4.47. These graphs include time of arrival, pressure, positive phase duration, and impulse, plotted principally as functions of ground range. This section of the report will deal with the as-read results in an effort to demonstrate how the various air blast phenomena varied from shot to shot in this test. A detailed discussion of the more important aspects of the test and comparisons with other tests will be based upon the A-scaled curves presented in Chapter 5.

4.5.1 Times of Arrival

Graphs of times of arrival for Shots 9, 10, and 11 are shown in Figs. 4.16 through 4.18. (The arrival time data for Shots 3 and 4 appear to have no significance and are not shown in graphical form.)

The graph for time of arrival vs ground range for Shot 9 is shown in Fig. 4.16, based on arrival times at ground level gages. This curve is included primarily because of its possible usefulness to elements of Programs 3, 8, and 9, and is plotted against ground range mainly for this reason. It should be noted, however, that the majority of these data are from gages located in the Mach reflection region, where reference to slant range would be meaningless. Figure 4.17 shows the arrival time curve for Shot 10, with an enlargement of the early portion of this curve for clarity. Although the exact shape of the main shock arrival curve in the early region is questionable, the advance arrival of the precursor is evident from this presentation.

Arrival time data for Shot 11 are shown in Fig. 4.18. Again the advance arrival of the precursor is evident, although the precise curve for the main shock arrival in the precursor region is even more indeterminate.

TABLE 4.1 - Air Pressure, Shot 3, Surface Level

Sta. No.	Gage Code No.	Grnd. Range (ft)	Slant Range (ft)	Pressure (psi)			Time (sec)					Duration (sec)		Impulse (psi-sec)
				P_a	P_n	P_b	t_s	t_a	t_x	t_n	t_b	Δt_s	Δt_-	I_+
As-Read														
200	0B	1410	1441	3.4	0.7	0.3 [a]	0.9445	0.946	1.1745	1.46	1.5655 [a]	0.0015	0.230	0.34
280	80B	1094	1134	4.4	1.1	0.7 [a]	0.694	0.6955	0.9145	1.17	1.292 [a,b]	0.0015	0.2205	0.34
281	81B	1553	1581	2.77	0.73	0.3 [a]	1.0695	1.0715	1.2985	1.60	1.71 [a]	0.002	0.229	0.24
204	4B	2370	2384	1.29	0.34	0.14 [a]	1.7665	1.7685	2.027	2.37	2.480 [a]	0.002	0.2605	0.19
282	82B	3291	3304	0.67	0.18	0.16	2.574	2.576	2.8615	3.19	3.339	0.002	0.2875	0.092
283	83B	4247	4258	0.80	0.22	0.30	3.424	3.4265	3.6995	4.06	4.2185	0.0025	0.2780	0.093
208	8B	5220	5229	0.73	0.19	0.32	4.2845	4.286	4.592	5.00	5.1045	0.0015	0.3075	0.078
284	84B	6201	6209	0.67	0.20	0.28	5.1695	5.1715	5.4725	5.88	6.009	0.002	0.303	0.067
285	85B	7188	7194	0.52	0.14	0.30	6.055	6.057	6.368	6.80	6.9105	0.002	0.331	0.053
286	86B	8674	8679	0.49	0.08	0.34	7.3915	7.3925	7.719	8.17	8.2695	0.001	0.3275	0.052
287	87B	10164	10168	0.53	0.15	0.29	8.732	8.7335	9.050	9.52	9.6265	0.0015	0.318	0.035
288	88B	12154	12158	0.56	0.08	0.31	10.5285	10.5295	10.931	11.31	11.4405	0.001	0.4025	0.042
A-Scaled to 1 KT Radiochemical Release at Sea Level														
200	0B	2286	2336	3.99	0.82	0.4 [a]	1.500	1.502	1.865	2.31	2.486 [a]	0.002	0.365	0.64
280	80B	1773	1838	5.2	1.29	0.8 [a]	1.102	1.104	1.452	1.86	2.052 [a,c]	0.002	0.350	0.64
281	81B	2517	2563	3.25	0.86	0.4 [a]	1.698	1.701	2.062	2.54	2.72 [a]	0.003	0.363	0.44
204	4B	3842	3864	1.5	0.40	0.16 [a]	2.805	2.808	3.219	3.76	3.938 [a]	0.003	0.414	0.36
282	82B	5335	5356	0.79	0.21	0.19	4.088	4.091	4.544	5.07	5.302	0.003	0.457	0.17
283	83B	6884	6902	0.94	0.26	0.35	5.437	5.441	5.875	6.45	6.699	0.004	0.442	0.17
208	8B	8462	8476	0.86	0.22	0.38	6.804	6.806	7.292	7.94	8.106	0.002	0.488	0.15
284	84B	10052	10065	0.79	0.24	0.33	8.209	8.212	8.690	9.34	9.542	0.003	0.481	0.125
285	85B	11652	11663	0.61	0.16	0.35	9.615	9.618	10.141	10.79	10.974	0.003	0.525	0.099
286	86B	14061	14069	0.58	0.09	0.40	11.738	11.7396	12.258	12.97	13.132	0.0016	0.520	0.097
287	87B	16476	16482	0.62	0.18	0.34	13.866	13.868	14.371	15.12	15.287	0.002	0.505	0.067
288	88B	19702	19708	0.66	0.09	0.36	16.719	16.7206	17.358	17.96	18.168	0.0016	0.639	0.078

a - Gradual rise
b - Another blip at 0.988 sec
c - Another blip at 1.57 sec

For meaning of symbols see Fig. 4.2

TABLE 4.2 – Air Pressure, Shot 3, 10 Ft Level*

Sta. No.	Gage Code No.	Grnd. Range (ft)	Slant Range (ft)	Pressure (psi)			Time (sec)					Duration (sec)		Impulse (psi-sec)
				P_m	P_n	P_b	t_s	t_m	t_x	t_n	t_b	Δt_s	Δt_+	I_+
As-Read														
200	0B10	1414	1444	3.8	0.9	0.4 [a]	0.948	0.9505	1.155	1.45	1.572[a]	0.0025	0.207	0.27
280	80B10	1100	1138	4.4	1.1	0.4 [a]	0.698	0.7005	0.903	1.17	1.3085[a]	0.0025	0.205	0.35
281	81B10	1556	1583	2.3	0.60	0.15[a]	1.0725	1.0735	1.313	1.62	1.725[a]	0.001	0.2425	0.27
204	4B10	2373	2390	1.45	0.41	0.17[a]	1.7685	1.771	2.0195	2.36	2.49 [a]	0.0025	0.251	0.13
282	82B10	3297	3305	0.95	0.33	0.24	2.5755	2.5775	2.845	3.20	3.340	0.002	0.2705	0.107
283	83B10	4249	4258	0.63	0.21	0.20	3.4225	3.424	3.720	4.13	4.2185	0.0015	0.2975	0.079
208	8B10	5221	5229	0.68	0.22	0.26	4.285	4.287	4.595	4.977	5.1055	0.002	0.310	0.096
284	84B10	6202	6209	0.46	0.12	0.20	5.169	5.171	5.478	5.90	6.085	0.002	0.309	0.056
285	85B10	7189	7195	0.37	0.15	0.18	6.0555	6.057	6.325	6.77	6.910	0.0015	0.277	0.035
286	86B10	8674	8679	0.47	0.12	0.26	7.391	7.3925	7.6985	8.16	8.269	0.0015	0.3075	0.047
287	87B10	10164	10168	0.37	0.07	0.20	8.7325	8.734	9.086	9.53	9.626	0.0015	0.3535	0.038
288	88B10	12154	12158	0.46	0.11	0.25	10.527	10.529	10.769	11.39	11.437	0.002	0.242	0.036
A-Scaled to 1 KT Radiochemical Release at Sea Level														
200	0B10	2292	2341	4.46	1.26	0.5 [a]	1.505	1.509	1.834	2.30	2.496[a]	0.004	0.329	0.51
280	80B10	1783	1845	5.17	1.29	0.5 [a]	1.108	1.112	1.434	1.86	2.078[a]	0.004	0.326	0.65
281	81B10	2522	2566	2.7	0.70	0.18[a]	1.703	1.7046	2.085	2.57	2.739[a]	0.0016	0.385	0.50
204	4B10	3847	3875	1.70	0.48	0.20[a]	2.332	2.336	3.207	3.75	3.95 [a]	0.004	0.399	0.24
282	82B10	5347	5357	1.11	0.39	0.28	4.090	4.093	4.519	5.08	5.304	0.003	0.430	0.20
283	83B10	6888	6902	0.74	0.25	0.23	5.435	5.437	5.907	6.56	6.699	0.002	0.472	0.15
208	8B10	8463	8476	0.80	0.26	0.31	6.805	6.808	7.297	7.90	8.108	0.003	0.492	0.18
284	84B10	10053	10065	0.54	0.14	0.23	8.208	8.211	8.699	9.37	9.663	0.003	0.491	0.104
285	85B10	11653	11663	0.43	0.18	0.21	9.616	9.618	10.056	10.75	10.973	0.002	0.440	0.067
286	86B10	14061	14069	0.55	0.14	0.31	11.737	11.739	12.225	12.96	13.132	0.002	0.488	0.088
287	87B10	16476	16482	0.43	0.08	0.23	13.867	13.869	14.429	15.13	15.286	0.002	0.561	0.071
288	88B10	19702	19708	0.54	0.13	0.29	16.717	16.720	17.101	18.09	18.162	0.003	0.384	0.067

a – Gradual rise

* – Actual gage height, 10 ft; A-scaled gage height, 16.2 ft

For meaning of symbols see Fig. 4.2

TABLE 4.3 - Air Pressure, Shot 4, Surface Level

Sta. No.	Gage Code No.	Effective Ground Range (ft)	Slant Range (ft)	Pressure (psi)			Time (sec)					Duration (sec)			Impulse (psi-sec)	
				P_s	P_m	P_n	t_s	t_m	t_x	t_n	t_{x2}	Δt_s	Δt_+	Δt_-	I_+	I_-
As-Read																
200	0B	610	6051	2.37	2.37	0.62	4.232	4.234	5.054	5.8	7.5	0.002	0.822	2.4	0.87	0.88
280	80B	1346	6169	2.42	2.42	0.61	4.339	4.341	5.120	5.9	7.7	0.002	0.781	2.6	0.83	0.83
281	81B	2292	6442	2.45	2.50	0.53	4.5765	4.585	5.402	6.0	8.1	0.001	0.8255	2.7	0.84	0.72
204	4B	3271	6851	2.04	2.04	0.46	4.932	4.934	5.7595	6.6	8.3	0.002	0.8275	2.5	0.73	0.61
282	82B	4259	7374	1.57	1.57	0.37	5.3855	5.388	6.2485	7.1	8.8	0.0025	0.863	2.6	0.59	0.52
283	83B	5252	7989	1.66	1.72	0.51	5.919	5.928	6.7825	7.6	9.3	0.002	0.8635	2.5	0.66	0.65
208	8B	6247	8675	1.35	1.49	0.41	6.5125	6.520	7.397	8.3	9.8	0.002	0.8845	2.4	0.59	0.63
284	84B	7243	9418	1.13	1.20	0.40	7.166	7.173	8.069	8.9	10.7	0.002	0.903	2.6	0.48	0.52
285	85B	8241	10205	1.05	1.05	0.32	7.855	7.857	8.7995	9.7	11.0	0.002	0.9445	2.2	0.47	0.42
286	86B	9738	11448	0.89	0.95	0.29	8.950	8.980	9.880	10.80	12.7	0.001	0.930	2.8	0.41	0.42
287	87B	11235	12746	0.86	0.91	0.31	10.0975	10.1165	11.1205	11.90	13.6	0.0025	1.023	2.5	0.40	0.36
288	88B	13233	14538	0.79	0.83	0.26	11.6795	11.6975	12.67	13.4	14.9	0.0015	0.9905	2.2	0.34	0.35
A-Scaled to 1 KT Radiochemical Release at Sea Level																
200	0B	241	2389	3.50	3.50	0.92	1.611	1.6113	1.924	2.2	2.9	0.0008	0.313	0.91	0.49	0.49
280	80B	531	2436	3.57	3.57	0.90	1.652	1.6528	1.949	2.3	2.9	0.0008	0.297	0.99	0.47	0.47
281	81B	905	2543	3.62	3.69	0.78	1.742	1.746	2.057	2.3	3.1	0.0004	0.314	1.0	0.47	0.40
204	4B	1291	2705	3.01	3.01	0.68	1.878	1.8788	2.193	2.5	3.2	0.0008	0.315	0.95	0.41	0.35
282	82B	1681	2911	2.32	2.32	0.55	2.060	2.051	2.379	2.7	3.4	0.001	0.329	0.99	0.33	0.29
283	83B	2073	3154	2.45	2.54	0.75	2.253	2.257	2.582	2.9	3.5	0.0008	0.329	0.95	0.37	0.37
208	8B	2466	3425	1.99	2.20	0.61	2.479	2.482	2.816	3.2	3.7	0.0008	0.337	0.91	0.33	0.35
284	84B	2860	3718	1.66	1.77	0.59	2.728	2.731	3.072	3.4	4.07	0.0008	0.344	0.99	0.27	0.29
285	85B	3254	4029	1.55	1.55	0.47	2.990	2.9908	3.350	3.7	4.19	0.0008	0.360	0.84	0.26	0.24
286	86B	3845	4520	1.31	1.40	0.43	3.407	3.419	3.761	4.11	4.84	0.001	0.354	1.07	0.23	0.24
287	87B	4436	5032	1.27	1.34	0.46	3.844	3.851	4.234	4.53	5.18	0.001	0.389	0.95	0.22	0.20
288	88B	5224	5740	1.2	1.23	0.38	4.446	4.453	4.82	5.10	5.67	0.0006	0.377	0.84	0.19	0.20

For meaning of symbols see Fig. 4.2

TAPLE 4.4 - Air Pressure (Incident), Shot 4, 10 Ft Level*

Sta. No.	Gage Code No.	Effective Ground Range (ft)	Slant Range (ft)	Pressure (psi)		Time (sec)		Duration (sec)	
				P_i	P_{12}	t_i	t_r	Δt_i	Δt_{ir}
As-Read									
200	0B10	604	6040	1.02	1.05	4.2245	4.239	0.002	0.0145
280	80B10	1344	6158	1.32	1.26	4.330	4.3465	0.002	0.0165
281	81B10	2291	6432	1.05	1.05	4.569	4.5835	0.002	0.0145
204	4B10	3270	6842	1.01	0.90	4.925	4.9385	0.001	0.0135
282	82B10	4258	7366	0.83	0.79	5.378	5.392	0.0015	0.0140
283	83B10	5251	7981	0.78	0.80	5.911	5.9245	0.002	0.0135
208	8B10	6246	8668	0.72	0.72	6.5065	6.518	0.002	0.0115
284	84B10	7242	9412	0.59	0.61	7.160	7.1705	0.001	0.0105
285	85B10	8240	10199	0.41	0.40	7.849	7.8585	0.0015	0.0095
286	86B10	9737	11443	0.44	0.42	8.9495	8.953	0.0015	0.0085
287	87B10	11235	12742	0.37	0.37	10.0945	10.1015	0.002	0.0070
288	88B10	13233	14534	0.35	0.36	11.676	11.6825	0.002	0.0065
A-Scaled to 1 KT Radiochemical Release at Sea Level									
200	0B10	238	2385	1.51	1.55	1.608	1.614	0.0008	0.00552
280	80B10	531	2431	1.95	1.86	1.648	1.655	0.0008	0.00628
281	81B10	904	2539	1.55	1.55	1.739	1.745	0.0008	0.00552
204	4B10	1291	2701	1.49	1.33	1.875	1.880	0.0004	0.00514
282	82B10	1681	2908	1.22	1.17	2.047	2.053	0.0006	0.00533
283	83B10	2073	3151	1.15	1.18	2.250	2.262	0.0008	0.00514
208	8B10	2466	3422	1.06	1.06	2.477	2.481	0.0008	0.00438
284	84B10	2860	3716	0.87	0.90	2.726	2.730	0.0004	0.00399
285	85B10	3254	4027	0.61	0.59	2.988	2.992	0.0006	0.0036
286	86B10	3845	4518	0.65	0.62	3.407	3.408	0.0006	0.0032
287	87B10	4436	5031	0.55	0.55	3.843	3.846	0.0008	0.0027
288	88B10	5224	5738	0.52	0.53	4.445	4.448	0.0008	0.0025

* - Actual gage height 10 ft; A-scaled gage height 3.95 ft

For meaning of symbols see Fig. 4.2

TABLE 4.5 - Air Pressure (Reflected), Shot 4, 10 Ft Level*

Sta. No.	Gage Code No.	Effective Ground Range (ft)	Slant Range (ft)	Pressure (psi)			Time (sec)					Duration (sec)			Impulse (psi-sec)	
				P_r	P_m	P_n	t_r	t_m	t_x	t_n	t_{x2}	Δt_r	Δt_+	Δt_-	I_+	I_-
As-Read																
200	0B10	604	6040	2.17	2.34	0.70	4.239	4.2625	5.0295	5.75	8.0	0.0025	0.805	3.0	0.99	0.98
280	80B10	1344	6158	2.58	2.58	0.73	4.3465	4.3485	5.151	5.8	7.4	0.002	0.821	2.2	0.89	0.92
281	81B10	2291	6432	2.29	2.33	0.58	4.5835	4.598	5.4065	6.15	7.7	0.002	0.8375	2.3	0.86	0.75
204	4B10	3270	6842	1.94	2.01	0.54	4.9385	4.954	5.7645	6.4	8.6	0.0015	0.8395	2.8	0.72	0.75
282	82B10	4258	7366	1.75	1.75	0.48	5.392	5.394	6.2195	7.1	8.5	0.002	0.8415	2.3	0.69	0.67
283	83B10	5251	7981	1.56	1.68	0.53	5.9245	5.935	6.760	7.6	9.4	0.002	0.849	2.6	0.64	0.73
208	8B10	6246	8668	1.48	1.52	0.46	6.518	6.532	7.404	8.2	9.9	0.0015	0.8975	2.5	0.62	0.61
284	84B10	7242	9412	1.25	1.31	0.39	7.1705	7.1825	8.0965	8.9	10.5	0.0015	0.9365	2.4	0.54	0.54
285	85B10	8240	10199	0.87	1.00	0.33	7.8585	7.8765	8.7805	9.65	11.5	0.0015	0.9315	2.7	0.46	0.49
286	86B10	9737	11443	0.86	0.97	0.27	8.953	8.980	9.8745	10.7	12.3	0.0015	0.930	2.4	0.39	0.43
287	87B10	11235	12742	0.73	0.85	0.25	10.1015	10.2135	11.070	12.0	13.3	0.0025	0.9755	2.2	0.36	0.32
288	88B10	13233	14534	0.73	0.80	0.25	11.6825	11.696	12.634	13.5	15.4	0.0015	0.958	2.8	0.36	0.35
A-Scaled to 1 KT Radiochemical Release at Sea Level																
200	0B10	238	2385	3.20	3.46	1.0	1.614	1.623	1.915	2.19	3.05	0.001	0.307	1.14	0.56	0.55
280	80B10	531	2431	3.81	3.81	1.1	1.655	1.6558	1.961	2.21	2.8	0.0008	0.313	0.84	0.50	0.52
281	81B10	904	2539	3.38	3.44	0.86	1.745	1.751	2.058	2.34	2.9	0.0008	0.319	0.88	0.48	0.42
204	4B10	1291	2701	2.89	2.97	0.80	1.880	1.886	2.195	2.44	3.3	0.0006	0.320	1.07	0.40	0.42
282	82B10	1681	2908	2.58	2.58	0.71	2.053	2.0538	2.368	2.70	3.2	0.0008	0.320	0.88	0.39	0.38
283	83B10	2073	3151	2.30	2.48	0.78	2.262	2.260	2.574	2.89	3.6	0.0008	0.323	0.99	0.36	0.41
208	8B10	2466	3422	2.19	2.25	0.68	2.481	2.487	2.819	3.12	3.8	0.0006	0.342	0.95	0.35	0.35
284	84B10	2860	3716	1.85	1.93	0.58	2.730	2.734	3.082	3.39	4.00	0.0006	0.357	0.91	0.30	0.30
285	85B10	3254	4027	1.29	1.48	0.49	2.992	2.999	3.343	3.67	4.38	0.0006	0.355	1.03	0.26	0.28
286	86B10	3845	4518	1.27	1.43	0.40	3.408	3.419	3.759	4.07	4.68	0.0006	0.354	0.91	0.22	0.24
287	87B10	4436	5031	1.08	1.26	0.47	3.846	3.888	4.214	4.57	5.06	0.001	0.371	0.84	0.20	0.18
288	88B10	5224	5738	1.08	1.18	0.47	4.448	4.453	4.810	5.14	5.86	0.0006	0.365	1.07	0.20	0.20

* - Actual gage height 10 ft; A-scaled gage height 3.95 ft

For meaning of symbols see Fig. 4.2

TABLE 4.6 - Air Pressure, Shot 9, Surface Level

Sta. No.	Gage Code No.	Grnd. Range (ft)	Slant Range (ft)	Pressure (psi) P_s	P_m	P_n	P_b	Time (sec) t_s	t_m	t_x	t_n	t_b	t_{x2}	Duration (sec) Δt_s	Δt_+	Δt_-	Impulse (psi-sec) I_+	I_- #
As-Read																		
214	14B	820	2558	19.7[e]	21.2	2.3	——	1.097	1.108	1.80	2.57	——	3.8	0.0045	0.70	2.0	4.4	2.6
215	15B	952	2603	NR	NR	NR	NR	NR	NR	NR	NR	NR	NR	NR	NR	NR	NR	NR
216	16B	1281	2741	15.5	16.7	2.7	——	1.237	1.2465	1.90	2.8	——	5.1	0.002	0.66	3.2	3.8	4.8
217	17B	1696	2958	12.1[f]	13.9	1.8	——	1.400	1.416	2.14	2.82	——	5.0	0.0025	0.74	2.9	3.6	3.0
200	OB	2148	3238	10.7[g]	11.2	1.7	——	1.613	1.630	2.38	3.3	——	5.3	0.006	0.77	2.9	3.2	2.8
202	2B	2617	3566	9.8	10.2	1.7	——	1.873	1.880	2.54	3.47	——	5.7	0.002	0.77	3.1	2.8	3.0
204	4B	3094	3930	9.85	10.4	1.7	——	2.165	2.175	2.99	3.85	——	6.2	0.002	0.83	3.2	2.6	3.0
206	6B	3580	4323	7.42	7.85	1.2	——	2.462	2.492	3.32	4.2	——	6.3	0.003	0.84	3.0	2.2	2.0
208	8B	4068	4735	7.26	7.50	1.1	——	2.8215	2.828	3.72	4.6	——	6.5	0.003	0.90	2.8	2.0	1.7
209	9B	4559	5163	6.28	7.00	0.90	——	3.176	3.185	4.08	5.1	——	6.9	0.003	0.90	2.8	1.8	1.4
210	10B	5052	5603	6.15	6.15	0.98	——	3.544	3.5455	4.50	5.3	——	7.46	0.0015	0.96	3.0	1.6	1.7
211	11B	6041	6509	4.98	4.98	0.66	0.18	4.306	4.3075	5.32	6.35	7.609	8.35	0.0015	1.01	3.03	1.6	1.1
285	85B	6537	6971	4.06	4.06	0.48	0.24	4.699	4.701	5.69	6.6	8.0355	9.0	0.002	0.99	3.3	1.4	0.9
293	93B	7530	7910	3.16	3.19	0.65	0.15	5.4765	5.490	6.52	7.5	8.875	9.6	0.0025	1.04	3.1	1.2	1.1
A-Scaled to 1 KT Radiochemical Release at Sea Level																		
214	14B	259	809	24.2[h]	26.0	2.82	——	0.3397	0.343	0.558	0.796	——	1.18	0.0014	0.22	0.62	1.7	0.99
215	15B	301	823	NR	NR	NR	NR	NR	NR	NR	NR	NR	NR	NR	NR	NR	NR	NR
216	16B	405	867	19.0	20.5	3.32	——	0.3831	0.386	0.588	0.867	——	1.58	0.0006	0.20	0.99	1.4	1.3
217	17B	536	935	14.9[i]	17.1	2.21	——	0.4336	0.439	0.663	0.873	——	1.55	0.0008	0.23	0.90	1.4	1.1
200	OB	679	1024	13.1[j]	13.8	2.09	——	0.4996	0.505	0.737	1.02	——	1.64	0.0019	0.24	0.90	1.2	1.06
202	2B	828	1128	12.0	12.5	2.09	——	0.5801	0.282	0.818	1.08	——	1.77	0.0006	0.24	0.96	1.1	1.1
204	4B	978	1243	12.1	12.8	2.09	——	0.6705	0.674	0.926	1.19	——	1.92	0.0006	0.26	0.99	0.98	1.1
206	6B	1132	1367	9.11	9.64	1.47	——	0.7687	0.772	1.03	1.30	——	1.95	0.0009	0.26	0.93	0.83	0.76
208	8B	1286	1497	8.92	9.21	1.35	——	0.8738	0.876	1.15	1.42	——	2.01	0.0009	0.28	0.87	0.76	0.64
209	9B	1442	1633	7.71	8.60	1.11	——	0.9836	0.986	1.26	1.58	——	2.14	0.0009	0.28	0.87	0.68	0.53
210	10B	1597	1772	7.55	7.55	1.20	——	1.0976	1.0981	1.39	1.64	——	2.31	0.0005	0.30	0.93	0.61	0.64
211	11B	1910	2058	6.12	6.12	0.81	0.22	1.3336	1.3341	1.65	1.97	2.357	2.59	0.0005	0.32	0.94	0.61	0.42
285	85B	2067	2204	4.99	4.99	0.59	0.30	1.4553	1.4559	1.76	2.04	2.489	2.79	0.0006	0.31	1.02	0.53	0.34
293	93B	2381	2501	3.88	3.92	0.80	0.18	1.6961	1.700	2.02	2.32	2.749	2.97	0.0008	0.32	0.96	0.45	0.42

NR - No record
e - Slight hesitation at 1.0995 sec and 15.7 psi
f - Slight hesitation at 1.402 sec and 12.3 psi
g - Slight hesitation at 1.6145 sec and 5.7 psi, also at 1.617 sec and 10.0 psi
h - Slight hesitation at 0.341 sec and 19.3 psi
i - Slight hesitation at 0.434 sec and 15.1 psi
j - Slight hesitation at 0.500 sec and 7.0 psi, also at 0.501 sec and 12.3 psi
- Negative impulse : $I_- = 1.115 \times 1/2\ P_n\ \Delta t_-$

For meaning of symbols see Fig. 4.2

TABLE 4.7 – Air Pressure (Incident), Shot 9, 10 Ft Level*

Sta. No.	Gage Code No.	Grnd. Range (ft)	Slant Range (ft)	Pressure (psi)		Time (sec)		Duration (sec)	
				P_i	P_{12}	t_i	t_r	Δt_i	Δt_{ir}
As-Read									
214	14B10	837	2554	9.8	5.9	1.096	1.108	0.0025	0.012
215	15B10	967	2600	7.3y	6.7y	1.133	1.144	0.001	0.011
216	16B10	1283	2733	7.3	6.8	1.234	1.244	0.001	0.010
217	17B10	1697	2950	6.8	6.0	1.399	1.4055	0.002	0.0065
200	0B10	2154	3235	6.2	6.2	1.618	1.619	0.001	0.001
202	2B10	2622	3564	4.40	3.6	1.875	1.8775	0.001	0.0025
204	4B10	3100	3929	K	K	K	2.1685	K	K
206	6B10	3584	4321	K	K	K	2.487	K	K
208	8B10	4072	4733	K	K	K	2.8245	K	K
209	9B10	4562	5161	K	K	K	3.180	K	K
210	10B10	5055	5601	K	K	K	3.545	K	K
285	85B10	6539	6970	K	K	K	4.700	K	K
A-Scaled to 1 KT Radiochemical Release at Sea Level									
214	14B10	265	808	12.0	7.2	0.3394	0.343	0.0008	0.0036
215	15B10	306	822	8.96y	8.2y	0.3509	0.354	0.0003	0.0034
216	16B10	406	864	8.96	8.4	0.3822	0.385	0.0003	0.0031
217	17B10	537	933	8.3	7.4	0.4333	0.435	0.0006	0.0020
200	0B10	681	1023	7.6	7.6	0.5011	0.501	0.0003	0.0003
202	2B10	829	1127	5.4	4.4	0.5807	0.582	0.0003	0.0008
204	4B10	980	1242	K	K	K	0.6772	K	K
206	6B10	1133	1366	K	K	K	0.7702	K	K
208	8B10	1288	1497	K	K	K	0.8748	K	K
209	9B10	1443	1632	K	K	K	0.9849	K	K
210	10B10	1598	1771	K	K	K	1.098	K	K
285	85B10	2068	2204	K	K	K	1.456	K	K

K – Mach stem height is greater than gage height
* – Actual gage height, 10 ft; A-scaled gage height, 3.16 ft
y – Validity of data doubtful; inconsistent autocal.

For meaning of symbols see Fig. 4.2

TABLE 4.8 - Air Pressure (Reflected), Shot 9, 10 Ft Level*

Sta. No.	Gage Code No.	Grnd. Range (ft)	Slant Range (ft)	Pressure (psi)				Time (sec)						Duration (sec)			Impulse (psi-sec)	
				P_r	P_m	P_n	P_b	t_r	t_m	t_x	t_n	t_b	t_{x2}	Δt_r	Δt_+	Δt_-	I_+	I_-#
As-Read																		
214	14B10	837	2554	23.6	23.6	2.4	----	1.108	1.109	1.740	2.4	-----	4.5	0.001	0.649	2.8	4.5	3.6
215	15B10	967	2600	14.6y	19.2y	2.4y	----	1.144	1.156	1.799	2.68	-----	5.0	0.002	0.666	3.2	4.4	4.4
216	16B10	1283	2733	17.1	18.2	2.8	----	1.244	1.249	1.935	2.6	-----	4.6	0.0015	0.701	2.7	4.3	4.2
217	17B10	1697	2950	15.6	15.6	2.4	----	1.4055	1.407	2.135	2.9	-----	5.1	0.0015	0.736	3.0	3.8	4.0
200	0B10	2154	3235	13.1	13.4m	1.6	----	1.619	1.630	2.382	3.05	-----	5.1	0.0025	0.764	2.7	3.5	2.3
202	2B10	2622	3564	12.27	12.27	1.5	----	1.8775	1.8785	2.706	3.55	-----	5.6	0.001	0.831	2.9	3.2	2.5
204	4B10	3100	3929	12.0	12.0	1.5	----	2.1685	2.170	2.980	3.9	-----	6.2	0.0015	0.8115	3.2	2.9	2.8
206	6B10	3584	4321	12.0	12.0	1.3	----	2.487	2.4875	3.3405	4.53	-----	6.3	0.0005	0.8535	3.0	3.0	2.2
208	8B10	4072	4733	8.5	8.5	1.0	----	2.8245	2.826	3.761	4.6	-----	6.6	0.0015	0.9365	2.8	2.4	1.6
209	9B10	4562	5161	7.60	7.60	1.1	----	3.180	3.181	4.129	5.2	-----	7.08	0.001	0.949	3.0	2.0	1.8
210	10B10	5055	5601	7.08	7.08	1.0	----	3.545	3.547	4.4955	5.55	-----	7.3	0.002	0.9505	2.8	2.2	1.6
285	85B10	6539	6970	4.21	4.21	0.72	0.16	4.700	4.7025	5.6915	6.54	8.038	8.15	0.0025	0.9915	2.5	1.4	1.0
A-Scaled to 1 KT Radiochemical Release at Sea Level																		
214	14B10	265	808	28.9	28.9	3.0	----	0.343	0.3433	0.539	0.743	-----	1.4	0.0003	0.201	0.87	1.7	1.4
215	15B10	306	822	17.9y	23.6y	3.0y	----	0.354	0.358	0.557	0.830	-----	1.6	0.0006	0.206	0.99	1.7	1.7
216	16B10	406	864	21.0	22.3	3.4	----	0.385	0.387	0.599	0.805	-----	1.4	0.0005	0.217	0.84	1.6	1.6
217	17B10	537	933	19.2	19.2	3.0	----	0.435	0.4355	0.661	0.898	-----	1.6	0.0005	0.228	0.96	1.4	1.5
200	0B10	681	1023	16.1	16.5n	2.0	----	0.501	0.505	0.738	0.945	-----	1.6	0.0008	0.237	0.84	1.3	0.87
202	2B10	829	1127	15.1	15.1	1.8	----	0.582	0.5823	0.838	1.10	-----	1.7	0.0003	0.257	0.90	1.2	0.95
204	4B10	980	1242	14.7	14.7	1.8	----	0.6772	0.6777	0.923	1.21	-----	1.9	0.0005	0.251	0.99	1.1	1.06
206	6B10	1133	1366	14.7	14.7	1.6	----	0.7702	0.7704	1.035	1.40	-----	2.0	0.0002	0.264	0.93	1.1	0.83
208	8B10	1288	1497	10.4	10.4	1.2	----	0.8748	0.8753	1.165	1.42	-----	2.1	0.0005	0.290	0.87	0.91	0.60
209	9B10	1443	1632	9.33	9.33	1.4	----	0.9849	0.9852	1.279	1.61	-----	2.2	0.0003	0.294	0.93	0.76	0.68
210	10B10	1598	1771	8.69	8.69	1.2	----	1.098	1.0986	1.392	1.72	-----	2.3	0.0006	0.294	0.87	0.83	0.60
285	85B10	2068	2204	5.17	5.17	0.88	0.20	1.456	1.4568	1.763	2.03	2.489	2.5	0.0008	0.307	0.77	0.53	0.38

m - Smoothed value; actual record maximum is 16.9 psi
n - Smoothed value; actual record maximum is 20.3 psi
- Negative impulse: $I_- = 1.115 \times 1/2\ P_n\ \Delta t_-$
* - Actual gage height, 10 ft; A-scaled gage height, 3.16 ft
y - Validity of data doubtful; inconsistent autocal

For meaning of symbols see Fig. 4.2

TABLE 4.9 - Air Pressure (Incident), Shot 9; 30, 35, and 40 Ft Levels*

Sta. No.	Gage Code No.	Grnd. Range (ft)	Slant Range (ft)	Pressure (psi)		Time (sec)		Duration (sec)	
				P_i	P_{12}	t_i	t_r	Δt_i	Δt_{ir}
As-Read									
30-ft level									
214	14E30	837	2535	8.5	7.6	1.0835	1.125	0.002	0.0415
215	15B30	967	2581	8.1	5.8	1.120	1.1625	0.001	0.0425
216	16E30	1293	2720	7.5	6.3	1.2235	1.262	0.0005	0.0385
217	17E30	1705	2938	6.7	5.7	1.390	1.421	0.001	0.031
200	0E30	2154	3220	4.54	4.3	1.606	1.6295	0.002	0.0235
202	2E30	2622	3550	4.40	4.2	1.864	1.886	0.0015	0.022
204	4E30	3100	3916	4.26	3.96	2.160	2.1755	0.0005	0.016
206	6E30	3584	4310	3.70	3.20	2.479	2.490	0.0015	0.012
208	8E30	4072	4723	2.84	2.71	2.821	2.825	0.001	0.004
35-ft level									
285	85B35	6539	6961	K	K	K	4.700	K	K
40-ft level									
204	4E40	3100	3910	3.6	3.5	2.1545	2.1775	0.0015	0.023
206	6E40	3584	4304	3.4	3.3	2.475	2.4925	0.001	0.0175
208	8E40	4072	4718	2.7	2.7	2.8175	2.8265	0.001	0.0105
209	9E40	4562	5147	K	K	K	3.178	K	K
A-Scaled to 1 KT Radiochemical Release at Sea Level									
30-ft level *									
214	14E30	765	802	10.4	9.3	0.3356	0.348	0.0006	0.0129
215	15E30	906	816	9.95	7.1	0.3469	0.360	0.0003	0.0132
216	16E30	409	860	9.2	7.7	0.3789	0.391	0.0002	0.0119
217	17E30	539	929	8.2	7.0	0.4305	0.440	0.0003	0.0096
200	0E30	681	1018	5.56	5.3	0.4974	0.505	0.0006	0.0073
202	2E30	829	1123	5.40	5.2	0.5773	0.584	0.0005	0.0068
204	4E30	980	1238	5.23	4.9	0.6690	0.674	0.0002	0.0050
206	6E30	1133	1363	3.93	3.9	0.7678	0.771	0.0005	0.0037
208	8E30	1288	1493	3.49	3.3	0.8737	0.875	0.0003	0.0012
35-ft level *									
285	85B35	2068	2201	K	K	K	1.456	K	K
40-ft level *									
204	4E40	980	1237	4.4	4.3	0.6673	0.674	0.0005	0.0071
206	6E40	1133	1361	4.2	4.1	0.7665	0.772	0.0003	0.0054
208	8E40	1288	1492	3.3	3.3	0.8726	0.875	0.0003	0.0033
209	9E40	1443	1628	K	K	K	0.984	K	K

K - Mach stem height is greater than gage height

* - Actual gage heights, 30, 35, and 40 ft; A-scaled gage heights, 9.49, 11.07, and 12.65 ft

For meaning of symbols see Fig. 4.2

TABLE 4.10 - Air Pressure (Reflected), Shot 9; 30, 35, and 40 Ft Levels*

Sta. No.	Gage Code No.	Grnd. Range (ft)	Slant Range (ft)	Pressure (psi)				Time (sec)						Duration (sec)			Impulse (psi-sec)	
				P_r	P_m	P_n	P_b	t_r	t_m	t_x	t_n	t_b	t_{x2}	Δt_r	Δt_+	Δt_-	I_+	I_-#
As-Read																		
30-ft Level																		
214	14B30	837	2535	20.5	20.5	2.7	——	1.125	1.1265	1.679	2.34	——	4.25	0.0015	0.5955	2.57	4.1	3.8
215	15B30	967	2581	17.9	18.5	2.6	——	1.1625	1.167	1.940	2.6	——	4.3	0.0005	0.820	2.4	4.7	3.4
216	16B30	1293	2720	15.2	15.4	2.1	——	1.262	1.270	1.9405	2.55	——	4.7	0.0015	0.717	2.8	4.0	3.2
217	17B30	1705	2938	13.4	13.9	2.0	——	1.421	1.4335	2.157	2.8	——	4.9	0.0025	0.768	2.7	3.8	3.1
200	0B30	2154	3220	8.6	9.60	1.5	——	1.6295	1.643	2.4015	3.2	——	5.3	0.001	0.7955	2.9	4.2	2.4
202	2B30	2622	3550	10.08	10.08	1.6	——	1.886	1.887	2.690	3.6	——	5.6	0.001	0.826	2.9	2.7	2.7
204	4B30	3100	3916	10.47	10.47	1.5	——	2.1755	2.176	2.977	4.05	——	6.0	0.0005	0.817	3.0	2.7	2.5
206	6B30	3584	4310	8.50	8.50	1.2	——	2.490	2.491	3.3415	4.3	——	6.25	0.001	0.8625	2.91	2.3	1.8
208	8B30	4072	4723	7.52	7.65	1.1	——	2.825	2.831	3.746	4.42	——	6.7	0.002	0.925	3.0	2.3	1.8
35-ft Level																		
285	85B35	6539	6961	4.6	4.6	0.71	0.12	4.700	4.7015	5.6695	6.6	8.0295	8.9	0.0015	0.9695	3.2	1.5	1.3
40-ft Level																		
204	4B40	3100	3910	9.0	9.0	1.1	——	2.1775	2.179	3.0475	3.9	——	5.3	0.0015	0.893	2.3	2.7	1.4
206	6B40	3584	4310	8.5	8.5	1.4	——	2.4925	2.4935	3.311	4.3	——	6.4	0.001	0.836	3.1	2.3	2.3
208	8B40	4072	4718	7.3	7.3	1.0	——	2.8265	2.828	3.713	4.65	——	6.5	0.0015	0.8955	2.8	2.2	1.6
209	9B40	4562	5147	6.09	6.09	0.9	——	3.178	3.180	4.056	5.0	——	7.45	0.002	0.878	3.4	1.8	1.7
A-Scaled to 1 KT Radiochemical Release at Sea Level																		
30-ft Level*																		
214	14B30	265	802	25.2	25.2	3.3	——	0.348	0.3485	0.520	0.73	——	1.31	0.0005	0.184	0.796	1.6	1.4
215	15B30	306	816	22.0	22.7	3.2	——	0.360	0.361	0.601	0.81	——	1.33	0.0002	0.230	0.743	1.8	1.3
216	16B30	409	860	18.7	18.9	2.6	——	0.391	0.393	0.601	0.79	——	1.5	0.0005	0.220	0.867	1.5	1.2
217	17B30	539	929	16.5	17.1	2.5	——	0.440	0.444	0.668	0.87	——	1.5	0.0008	0.238	0.836	1.4	1.17
200	0B30	681	1018	11.8	10.6	1.8	——	0.505	0.509	0.744	0.99	——	1.6	0.0003	0.246	0.898	1.6	0.91
202	2B30	829	1123	12.38	12.38	2.0	——	0.584	0.5843	0.833	1.11	——	1.7	0.0003	0.256	0.898	1.0	1.02
204	4B30	980	1238	12.86	12.86	1.8	——	0.674	0.6742	0.922	1.25	——	1.9	0.0002	0.253	0.929	1.0	0.95
206	6B30	1133	1363	10.4	10.4	1.5	——	0.771	0.7713	1.04	1.3	——	1.9	0.0003	0.267	0.898	0.87	0.68
208	8B30	1288	1493	9.23	9.39	1.4	——	0.875	0.877	1.16	1.4	——	2.1	0.0006	0.267	0.929	0.87	0.68
35-ft Level*																		
285	85B35	2068	2201	5.7	5.7	0.87	0.14	1.456	1.4565	1.76	2.0	2.487	2.8	0.0005	0.300	0.991	0.57	0.49
40-ft Level*																		
204	4B40	980	1237	11.1	11.1	1.4	——	0.674	0.6745	0.944	1.2	——	1.6	0.0005	0.277	0.712	1.0	0.53
206	6B40	1133	1361	10.4	10.4	1.7	——	0.772	0.7723	1.03	1.3	——	2.0	0.0003	0.259	0.960	0.87	0.87
208	8B40	1288	1492	8.96	8.96	1.2	——	0.875	0.8755	1.15	1.4	——	2.0	0.0005	0.277	0.867	0.83	0.61
209	9B40	1443	1628	7.48	7.48	1.1	——	0.984	0.9846	1.26	1.5	——	2.3	0.0006	0.272	1.05	0.68	0.64

- Negative impulse: $I_- = 1.115 \times 1/2\ P_n\ \Delta t_-$

* - Actual gage heights, 30, 35, and 40 ft; A-scaled gage heights, 9.49, 11.07, and 12.65 ft

For meaning of symbols see Fig. 4.2

TABLE 4.11 - Air Pressure (Incident), Shot 9, 50 Ft Level*

Sta. No.	Gage Code No.	Grnd. Range (ft)	Slant Range (ft)	Pressure (psi)		Time (sec)		Duration (sec)	
				P_i	P_{12}	t_i	t_r	Δt_i	Δt_{ir}
As-Read									
214	14B50	837	2516	9.4	7.0	1.0705	1.142	0.001	0.0715
215	15B50	967	2563	8.5	6.4	1.107	1.179	0.002	0.072
216	16B50	1293	2702	7.2	5.7	1.2115	1.2785	0.001	0.067
217	17B50	1705	2922	6.1	5.5	1.378	1.436	0.0015	0.058
200	0B50	2154	3205	5.52	5.34	1.596	1.6425	0.001	0.0465
202	2B50	2622	3537	4.50	4.27	1.854	1.895	0.0015	0.041
204	4B50	3100	3904	NR	NR	NR	NR	NR	NR
206	6B50	3584	4299	2.2y	2.6y	2.4705	2.4945	0.001	0.024
208	8B50	4072	4713	2.8	2.75	2.8145	2.830	0.0015	0.0155
209	9B50	4562	5143	2.40	2.40	3.1745	3.179	0.0015	0.0045
210	10B50	5055	5584	K	K	K	3.5445	K	K
A-Scaled to 1 KT Radiochemical Release at Sea Level									
214	14B50	265	796	11.5	8.6	0.3315	0.354	0.0003	0.0221
215	15B50	306	810	10.4	7.9	0.3428	0.365	0.0006	0.0223
216	16B50	409	854	8.8	7.0	0.3752	0.396	0.0003	0.0208
217	17B50	539	924	7.5	6.8	0.4268	0.445	0.0005	0.0180
200	0B50	681	1013	6.78	6.6	0.4943	0.508	0.0003	0.0144
202	2B50	829	1118	5.53	5.2	0.5742	0.587	0.0005	0.0127
204	4B50	980	1234	NR	NR	NR	NR	NR	NR
206	6B50	1133	1359	2.70y	3.2y	0.7651	0.773	0.0003	0.0074
208	8B50	1288	1490	3.4	3.4	0.8717	0.877	0.0005	0.0048
209	9B50	1443	1626	2.95	3.0	0.9831	0.985	0.0005	0.0014
210	10B50	1598	1766	K	K	K	1.0977	K	K

K - Mach stem height is greater than gage height
NR - No record
* - Actual gage height, 50 ft; A-scaled gage height, 15.81 ft
y - Validity of data doubtful; inconsistent autocal

For meaning of symbols see Fig. 4.2

TABLE 4.12 - Air Pressure (Reflected), Shot 9, 50 Ft Level*

Sta. No.	Gage Code No.	Grnd. Range (ft)	Slant Range (ft)	Pressure (psi)				Time (sec)						Duration (sec)			Impulse (psi-sec)	
				P_r	P_m	P_n	P_b	t_r	t_m	t_x	t_n	t_b	t_{x2}	Δt_r	Δt_+	Δt_-	I_+	I_-#
As-Read																		
214	14B50	837	2516	18.4	18.4	2.6	—	1.142	1.144	1.771	2.45	—	4.25	0.002	0.7005	2.48	3.8	3.6
215	15B50	967	2563	17.4	17.4	2.2	—	1.179	1.181	1.850	2.47	—	4.7	0.002	0.743	2.8	3.8	3.6
216	16B50	1293	2702	14.6	14.8	2.4	—	1.2785	1.288	1.959	2.8	—	5.0	0.0015	0.7475	3.0	3.3	4.1
217	17B50	1705	2922	12.5	13.5	2.0	—	1.436	1.446	2.142	2.96	—	5.1	0.0015	0.764	3.0	3.4	3.3
200	0B50	2154	3205	10.1	11.5	1.8	—	1.6425	1.6575	2.379	3.1	—	5.2	0.0005	0.783	2.8	3.3	4.0
202	2B50	2622	3537	10.2	10.2	1.5	—	1.895	1.8955	2.734	3.5	—	5.4	0.0005	0.880	2.7	2.7	2.1
204	4B50	3100	3904	NR	NR	NR	NR	NR	NR	NR	NR	NR	NR	NR	NR	NR	NR	NR
206	6B50	3584	4299	6.4y	7.3y	1.2y	—	2.4945	2.506	3.4405	4.3	—	6.4	0.0015	0.970	3.0	2.5	1.9
208	8B50	4072	4713	7.01	7.01	1.1	—	2.830	2.8315	3.704	4.6	—	6.67	0.0015	0.8895	2.97	2.0	1.8
209	9B50	4562	5143	6.20	6.60	1.4	—	3.179	3.186	4.096	5.03	—	7.1	0.0025	0.9215	3.0	2.0	2.0
210	10B50	5055	5584	6.3	6.3	0.9	—	3.5445	3.546	4.491	5.65	—	7.35	0.0015	0.9465	2.86	1.9	1.5
A-Scaled to 1 KT Radiochemical Release at Sea Level																		
214	14B50	265	796	22.6	22.6	3.2	—	0.354	0.3546	0.549	0.76	—	1.32	0.0006	0.217	0.768	1.4	1.4
215	15B50	306	810	21.4	21.4	2.7	—	0.365	0.3656	0.573	0.76	—	1.5	0.0006	0.246	0.867	1.4	1.4
216	16B50	409	854	17.9	18.2	3.0	—	0.396	0.399	0.607	0.87	—	1.5	0.0005	0.232	0.929	1.3	1.6
217	17B50	539	924	15.3	16.6	2.5	—	0.445	0.448	0.663	0.92	—	1.6	0.0005	0.237	0.929	1.4	1.3
200	0B50	681	1013	12.4	14.1	2.2	—	0.508	0.513	0.737	0.96	—	1.6	0.0002	0.243	0.867	1.3	1.5
202	2B50	829	1118	12.5	12.5	1.8	—	0.587	0.5872	0.847	1.1	—	1.7	0.0002	0.273	0.836	1.0	0.80
204	4B50	980	1234	NR	NR	NR	NR	NR	NR	NR	NR	NR	NR	NR	NR	NR	NR	NR
206	6B50	1133	1359	7.9y	8.9y	1.5y	—	0.773	0.776	1.066	1.3	—	2.0	0.0005	0.300	0.929	0.95	0.72
208	8B50	1288	1490	8.6	8.6	1.4	—	0.877	0.8775	1.147	1.4	—	2.07	0.0005	0.276	0.920	0.76	0.68
209	9B50	1443	1626	7.6	8.1	1.7	—	0.985	0.987	1.269	1.6	—	2.2	0.0002	0.285	0.929	0.76	0.76
210	10B50	1598	1766	7.74	7.74	1.1	—	1.0977	1.0982	1.391	1.8	—	2.3	0.0005	0.293	0.886	0.72	0.57

NR - No record
- Negative impulse: $I_- = 1.115 \times 1/2\ P_n\ \Delta t_-$
* - Actual gage height, 50 ft; A-scaled gage height, 15.81 ft
y - Validity of data doubtful; inconsistent autocal

For meaning of symbols see Fig. 4.2

TABLE 4.13 – Air Pressure (Precursor), Shot 10, Surface and 10 Ft Levels*

Sta. No.	Gage Code No.	Grnd. Range (ft)	Slant Range (ft)	Pressure (psi)			Time (sec)			Duration (sec)		Impulse (psi-sec)	$\frac{\Delta t_{cs}}{\Delta t_+}$	$\frac{I_p}{I_+}$
				P_{p1}	P_{pm}	P_{p2}	t_p	t_{pm}	t_s	Δt_p	Δt_{ps}	I_p		
As-Read														
Surface Level														
215	15B	430	678	38	53	53	0.0915	0.0965	0.0965	0.0025	0.005	0.18	0.027	0.021
3.7	16BA	765	926	23.2	36	36	0.1605	0.189	0.189	0.0015	0.0285	0.80	CB	0.154
3.7	16BB	782	941	22.7	33.4	33.4	0.1685	0.193	0.193	0.003	0.0245	0.58	CB	CB
3.8	16BC	865	1011	10.7	15.0	0.7	0.173	0.1875	0.221	0.0025	0.048	0.50	0.178	0.111
3.8	16BD	893	1035	11.6	19.4	4.2	0.1765	0.203	0.237	0.002	0.0605	0.81	0.216	0.169
216	16B	921	1060	14.4	16.9	13.7	0.1915	0.2035	0.251	0.0025	0.0595	0.77	0.212	0.168
217	17B	1419	1513	10.3	11.6	s	0.351	0.397	s	0.017	s	s	s	s
200	OB	1918	1988	6.2	7.7	s	0.596	0.657	s	0.024	s	s	s	s
202	2B	2417	2473	2.9	7.2	7.2	0.974	1.041	1.041	0.005	0.067	0.33	0.10	0.143
10 Ft Level														
216	16B10	922	1056	——	53.5	CB	0.194	0.230	CB	——	CB	CB	CB	CB
216	16B10A	922	1056	14.5	16.7	CB	0.195	0.21	CB	0.003	CB	CB	CB	CB
217	17B10	1419	1510	11.4	12.7	t	0.3585	0.375	t	0.0055	t	t	CB	CB
217	17B10A	NR	NR	NR	NR	NR	NR	NR	NR	NR	NR	NR	NR	NR
200	OB10	1919	1987	8.3	t	t	0.605	t	t	0.031	t	t	t	t
202	2B10	2418	2472	3.35	6.86	6.86	0.979	1.042	1.042	0.063	0.063	0.32	0.104	0.152
A-Scaled to 1 KT Radiochemical Release at Sea Level														
Surface Level														
215	15B	167	263	44	61	61	0.0351	0.0370	0.0370	0.0010	0.0019	0.077	0.027	0.021
3.7	16BA	297	360	26.7	41	41	0.0616	0.0725	0.0725	0.0006	0.0109	0.35	CB	0.154
3.7	16BB	304	365	26.0	38.3	38.3	0.0647	0.0741	0.0741	0.0012	0.0094	0.25	CB	CB
3.8	16BC	336	393	12.3	17.2	0.8	0.0664	0.0719	0.0848	0.0010	0.0184	0.22	0.178	0.111
3.8	16BD	347	402	13.3	22.2	4.8	0.0677	0.0779	0.0909	0.0008	0.0232	0.36	0.216	0.169
216	16B	358	412	16.5	19.4	15.7	0.0735	0.0781	0.0963	0.0010	0.0228	0.34	0.212	0.168
217	17B	551	587	11.8	13.3	s	0.1347	0.1523	s	0.0065	s	s	s	s
200	OB	745	772	7.1	8.8	s	0.2287	0.2521	s	0.0092	s	s	s	s
202	2B	939	960	3.3	8.3	8.3	0.3737	0.3994	0.3994	0.0019	0.0257	0.15	0.10	0.143
10 Ft Level*														
216	16B10	358	410	——	61.3	CB	0.0744	0.0883	CB	——	CB	CB	CB	CB
216	16B10A	358	410	16.6	19.1	CB	0.0748	0.081	CB	0.0012	CB	CB	CB	CB
217	17B10	551	586	13.1	14.6	t	0.1376	0.1439	t	0.0021	t	t	CB	CB
217	17B10A	NR	NR	NR	NR	NR	NR	NR	NR	NR	NR	NR	NR	NR
200	OB10	745	772	9.5	t	t	0.2321	t	t	0.0119	t	t	t	t
202	2B10	939	960	3.83	7.86	7.86	0.3756	0.3998	0.3998	0.0012	0.0242	0.14	0.104	0.152

NR – No record
CB – Cable broke
s – No distinguishable main shock
t – Irregular wave form
* – Actual gage heights, 0 and 10 ft; A-Scaled gage heights, 0 and 3.88 ft
For meaning of symbols see Fig. 4.3

TABLE 4.14 - Air Pressure (Precursor), Shot 10; 30 and 50 Ft Levels*

Sta. No.	Gage Code No.	Grnd. Range (ft)	Slant Range (ft)	Pressure (psi)			Time (sec)			Duration (sec)		Impulse (psi-sec)	$\frac{\Delta t_{ps}}{\Delta t_+}$	$\frac{I_p}{I_+}$
				P_{p1}	P_{pm}	P_{p2}	t_p	t_{pm}	t_s	Δt_p	Δt_{ps}	I_p		
As-Read														
30 Ft Level														
216	16B30	NR	NR	NR	NR	NR	NR	NR	NR	NR	NR	NR	NR	NR
217	17B30	1421	1504	10.2	12.1	t	0.3665	0.390	t	0.0065	t	t	CB	CB
200	0B30	1919	1982	6.6	t	t	0.6175	t	t	0.018	t	t	t	t
202	2B30	NR	NR	NR	NR	NR	NR	NR	NR	NR	NR	NR	NR	NR
50 Ft Level														
216	16B50	925	1039	8.3	15.3	10.0	0.207	0.234	0.2405	0.015	0.0335	0.30	CB	CB
216	16B50A	925	1039	——	22.2	8.4	0.2065	0.235	0.240	——	0.0335	0.36	CB	CB
217	17B50	1421	1498	12.0	12.8	t	0.3755	0.401	t	0.016	t	t	CB	CB
217	17B50A	1421	1498	8.4	12.5	CB	0.3765	0.408	CB	0.0075	CB	CB	CB	CB
200	0B50	1919	1977	6.4	t	t	0.6305	t	t	0.002	t	t	t	t
202	2B50	2418	2464	4.2	6.0	6.0	0.983	1.035	1.035	0.0015	0.052	0.25	0.091	0.12
A-Scaled to 1 KT Radiochemical Release at Sea Level														
30 Ft Level*														
216	16B30	NR	NR	NR	NR	NR	NR	NR	NR	NR	NR	NR	NR	NR
217	17B30	552	584	11.7	13.9	t	0.141	0.150	t	0.0025	t	t	CB	CB
200	0B30	745	770	7.6	t	t	0.237	t	t	0.0069	t	t	t	t
202	2B30	NR	NR	NR	NR	NR	NR	NR	NR	NR	NR	NR	NR	NR
50 Ft Level*														
216	16B50	359	403	9.5	17.5	11.5	0.079	0.090	0.092	0.0058	0.0129	0.131	CB	CB
216	16B50A	359	403	——	25.4	9.6	0.079	0.090	0.092	——	0.0129	0.158	CB	CB
217	17B50	552	582	13.8	14.7	t	0.144	0.154	t	0.0061	t	t	CB	CB
217	17B50A	552	582	9.6	14.3	CB	0.145	0.157	CB	0.0029	CB	CB	CB	CB
200	0B50	745	768	7.2	t	t	0.242	t	t	0.0008	t	t	t	t
202	2B50	939	957	4.8	6.9	6.9	0.377	0.397	0.397	0.0006	0.0199	0.110	0.091	0.12

NR - No record
CB - Cable broke
t - Irregular wave form
* - Actual gage heights, 30 and 50 ft; A-scaled gage heights, 11.65 and 19.42 ft

For meaning of symbols see Fig. 4.3

TABLE 4.15 – Air Pressure, Shot 10, Surface Level

Sta. No.	Gage Code No.	Grnd. Range (ft)	Slant Range (ft)	Pressure (psi)				Time (sec)					Duration (sec)			Impulse (psi-sec)
				P_s	P_m	P_n	P_b	t_s	t_m	t_x	t_n	t_b	Δt_s	Δt_{sm}	Δt_+	I_+
As-Read																
215	15B	430	678	——	>200[r]	3	——	0.0965	0.105	0.279	0.34	——	——	0.0085	0.1875	8.4[w]
3.7	16BA	765	926	——	112	CB	CB	0.189	0.198	CB	CB	CB	——	0.009	CB	5.2[w]
3.7	16BB	782	941	——	152	CB	CB	0.193	0.2055	CB	CB	CB	——	0.0125	CB	CB
3.8	16BC	865	1011	——	63.8	2.5	——	0.221	0.235	0.44	0.49	——	——	0.014	0.27	4.5
3.8	16BD	893	1035	——	69.7	2.8	——	0.237	0.2485	0.46	0.60	——	——	0.0115	0.28	4.8
216	16B	921	1060	——	71.5	2.8	1.8	0.251	0.2625	0.47	0.59	0.704	——	0.0115	0.28	4.6
217	17B	1419	1513	——	14.3	2.2	0.6	s	0.571	0.808	1.09	1.129	s	s	0.457	3.3
200	OB	1918	1988	——	8.1	1.0	1.4	s	0.718	1.2665	1.55	1.571	s	s	0.6705	2.5
202	2B	2417	2473	——	8.1	1.5	——	1.041	1.045	1.64	1.85	——	——	0.004	0.67	2.3
204	4B	2916	2963	7.15	7.15	1.2	0.36	1.3665	1.369	2.0075	2.39	2.42[a]	0.0025	——	0.641	1.84
206	6B	3416	3456	4.99	5.33	0.99	0.12	1.7435	1.779	2.449	2.86	2.960	0.0025	0.0355	0.7055	1.57
208	8B	3916	3951	4.73	4.73	0.85	0.29	2.130	2.135	2.9395	3.31	3.4105	0.005	——	0.8095	1.51
209	9B	4416	4447	4.08	4.08	0.63	0.20	2.525	2.5285	3.367	3.83	3.867	0.0035	——	0.842	1.33
210	10B	4916	4943	3.28	3.40	0.72	0.22	2.927	2.937	3.813	4.29	4.328	0.003	0.010	0.886	1.28
211	11B	5915	5938	2.37	2.37	0.50	0.14	3.752	3.753	4.698	5.24	5.252	0.001	——	0.946	0.96
285	85B	NR	NR	NR	NR	NR	NR	NR	NR	NR	NR	NR	NR	NR	NR	NR
293	93B	7415	7433	1.35	1.48	0.36	0.14	5.026	5.035	6.065	6.63	6.642[a]	0.002	0.009	1.039	0.76
A-Scaled to 1 KT Radiochemical Release at Sea Level																
215	15B	167	263	——	>230[r]	3	——	0.0370	0.0403	0.1071	0.13	——	——	0.0033	0.0719	3.7[w]
3.7	16BA	297	360	——	128	CB	CB	0.0725	0.0760	CB	CB	CB	——	0.0035	CB	2.3[w]
3.7	16BB	304	365	——	174	CB	CB	0.0741	0.0789	CB	CB	CB	——	0.0048	CB	CB
3.8	16BC	336	393	——	73.1	2.9	——	0.0848	0.0902	0.17	0.188	——	——	0.0054	0.104	2.0
3.8	16BD	347	402	——	79.9	3.2	——	0.0909	0.0953	0.18	0.230	——	——	0.0044	0.108	2.1
216	16B	358	412	——	81.9	3.2	2.1	0.0963	0.1007	0.18	0.226	0.2701	——	0.0044	0.108	2.0
217	17B	521	587	——	16.4	2.5	0.7	s	0.2191	0.3100	0.418	0.4332	s	s	0.1754	1.5
200	OB	745	772	——	9.3	1.1	1.6	s	0.2755	0.4860	0.595	0.6028	s	s	0.2573	1.1
202	2B	939	960	——	9.3	1.7	——	0.3994	0.4010	0.629	0.710	——	——	0.0015	0.257	1.0
204	4B	1132	1151	8.19	8.19	1.4	0.41	0.5243	0.5253	0.7703	0.917	0.929[a]	0.0010	——	0.2460	0.81
206	6B	1326	1342	5.72	6.11	1.13	0.14	0.6690	0.6826	0.9397	1.09	1.136	0.0010	0.0136	0.2707	0.69
208	8B	1521	1534	5.42	5.42	0.97	0.33	0.8173	0.8192	1.1279	1.27	1.309	0.0019	——	0.3106	0.66
209	9B	1715	1727	4.68	4.68	0.72	0.23	0.9688	0.9701	1.2919	1.47	1.484	0.0013	——	0.3231	0.58
210	10B	1909	1919	3.76	3.90	0.83	0.25	1.1231	1.1269	1.4630	1.65	1.661	0.0012	0.0038	0.3400	0.56
211	11B	2297	2306	2.72	2.72	0.57	0.16	1.4396	1.4400	1.8026	2.01	2.015	0.0004	——	0.3630	0.42
285	85B	NR	NR	NR	NR	NR	NR	NR	NR	NR	NR	NR	NR	NR	NR	NR
293	93B	2879	2886	1.55	1.70	0.41	0.16	1.9285	1.9319	2.3271	2.54	2.549[a]	0.0008	0.0035	0.3987	0.33

NR – No record
CB – Cable broke
a – Gradual rise
r – Record shows evidence of gage overload
s – No distinguishable main shock
w – Extrapolated value
For meaning of symbols see Figs. 4.2 and 4.3

TABLE 4.16 – Air Pressure, Shot 10; 10 Ft Level*

Sta. No.	Gage Code No.	Grnd. Range (ft)	Slant Range (ft)	Pressure (psi)				Time (sec)					Duration (sec)			Impulse (psi-sec)
				P_s	P_m	P_n	P_b	t_s	t_m	t_x	t_n	t_b	Δt_s	Δt_{sm}	Δt_+	I_+
As-Read																
216	16B10	922	1056	CB	CB	CB	CB	CB	CB	CB	CB	CB	CB	CB	CB	CB
216	16B10A	922	1056	CB	CB	CB	CB	CB	CB	CB	CB	CB	CB	CB	CB	CB
217	17B10	1419	1510	t	CB	CB	CB	t	CB	CB	CB	CB	t	CB	CB	CB
217	17B10A	NR	NR	NR	NR	NR	NR	NR	NR	NR	NR	NR	NR	NR	NR	NR
200	0B10	1919	1987	t	14.5	CB	CB	t	0.669	t	CB	CB	t	t	t	1.7^t
202	2B10	2418	2472	——	8.9	1.56	——	1.042	1.043	1.5835	1.98	——	0.001	0.001	0.6045	2.1
204	4B10	2917	2962	6.41	6.41	1.16	——	1.367	1.369	2.030	3.15	——	0.002	——	0.663	1.71
206	6B10	NR	NR	NR	NR	NR	NR	NR	NR	NR	NR	NR	NR	NR	NR	NR
208	8B10	3917	3950	4.72	4.72	0.89	0.30	2.1305	2.132	2.925	3.37	3.411	0.0015	——	0.7945	1.47
209	9B10	4416	4446	3.85	4.00	0.95	0.23	2.526	2.546	3.3505	3.788	3.8685	0.001	0.020	0.8245	1.28
210	10B10	NR	NR	NR	NR	NR	NR	NR	NR	NR	NR	NR	NR	NR	NR	NR
285	85B10	6416	6436	1.85	1.85	0.52	0.10	4.1725	4.175	5.139	5.69	5.7155	0.0025	——	0.9665	0.83
A-Scaled to 1 KT Radiochemical Release at Sea Level																
216	16B10	358	410	CB	CB	CB	CB	CB	CB	CB	CB	CB	CB	CB	CB	CB
216	16B10A	358	410	CB	CB	CB	CB	CB	CB	CB	CB	CB	CB	CB	CB	CB
217	17B10	551	586	t	CB	CB	CB	t	CB	CB	CB	CB	t	CB	CB	CB
217	17B10A	NR	NR	NR	NR	NR	NR	NR	NR	NR	NR	NR	NR	NR	NR	NR
200	0B10	745	772	t	16.6	CB	CB	t	0.2567	t	CB	CB	t	t	t	0.7^t
202	2B10	939	960	——	10.2	1.79	——	0.3998	0.4002	0.6076	0.760	——	0.0004	0.0004	0.2319	0.9
204	4B10	1133	1150	7.35	7.35	1.33	——	0.5245	0.5253	0.7789	1.209	——	0.0008	——	0.2544	0.75
206	6B10	NR	NR	NR	NR	NR	NR	NR	NR	NR	NR	NR	NR	NR	NR	NR
208	8B10	1521	1534	5.41	5.41	1.02	0.34	0.8175	0.8181	1.1223	1.293	1.309	0.0006	——	0.3048	0.65
209	9B10	1715	1726	4.41	4.58	1.09	0.26	0.9692	0.9769	1.2856	1.453	1.484	0.0004	0.0077	0.3164	0.56
210	10B10	NR	NR	NR	NR	NR	NR	NR	NR	NR	NR	NR	NR	NR	NR	NR
285	85B10	2491	2499	2.12	2.12	0.60	0.11	1.6010	1.6020	1.9718	2.183	2.193	0.0010	——	0.3708	0.36

NR – No record
CB – Cable broke
t – Irregular wave form
* – Actual gage height, 10 ft; A-scaled gage height, 3.88 ft

For meaning of symbols see Figs. 4.2 and 4.3

TABLE 4.17 – Air Pressure, Shot 10; 30, 35, and 40 Ft Levels*

Sta. No.	Gage Code No.	Grnd. Range (ft)	Slant Range (ft)	Pressure (psi)				Time (sec)					Duration (sec)			Impulse (psi-sec)
				P_s	P_m	P_n	P_b	t_s	t_m	t_x	t_n	t_b	Δt_s	Δt_{sm}	Δt_+	I_+
As-Read																
30 Ft Level																
216	16B30	NR	NR	NR	NR	NR	NR	NR	NR	NR	NR	NR	NR	NR	NR	NR
217	17B30	1421	1504	t	CB	CB	CB	t	CB	CB	CB	CB	t	CB	CB	CB
200	0B30	1919	1982	t	15.4	CB	CB	t	0.771	1.11	CB	CB	t	t	0.49	1.86[t]
202	2B30	NR	NR	NR	NR	NR	NR	NR	NR	NR	NR	NR	NR	NR	NR	NR
204	4B30	2917	2959	7.50	7.50	1.28	——	1.367	1.369	2.001	2.38	——	0.002	——	0.634	2.06
206	6B30	3417	3452	5.13	5.33	0.81	0.12	1.744	1.7835	2.495	2.87	2.956	0.002	0.0395	0.751	1.64
208	8B30	3917	3948	4.64	4.64	0.81	0.26	2.1305	2.132	2.920	3.365	3.409	0.0015	——	0.7895	1.45
35 Ft Level																
285	85B35	6416	6434	1.65	1.70	0.43	0.09	4.173	4.214	5.1445	5.72	5.736	0.002	0.041	0.9715	0.75
40 Ft Level																
204	4B40	2917	2957	6.74	6.74	1.07	——	1.367	1.369	2.0395	3.15	——	0.002	——	0.6725	1.84
206	6B40	3417	3451	5.35	5.46	0.62	0.07	1.744	1.775	2.5195	2.85	2.954	0.001	0.031	0.7755	1.36
208	8B40	3917	3946	4.53	4.53	0.61	0.20	2.1305	2.132	2.987	3.365	3.408	0.0015	——	0.8565	1.48
209	9B40	NR	NR	NR	NR	NR	NR	NR	NR	NR	NR	NR	NR	NR	NR	NR
A-Scaled to 1 KT Radiochemical Release at Sea Level																
30 Ft Level*																
216	16B30	NR	NR	NR	NR	NR	NR	NR	NR	NR	NR	NR	NR	NR	NR	NR
217	17B30	552	584	t	CB	CB	CB	t	CB	CB	CB	CB	t	CB	CB	CB
200	0B30	745	770	t	17.6	CB	CB	t	0.296	0.43	CB	CB	t	t	0.188	0.82[t]
202	2B30	NR	NR	NR	NR	NR	NR	NR	NR	NR	NR	NR	NR	NR	NR	NR
204	4B30	1133	1149	8.59	8.59	1.47	——	0.525	0.5258	0.768	0.913	——	0.0008	——	0.243	0.91
206	6B30	1327	1340	5.88	6.11	0.93	0.14	0.669	0.684	0.957	1.10	1.134	0.0008	0.015	0.288	0.72
208	8B30	1521	1533	5.32	5.32	0.93	0.30	0.817	0.8176	1.120	1.29	1.308	0.0006	——	0.303	0.64
35 Ft Level*																
285	85B35	2491	2498	1.89	1.95	0.49	0.10	1.601	1.617	1.974	2.20	2.201	0.0008	0.016	0.373	0.33
40 Ft Level*																
204	4B40	1133	1148	7.72	7.72	1.23	——	0.525	0.5258	0.783	1.21	——	0.0008	——	0.258	0.81
206	6B40	1327	1340	6.13	6.26	0.71	0.08	0.669	0.681	0.967	1.09	1.133	0.0004	0.012	0.298	0.60
208	8B40	1521	1532	5.19	5.19	0.70	0.23	0.817	0.8176	1.15	1.29	1.308	0.0006	——	0.329	0.65
209	9B40	NR	NR	NR	NR	NR	NR	NR	NR	NR	NR	NR	NR	NR	NR	NR

NR – No record
CB – Cable broke
t – Irregular wave form
* – Actual gage heights, 30, 35, and 40 ft; A-scaled gage heights, 11.65, 13.59, and 15.53 ft

For meaning of symbols see Figs. 4.2 and 4.3

TABLE 4.18 - Air Pressure, Shot 10; 50 Ft Level*

Sta. No.	Gage Code No.	Grnd. Range (ft)	Slant Range (ft)	Pressure (psi) P_s	P_m	P_n	P_b	Time (sec) t_s	t_m	t_x	t_n	t_o	Duration (sec) Δt_s	Δt_{sm}	Δt_+	Impulse (psi-sec) I_+
As-Read																
216	16B50	925	1039	u	88.5[u]	CB	CB	u	0.2645	CB	CB	CB	u	u	CB	CB
216	16B50A	925	1039	----	CB	CB	CB	0.240	CB	CB	CB	CB	------	CB	CB	CB
217	17B50	1421	1498	CB	CB	CB	CB	t	CB	CB	CB	CB	CB	CB	CB	CB
217	17B50A	1421	1498	CB	CB	CB	CB	CB	CB	CB	CB	CB	CB	CB	CB	CB
200	0B50	1919	1977	----	13.1	CB	CB	t	0.722	1.10[w]	CB	CB	t	t	0.47[w]	2.2[t,w]
202	2B50	2418	2464	----	9.6	1.6	----	1.035	1.0365	1.554	2.72	------	0.0015	0.0015	0.571	2.1
204	4B50	NR	NR	NR	NR	NR	NR	NR	NR	NR	NR	NR	NR	NR	NR	NR
206	6B50	3417	3450	5.18	5.32	1.00	0.11	1.744	1.7745	2.428	2.87	2.9505	0.002	0.0305	0.674	1.57
208	8B50	3917	3945	5.02	**5.02**	0.75	0.23	2.1315	**2.132**	2.961	3.35	3.408	0.0005	------	0.8295	1.62
209	9B50	4416	4442	3.62	**3.62**	0.68	0.16	2.5265	**2.529**	3.375	3.83	3.868	0.0025	------	0.8485	1.24
210	10B50	4916	4939	3.40	**3.40**	0.61	0.20	2.928	**2.9295**	3.850	4.30	4.328	0.0015	------	0.922	1.23
A-scaled to 1 KT Radiochemical Release at Sea Level																
216	16B50	359	403	v	101[v]	CB	CB	v	0.102	CB	CB	CB	v	v	CB	CB
216	16B50A	359	403	----	CB	CB	CB	0.092	CB	CB	CB	CB	------	CB	CB	CB
217	17B50	552	582	CB	CB	CB	CB	t	CB	CB	CB	CB	CB	CB	CB	CB
217	17B50A	552	582	CB	CB	CB	CB	CB	CB	CB	CB	CB	CB	CB	CB	CB
200	0B50	745	768	----	15.0	CB	CB	t	0.277	0.42[w]	CB	CB	t	t	0.180[w]	0.97[t,w]
202	2B50	939	957	----	11.0	1.8	----	0.397	0.398	0.596	1.04	------	0.0006	0.0006	0.219	0.92
204	4B50	NR	NR	NR	NR	NR	NR	NR	NR	NR	NR	NR	NR	NR	NR	NR
206	6B50	1327	1340	5.94	6.10	1.15	0.13	0.669	0.681	0.932	1.10	1.132	0.0008	0.012	0.259	0.69
208	8B50	1521	1532	5.75	5.75	0.86	0.26	0.818	**0.8182**	1.136	1.29	1.308	0.0002	------	0.318	0.71
209	9B50	1715	1725	4.15	4.15	0.78	0.18	0.969	**0.970**	1.295	1.47	1.484	0.0010	------	0.326	0.54
210	10B50	1909	1918	3.90	3.90	0.70	0.23	1.1 3	**1.1236**	1.477	1.65	1.661	0.0006	------	0.354	0.54

NR - No record
CB - Cable broke
t - Irregular wave form
u - P_1 = 65, P_{12} = 17.1, P_r = 88.5 psi; t_1 = 0.2405, t_r = 0.262 sec; $\Delta t_1 = \Delta t_r$ = 0.0025 sec, Δt_{ir} = 0.0215 sec
v - P_1 = 74, P_{12} = 19.6, P_r = 101 psi; t_1 = 0.092, t_r = 0.101 sec; $\Delta t_1 = \Delta t_r$ = 0.0010 sec, Δt_{ir} = 0.0082 sec
w - Extrapolated value
* - Actual gage height, 50 ft; A-scaled gage height, 19.42 ft

For meaning of symbols see Figs. 4.2 and 4.3

TABLE 4.19 - Air Pressure (Precursor), Shot 11, Surface, 5 and 10 Ft Levels*

Sta. No.	Gage Code No.	Effective Ground Range (ft)	Slant Range (ft)	Pressure (psi) P_{p1}	P_{pm}	P_{p2}	Time (sec) t_p	t_{pm}	t_s	Duration (sec) Δt_p	Δt_{ps}	Impulse (psi-sec) I_p	$\frac{\Delta t_{ps}}{\Delta t_+}$	$\frac{I_p}{I_+}$
As-Read														
Surface Level														
280	80B	1552	2047	8.3	9.9	3.3	0.472	0.5055	0.571	0.0045	0.099	0.80	0.170	0.129
202	2B	2011	2413	5.8	8.4	6.1	0.6205	0.744	0.7965	0.0075	0.176	1.15	0.257	0.202
281	81B	2485	2820	6.8	8.8	d	0.849	0.993	d	0.0315	-----	----	-----	-----
289	89B	2967	3253	9.4	9.7	d	1.1545[d]	1.226	d	0.0495	-----	----	-----	-----
290	90B	3946	4165	7.9 [z]	z	----	1.830	z	-----	0.012	-----	----	-----	-----
5 Ft Level														
204	4B5	3456	3703	5.0	8.7	8.7	1.493	1.530	1.530	0.011	0.037	0.20	0.037	0.043
204	4B5	3456	3703	1.18	3.73	3.73	1.493	1.5305	1.5305	0.011	0.0375	----	0.018	-----
10 Ft Level														
281	81B10	2486	2817	7.1	8.8	CB	0.851	0.961	CB	0.024	CB	CB	CB	CB
A-Scaled to 1 KT Radiochemical Release at Sea Level														
Surface Level														
280	80B	368	486	10.2	12.2	4.1	0.111	0.118	0.134	0.001	0.023	0.23	0.170	0.129
202	2B	477	573	7.1	10.3	7.5	0.145	0.174	0.187	0.002	0.041	0.33	0.257	0.202
281	81B	590	669	8.4	10.8	d	0.199	0.233	d	0.007	-----	----	-----	-----
289	89B	704	772	11.6	11.9	d	0.270[d]	0.287	d	0.012	-----	----	-----	-----
290	90B	937	989	9.7 [z]	z	---	0.429	z	-----	0.003	-----	----	-----	-----
5 Ft Level*														
204	4B5	820	879	6.2	10.7	10.7	0.350	0.358	0.358	0.003	0.0087	0.058	0.037	0.043
204	4B5	820	879	1.45	4.59	4.59	0.350	0.358	0.358	0.003	0.0088	----	0.018	-----
10 Ft Level*														
281	81B10	590	669	8.7	10.8	CB	0.199	0.225	CB	0.007	CB	CB	CB	CB

CB - Cable broke
d - Region of large base line shift
* - Actual gage heights, 0, 5, and 10 ft; A-scaled gage heights, 0, 1.19 and 2.37 ft
z - Initial precursor pressure not definitely distinguishable from main shock pressure

For meaning of symbols see Fig. 4.3

TABLE 4.20 – Air Pressure, Shot 11, Surface Level

Sta. No.	Gage Code No.	Effective Ground Range (ft)	Slant Range (ft)	Pressure (psi)			Time (sec)				Duration (sec)			Impulse (psi-sec)
				P_s	P_m	P_n	t_s	t_m	t_x	t_n	Δt_s	Δt_{sm}	Δt_+	I_+
As-Read														
280	80B	1552	2047	——	39.6	p	0.571	0.617	1.0545	p	——	0.046	0.5825	6.2
202	2B	2011	2413	——	24.3	p	0.7965	0.864	1.305	p	——	0.0675	0.6845	5.7
281	81B	2485	2820	d	d	p	d	d	1.841	p	d	d	0.992	6.5
289	89B	2967	3253	——	9.9	p	d	1.251	2.095	p	——	——	0.9405	4.5
290	90B	3946	4165	——	8.9	1.6	——	1.847	2.837	4.0	——	——	1.007	3.9
282	82B	4438	4634	7.83	8.60	1.3	2.177	2.1945	3.243	4.2	0.0025	0.0175	1.066	3.6
206	6B	4932	5109	6.74	7.19	1.1	2.537	2.5475	3.793	4.8	0.0025	0.0105	1.256	3.4
283	83B	5428	5589	5.12	5.96	1.3	2.896	2.907	4.0575	5.2	0.002	0.011	1.1555	3.0
208	8B	6420	6558	5.13	5.13	1.22	3.642	3.6435	4.823	6.3	0.0015	——	1.181	2.5
284	84B	7415	7534	4.03	4.03	0.92	4.416	4.417	5.777	7.1	0.001	——	1.361	2.4
285	85B	8411	8516	3.47	3.47	0.86	5.2045	5.206	6.4995	8.2	0.0015	——	1.2945	1.9
286	86B	9906	9996	2.33	2.33	0.69	6.414	6.4155	7.9705	9.5	0.0015	——	1.5565	1.5
287	87B	11403	11481	2.62	2.62	0.70	7.6435	7.6445	9.180	10.9	0.001	——	1.5365	1.4
288	88B	13400	13466	2.43	2.43	0.37	9.304	9.3055	10.890	12.2	0.0015	——	1.586	1.1
A-Scaled to 1 KT Radiochemical Release at Sea Level														
280	80B	368	486	——	45.4	p	0.134	0.145	0.247	p	——	0.011	0.136	1.78
202	2B	477	573	——	29.9	p	0.187	0.202	0.306	p	——	0.016	0.160	1.64
281	81B	590	669	d	d	p	d	d	0.431	p	d	d	0.232	1.87
289	89B	704	772	——	12.2	p	d	0.293	0.491	p	——	——	0.220	1.29
290	90B	937	989	——	10.9	1.97	——	0.433	0.664	0.94	——	——	0.236	1.12
282	82B	1054	1100	9.63	10.6	1.60	0.510	0.514	0.760	0.98	0.0006	0.0041	0.250	1.04
206	6B	1171	1213	8.29	8.8	1.35	0.594	0.597	0.888	1.1	0.0006	0.0025	0.294	0.98
283	83B	1289	1327	6.29	7.33	1.60	0.678	0.681	0.950	1.2	0.0005	0.0026	0.271	0.86
208	8B	1524	1557	6.30	6.30	1.50	0.853	0.853	1.130	1.5	0.0004	——	0.277	0.72
284	84B	1760	1789	4.96	4.96	1.13	1.03	1.03	1.35	1.7	0.0002	——	0.319	0.69
285	85B	1997	2022	4.27	4.27	1.06	1.219	1.219	1.52	1.9	0.0004	——	0.303	0.55
286	86B	2352	2373	2.87	2.87	0.85	1.50	1.50	1.87	2.2	0.0004	——	0.365	0.43
287	87B	2707	2725	3.22	3.22	0.86	1.79	1.79	2.15	2.6	0.0002	——	0.360	0.40
288	88B	3181	3197	2.99	2.99	0.46	2.16	2.16	2.55	2.9	0.0004	——	0.371	0.32

d – Region of large base line shift
p – Base line uncertain

For meaning of symbols see Figs. 4.2 and 4.3

TABLE 4.21 - Air Pressure, Shot 11; 5 and 10 Ft Levels*

Sta. No.	Gage Code No.	Effective Ground Range (ft)	Slant Range (ft)	Pressure (psi)			Time (sec)				Duration (sec)			Impulse (psi-sec)
				P_s	P_m	P_n	t_s	t_m	t_x	t_n	Δt_s	Δt_{sm}	Δt_+	I_+
As-Read														
5 Ft Level														
204	4B5	3456	3703	——	11.4	p	1.530	1.536	2.4835	p	——	0.006	0.9905	4.7
204	495	3456	3703	——	6.39	r	1.5305	1.539	3.6	r	——	0.0085	2.1	——
10 Ft Level														
281	81B10	2486	2817	CB	CB	CB	CB	CB	CB	CB	CB	CB	CB	CB
282	82B10	4439	4632	7.37	7.98	p	2.178	2.193	3.288	p	0.002	0.015	1.110	3.8
283	83B10	5428	5587	5.95	6.05	1.24	2.897	2.9055	4.065	4.9	0.0025	0.0085	1.168	2.5
208	8B10	6421	6556	5.09	5.31	0.77	3.642	3.674	4.973	6.2	0.001	———	1.331	2.8
284	84B10	7416	7533	4.16	4.16	1.01	4.416	4.4175	5.770	7.1	0.0015	———	1.354	2.2
285	85B10	8411	8515	3.28	3.28	0.79	5.2045	5.207	6.655	8.3	0.0025	———	1.4455	2.0
286	86B10	9907	9995	2.91	2.91	0.78	6.414	6.415	7.877	9.4	0.001	———	1.463	1.7
287	87B10	11403	11480	2.40	2.40	0.67	7.643	7.645	9.220	11.1	0.002	———	1.577	1.6
A-Scaled to 1 KT Radiochemical Release at Sea Level														
5 Ft Level*														
204	4B5	820	879	——	14.0	p	0.358	0.360	0.582	p	——	0.0014	0.232	1.35
204	495	820	879	——	7.86	r	0.358	0.360	0.843	r	——	0.002	0.492	——
10 Ft Level*														
281	81B10	590	669	CB	CB	CB	CB	CB	CB	CB	CB	CB	CB	CB
282	82B10	1054	1100	9.06	9.8	p	0.510	0.513	0.770	p	0.0005	0.004	0.260	1.09
283	83B10	1289	1326	7.32	7.44	1.52	0.679	0.681	0.952	1.1	0.0006	0.002	0.274	0.72
208	8B10	1524	1556	6.26	6.53	0.95	0.853	0.861	1.16	1.5	0.0002	———	0.312	0.81
284	84B10	1761	1788	5.11	5.11	1.24	1.03	1.03	1.35	1.7	0.0004	———	0.317	0.63
285	85B10	1997	2021	4.03	4.03	0.97	1.219	1.2196	1.56	1.9	0.0006	———	0.339	0.58
286	86B10	2352	2373	3.58	3.58	0.96	1.50	1.50	1.85	2.2	0.0002	———	0.343	0.49
287	87B10	2707	2725	2.95	2.95	0.82	1.79	1.79	2.16	2.6	0.0005	———	0.369	0.46

CB - Cable broke
p - Base line uncertain
r - No negative phase
* - Actual gage heights, 5 and 10 ft; A-scaled gage heights, 1.19 and 2.37 ft

For meaning of symbols see Figs. 4.2 and 4.3

TABLE 4.22 – Air Pressure (Secondary Blips), Shot 11, Surface; 5 and 10 Ft Levels*

Sta. No.	Gage Code No.	Effect. Ground Range (ft)	Slant Range (ft)	Pressure (psi)			Time (sec)			Gage Code No.	Effect. Ground Range (ft)	Slant Range (ft)	Pressure (psi)			Time (sec)		
				P_{b1}	P_{b2}	P_{b3}	t_{b1}	t_{b2}	t_{b3}				P_{b1}	P_{b2}	P_{b3}	t_{b1}	t_{b2}	t_{b3}
As-Read																		
280	80B	1992	2047	——	——	——	———	———	———	**	**	**	**	**	**	**	**	**
202	2B	2011	2413	——	——	1.0	———	———	2.65[a]	**	**	**	**	**	**	**	**	**
281	81B	2485	2820	——	1.0	0.6	———	1.4645	3.07[a]	81B10	2486	2817	CB	CB	CB	CB	CB	CB
289	89B	2967	3253	——	1.0	0.1	———	1.7255	3.505[a]	**	**	**	**	**	**	**	**	**
204	**	**	**	**	**	**	**	**	**	4B5	3456	3703	——	——	0.6	———	———	3.90[a]
204	**	**	**	**	**	**	**	**	**	4-5	3456	3703	q	q	q	q	q	q
290	90B	3946	4165	0.9	0.4	——	2.048	2.37	———	**	**	**	**	**	**	**	**	**
282	82B	4438	4634	1.3	0.7	0.4	2.3585	2.686	4.85	82B10	4439	4632	1.2	0.7	0.5	2.3565	2.682	4.85
206	6B	4932	5109	0.6	0.5	——	2.6745	3.0305	———	**	**	**	**	**	**	**	**	**
283	83B	5428	5589	0.4	0.3	0.4	2.9975	3.3785	5.76	83B10	5428	5587	0.5	0.3	0.3	2.9995	3.3765	5.76
208	8B	6420	6558	0.3	0.2	0.3	3.665	4.099	6.696	8B10	6421	6556	——	0.23	0.35	———	4.097	6.697
284	84B	7415	7534	——	0.24	0.4	———	4.845	7.623	84B10	7416	7533	——	0.16	0.40	———	4.8435	7.624
285	85B	8411	8516	——	0.16	0.52	———	5.602	8.545	85B10	8411	8515	——	0.17	0.47	———	5.599	8.544
286	86B	9906	9996	——	0.07	0.51	———	6.7575	9.918	86B10	9907	9995	——	0.07	0.60	———	6.7555	9.918
287	87B	11403	11481	——	0.07	0.70	———	7.9315	11.286	87B10	11403	11480	——	——	0.67	———	———	11.2685
288	88B	13400	13466	——	0.04	0.88	———	9.5165	13.104	**	**	**	**	**	**	**	**	**
n-Scaled to 1 KT Radiochemical Release at Sea Level																		
280	80B	368	486	——	——	——	———	———	———	**	**	**	**	**	**	**	**	**
202	2B	477	573	——	——	1.2	———	———	0.621[a]	**	**	**	**	**	**	**	**	**
281	81B	590	669	——	1.2	0.7	———	0.343	0.719[a]	81B10	590	669	CB	CB	CB	CB	CB	CB
289	89B	704	772	——	1.2	0.12	———	0.404	0.821[a]	**	**	**	**	**	**	**	**	**
204	**	**	**	**	**	**	**	**	**	4B5	820	879	——	——	0.70	———	———	0.913[a]
204	**	**	**	**	**	**	**	**	**	4-5	820	879	q	q	q	q	q	q
290	90B	937	989	1.1	0.5	——	0.480	0.555	———	**	**	**	**	**	**	**	**	**
282	82B	1054	1100	1.60	0.9	0.5	0.552	0.629	1.14	82B10	1054	1100	1.4	0.9	0.6	0.552	0.628	1.16
206	6B	1171	1213	0.7	0.6	——	0.626	0.710	———	**	**	**	**	**	**	**	**	**
283	83B	1289	1327	0.5	0.4	0.5	0.702	0.791	1.35	83B10	1289	1326	0.6	0.4	0.4	0.703	0.791	1.35
208	8B	1524	1557	0.4	0.3	0.4	0.858	0.960	1.57	8B10	1524	1556	——	0.28	0.43	———	0.960	1.57
284	84B	1760	1789	——	0.30	0.5	———	1.13	1.79	84B10	1761	1788	——	0.20	0.49	———	1.13	1.79
285	85B	1997	2022	——	0.20	0.64	———	1.31	2.00	85B10	1997	2021	——	0.21	0.58	———	1.31	2.00
286	86B	2352	2373	——	0.09	0.63	———	1.35	2.32	86B10	2352	2373	——	0.09	0.74	———	1.58	2.32
287	87B	2707	2725	——	0.09	0.9	———	1.86	2.64	87B10	2707	2725	——	——	0.82	———	———	2.64
288	88B	3181	3197	——	0.05	1.1	———	2.23	3.07	**	**	**	**	**	**	**	**	**

CB – Cable broke
a – Gradual rise
q – Record too noisy to show blip
* – actual gage heights, 0-, 5-, and 10-ft; n-scaled gage heights, 0, 1.19, and 2.37 ft
** – No measurement taken
For meaning of symbols see Fig. 4.2

TABLE 4.23 – Earth Acceleration and Velocity, Shot 9

Sta. No.	Gage Code No.	Grnd. Range (ft)	Slant Range to Surface (ft)	Acceleration (g)				Time (sec)						Duration (sec)	Velocity (fps)
				A_1	A_2	A_m	A_1-A_2	t_e	t_a	t_1	t_x	t_2	t_m	$t_x - t_a$	V_s
Vertical Acceleration 1 Ft Deep															
214	14V1	785	2547	-32.8	7.8	——	40.6	——	1.089	1.093	1.095	1.0955	——	0.006	-2.7
215	15V1	922	2593	-32.0	20.1	——	52.1	——	1.1235	1.126	1.1275	1.128	——	0.004	-1.3
216	16V1	1259	2731	-23.3	8.6	——	31.9	——	1.228	1.230	1.231	1.282	——	0.0035	-1.4
217	17V1	1680	2948	-33.3	30.4	——	52.3	——	1.391	1.393	1.3935	1.394	——	0.0025	-1.6
200	0V1	2134	3229	-24.7	13.3	——	38.0	1.593	1.6075	1.610	1.6105	1.611	——	0.003	-0.96
202	2V1	2606	3558	-17.6	8.64	——	26.2	1.667	1.8645	1.866	1.867	1.8675	——	0.0025	-0.68
204	4V1	3086	3924	-11.5	5.00	——	16.5	1.85	2.157	2.1595	2.161	2.162	——	0.004	-0.65
206	6V1	3572	4316	-14.9	6.21	——	22.11	1.79	2.478	2.478	2.4795	2.805	——	0.0015	-0.80
Radial Horizontal Acceleration 5 Ft Deep															
215	15H5	922	2592	- 0.8	1.5	-1.3	2.3	——	1.1285	1.1325	1.1335	1.1345	1.1435	0.0065	-0.06
216	16H5	1259	2730	1.5	-2.28	——	3.8	——	1.231	1.233	1.2355	1.237	——	0.0045	0.09
200	0H5	2134	3229	0.41	-0.11	-0.97	0.52	1.591	1.611	1.6145	1.619	1.620	1.653	0.008	0.11
202	2H5	2606	3558	1.31	-1.66	——	2.97	1.602	1.867	1.8715	1.8735	1.876	——	0.0065	0.10
204	4H5	3086	3924	1.44	-1.10	——	2.54	1.75	2.1615	2.164	2.167	2.1705	——	0.0055	0.10
206	6H5	3572	4316	1.62	-1.55	——	3.17	1.82	2.480	2.484	2.4855	2.4865	——	0.0065	0.11

For meaning of symbols see Fig. 4.4

TABLE 4.24 - Earth Acceleration and Velocity, Shot 10

Sta. No.	Gage Code No.	Grnd. Range (ft)	Slant Range To Surface (ft)	Acceleration (g)					Time (sec)							Duration (sec)	Velocity (fps)
				A_1	A_2	A_m	A_b	A_1-A_2	t_e	t_a	t_1	t_x	t_2	t_m	t_b	t_x-t_a	V_s
Vertical Acceleration 1 Foot Deep																	
215	15V1	423	673	-96.	4.	-351.	31.	100.	-----	0.091	0.0935	0.095	0.0955	0.099	0.7065	0.004	-34.
216	16V1	NR	NR	NR	NR	NR	NR	NR	NR	NR	NR	NR	NR	NR	NR	NR	NR
217	17V1	1417	1511	-12.6	6.3	11.2	-1.6 4.1	18.9	-----	0.3525	0.3565	0.3575	0.3585	0.465	1.13	0.006	- 0.77
200	0V1	1916	1986	- 2.7	2.0	-----	-2.0 1.8	4.7	0.599	0.6035	0.6085	0.6115	0.6125	-----	1.574	0.008	- 0.26
202	2V1	2416	2472	- 2.54	0.25	-----	-1.59 1.33	2.79	0.7125	0.974	0.9775	0.9805	0.981	-----	1.9875	0.0065	- 0.21
204	4V1	NR	NR	NR	NR	NR	NR	NR	NR	NR	NR	NR	NR	NR	NR	NR	NR
206	6V1	3415	3455	- 8.69	3.43	-----	-0.25 0.66	12.12	0.83	1.744	1.747	1.7485	1.7505	-----	2.942	0.0065	- 0.48
Radial Horizontal Acceleration 5 Feet Deep																	
215	15H5	423	673	18.8	-10.9	-----	-----	29.7	-----	0.097	0.107	0.109	0.1115	-----	-----	0.0055	2.2
216	16H5	918	1057	0.82	- 2.30	- 5.10	0.20[a] -0.50	3.12	-----	0.1965	0.2005	0.202	0.205	0.266	0.819	0.0055	-0.70
200	0H5	1916	1986	0.42	- 0.65	0.69	-0.15 0.42	1.07	0.584	0.584	0.6125	0.6235	0.6395	0.6795	1.588	0.0395	0.09
202	2H5	2416	2742	0.21	- 0.47	0.44	-0.13 0.12	0.68	0.7225	0.978	0.9815	0.985	1.003	1.0485	2.016	0.007	- 0.27
204	4H5	NR	NR	NR	NR	NR	NR	NR	NR	NR	NR	NR	NR	NR	NR	NR	NR
206	6H5	3415	3455	1.16	- 1.40	1.15	-0.08 0.10	2.56	0.832	1.748	1.762	1.7645	1.766	1.8225	2.950	0.0065	0.09

NR - No record
a - To an assumed base line

For meaning of symbols see Fig. 4.4

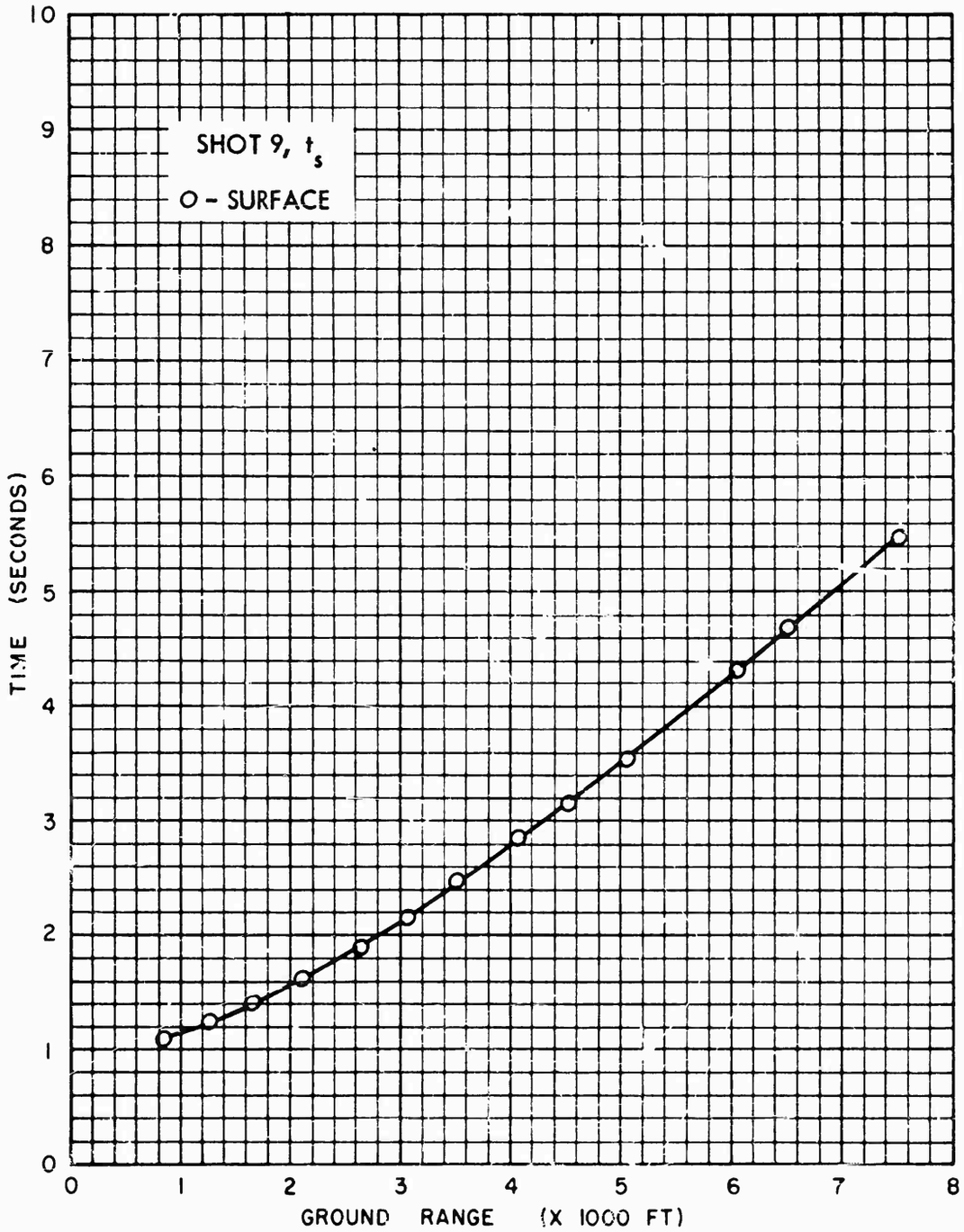

Fig. 4.16 Arrival Times at Surface Level, Main Shock, Shot 9

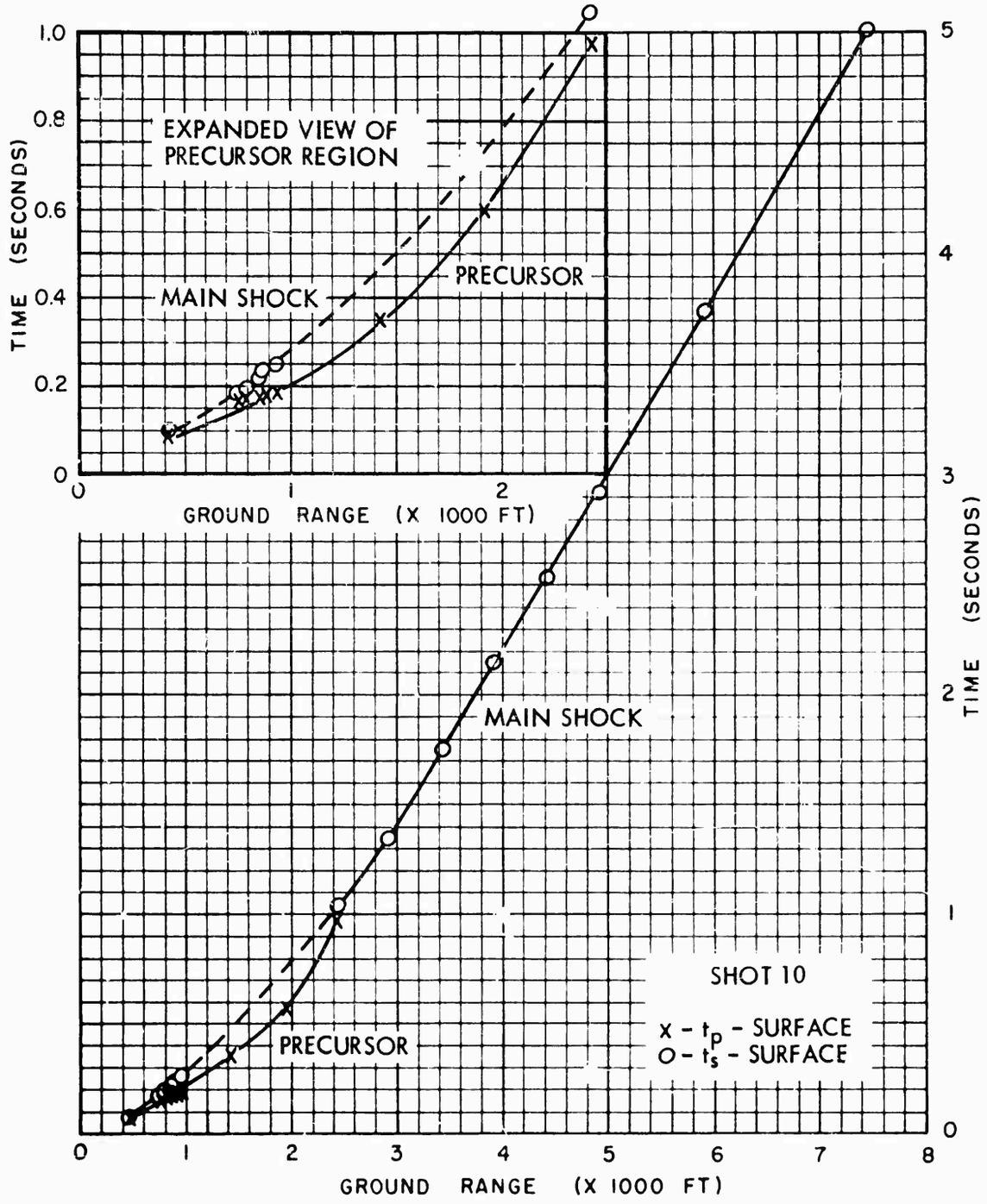

Fig. 4.17 Arrival Times at Surface Level, Precursor and Main Shock, Shot 10

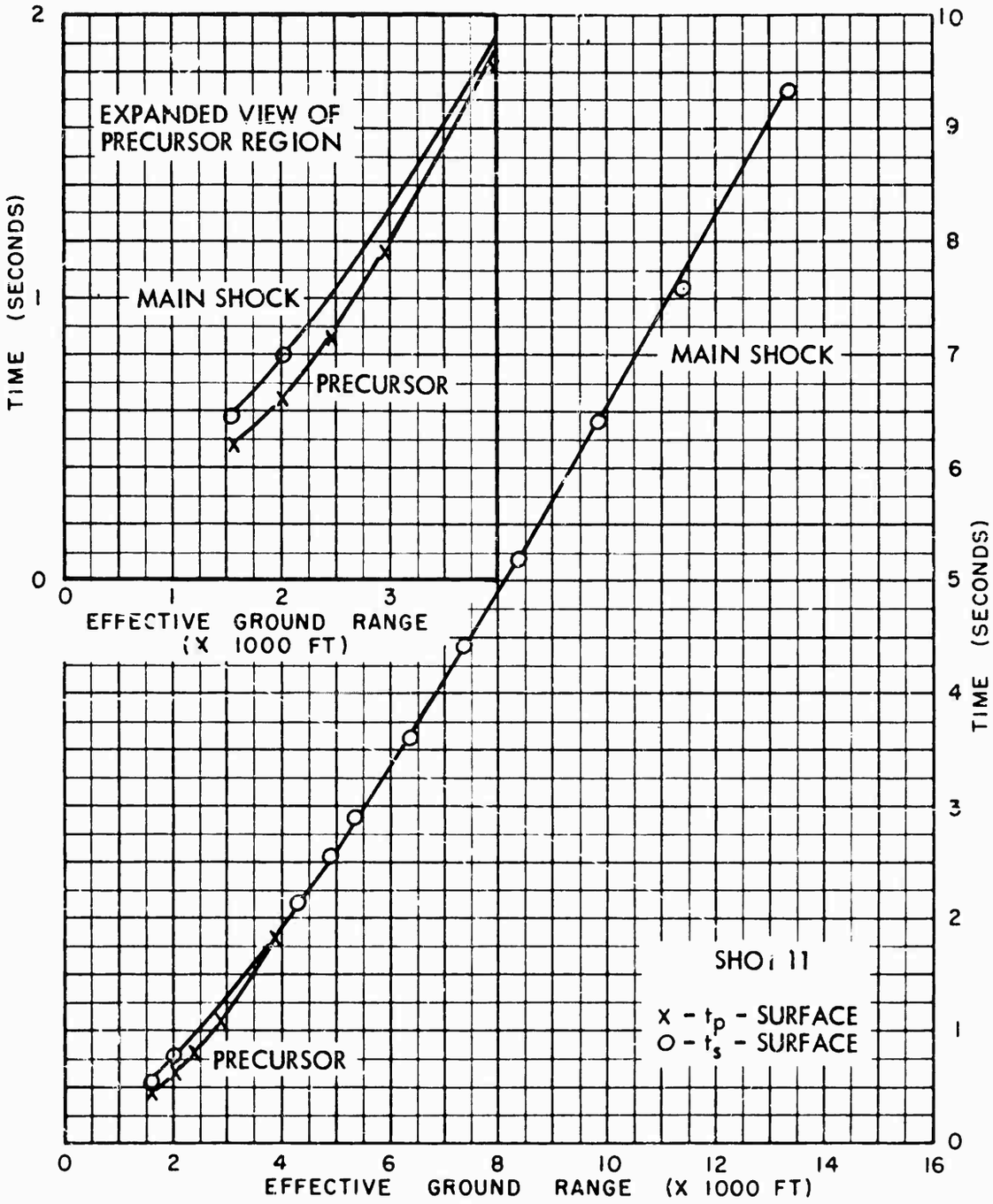

Fig. 4.18 Arrival Times at Surface Level, Precursor and Main Shock, Shot 11

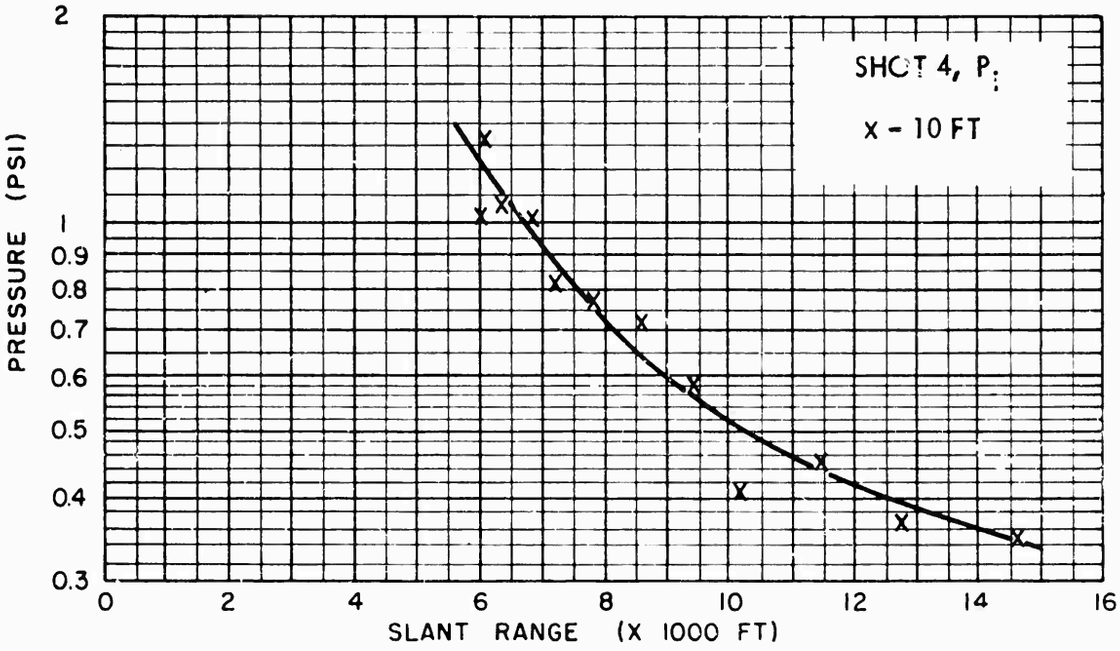

Fig. 4.19 Incident Air Pressure vs Slant Range, Shot 4

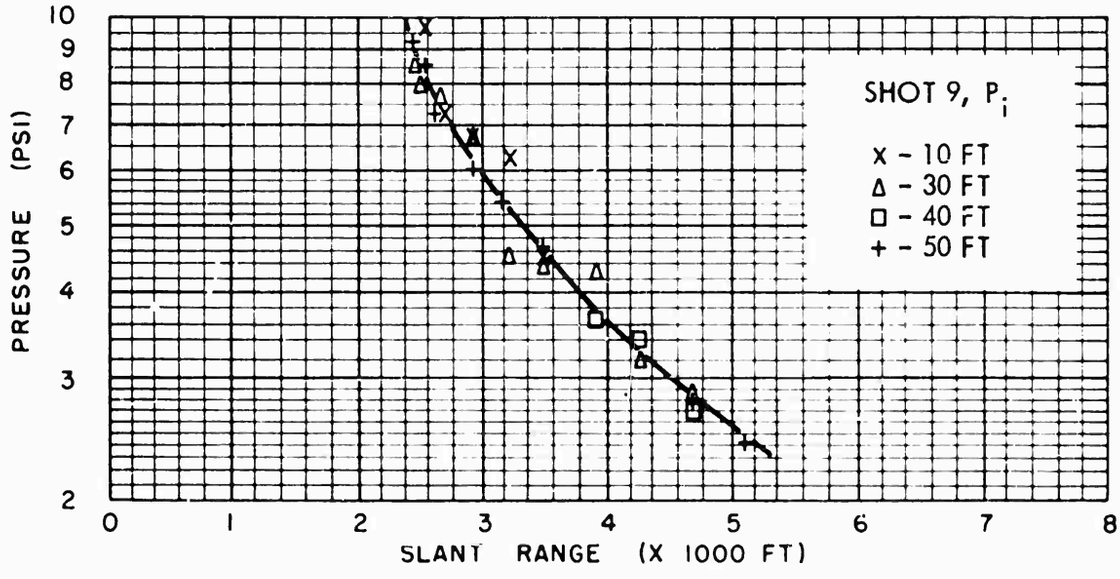

Fig. 4.20 Incident Air Pressure vs Slant Range, Shot 9

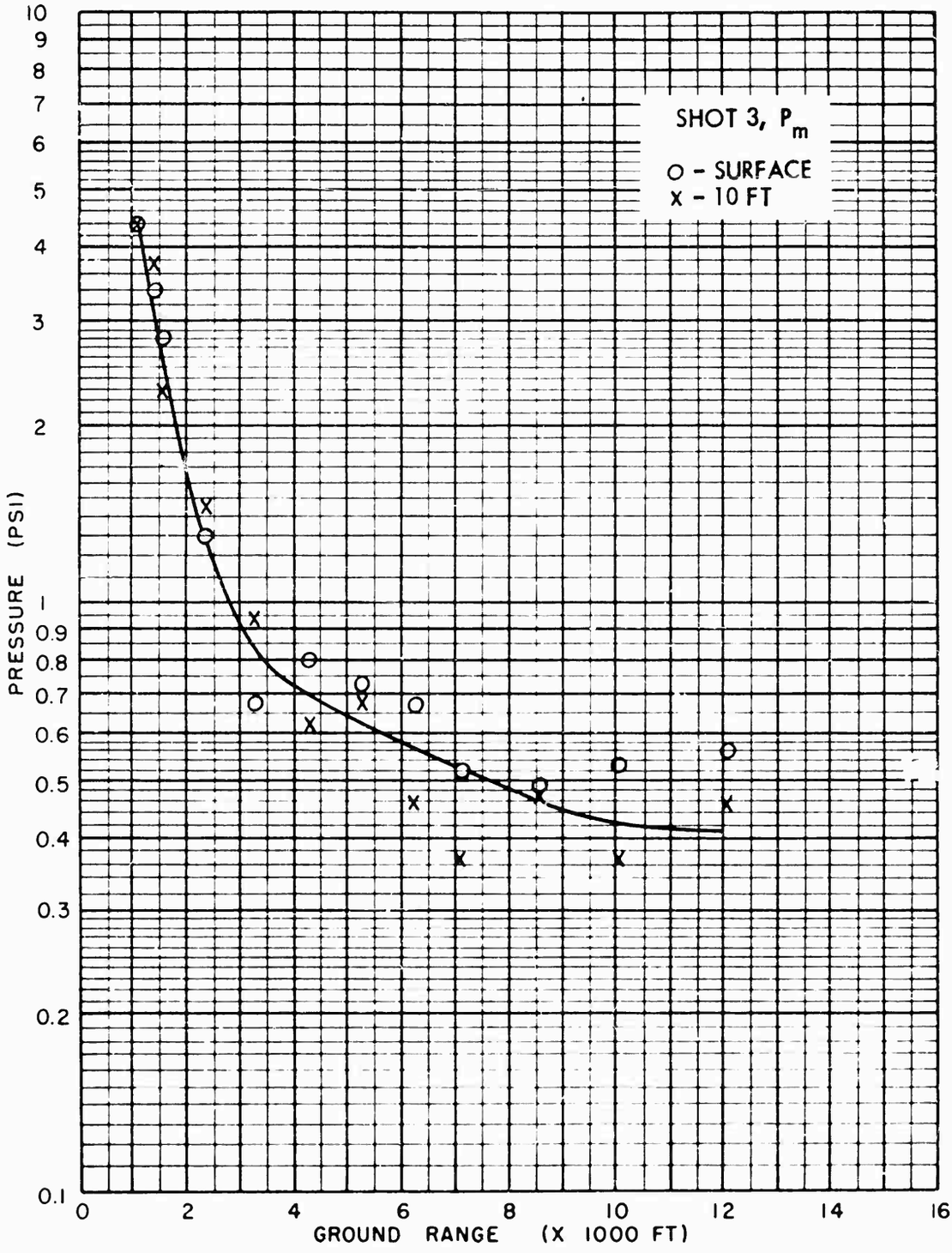

Fig. 4.21 Maximum Air Pressure, Shot 3

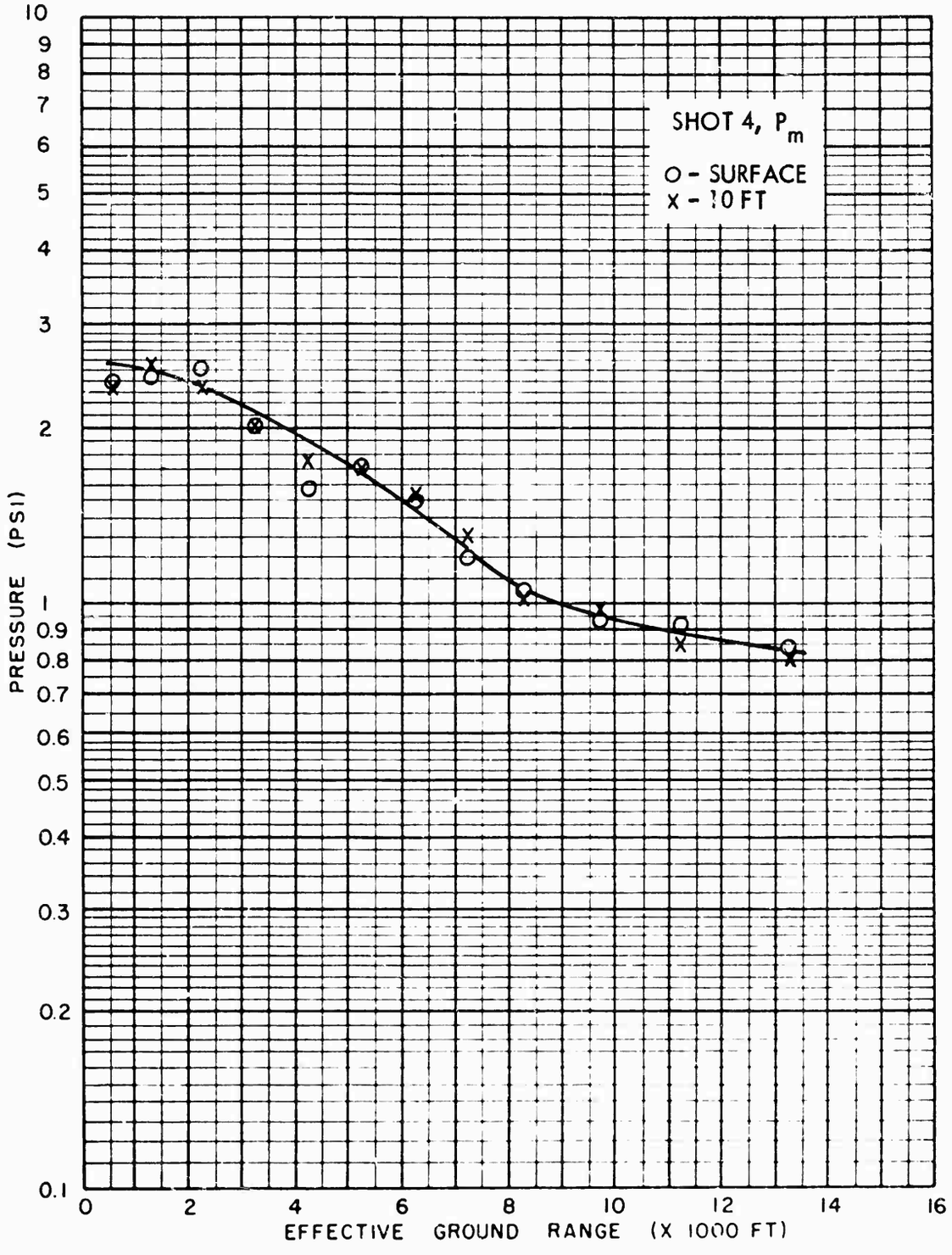

Fig. 4.22 Maximum Air Pressure, Shot 4

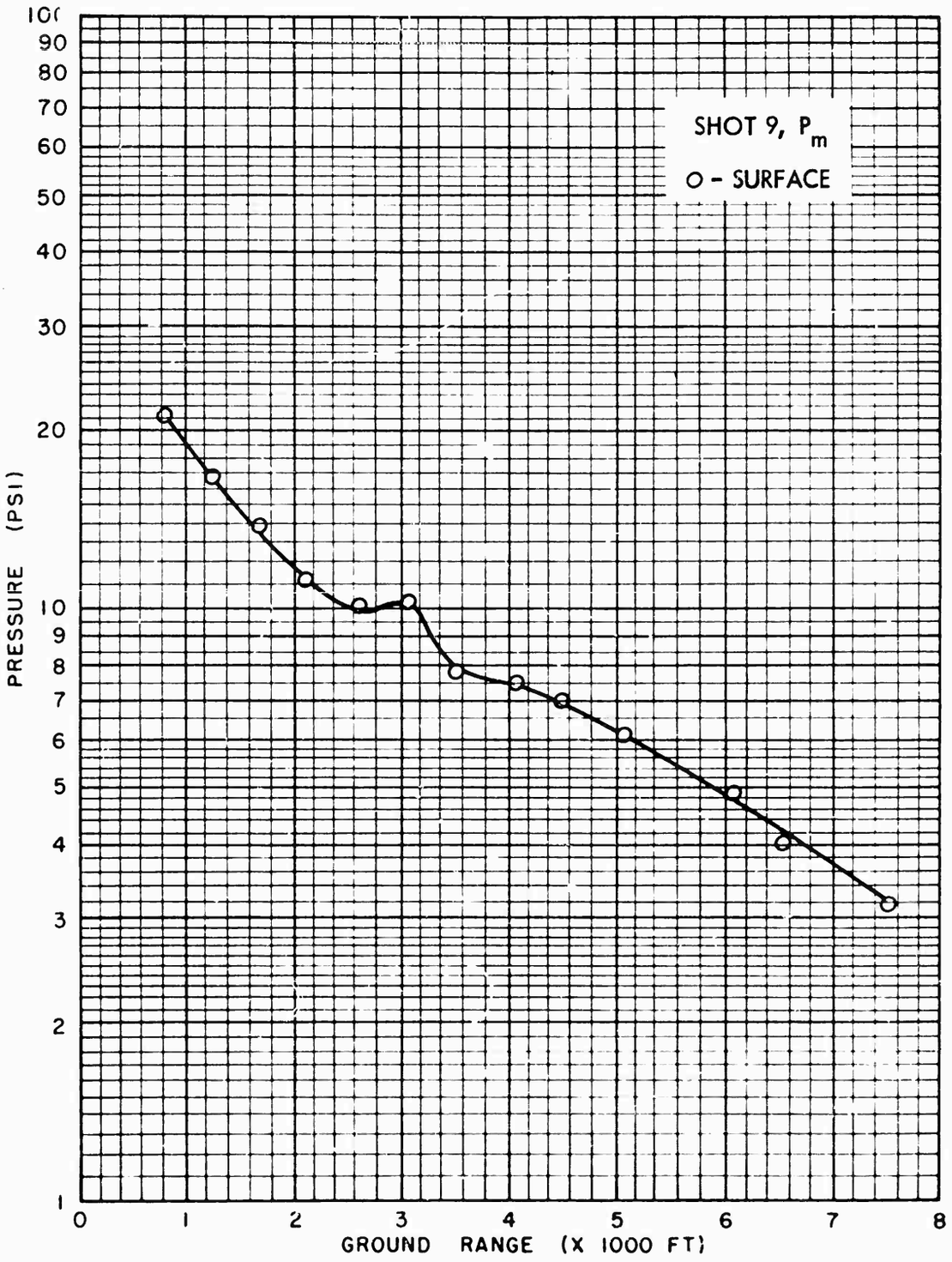

Fig. 4.23 Maximum Air Pressure, Shot 9, Surface Level

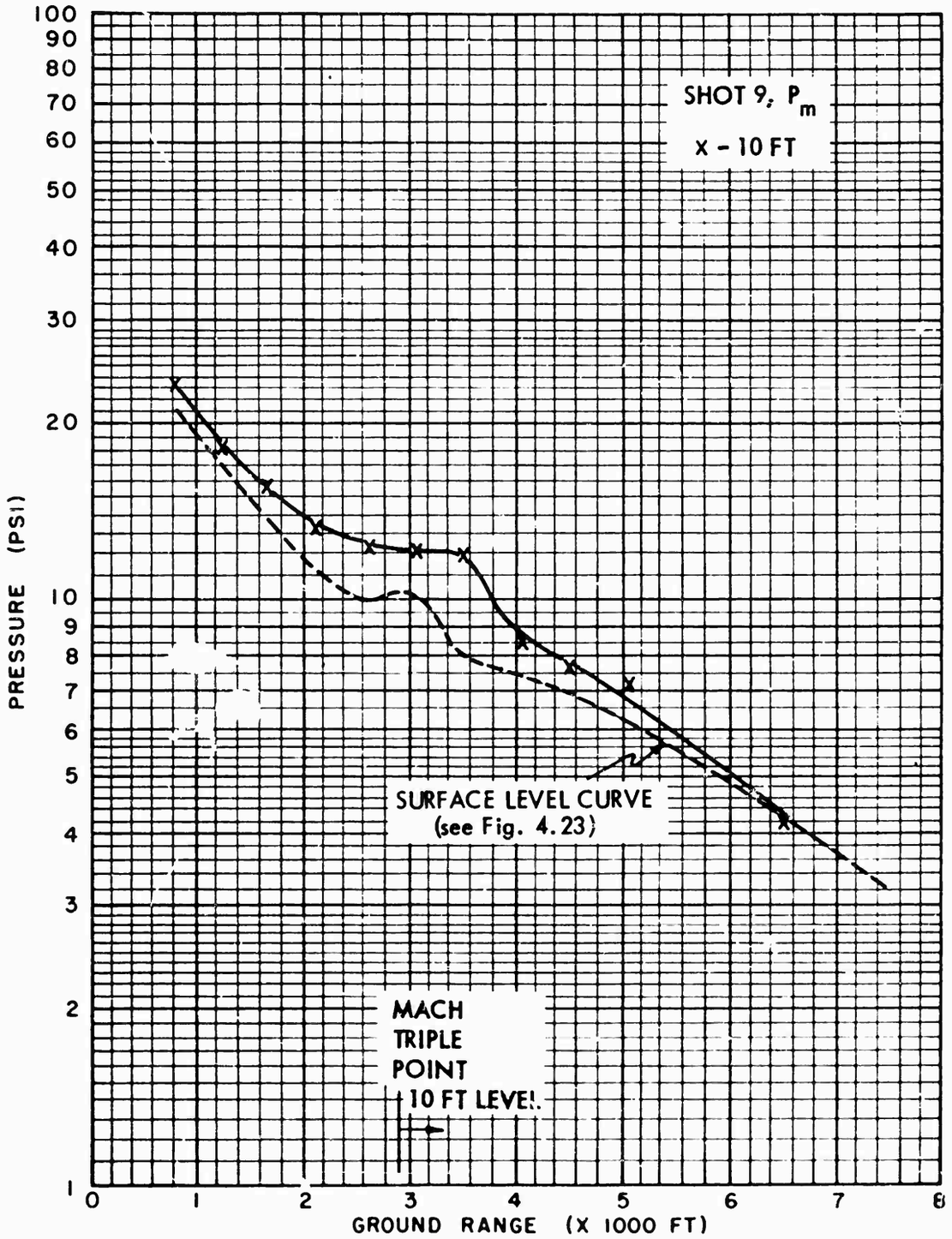

Fig. 4.24 Maximum Air Pressure, Shot 9, 10 ft Level

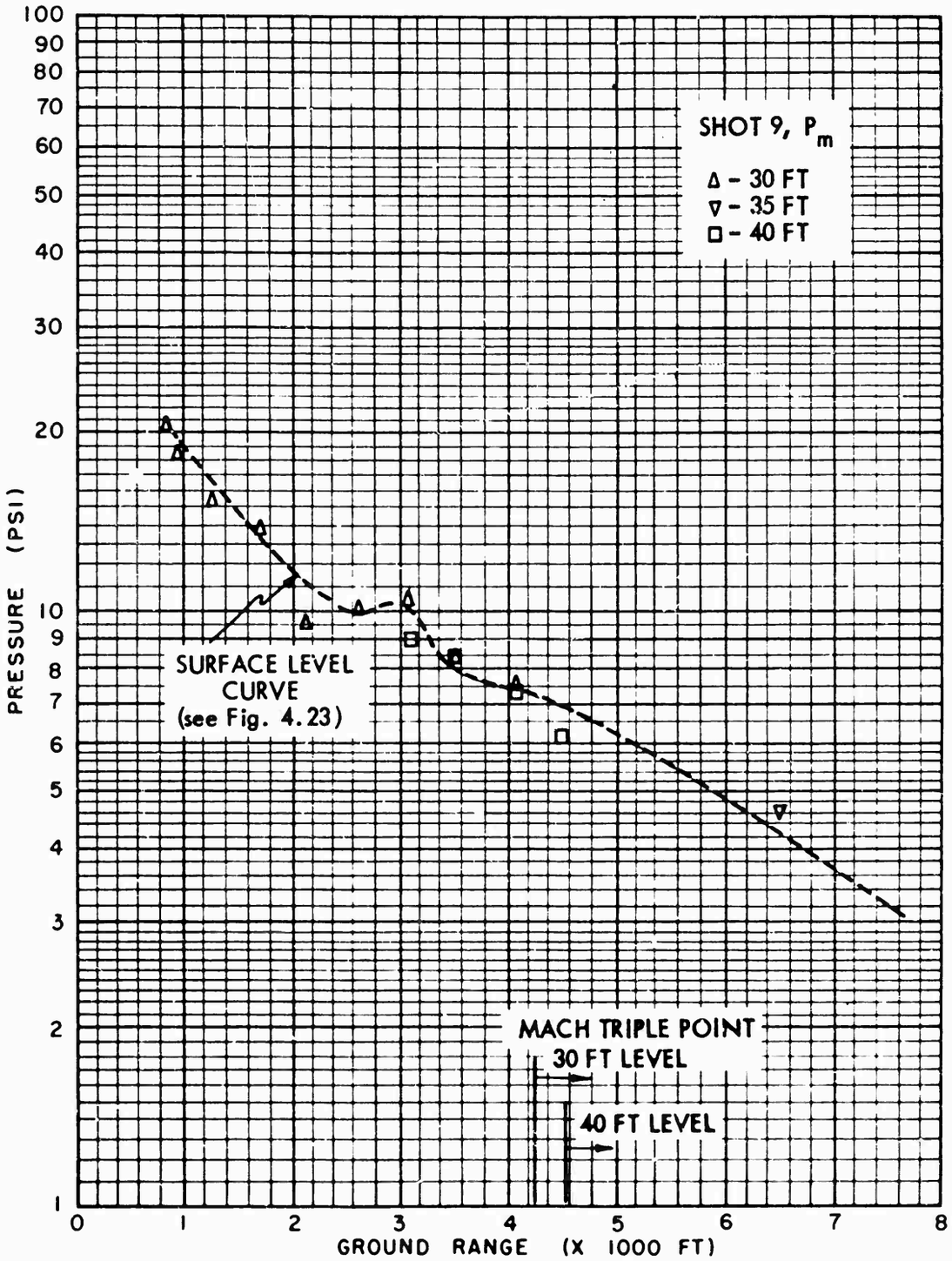

Fig. 4.25 Maximum Air Pressure, Shot 9; 30, 35, and 40 ft Levels

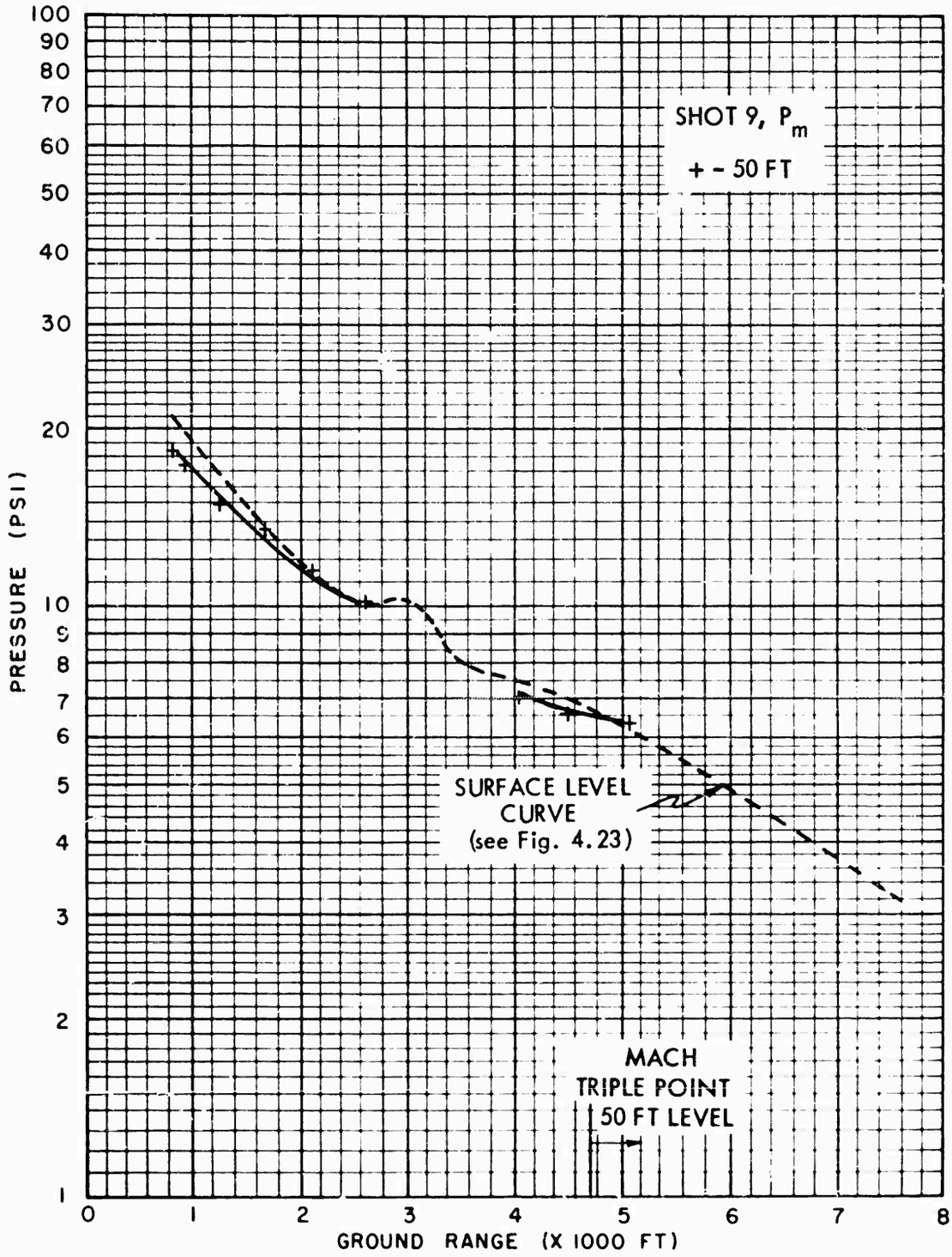

Fig. 4.26 Maximum Air Pressure, Shot 9, 50 ft Level

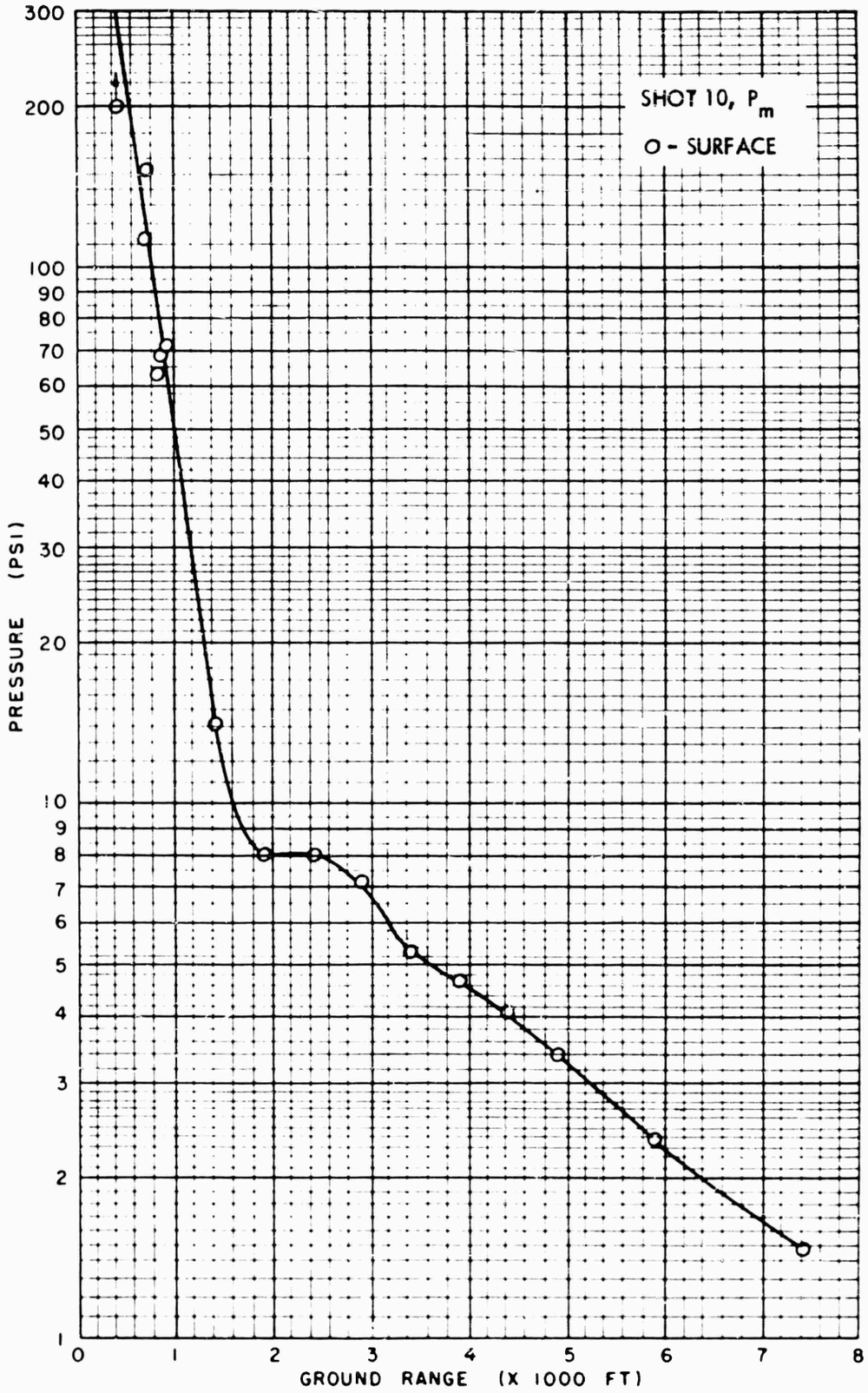

Fig. 4.27 Maximum Air Pressure, Shot 10, Surface Level

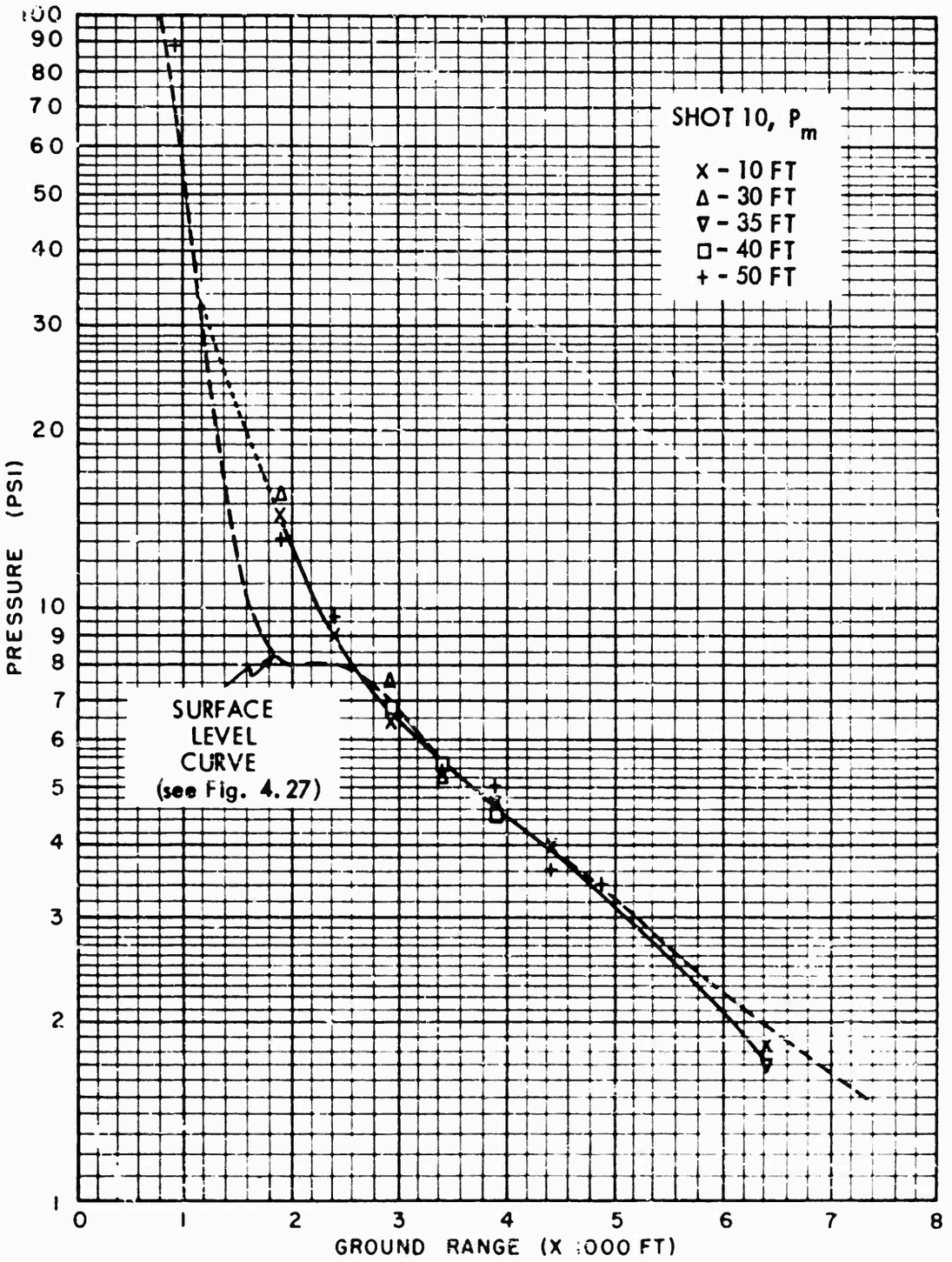

Fig. 4.28 Maximum Air Pressure, Shot 10, Aboveground Levels

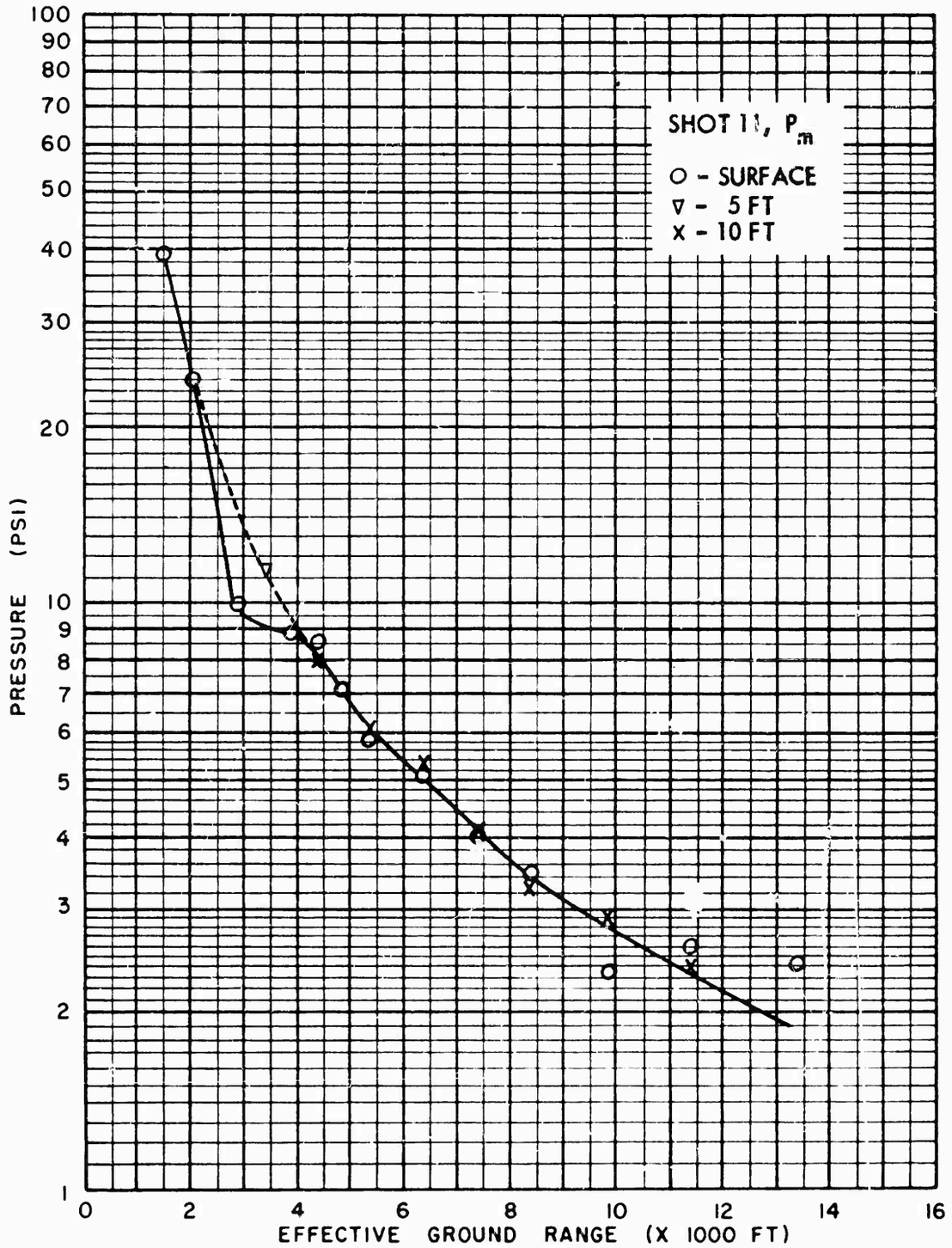

Fig. 4.29 Maximum Air Pressure, Shot 11, Surface and 10 ft Levels

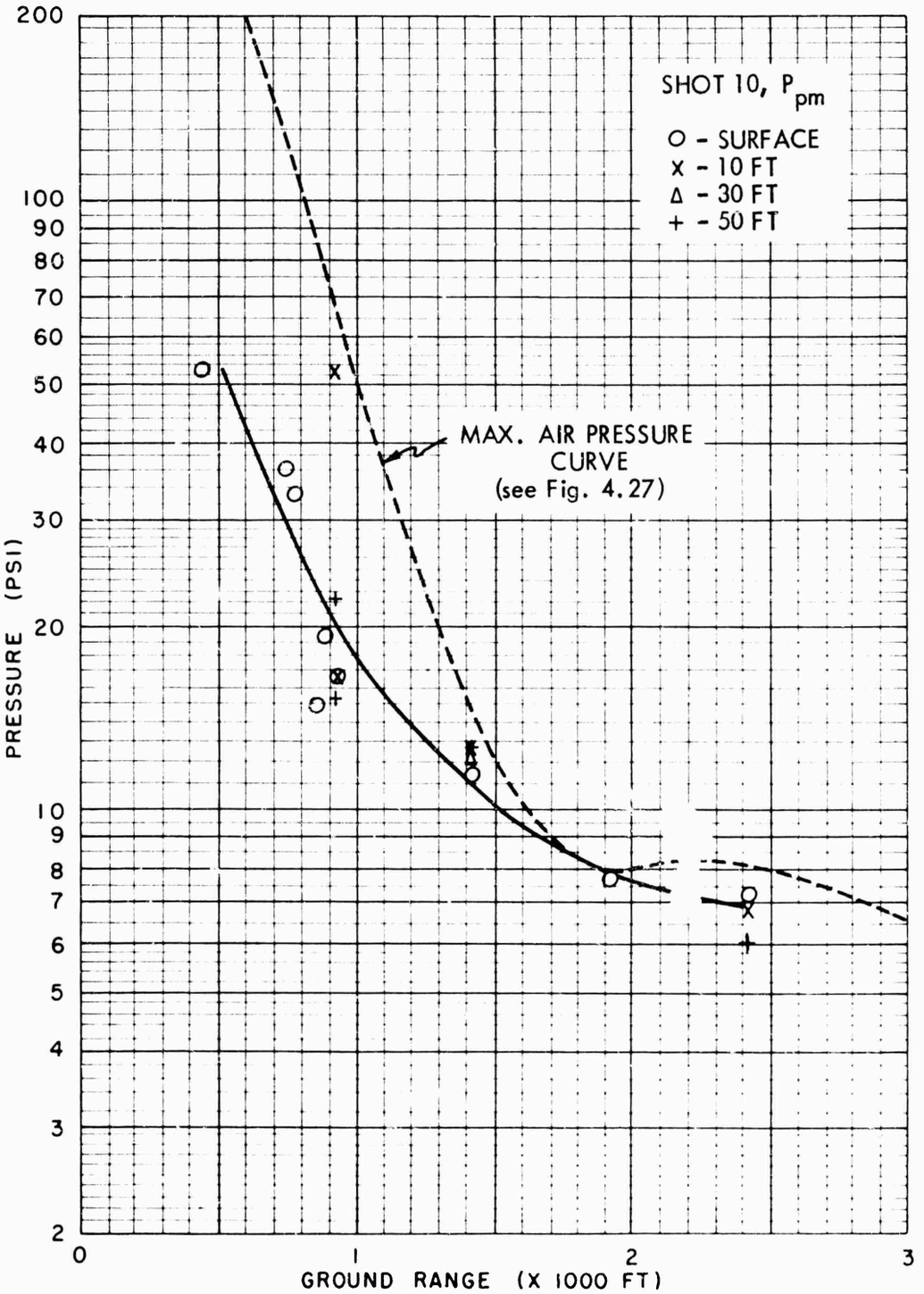

Fig. 4.30 Maximum Precursor Air Pressure, Shot 10

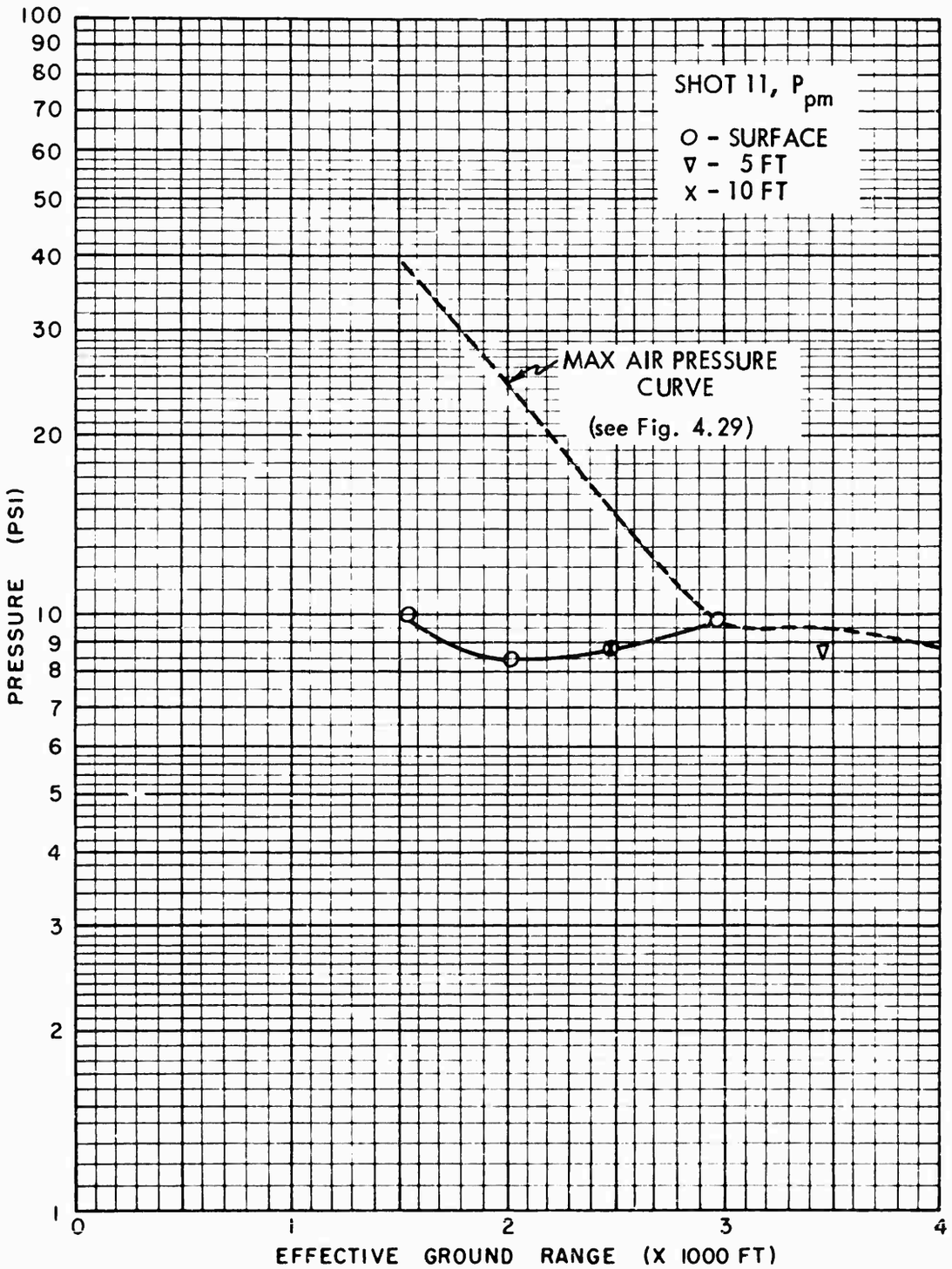

Fig. 4.31 Maximum Precursor Air Pressure, Shot 11

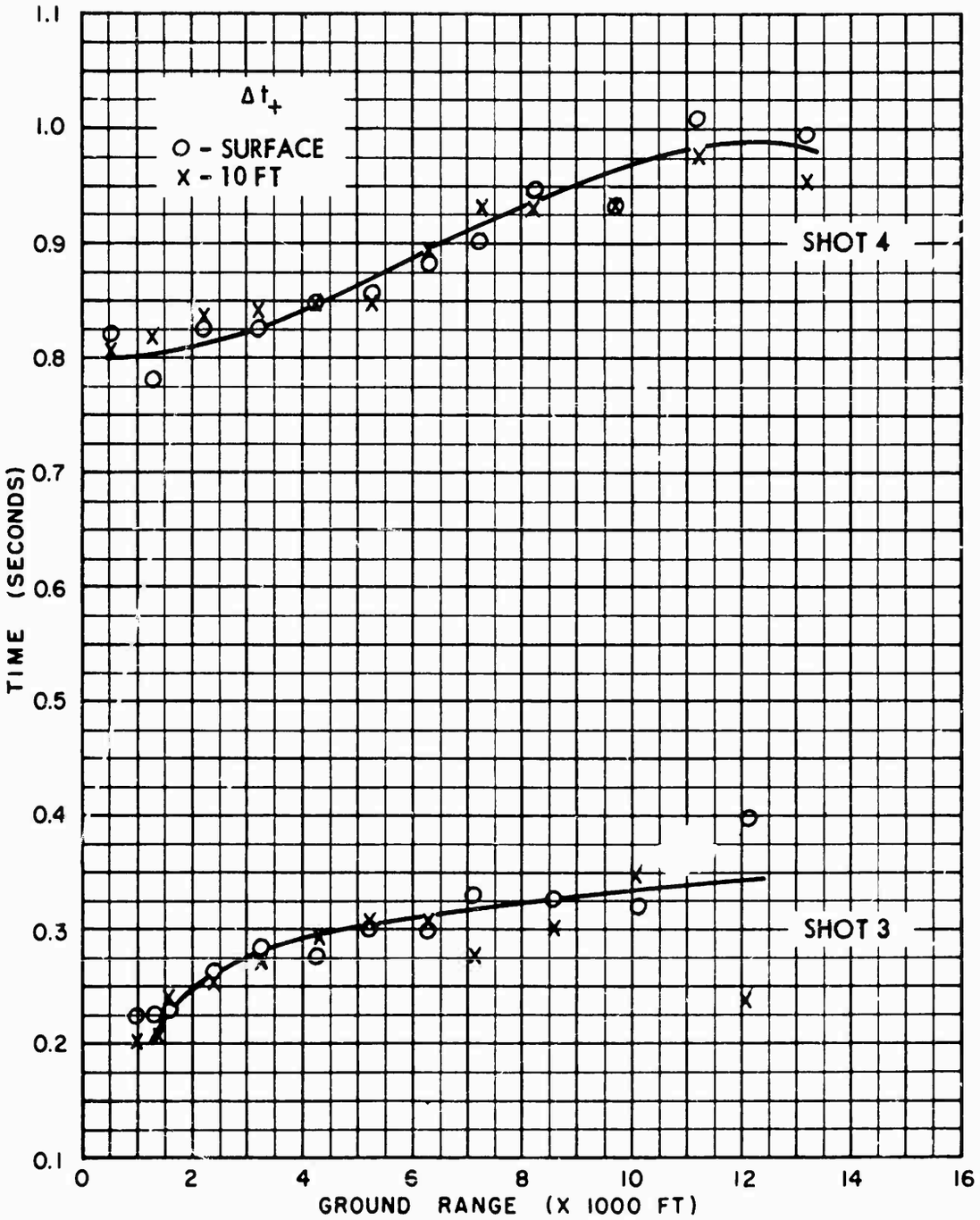

Fig. 4.32 Positive Phase Duration, Shots 3 and 4

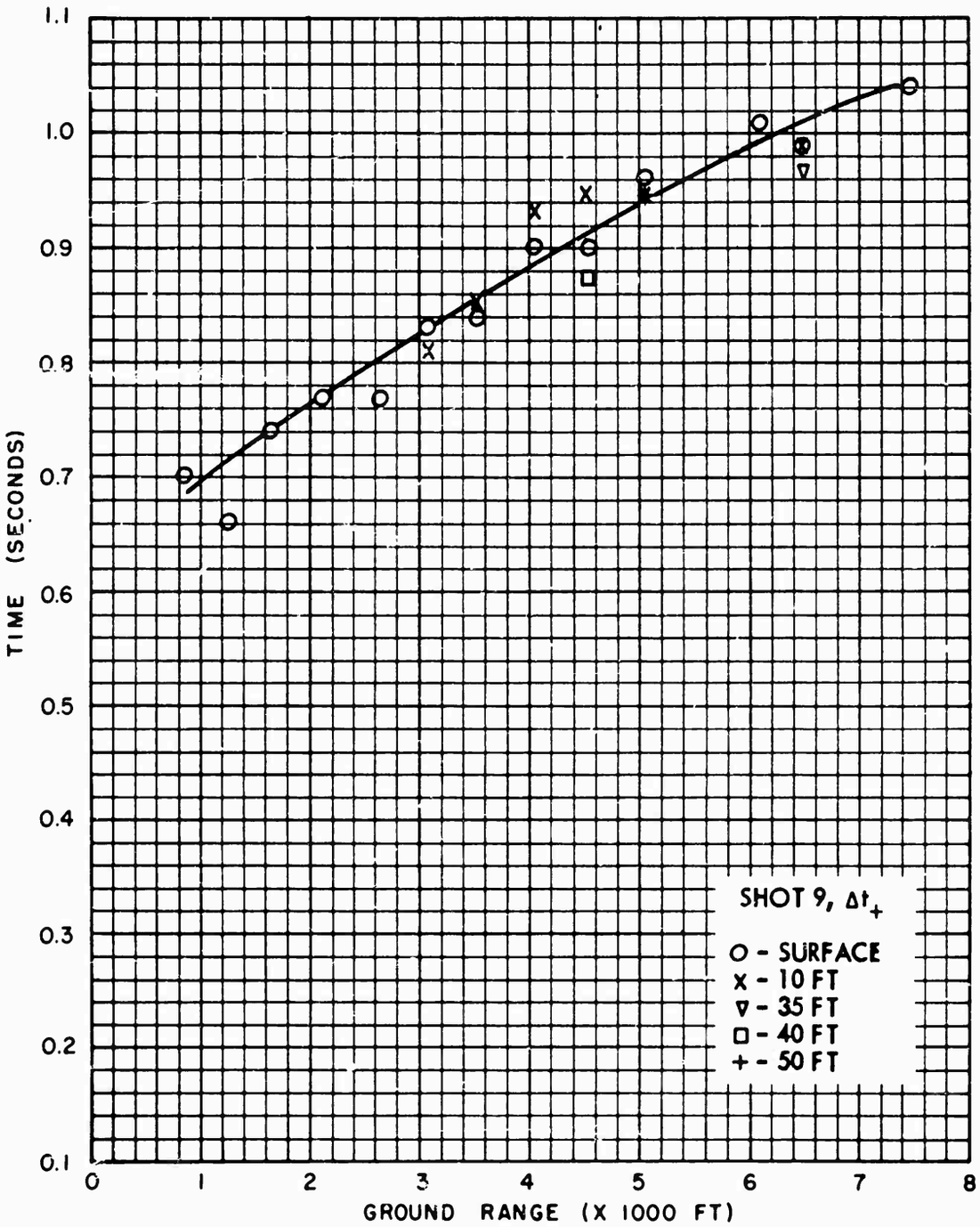

Fig. 4.33 Positive Phase Duration, Shot 9

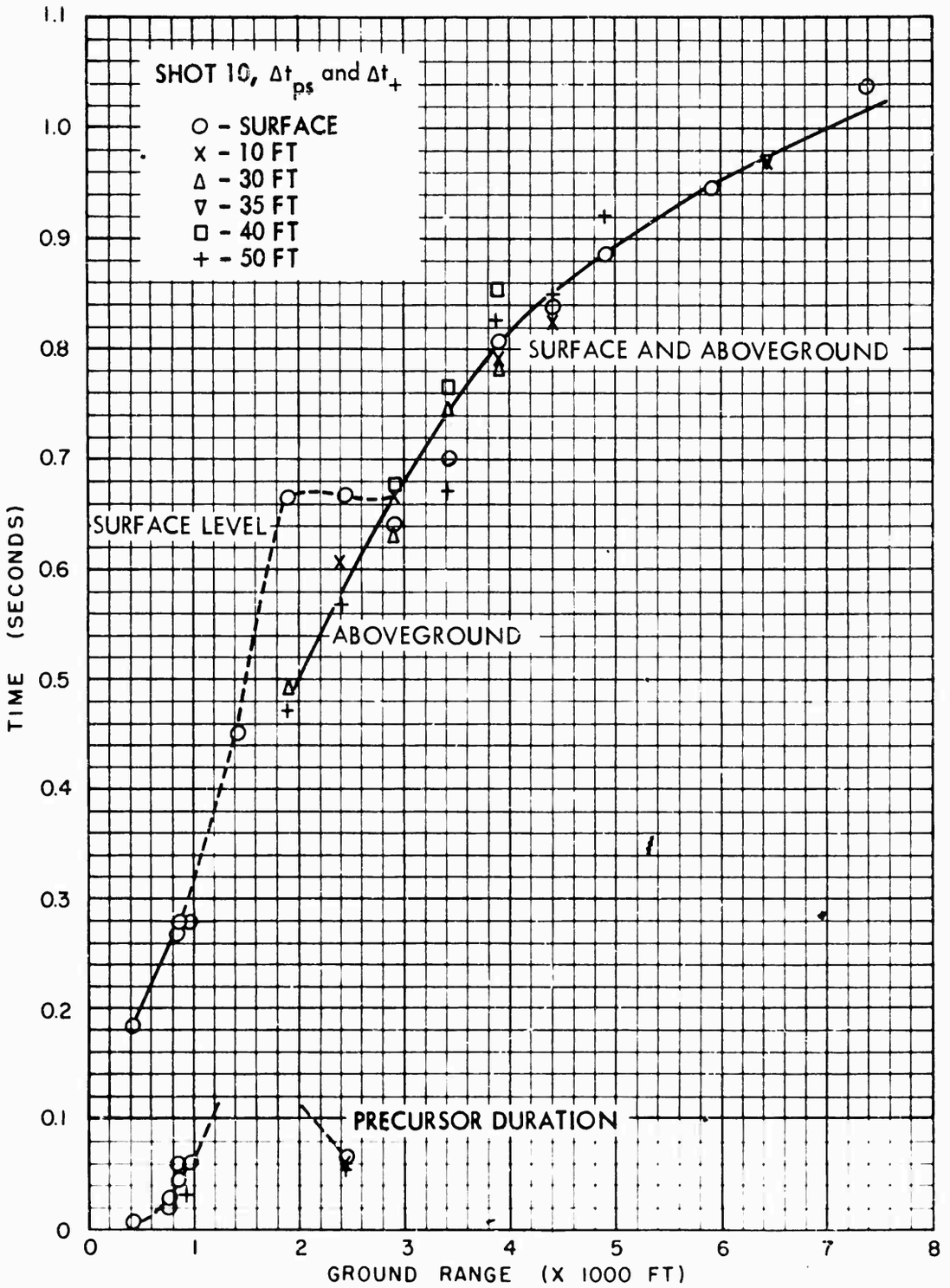

Fig. 4.34 Precursor and Positive Phase Duration, Shot 10

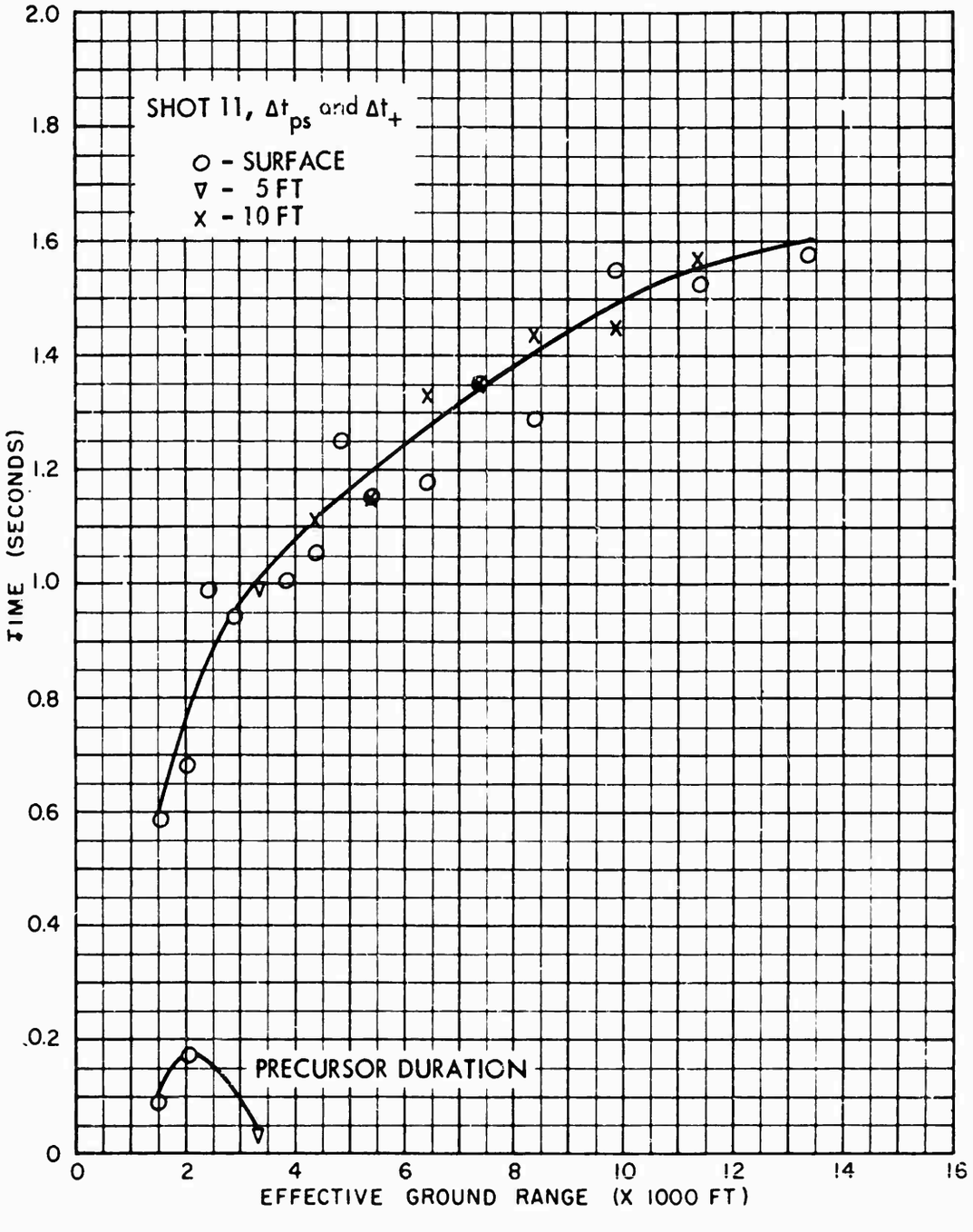

Fig. 4.35 Precursor and Positive Phase Duration, Shot 11

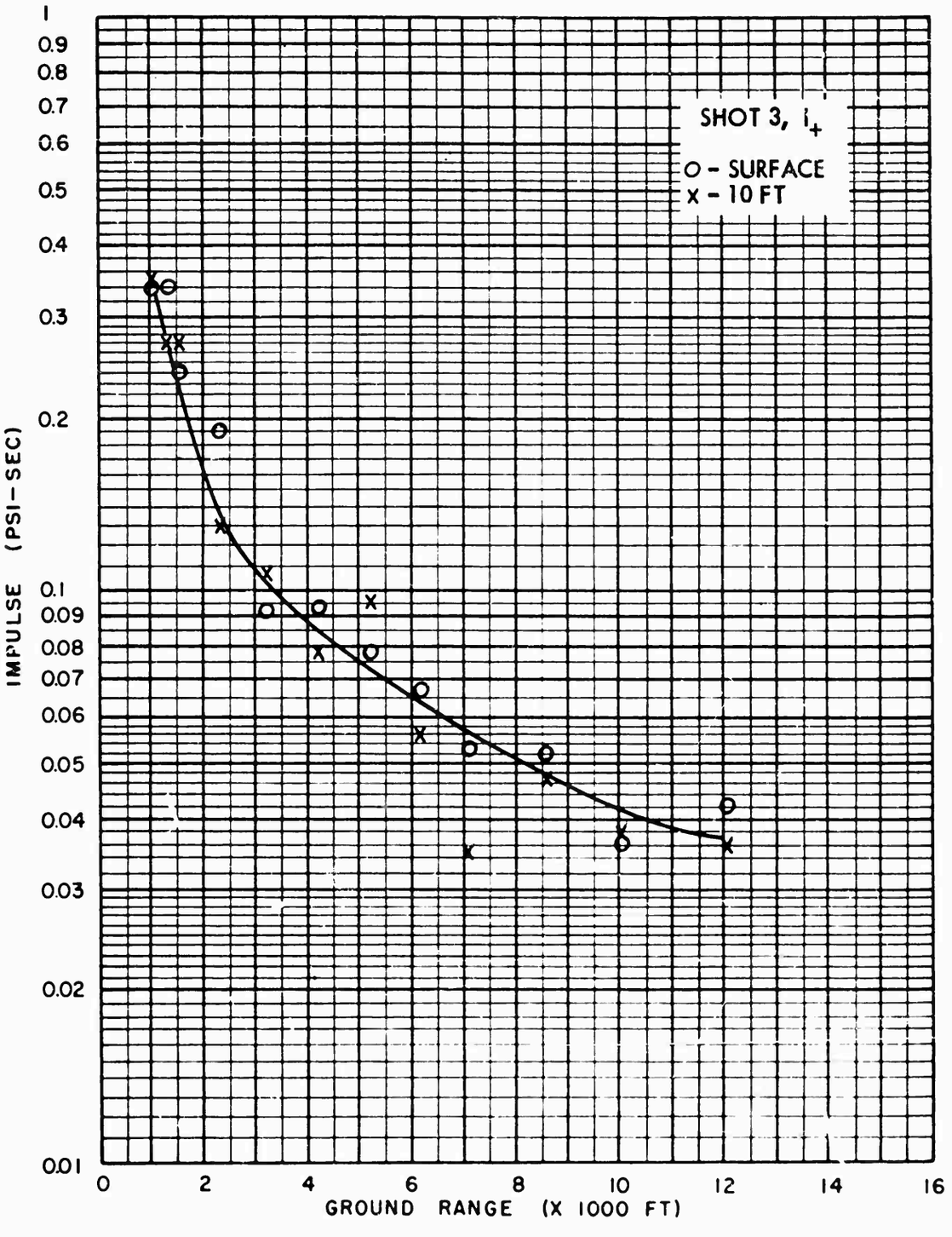

Fig. 4.36 Positive Impulse, Shot 3

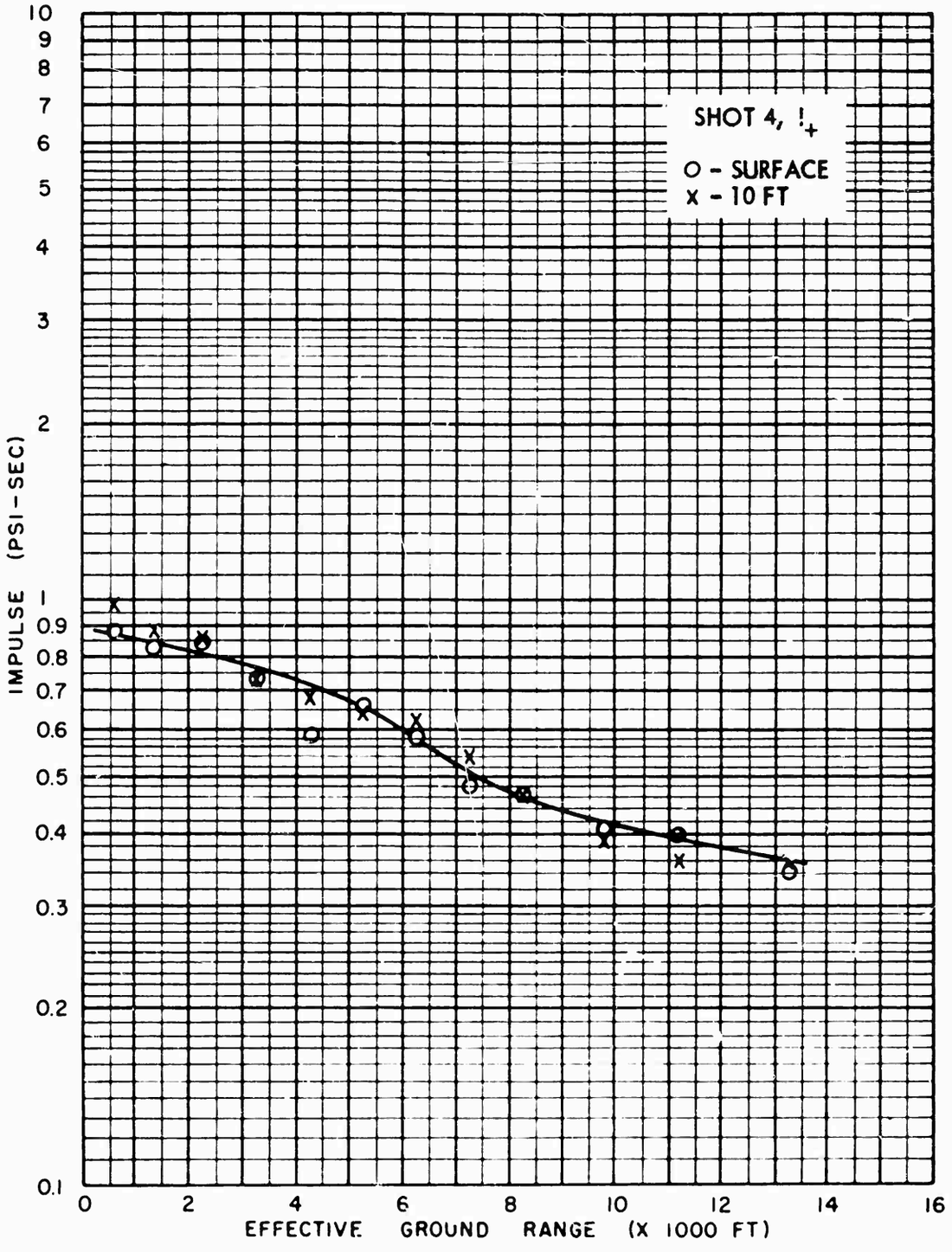

Fig. 4.37 Positive Impulse, Shot 4

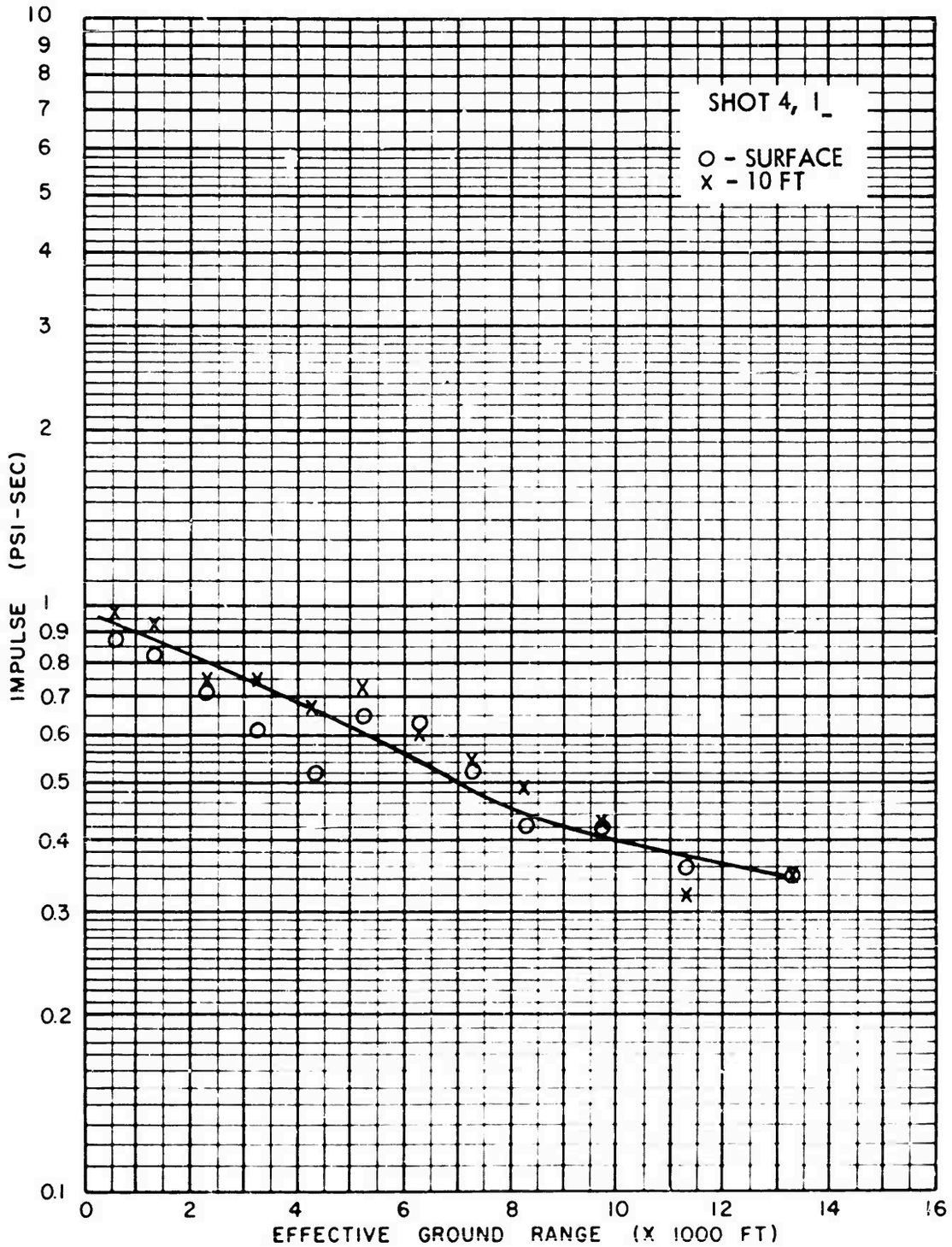

Fig. 4.38 Negative Impulse, Shot 4

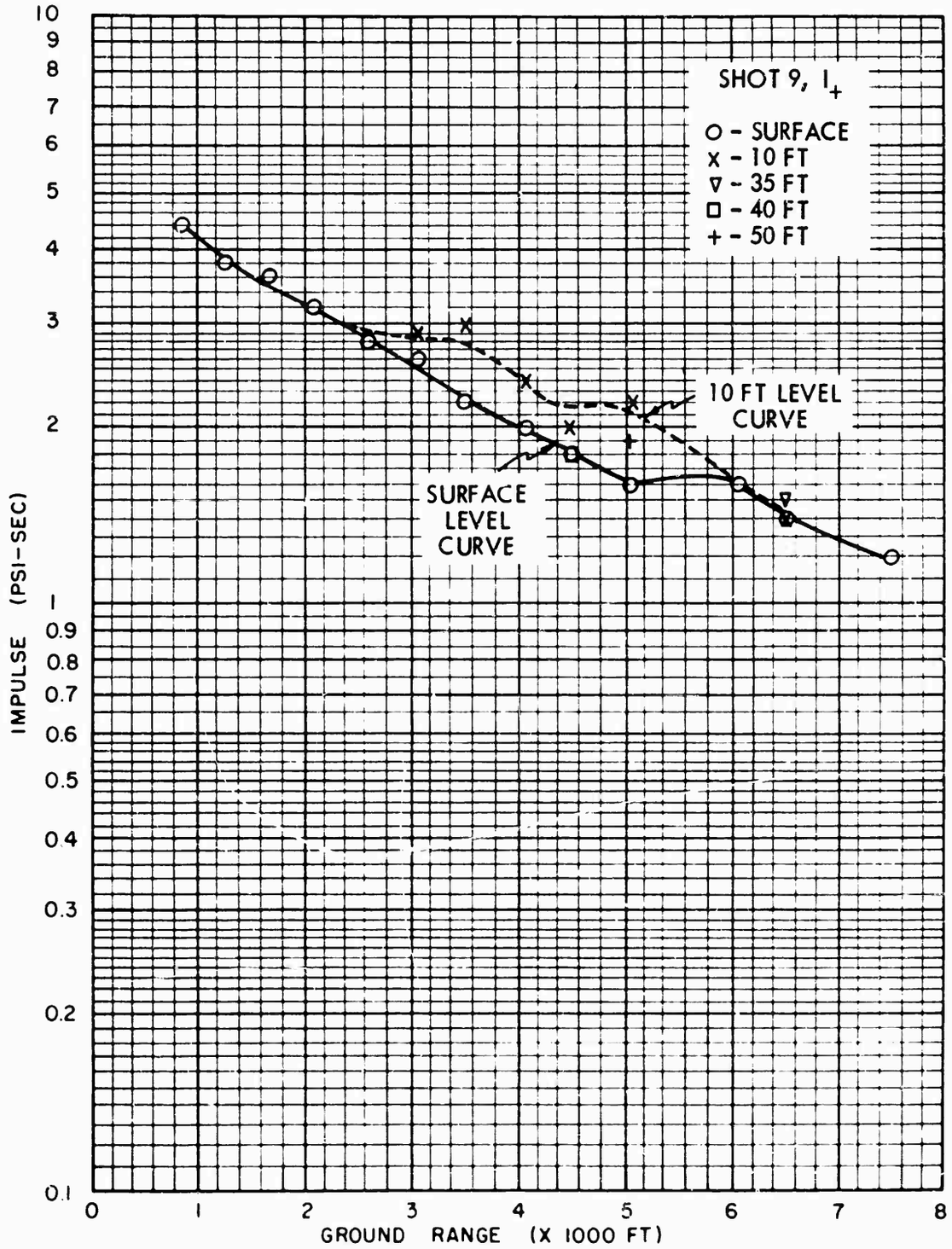

Fig. 4.39 Positive Impulse, Shot 9

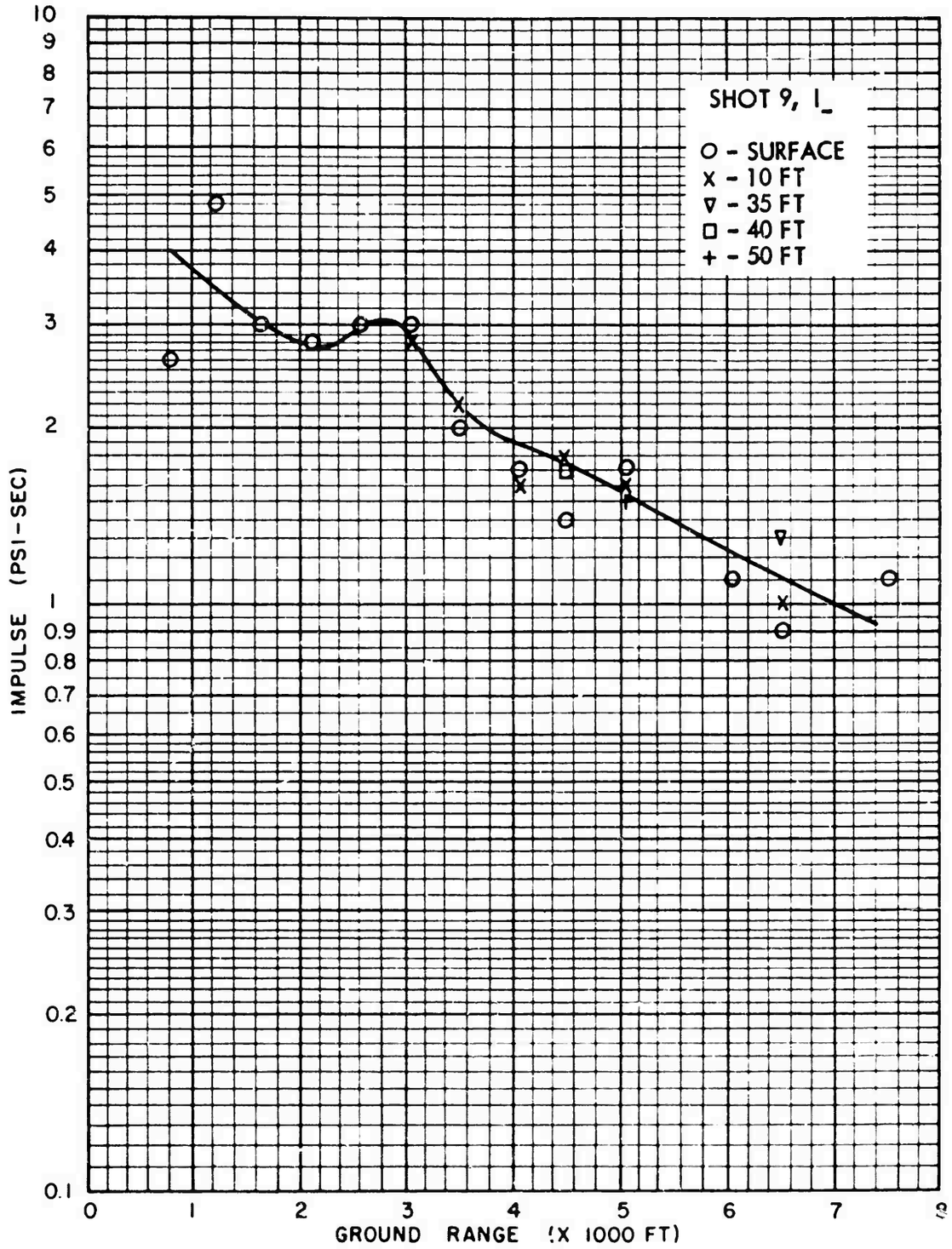

Fig. 4.40 Negative Impulse, Shot 9

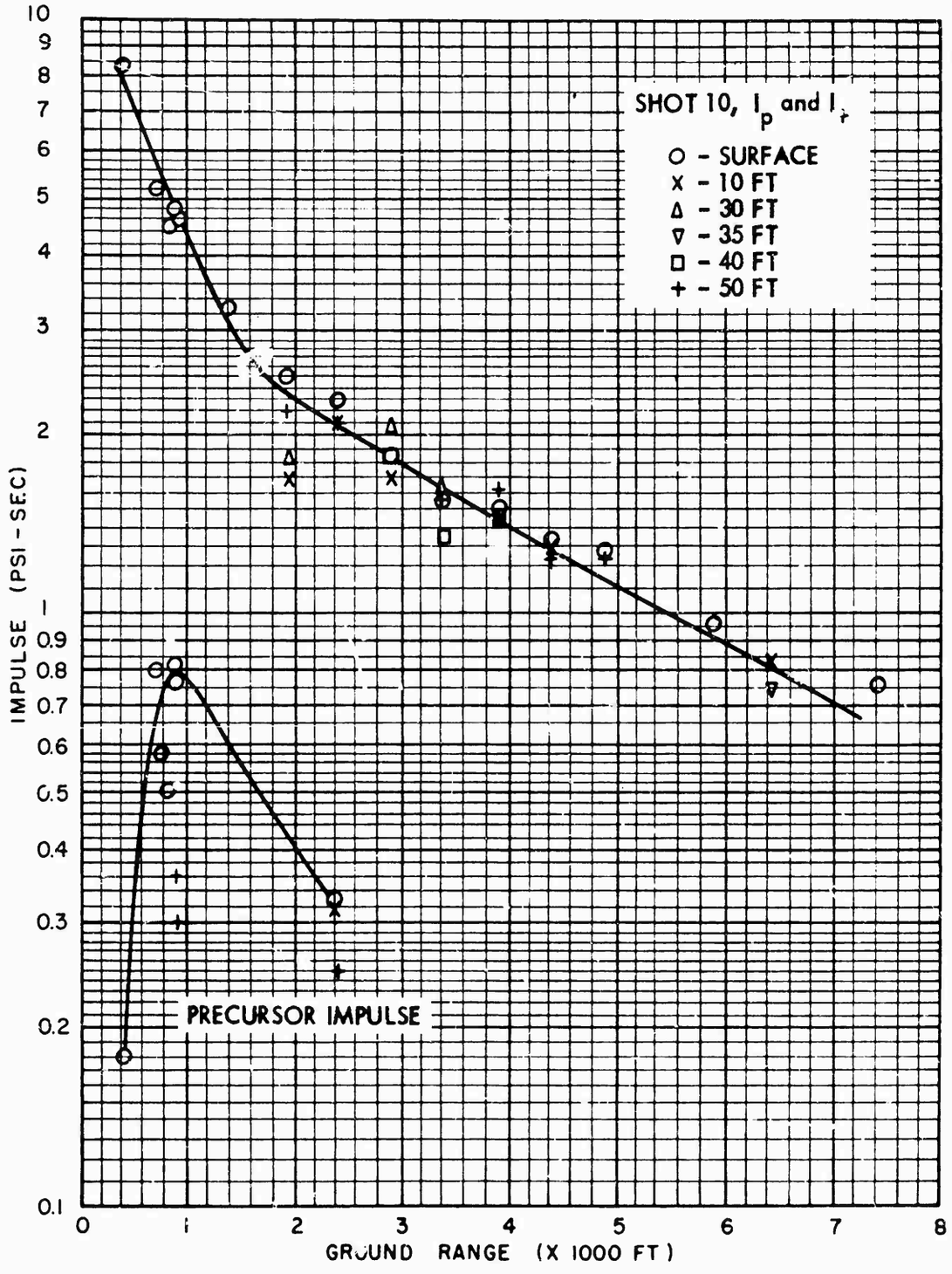

Fig. 4.41 Precursor and Positive Impulse, Shot 10

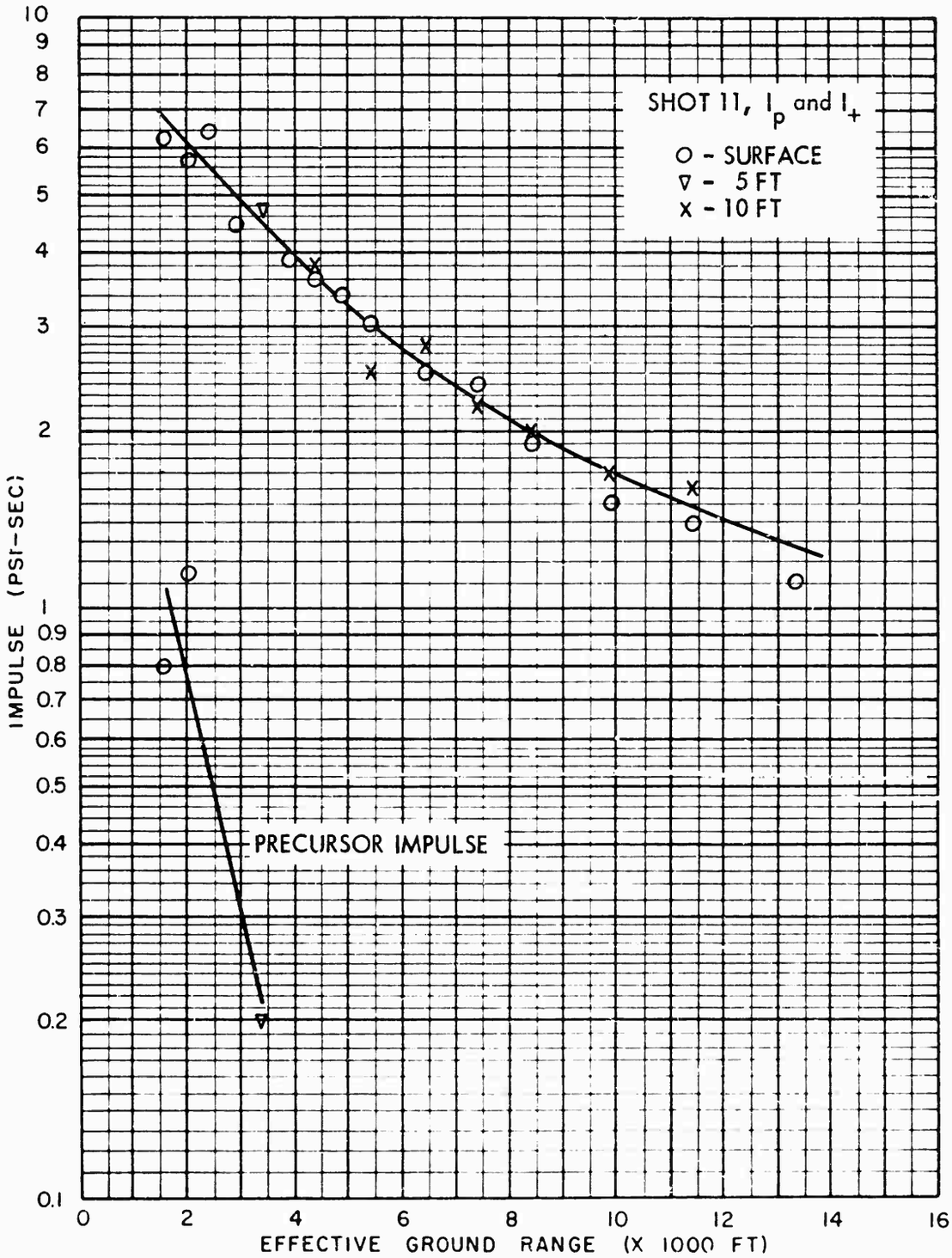

Fig. 4.42 Precursor and Positive Impulse, Shot 11

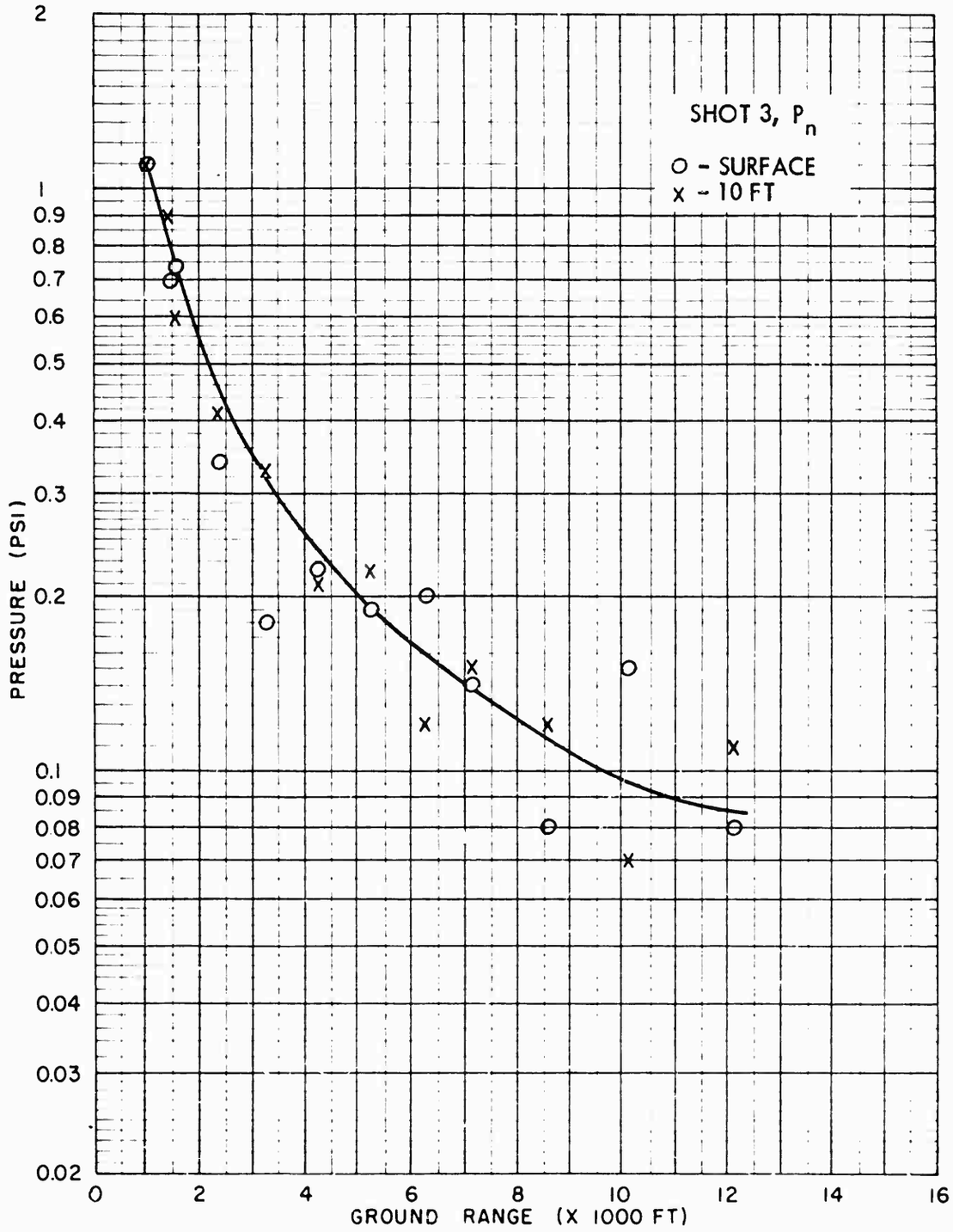

Fig. 4.43 Maximum Negative Air Pressure, Shot 3

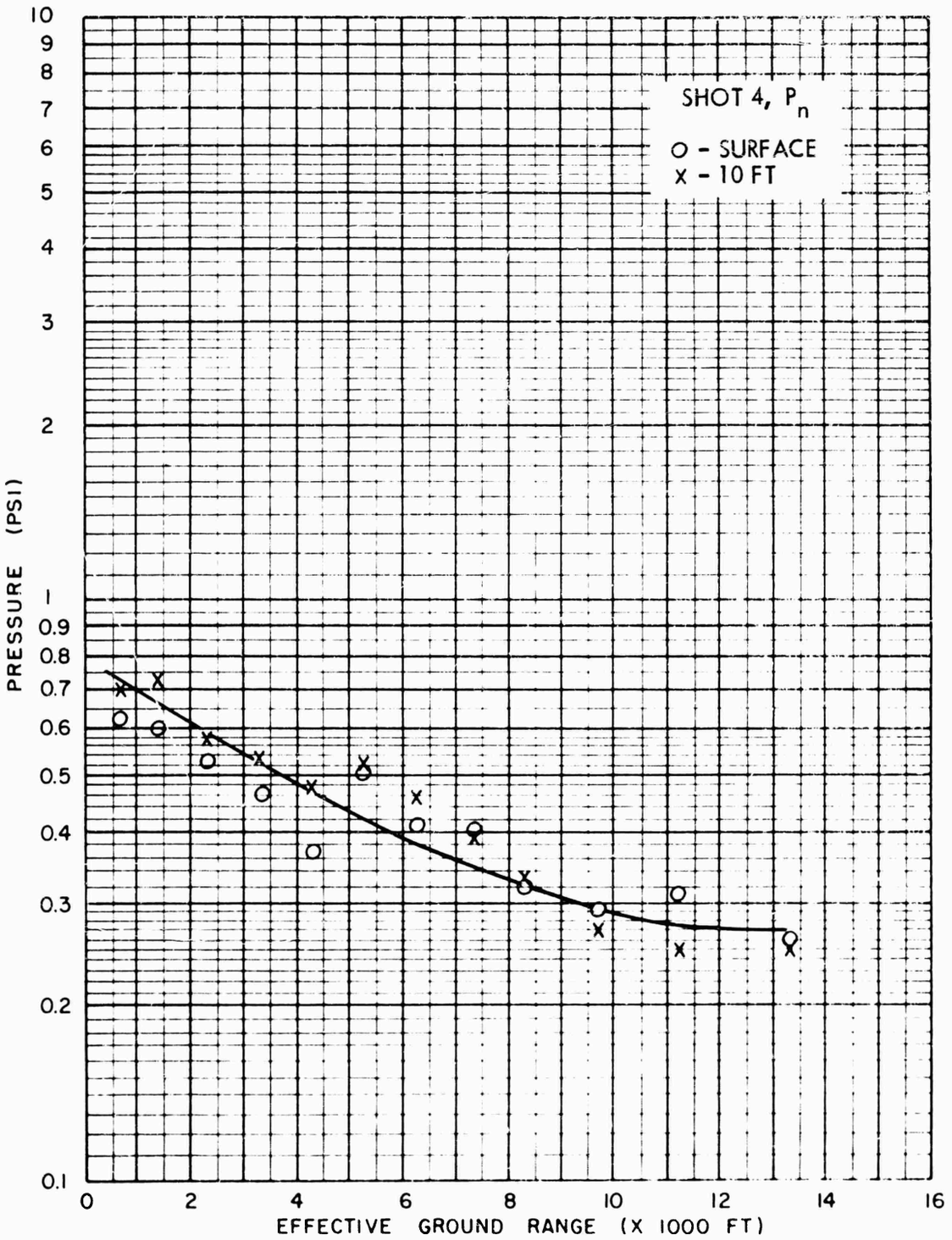

Fig. 4.44 Maximum Negative Air Pressure, Shot 4

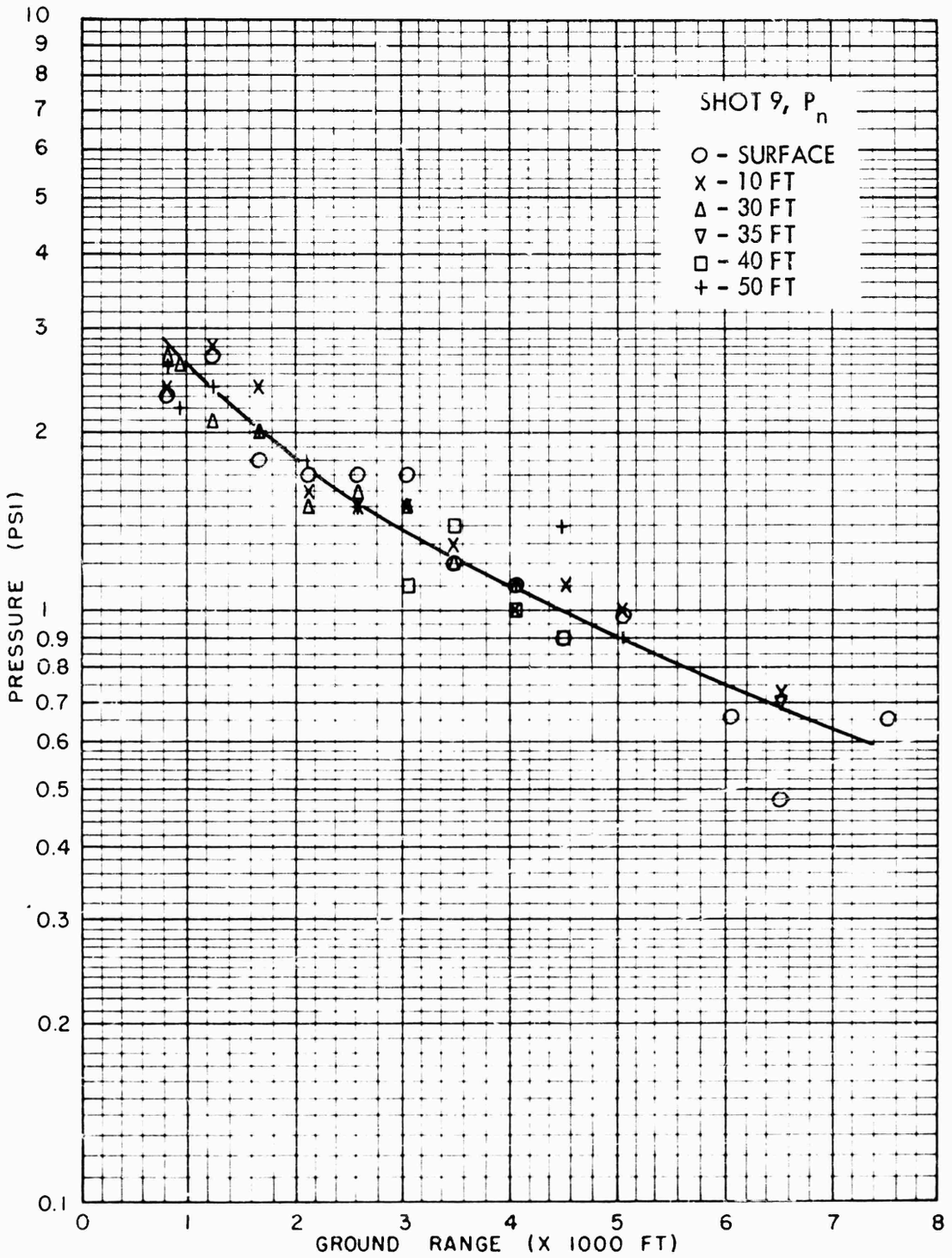

Fig. 4.45 Maximum Negative Air Pressure, Shot 9

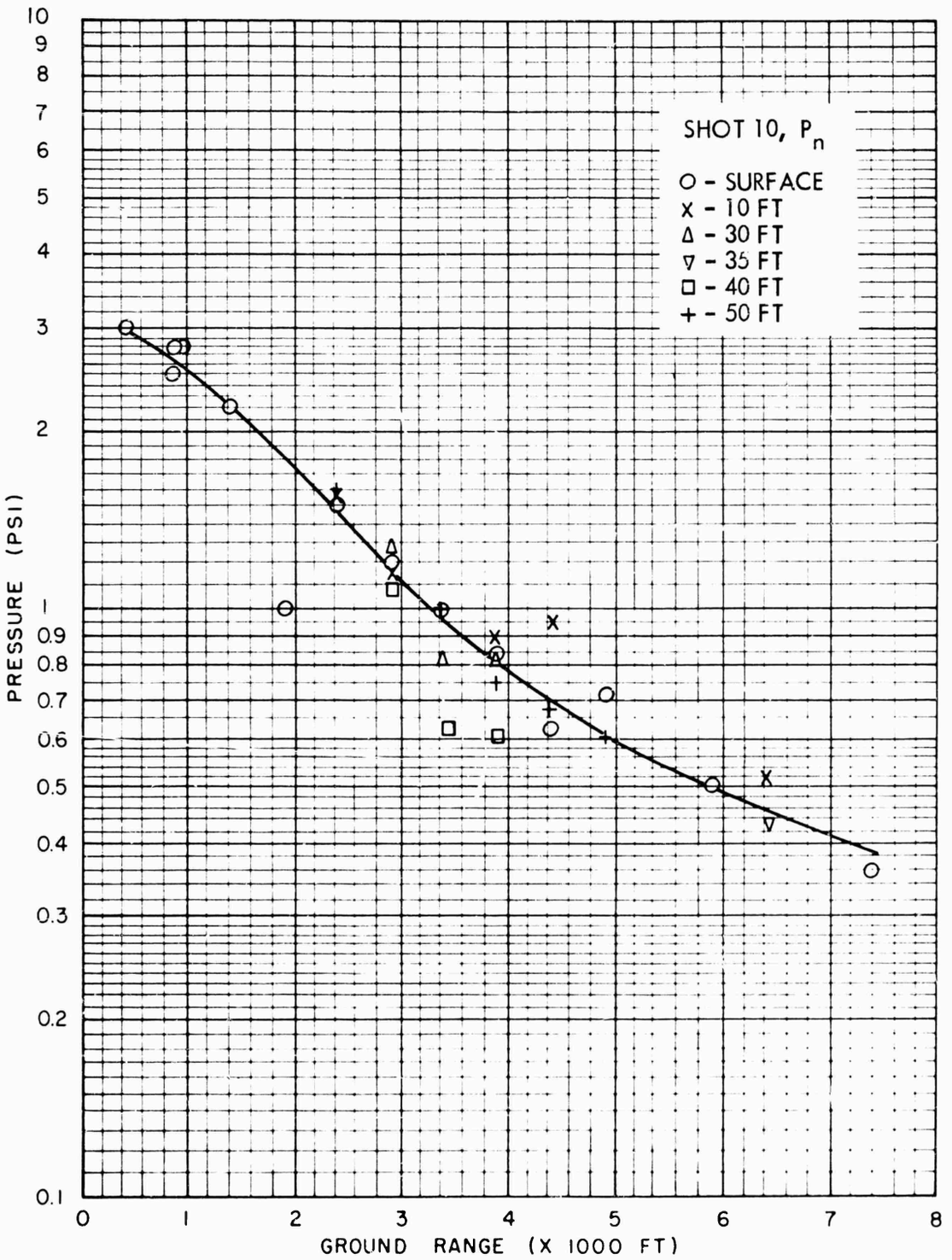

Fig. 4.46 Maximum Negative Air Pressure, Shot 10

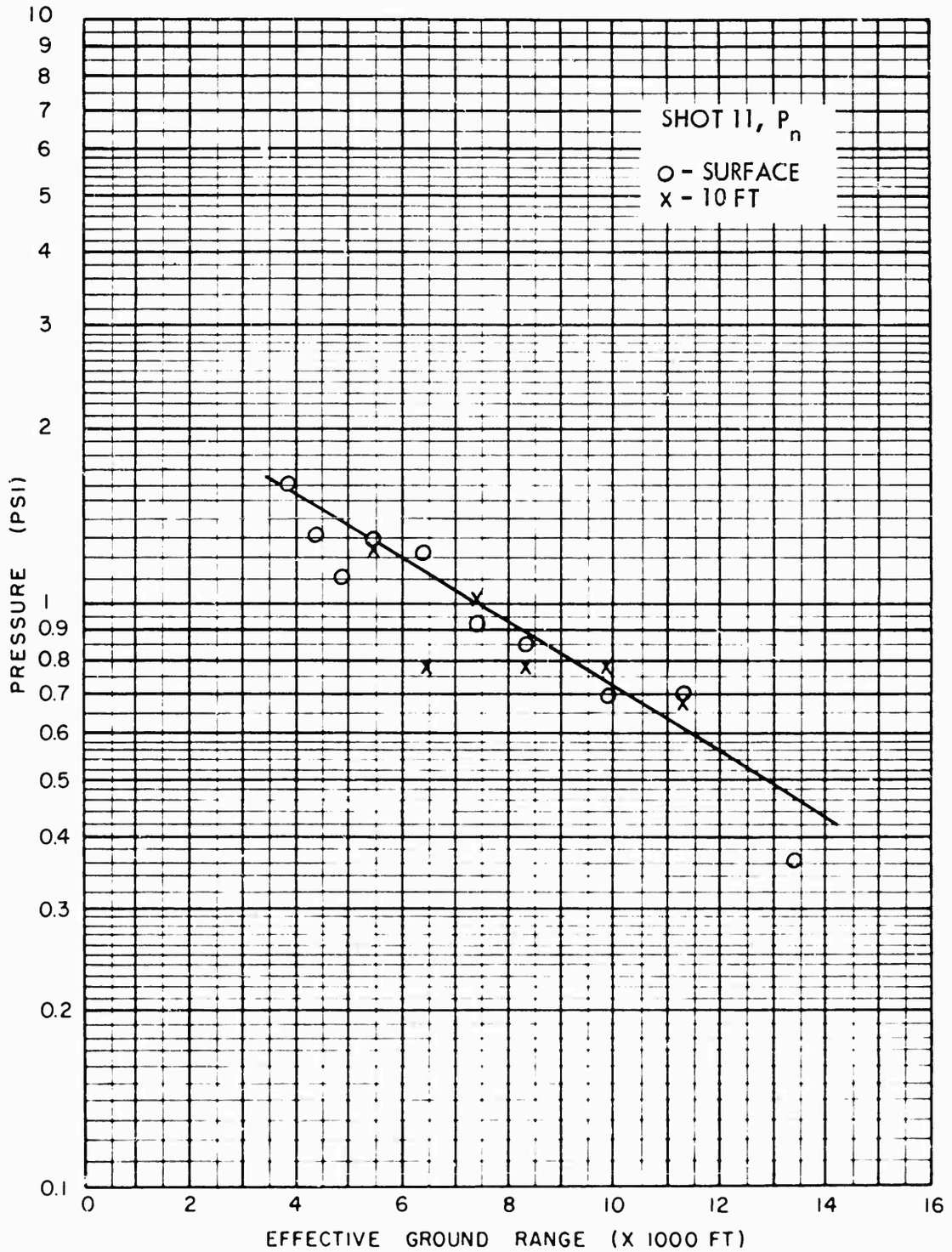

Fig. 4.47 Maximum Negative Air Pressure, Shot 11

4.5.2 Incident Free Air Pressure

Incident pressures could be measured only on Shot 4 and on a portion of the gages on Shot 9. These data are presented in Figs. 4.19 and 4.20, plotted against slant range. The scatter of the data points is somewhat large, but the curves shown are the best visual fit to the experimental points. The very small pressure levels measured on Shot 4 are probably the cause of the scatter in this case, whereas on Shot 9 it may be attributable to misorientation of the gage baffles, due to the bombing error, discussed in the next section.

4.5.3 Maximum Air Pressures

The graphs of maximum air pressures for each shot are included in Figs. 4.21 through 4.29.

The curve for maximum air pressure at the surface level and 10 ft level for Shot 3 is presented in Fig. 4.21. It can be seen from this figure that the maximum pressures at the two levels were similar out to a ground range of approximately 3000 ft, after which the data points seem to scatter badly. Part of the scatter is probably due to the inaccuracies inherent in measurement of pressures below 1 psi employing instrumentation of the type used by Project 1.1b. The curve represents the best visual fit to the data points.

The maximum air pressure vs effective ground range curve for Shot 4 is shown in Fig. 4.22. Points are plotted for both the surface and 10 ft level gages. A single curve represents the data from both gage elevations, although all gages were in the regular reflection region. The time intervals between the incident and reflected arrivals at the 10 ft gages were very small as compared with the total positive phase duration, so that there was very little pressure decay before the arrival of the reflected wave. As a consequence, the two sets of measurements are comparable.

A series of figures are used to show the maximum air pressures measured on Shot 9; the surface level data are shown in Fig. 4.23, while the aboveground data are shown in Figs. 4.24 through 4.26. It will be seen that each of these curves exhibits a pronounced inflection in the region of 2000 to 4000 ft ground range, with the possible exception of that for the 50 ft gage height. (Unfortunately, in this case the loss of one gage record, added to one questionable data point, leaves the shape of the curve indeterminate in this region.) These inflections are well-documented, and are similar to those noted from some TUMBLER shots (see Section 5.2.1). It is believed that the inflections in the maximum air pressure curves are due to the onset of Mach reflection near 2000 ft ground range.

In Figs. 4.24 through 4.26, the surface level curve is shown as a dotted curve for comparison. It is obvious from Fig. 4.24 that the maximum pressures measured at the 10 ft level are higher than the surface level pressure, especially in the intermediate ground ranges, although the shapes of the curves are similar. The maximum pressures measured at other heights (Figs. 4.25 and 4.26) compare more closely with those measured at the surface level. Under normal conditions, i.e., no thermal layer, slightly lower pressures are expected from

aboveground gages. It is generally conceded, however, from Mach stem data, that the Shot 9 detonation produced an effective thermal layer near the ground surface. This thermal layer probably acted to depress the peak pressures measured at the surface level, which may explain the results shown in Fig. 4.24.

Another possible explanation for this discrepancy between surface and aboveground pressures may be found in the large bombing error experienced on this shot (see Fig. 3.2). The resultant baffle misorientation would probably cause an increase in measured pressure, although the amount of this increase is unpredictable at present. The results of wind tunnel studies[13] on this effect, which predict higher peak pressures for the Shot 9 type of misorientation, were not well confirmed by experiments with deliberate misorientation under blast wave conditions on TUMBLER and other tests.[16] However, this discrepancy may be resolved by the aboveground pressure error due to baffle misorientation.

A comparison with results from other agencies tends to confirm this conclusion. Data from the Naval Ordnance Laboratory, Project 1.1a and 1.2, show the same type of comparison between surface level and 10 ft level gages. Each of these curves checks well with Figs. 4.23 and 4.24. This project used gage baffles almost identical with those used Project 1.1b. On the other hand, data from the Sandia Corporation, Project 1.1d,[15] on aboveground measurements at heights of 8 to 15 ft compare closely with those of Fig. 4.23 (surface level). These data, however, were obtained from the side orifice of Pitot tube gages, where the misorientation effects were probably quite different.

The Shot 10 data for maximum air pressure at surface level are shown in Fig. 4.27. This curve shows a decided break at approximately 1800 ft ground range, probably due to significant precursor dissipation in this region. The aboveground maximum air pressures are plotted in Fig. 4.28 and comparison is made in this figure with the maximum pressure at surface level (dashed curve). It is evident from this figure that the break exhibited on the surface level curve is absent in the case of the aboveground pressures; this is in contrast with the behavior on Shot 9, where similar breaks are observed at all levels. The maximum air pressures recorded on the surface level gages are significantly lower than the aboveground pressures in the region between 1000 and 2500 ft, giving the appearance that the formation of the precursor tends to depress the maximum pressures more at the surface than above the surface.

Figure 4.29 shows the maximum air pressure at surface level for Shot 11. If reliance is placed on the one surface level gage at a ground range of 2955 ft, a clear break is shown in the curve. Similarly, if the 5 ft high gage at 3445 ft was reliable, Shot 11 shows the same characteristic as Shot 10 in the precursor region where the surface pressures were consistently below the pressure aboveground. Beyond the precursor region for ground ranges greater than 4500 ft, the 10 ft high pressures were about the same as those at surface level.

4.5.4 Precursor Air Pressure

Precursor air pressures were observed on Shots 10 and 11, and these data are plotted in Figs. 4.30 and 4.31. For Shot 10, Fig. 4.30 shows the precursor pressure plotted vs ground range; also shown on this

figure is a portion (dotted) of the maximum air pressure curve for the surface level.

Figure 4.31 presents the precursor pressures associated with Shot 11; also shown (dotted) is a portion of the surface level maximum air pressure curve. The most noticeable feature of this curve is the essentially constant precursor pressures at all ranges where measurements were made.

4.5.5 Positive Phase Duration

The positive phase durations for all shots are plotted in Figs. 4.32 through 4.35. The curves of positive phase duration vs ground range for Shots 3 and 4 are shown in Fig. 4.32. In both cases, the points from records of gages at the surface and the 10 ft levels are included, and it will be seen that the curves drawn fit data points from both levels equally well. This is to be expected on Shot 3, since all measurements were made in the Mach region, but would not ordinarily be expected on Shot 4, where all measurements were made in the region of regular reflection. The 10 ft gage elevation, however, results in such a small separation between the incident and reflected shocks that the total positive phase duration is apparently not appreciably affected in this case.

The positive phase durations associated with the air pressure measurements for Shot 9 are shown in Fig. 4.33. Here, the points plotted include all surface measurements and the aboveground measurements where the Mach triple point was above the gage involved.

Figure 4.34 shows the positive phase durations for Shot 10. Here some of the surface level points fall so far from the smooth curve associated with points from other levels and other surface level points that a separate curve, shown dotted, appears to be justified for the surface level measurements. A difference in this region would be expected from an inspection of the records of Figs. 4.9 through 4.11, because of the much earlier arrivals at the surface level gages, but this does not justify the magnitude of this deviation. Where possible, precursor durations were measured (such measurements are dependent on identification of main shock arrival time), and a plot from these points is included in Fig. 4.34. The association between this curve and the deviation of the surface level curve from the smooth curve is apparent, in that the peaks occur at approximately the same ground range.

Similar curves are drawn for Shot 11 in Fig. 4.35. Here the difference between positive phase durations at the surface and at 10 ft is not obvious and the effect of the precursor duration is not so pronounced as on Shot 10.

4.5.6 Impulse

Graphs of positive and negative impulse are included in Figs. 4.36 through 4.42. Figure 4.36 shows a plot of positive impulse vs ground range for Shot 3. The points for the surface level and 10 ft level impulses are included in this figure. There seems to be no significant difference between positive impulses measured at the two levels on this shot, probably due to the fact that all measurements are in the Mach region.

The positive impulses measured on Shot 4 are plotted in Fig. 4.37. The plotted points indicate that the positive impulses measured at the surface and 10 ft levels on Shot 4 are not significantly different. It should be observed that these measurements are all in the regular reflection region, where the impulse for aboveground gages might be expected to be different from that for surface gages. However, this effect is not seen in Fig. 4.32 nor in Fig. 4.22, where the Shot 4 positive phase durations and maximum pressures are plotted. Therefore, the conclusion to be drawn from viewing these figures and Fig. 4.37 is that the pressure-time wave forms are conventional and invariant for Shot 4. A similar conclusion can be drawn from the negative impulse curve of Fig. 4.38.

The positive and negative impulses associated with Shot 9 are presented in Figs. 4.39 and 4.40. In each case, only such aboveground gages as were in the Mach reflection region were included as data points. Figure 4.39 shows that in the Mach region the 10 ft level impulses are significantly larger than those measured at the surface. This result is not inconsistent with the maximum pressure curves of Fig. 4.24, which indicate higher maximum air pressures at the 10 ft level on Shot 9. The negative impulse curve of Fig. 4.40 exhibits an obvious hump at about 2800 ft ground range, which is near the radius where true Mach reflection should begin.

The total positive impulse for Shot 10 is shown in Fig. 4.41. Data from aboveground gages in the Mach reflection region are included, and a single curve appears to fit all data points very well. The agreement between surface and aboveground impulses on this shot is due to a combination of circumstances: the surface air pressures out to ground ranges of about 3000 ft are lower than aboveground pressures (see Fig. 4.28); however, the surface level positive phase durations in this same region are longer than those associated with the aboveground levels (see Fig. 4.34). Apparently, these two facts compensate for each other, resulting in the single curve of Fig. 4.41. For comparison, the curve of the estimated precursor impulse is included in this figure.

Figure 4.42 presents the positive impulse results from Shot 11, plotted in the same fashion as in the previous figure. The precursor impulse curve is also included.

4.5.7 Negative Air Pressure

The data for maximum negative air pressures are plotted in Figs. 4.43 through 4.47. It should be observed that the pressure levels represented by these curves are always far below those expected for maximum positive pressure and for which the gage ranges and attenuator settings were designed. As a consequence, the accuracy of measurement of these minute pressures is somewhat poor, and a considerable scatter of data points is to be expected, particularly on Shots 3 and 4.

CHAPTER 5

DISCUSSION

5.1 GENERAL

In this chapter, the Project 1.1b A-scaled data will be considered and the following subjects will be discussed:

Verification of air blast scaling laws

Comparisons of air blast data obtained from the various UPSHOT-KNOTHOLE shots

Validity of an empirical relationship between positive duration, positive impulse, and maximum air pressure

Incident air pressures and altitude corrections

In addition, the main factors relating to general air blast phenomenology will be considered in the following order:

Regular reflection

Mach reflection

Precursor phenomena

Height of burst considerations

Finally, some attention will be given to the discussion of secondary air pressure shocks, earth acceleration, and earth particle velocity.

5.2 A-SCALED DATA AND COMPARISONS

To facilitate the intercomparison of results from the various shots of UPSHOT-KNOTHOLE and also comparison with results of other tests, it is necessary to normalize the data to a common set of hypothetical conditions. This is usually done by reducing the data from each shot to

conditions corresponding to a 1 KT radiochemical equivalent detonation at sea level. To obtain these A-scaled data, the as-read quantities are multiplied by the appropriate factors shown in Table 5.1. The subscripts "b" and "o" indicate burst and sea level ambient conditions respectively, W is the radiochemical yield in KT, and P and T are the atmospheric pressure and the absolute temperature respectively.

TABLE 5.1 - A-Scaling Factors

Shot	Pressure $\left(\frac{P_o}{P_b}\right)$	Distance $\left(\frac{P_b}{W\,P_o}\right)^{1/3}$	Time $\left(\frac{T_b}{T_o}\right)^{1/2}\left(\frac{P_b}{W\,P_o}\right)^{1/3}$	Impulse $\left(\frac{T_b}{T_o}\right)^{1/2}\left(\frac{P_o^2}{W\,P_b^2}\right)^{1/3}$
3	1.174	1.621	1.588	1.864
4	1.477	0.394	0.381	0.562
9	1.228	0.316	0.310	0.379
10	1.146	0.388	0.384	0.440
11	1.229	0.237	0.234	0.288

For easy reference, Table 5.2 presents the pertinent shot data for the UPSHOT-KNOTHOLE (Project 1.1b) and TUMBLER (Shots 1 and 4) tests.

TABLE 5.2 - Shot Data of TUMBLER and UPSHOT-KNOTHOLE

Shot	Scaled Height of Burst (ft)	Yield (KT)	Height of Burst (ft)	Location
U/K - Shot 10	203	14.9	524	FF
U/K - Shot 11	316	60.8	1334	T-7-3
TUMBLER - Shot 4	363	19.6	1040	T-7
U/K - Shot 3	486	0.20	300	T-7-5a
TUMBLER - Shot 1	747	1.05	793	FF
U/K - Shot 9	764	26	2423	FF
U/K - Shot 4	2378	11.0	6020	T-7-3

5.2.1 Direct Scaling

Shot 9 of UPSHOT-KNOTHOLE was planned as a scaled experiment of TUMBLER Shot 1. Table 5.2 shows that although the yield of Shot 9 was about 25 times larger than TUMBLER Shot 1, the scaled heights of burst of the two shots were approximately equal. The surface level A-scaled maximum pressures measured on these two shots are shown in Fig. 5.1; the curve is drawn through the U-K Shot 9 points. The figure indicates good agreement between shots except in the region of the inflection in the curve. Since these inflections give rise to the so-called "knees"

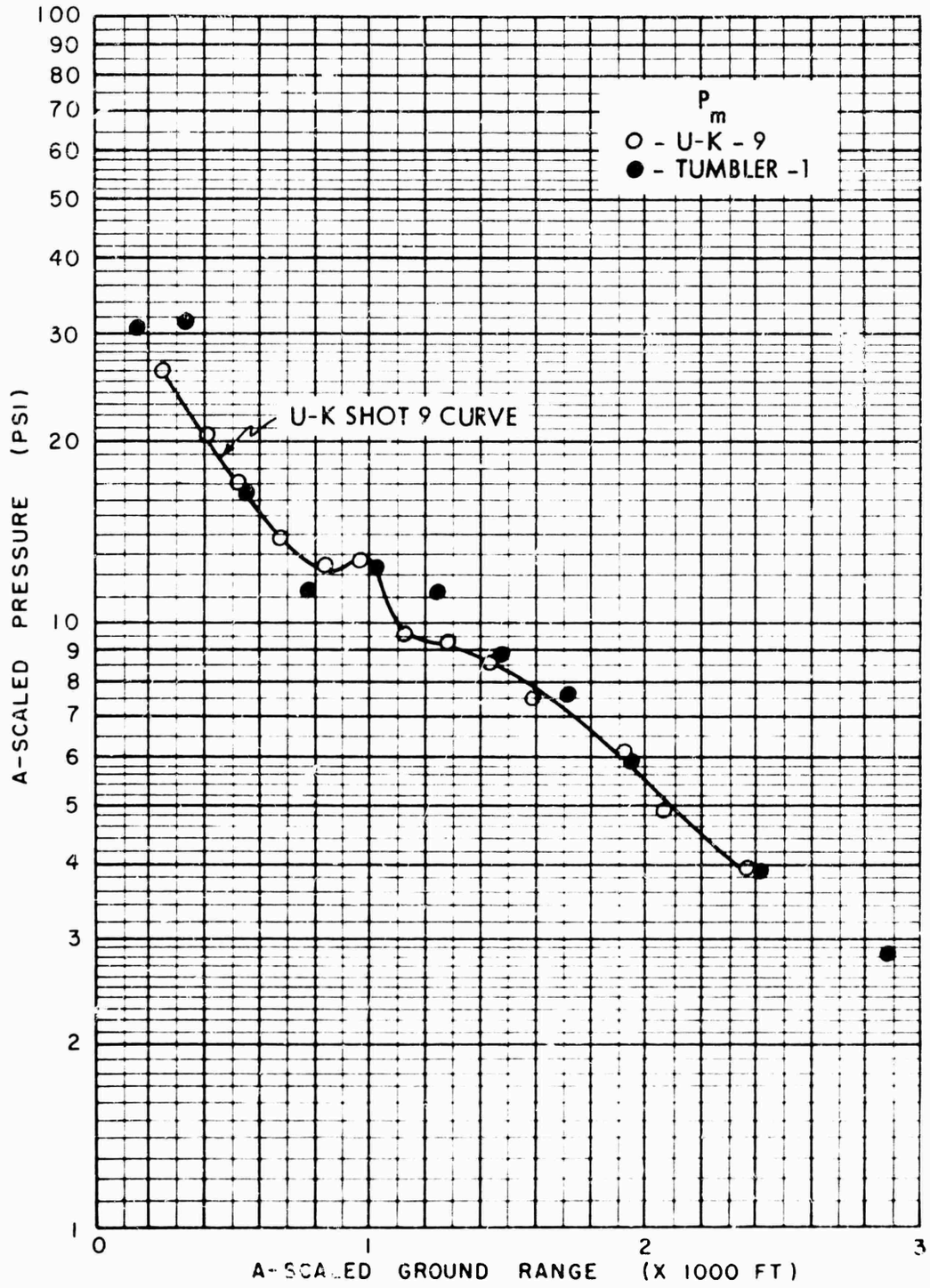

Fig. 5.1 A-Scaled Maximum Air Pressure, Shot 9, Compared to TUMBLER Shot 1, Surface Level

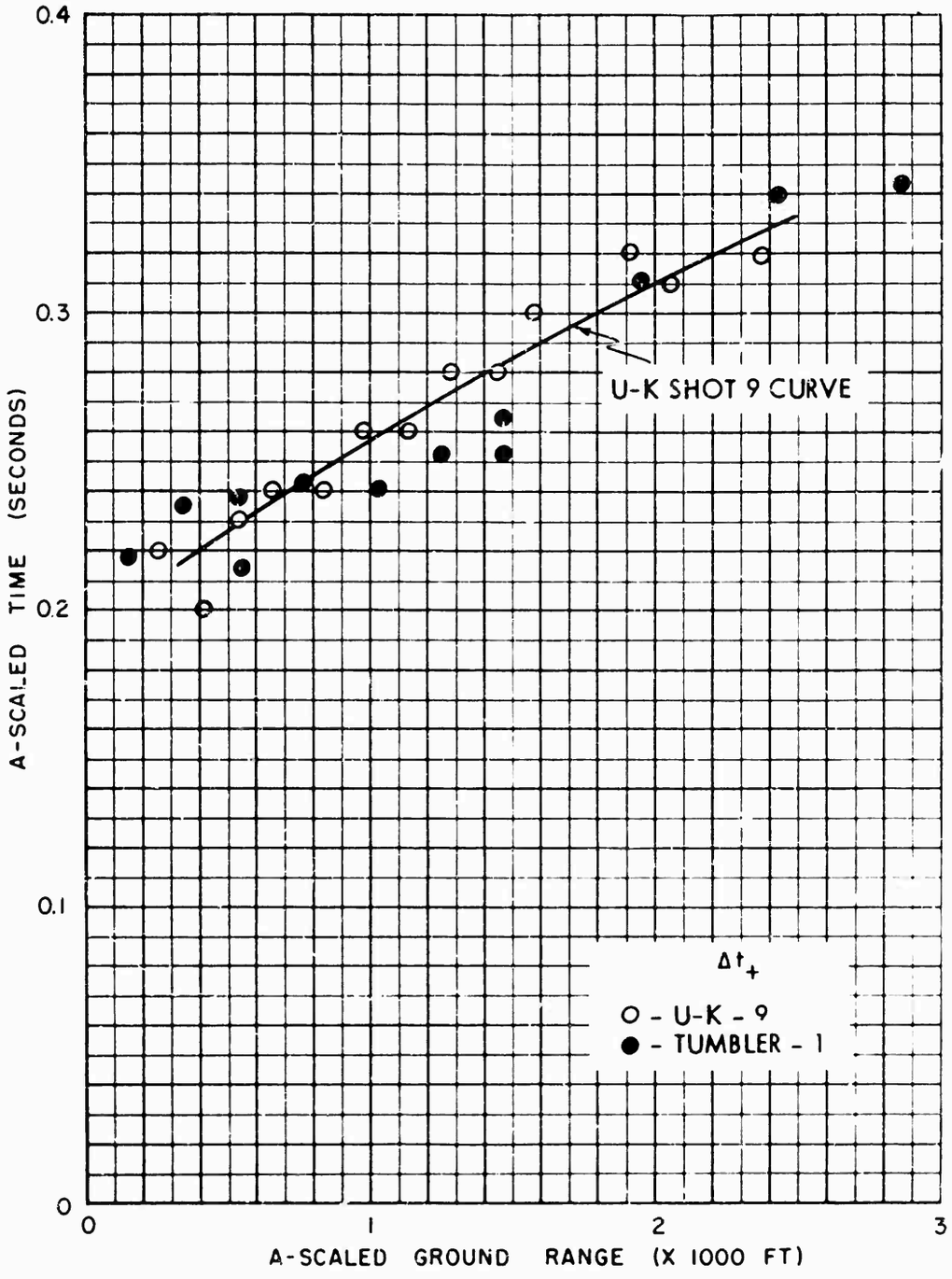

Fig. 5.2 A-Scaled Positive Phase Duration, Shot 9, Compared to TUMBLER Shot 1, Surface Level

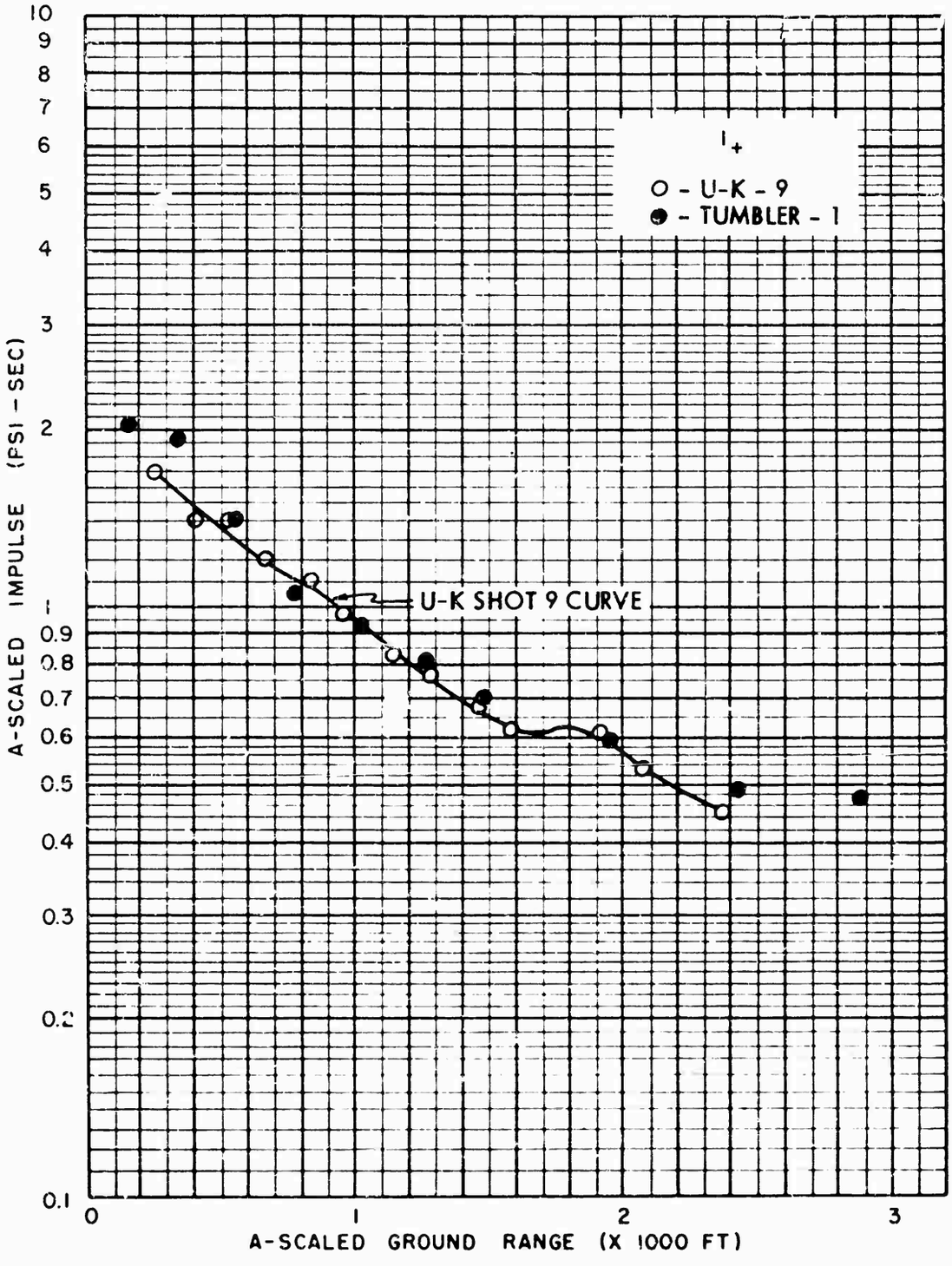

Fig. 5.3 A-Scaled Positive Phase Impulse, Shot 9, Compared to TUMBLER Shot 1, Surface Level

of the height of burst chart, it can be seen that the knee might be dependent upon localized thermal and other effects and could vary in magnitude and position from one shot to another.

The surface level A-scaled positive phase durations and impulses for U-K Shot 9 and TUMBLER Shot 1 are shown in Figs. 5.2 and 5.3, respectively. In each case, the curve is drawn through the U-K Shot 9 data points. There is fair correlation for the positive durations (Fig. 5.2), but the scatter of data points hampers any firm conclusions. The TUMBLER points at about 1200 ft A-scaled ground range are significantly low; however, reference to Fig. 5.1 indicates a high maximum pressure at this ground range. These two opposite effects compensate each other when impulse is measured. Figure 5.3 shows quite good agreement between the two scaled shots in regard to surface A-scaled impulse.

It can be concluded, therefore, that with the exception of minor differences, the surface level air pressure phenomenon followed conventional scaling laws between U-K Shot 9 and TUMBLER Shot 1. This conclusion is further substantiated by the comparisons of other factors discussed in Sections 5.4.1 and 5.4.2.

5.2.2 UPSHOT-KNOTHOLE Comparisons

A composite graph of the surface level A-scaled maximum air pressure vs ground range for all shots is presented in Fig. 5.4. In any such family of curves presenting the data from a number of shots at various A-scaled burst heights, certain general characteristics might be expected. The pressure at very low ground ranges should be highest for the lowest burst height and progressively lower as the burst height is increased. At very large ground ranges the situation should be reversed, the pressure being highest for the highest burst height. In general, each curve would be expected to cross each other curve only once, at a ground range such that the two burst heights involved would be expected to produce the same maximum pressure. Deviations from this general behavior might be caused by thermal effects or by variations in terrain and, at large ground ranges, in meteorology.

The curves of Fig. 5.4 follow the general behavior outlined above. The Shot 3 curve appears to connect well with that of Shot 9, which indicates that the terrain (Frenchman and Yucca Flat) was not a significant factor in the air pressure measurements. In the thermal region (500-1500 ft A-scaled ground range) the curves for Shots 10 and 11 are depressed. This effect is also perceptible on Shot 9, though not pronounced. It is noteworthy that inflections occur in the curves of Shots 9, 10, and 11 at about the same A-scaled range (1000 ft).

A composite graph of surface level A-scaled positive phase duration vs ground range for all shots is shown in Fig. 5.5. Since the scaled positive phase duration in general varies as an inverse function of the peak pressure, the general remarks concerning pressure vs ground range could be expected to apply inversely to this figure. Examination of the curves shows that this is generally true.

A composite graph of surface level A-scaled positive impulse vs ground range for all shots is shown in Fig. 5.6. These curves resemble generally those of Fig. 5.4 but the effect of burst height is not so pronounced. It is of interest to note that the inflections observed in

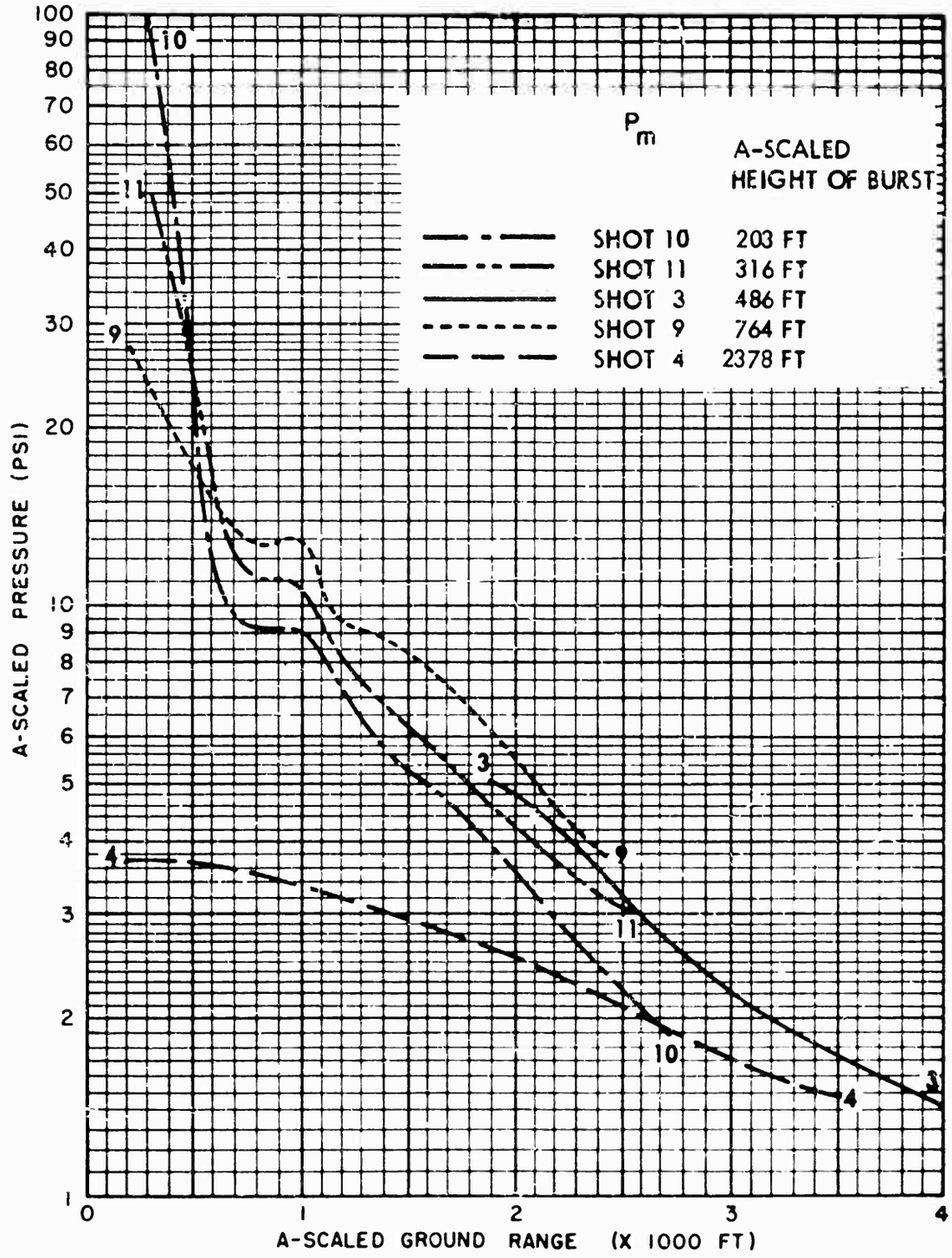

Fig. 5.4 A-Scaled Maximum Air Pressure, All Shots, Surface Level

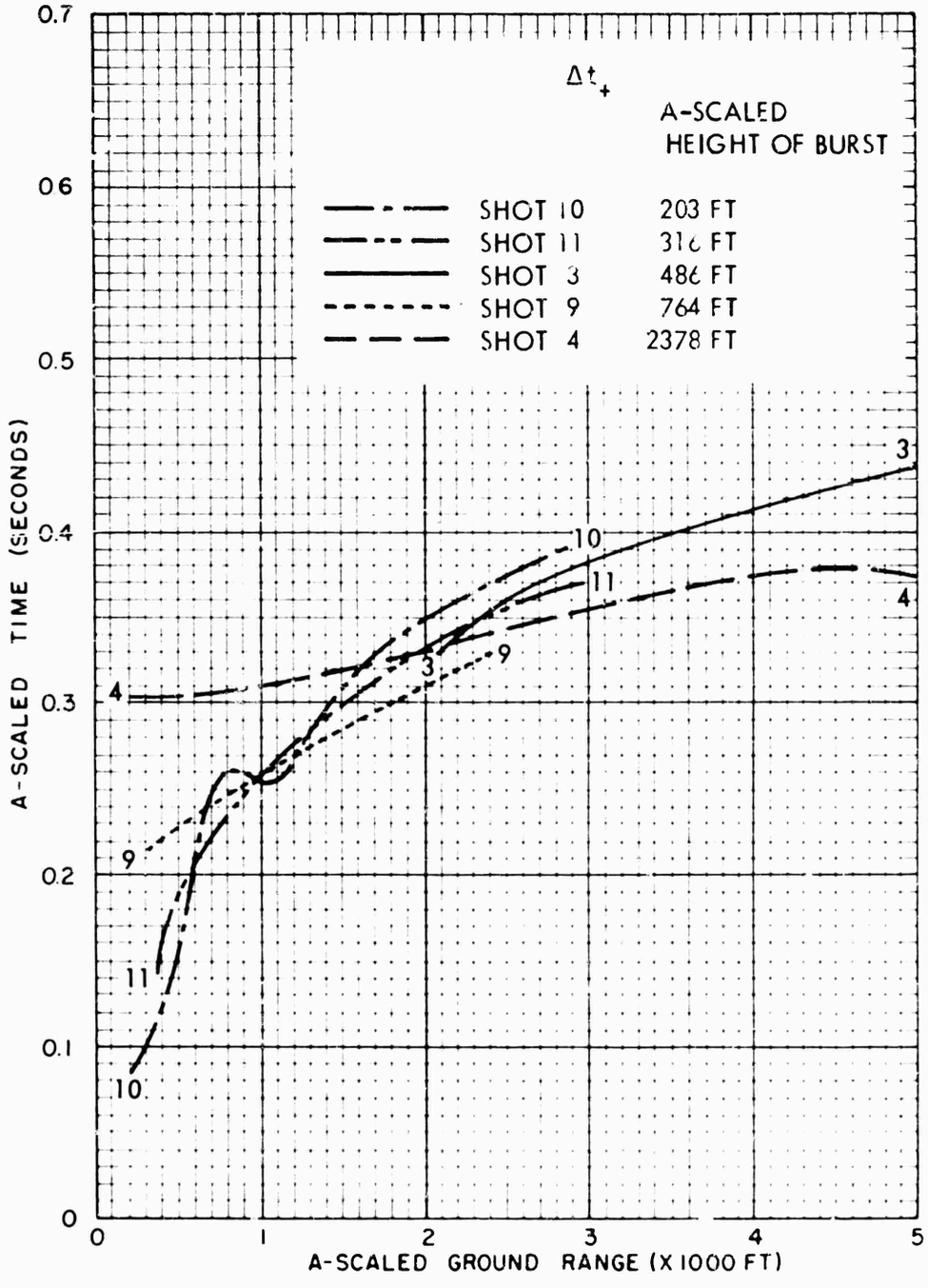

Fig. 5.5 A-Scaled Positive Phase Duration, All Shots, Surface Level

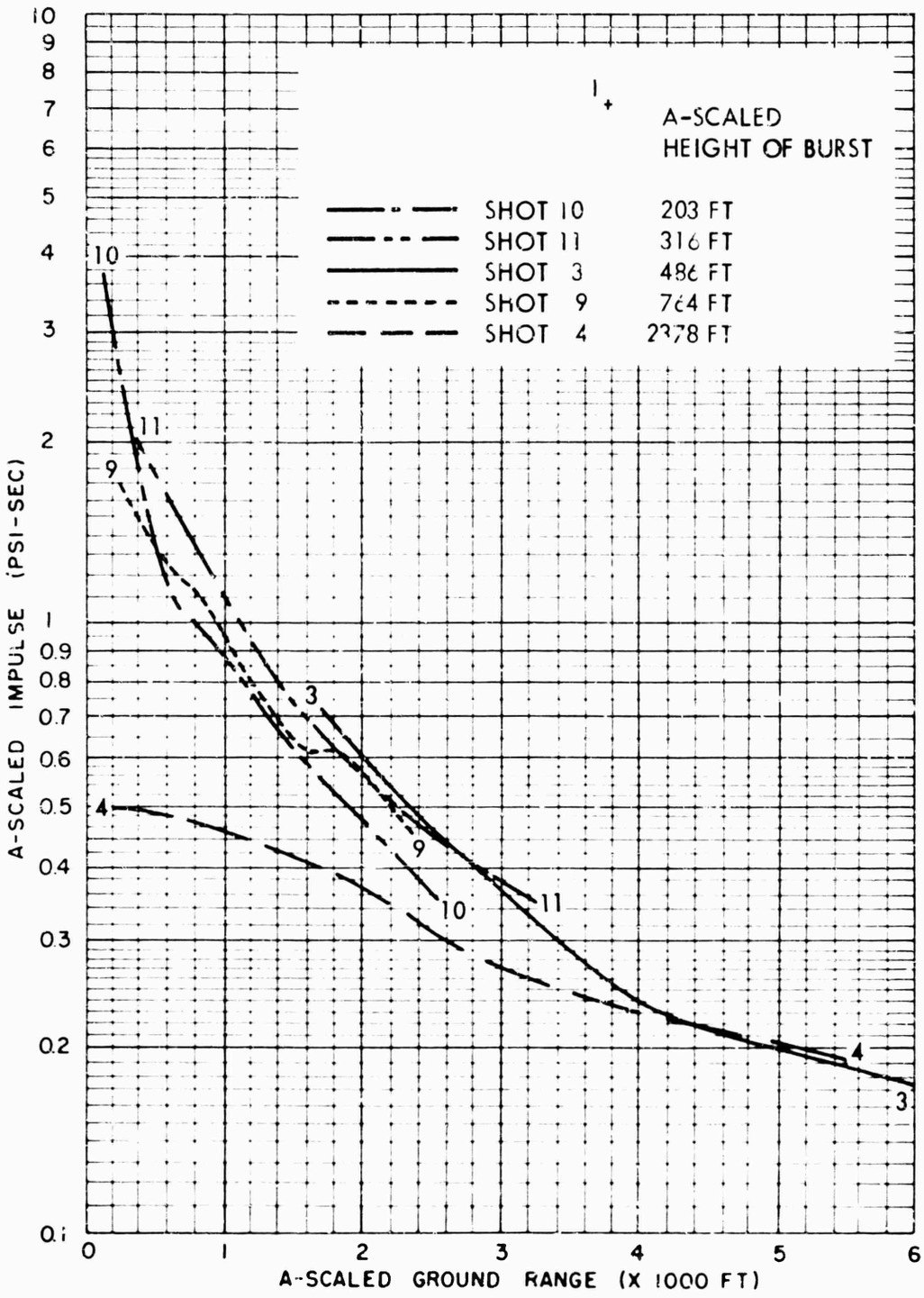

Fig. 5.6 A-Scaled Positive Phase Impulse, All Shots, Surface Level

the pressure vs ground range curves are not present in these impulse curves. Moreover, with the exception of the highest shot (U-K Shot 4), the agreement between UPSHOT-KNOTHOLE A-scaled impulse curves for A-scaled burst heights less than 1000 ft seems to be quite favorable.

5.2.3 Positive Duration and Impulse vs Maximum Air Pressure

An attempt was made in the TUMBLER Project 1.2 report to derive an empirical relation for positive phase duration and impulse as a function of shock pressure.[3] Such a relation implicitly includes effects of reflection which are not a function of burst height. The net result is a function that is considerably less sensitive to burst height than when ground range is the independent variable.

When surface level A-scaled positive phase duration was plotted against A-scaled maximum pressure for the TUMBLER shots (Shots 1, 2, 3, and 4), it was found that a single curve would satisfy the data to the extent that less than 20 per cent of the points lay outside plus or minus 10 per cent limits. The comparable data obtained on Project 1.1b of UPSHOT-KNOTHOLE are shown in Fig. 5.7 where separate coordinates are provided for each shot. The data shown on these graphs are taken, for each shot, directly from the tables found in Chapter 4 (surface level gages).

A result similar to that displayed in Fig. 5.7 is found when A-scaled positive impulse is plotted against maximum air pressure. These graphs for positive impulse are shown for each shot in Fig. 5.8.

Figure 5.9 presents a composite graph of all the positive phase duration curves found in Fig. 5.7; in addition, the figure shows a representation of the TUMBLER empirical relation.[3] This relation takes the form

$$\Delta t_+ = 0.42\ P_m^{-0.20} \qquad (5.1)$$

where Δt_+ is the A-scaled positive duration in secs and P_m is the A-scaled maximum air pressure in psi. Looking at Fig. 5.9, the conclusion is that the U-K data follow the TUMBLER curve out to A-scaled maximum pressures of about 10 psi. For higher pressures the U-K curves for Shots 10 and 11 slope downward, diverging from the TUMBLER curve. This pressure region corresponds to the range of strong thermal effects for these two shots and the empirical relation best applicable in this region is

$$\Delta t_+ = 0.50\ P_m^{-0.34} \qquad (5.2)$$

The composite graph of all the surface level impulse graphs (Fig. 5.8) is shown in Fig. 5.10; this figure also shows the representation of the TUMBLER (Shots 1, 2, and 3) empirical relation. This relation can be written

$$I_+ = 0.16\ P_m^{0.80} \qquad (5.3)$$

where I_+ is the A-scaled positive impulse in psi-secs and P_m is the A-scaled maximum air pressure in psi. Figure 5.10 indicates that the U-K

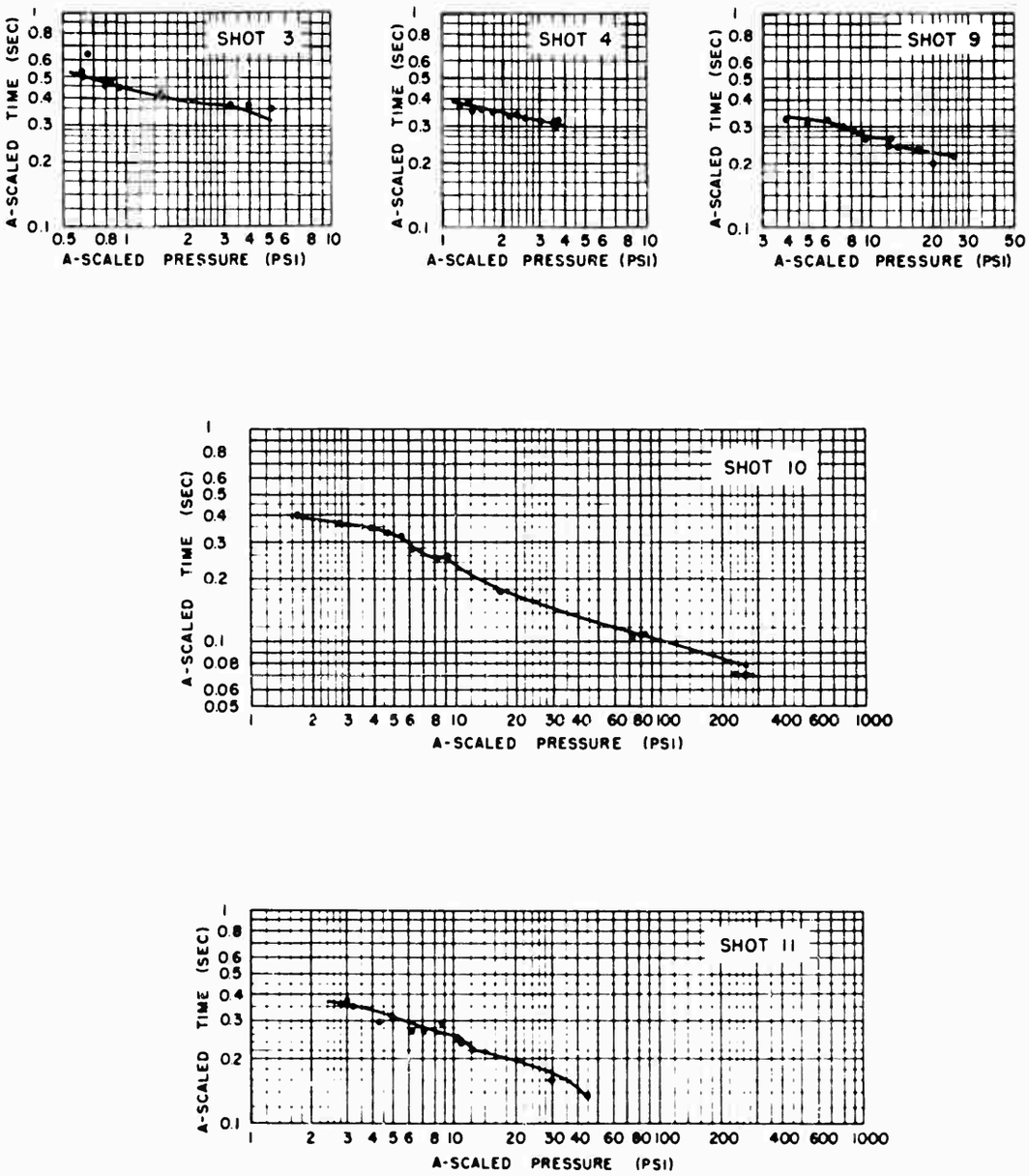

Fig. 5.7 A-Scaled Positive Phase Duration vs Maximum Air Pressure, All Shots, Surface Level

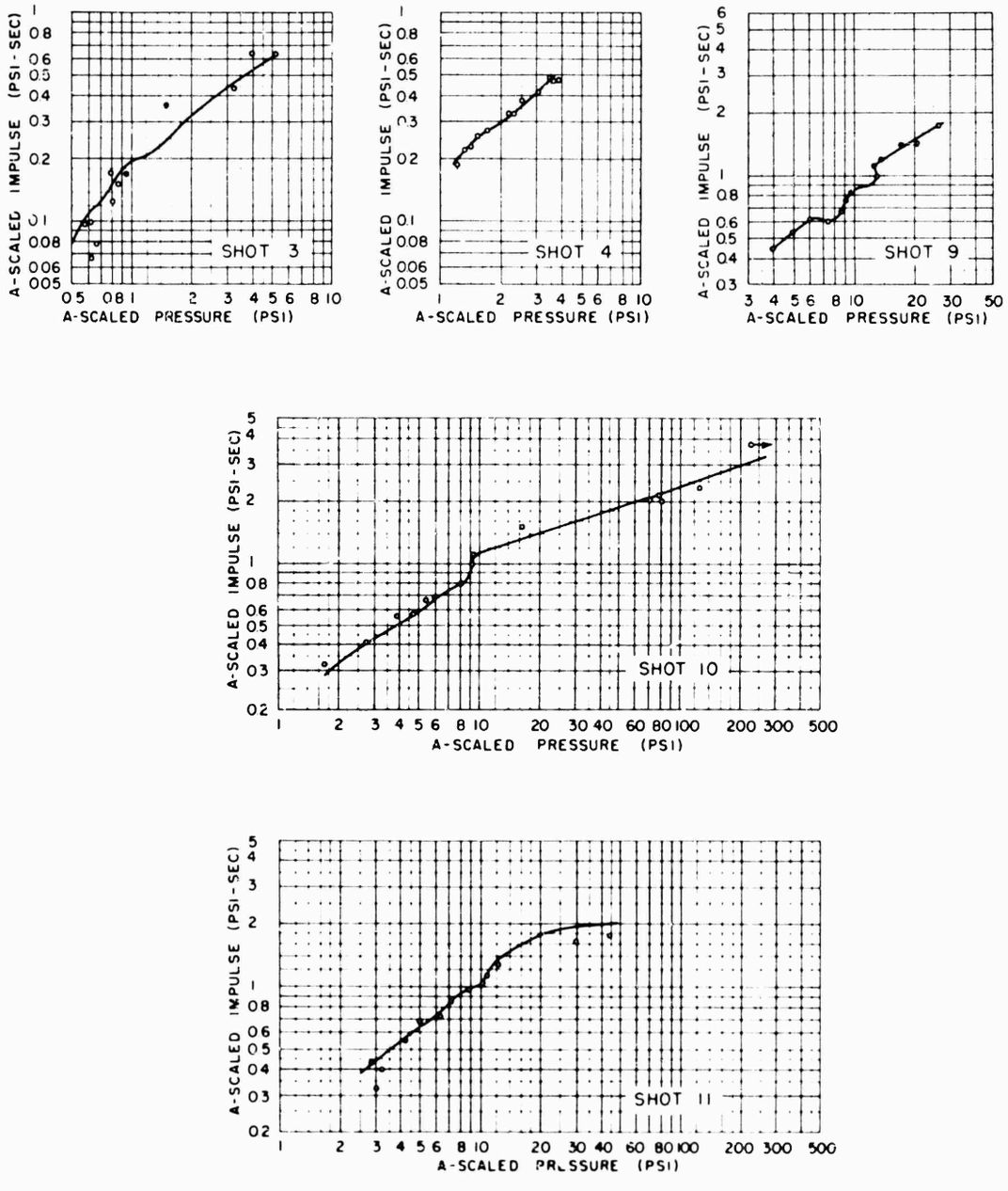

Fig. 5.8 A-Scaled Positive Phase Impulse vs Maximum Air Pressure, All Shots, Surface Level

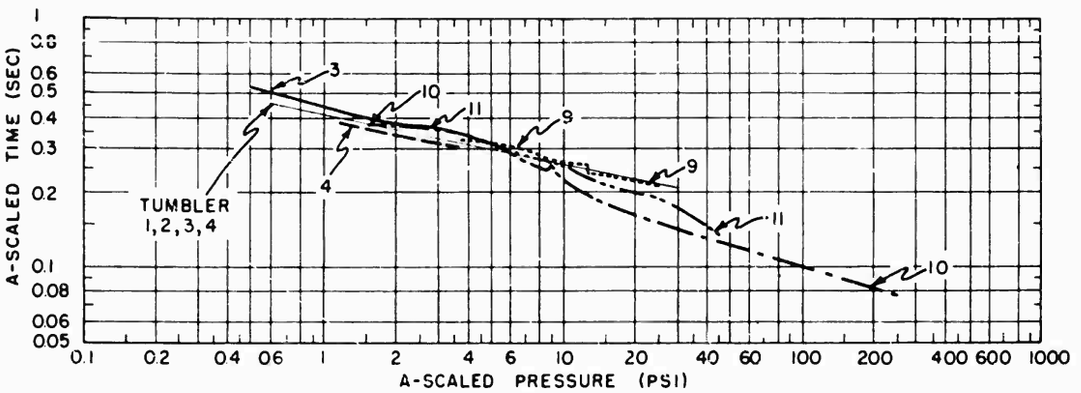

Fig. 5.9 A-Scaled Positive Phase Duration vs Maximum Air Pressure, Composite, All Shots, Compared to TUMBLER, Surface Level

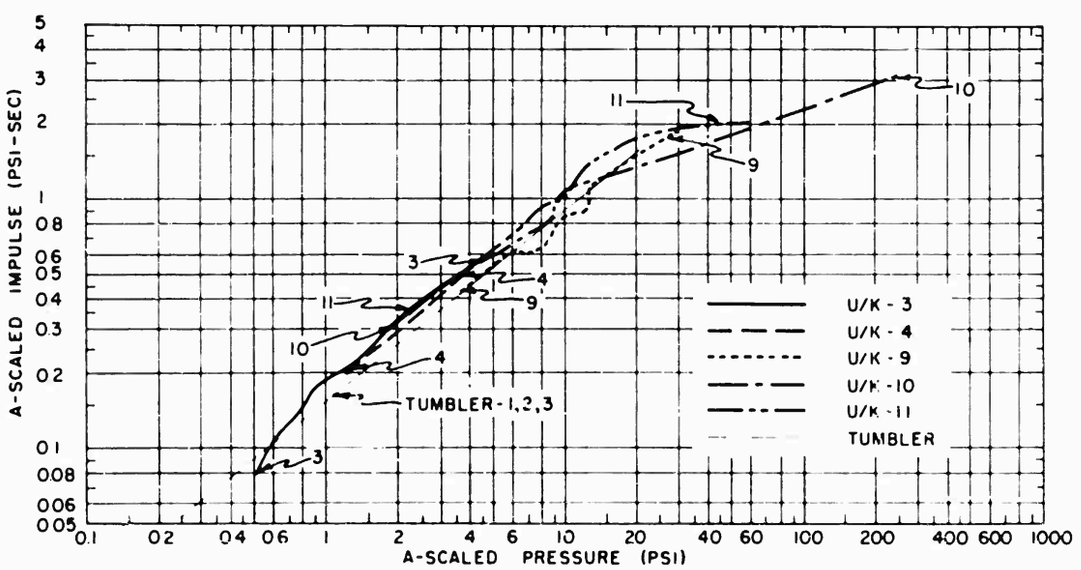

Fig. 5.10 A-Scaled Positive Phase Impulse vs Maximum Air Pressure, Composite, All Shots, Compared to TUMBLER, Surface Level

data follow TUMBLER data out to A-scaled maximum pressures of about 10 psi. For higher pressures, similar to the positive durations results, the Shots 10 and 11 curves exhibit a change in slope. The best empirical relation for this thermal region is given by

$$I_+ = 0.62\ P_m^{0.30} \qquad (5.4)$$

An interesting sidelight to this analysis is found when one considers the possible invariance of pressure wave shape as a function of maximum air pressure. It is well known that the theoretical equation giving pressure throughout the positive phase of a classic shock wave can be written

$$P(t) = P_m e^{-t/\Delta t_+} \left(1 - \frac{t}{\Delta t_+}\right), \qquad (5.5)$$

where P (t) is the pressure at time t. Integrating, one can obtain the classic positive impulse as

$$I_+ = \frac{1}{e} P_m \cdot \Delta t_+ = 0.37\ P_m \cdot \Delta t_+ \quad . \qquad (5.6)$$

The data from TUMBLER and U-K, as expressed by Equations 5.1 and 5.3, yield the following positive impulse relation:

$$I_+ = 0.38\ P_m \cdot \Delta t_+ \quad . \qquad (5.7)$$

This empirical relation compares favorably with the theoretical equation, (5.6), indicating that the pressure wave shape is invariant for maximum pressures to 10 psi. However, in the regions of higher pressure (and thermal effects) Equation 5.6 is not valid, confirming the observed fact that thermal effects disturb the shape of the pressure wave.

5.2.4 Free Air Pressures and Altitude Corrections

Free air pressures were measured on Shots 4 and 9 where aboveground gages were in the regular reflection region. The A-scaled pressure values for these shots are plotted vs A-scaled slant range in Fig. 5.11. The curve shown in this figure is the AFSWP free air curve which appears in the TUMBLER Summary Report.[7] Also plotted in Fig. 5.11 is the UPSHOT-KNOTHOLE Project 1.3 (AFCRC) Shot 9 free air pressure data obtained from airborne canisters.[17] The Shot 4 canister measurements were taken at A-scaled ranges beyond the limits of Fig. 5.11 and are therefore not included in the figure. Referring to the figure, it appears that the SRI Shot 9 data fit the AFSWP curve quite well; however, the SRI Shot 4 and AFCRC Shot 9 data seem to fall consistently lower than the composite curve.

For clarification, it should be mentioned that for free air pressures below 2 psi the composite curve is based upon only fragmentary data; therefore, disagreement in this pressure region is not surprising or very significant. Moreover, it becomes necessary to perform different altitude correction procedures if pressure measurements are taken at

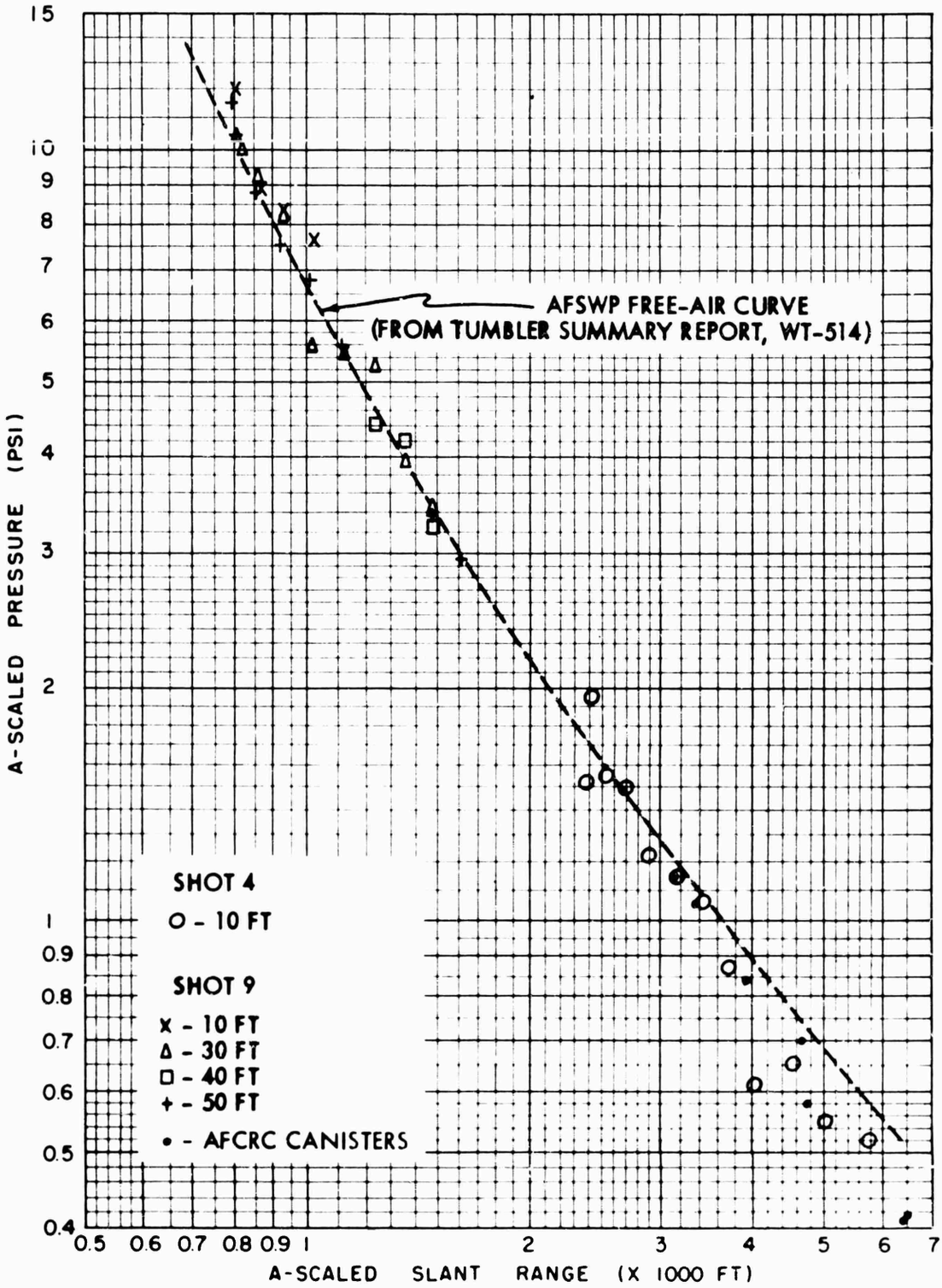

Fig. 5.11 A-Scaled Incident Air Pressure vs Slant Range, Shots 4 and 9, Compared to AFSWP Free Air Curve

altitudes greater than or comparable with burst height (AFCRC) as opposed to measurements taken near the ground surface (SRI).

In this regard it would be well to consider, in addition, the question of the altitude correction procedures, particularly for a very high burst height detonation. The correction used to normalize information from all tests to a common set of temperature and pressure conditions has led to considerable confusion. The problem involves the decision as to whether the burst height or the gage height conditions should be used in the transformation. If the combined Fuchs and Sachs corrections are used,[17,18,19] no confusion need arise when free air (incident) pressures in a uniform atmosphere are desired, for the corrections were devised for these conditions.

Figure 5.12 indicates the scheme for the combined corrections; the pressures are all incident (free air). If P_1 is measued at R_1, then the Fuchs corrections transfer the measurements to an infinite uniform atmosphere possessing burst height ambient conditions. The Sachs correction then ransforms this incident pressure to reference values (infinite uniform atmosphere at sea level). The corrections are discussed in detail in the TUMBLER Project 1.2 report.[3]

In this report the conventional procedure employed in TM 23-200, Capabilities of Atomic Weapons[20] is followed: that is, only the Sachs correction from burst height conditions is applied to reduce the data. However, the AFCRC Project 1.3 data are corrected to sea level conditions using the combined Fuchs-Sachs factors. In this section the Fuchs factors for Shot 4 are calculated, realizing that for this very high burst height one can expect to find significant differences between the various correction factors. Also, there is the question as to whether the burst height or gage height ambient pressure is the best to use in a single Sachs-type correction. Accordingly, Shot 4 has been used as an example to indicate the magnitude of the differences likely to occur.

The ambient conditions for Shot 4 are found in Table 3.1. Using these data, the correction factors of Table 5.3 are computed. For the Fuchs correction a linear interpolation between gage and burst heights is assumed. The results may be expressed in terms of the factors by multiplying the incident pressure P_1 measured at slant range R_1 (see Fig. 5.12) to obtain the sea level values P_2 and R_2.

TABLE 5.3 - Altitude Correction Factors for Shot 4

	Pressure	Distance
Fuchs - Sachs	1.588	0.332
Sachs (Burst Height)	1.477	0.394
Sachs (Gage Height)	1.177	0.425

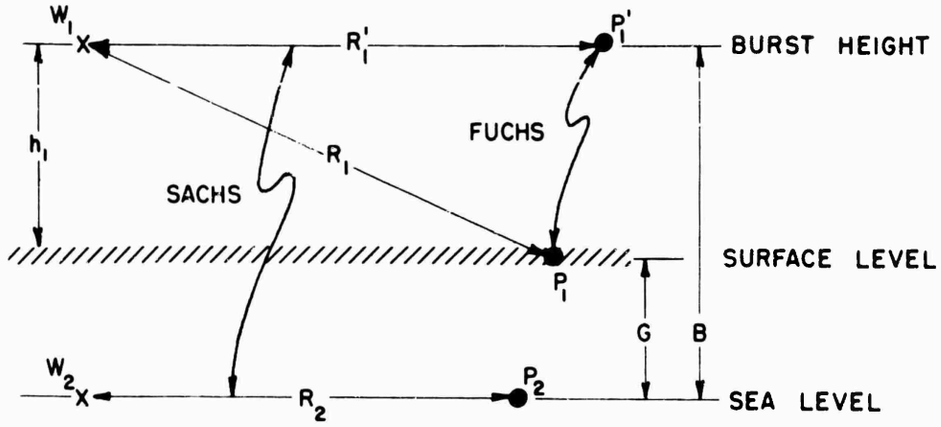

Fig. 5.12 Schematic Diagram of Levels and Radii for Altitude Correction

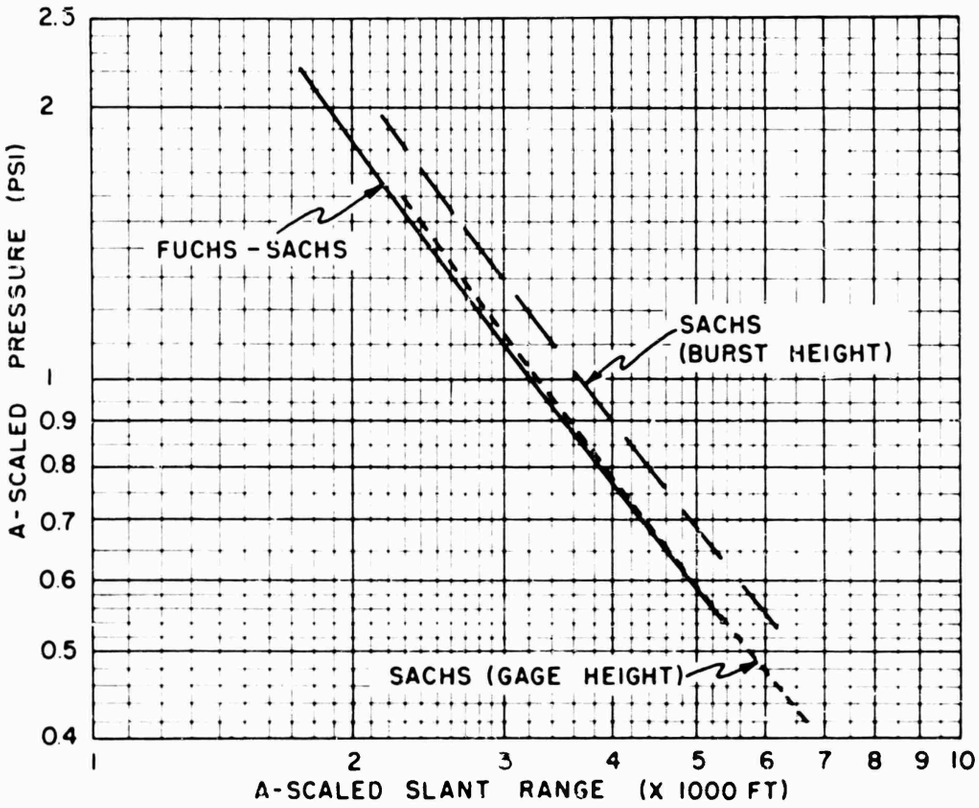

Fig. 5.13 A-Scaled Incident Air Pressure vs Slant Range, Shot 4, Using Three Altitude Correction Methods

To indicate the effects graphically, the free air (incident) pressure vs slant range curve was first obtained by fitting the Kirkwood-Brinkley TNT curve[21] to the experimental data. The fit was fair for a 4.4 KT TNT burst. The conversion factors of Table 5.3 were applied to the 4.4 KT curve and the transformed curves are plotted in Fig. 5.13.

The labels on the figure indicate that the Fuchs-Sachs and Sachs (gage height) altitude corrections led to approximately the same result, whereas the Sachs (burst height) corrections give pressure values which are higher by about 15 per cent at 1 psi (A-scaled). The TUMBLER Shot 3 (height of burst at 3447 ft) altitude corrections gave similar results in this pressure range.[3] Thus, referring back to Fig. 5.11, it can be concluded that the type of altitude correction chosen (Sachs burst height) produced higher pressures in this region than would be computed if either of the other two corrections (Fuchs-Sachs or Sachs gage height) had been used. If either of the other two altitude corrections had been applied to the SRI data, the deviation from the AFSWP composite curve would have been more pronounced. In fact, using the Fuchs-Sachs correction, which was also used by AFCRC, the SRI data points below 2 psi fall consistently below the AFCRC data points.

5.3 REGULAR REFLECTION

Investigation of the phenomenon of ground surface regular reflection of the air pressure wave from a nuclear explosion was presented in some detail in the TUMBLER report on Project 1.2.[3] Using the same general methods of analysis, it is possible to compute the reflecting ability of the earth on the UPSHOT-KNOTHOLE shots upon which incident air pressures were recorded, i.e., Shots 4 and 9.

Table 5.4 presents the experimental and calculated reflected pressures at the ground surface for Shot 4. An approximation of the surface level incident pressure at each station is taken as the average of the direct incident pressure (P_i) and the decayed incident pressure (P_{i2}) recorded on the 10 ft level gage. The "measured" reflection factor (β) of Table 5.4 is calculated by dividing the surface level maximum pressure by the surface level incident pressure referred to above. In addition, knowing the incident air pressure, it is possible from regular reflection theory to compute a "calculated" reflection factor (also found in Table 5.4) at each gage station. A major difficulty is that no theory exists that deals with the regular reflection of decaying shocks. Calculations here are based on the standard analysis for the reflection of uniform plane shocks from a perfectly reflecting plane surface[22] when the medium ahead of the shock is originally uniform. Both the measured and theoretical reflection pressures of Table 5.4 are plotted in Fig. 5.14.

A similar procedure for analysis was applied to the data from Shot 9 and the results for the surface level gages may be found in Table 5.5. The experimental and theoretical reflected pressures are shown graphically in Fig. 5.15.

These figures indicate that for Shot 4 there is good agreement between the measured and computed values of maximum reflected pressure; however, the Shot 9 results show that the calculated pressures are higher than the measurements in the vicinity of 2000 ft ground range. This difference might be ascribed to a combination of thermal effects

TABLE 5.4 - Reflection Factor, Shot 4, Surface Level
P_o = 12.5 psi

Sta. No.	Grnd. Range (ft)	θ (degrees)	P_i* (psi)	P_r		β	
				Measured (psi)	Calc. (psi)	Measured (psi)	Calc. (psi)
200	610	5.75	1.04	2.37	2.14	2.3	2.1
280	1346	12.6	1.29	2.42	2.70	1.9	2.1
281	2292	20.9	1.05	2.45	2.17	2.3	2.1
204	3271	28.5	0.96	2.04	1.96	2.1	2.1
282	4259	35.3	0.81	1.57	1.67	1.9	2.1
283	5252	41.0	0.79	1.66	1.62	2.1	2.1
208	6247	46.0	0.72	1.35	1.49	1.9	2.1
284	7243	50.3	0.60	1.13	1.24	1.9	2.1
285	8241	53.9	0.41	1.05	0.82	2.5	2.0
286	9738	58.2	0.43	0.89	0.88	2.1	2.0
287	11235	61.9	0.37	0.86	0.79	2.3	2.1
288	13233	65.5	0.36	0.79	0.74	2.2	2.1

* - Extrapolated

TABLE 5.5 - Reflection Factor, Shot 9, Surface Level
P_o = 13.05 psi

Sta. No.	Grnd Range (ft)	θ (degrees)	P_i* (psi)	P_r		β	
				Measured (psi)	Calc. (psi)	Measured (psi)	Calc. (psi)
214	837	19	8.0	19.7	19.5	2.5	2.4
215	967	22	7.2	NR	17.1	NR	2.4
216	1293	28	6.8	15.5	16.1	2.2	2.4
217	1705	35	6.1	12.1	14.3	1.9	2.3
200	2154	42	5.4	10.7	12.8	1.9	2.4
202	2622	47	4.2	9.8	10.2	2.3	2.4

* - Extrapolated
NR - No record

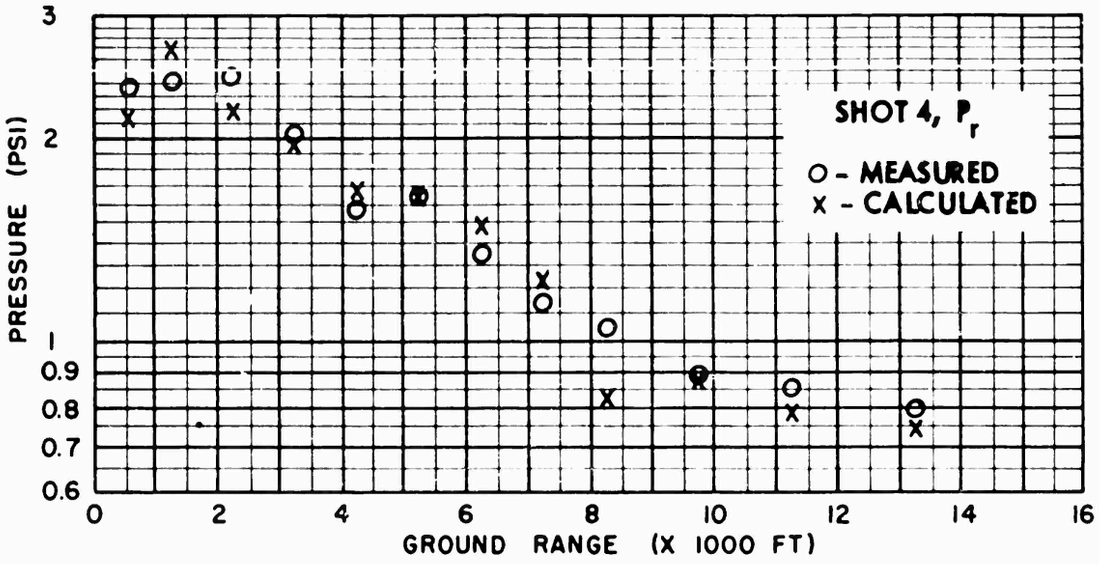

Fig. 5.14 Theoretical and Measured Reflected Air Pressure, Shot 4, Surface Level

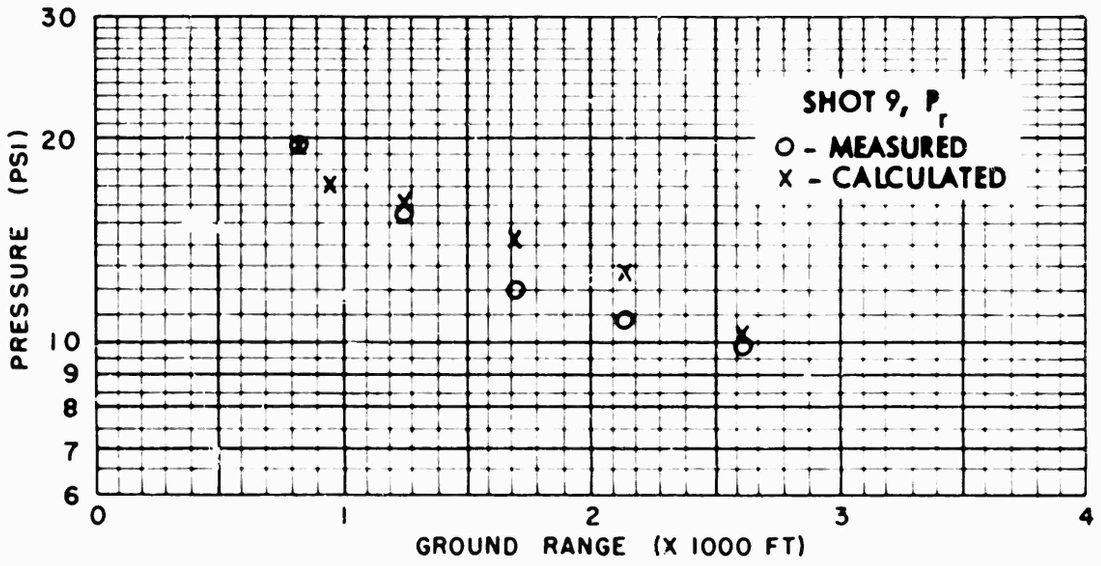

Fig. 5.15 Theoretical and Measured Reflected Air Pressure, Shot 9, Surface Level

(which decrease with increasing ground range due to the inverse-square and cosine laws) and the time of arrival of the shock wave. If this were the case, then gage records at close-in stations (very early shock arrivals) should be relatively ideal, while at intermediate ranges (1700-2200 ft) there should be a degradation of the shock with a subsequent return to ideal form at greater distances (small thermal effects). This general behavior is noted in the U-K Shot 9 surface level pressure-time records of Fig. 4.7, where the OB record (ground range 2147 ft) shows evidence of degradation. Comparisons between U-K Shot 4 and U-K Shot 9 reflection results are hampered by two facts; first, the pressure magnitudes are quite different, and second, the shots were detonated at locations possessing different ground surface conditions.

Efforts on TUMBLER[3] to determine the effects of terrain upon air pressure phenomena did not lead to any firm conclusions. However, the regular reflection data indicated that the Frenchman Flat and Yucca Flat areas present similar reflecting surfaces.

5.4 MACH REFLECTION

Of the five shots of Project 1.1b, Shot 3 measurements were entirely in the Mach region, Shot 4 showed only regular reflections, and the onset of Mach reflection on Shots 10 and 11 was obscured by thermal effects. Thus, all the useful information on Mach reflection is confined to Shot 9.

5.4.1 Triple Point Trajectory

One of the purposes of the multiple gage installations at several heights on Shot 9 was to obtain definitive data on the location of the Mach triple point at various ground ranges. The data required are the time intervals (Δt_{ir}) between the arrival of incident and reflected shocks as functions of both ground range and gage height. The method of analysis depends upon the assumption that, within the vertical extent of the gages, the Mach Y consists of plane wave fronts and that this configuration moves parallel to the ground without change of form.

Figure 5.16 shows a plot of Δt_{ir} for each gage level plotted against ground range. In each case, except the 30 ft level, a final gage is included whose Δt_{ir} is zero. The resultant curves are extrapolated to zero Δt_{ir}. The intercept of these extrapolations with $\Delta t_{ir} = 0$ is taken as the ground range at which the triple point reached the respective levels. It is evident that a peculiar inflection occurs in each of these curves at a ground range of approximately 2500 ft; the inflection is most pronounced at the 10 ft level.

Another means of using the data is shown in Fig. 5.17. Here the Δt_{ir} values are plotted against height for each gage station and the curves are extrapolated to zero Δt_{ir}. These zero intercepts indicate the height of the triple point at each gage station. The data from Figs. 5.16 and 5.17 are tabulated in Table 5.6 and plotted in Fig. 5.18. This curve shows the Mach triple point location as it varied with ground range. At the shortest ground ranges where measurements were taken (800-900 ft), the apparent triple point height, or reflecting plane, was 2 or 3 ft. This stem height remained constant to about 1500 ft,

where it rose abruptly to 8 or 9 ft. The figure shows that at a ground range of about 4750 ft the Mach stem is 50 ft high and rising rapidly.

TABLE 5.6 Mach Triple Point Height, Shot 9

As-Read		A-Scaled	
Grnd. Range (ft)	Height (ft)	Grnd. Range (ft)	Height (ft)
From Δt_{ir} vs Ground Range			
2850	10	895	3.14
4280	30	1344	9.42
4560	40	1432	12.56
4740	50	1488	15.70
From Δt_{ir} vs Height			
837	1.5	265	0.47
967	3.3	306	1.04
1293	2.9	409	0.91
1705	4.3	539	1.35
2154	9.3	681	2.92
2622	7.5	829	2.36
4072	25.5	1288	8.01

The curve of Fig. 5.18 plotted to A-scaled coordinates is shown in Fig. 5.19. It is interesting to compare the results shown on the latter figure with the theoretical curve for Mach stem formation. This is done in Fig. 5.20. The point for Shot 9 at about 200 ft ground range corresponds to the A-scaled ground range at which, on Fig. 5.20, Mach reflection appears to begin (the closest gage station to ground zero). However, the theoretical curve indicates that for the Shot 9 burst height Mach reflection should begin at about 750 ft A-scaled ground range. Referring to Fig. 5.19 again, it appears that the large hump in the curve occurs at about 700 ft A-scaled ground range. This evidence seems to support the type of reasoning developed in Section 1.3.2 of this report in which the concept of thermal-Mach reflection predominates out to an A-scaled range of about 500 ft, after which "true" irregular reflection begins to influence the triple point trajectory.

The Mach triple point behavior indicates two interfaces, one at about 2 or 3 ft and the other at 8 or 9 ft, where refraction and reflection occur. Such an hypothesis would explain the two levels of the triple point, the critical angle for the lower interface being greater than for the upper interface. The presence of such thermal layers would cause a rudimentary precursor wave (see Section 5.4.2), and the variation with angle of incidence of division of energy between reflected

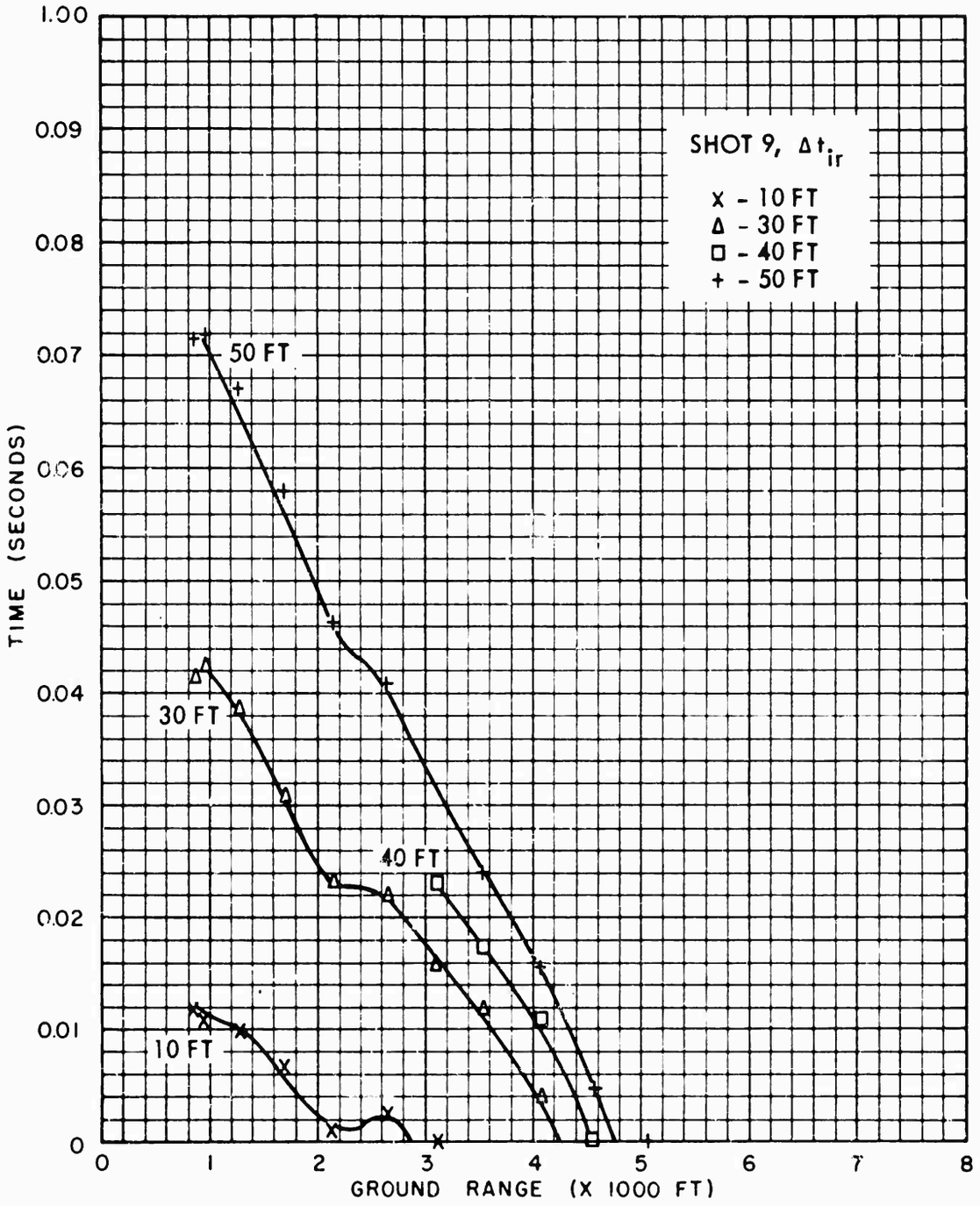

Fig. 5.16 Duration of Incident Air Pressure vs Ground Range, Snot 9

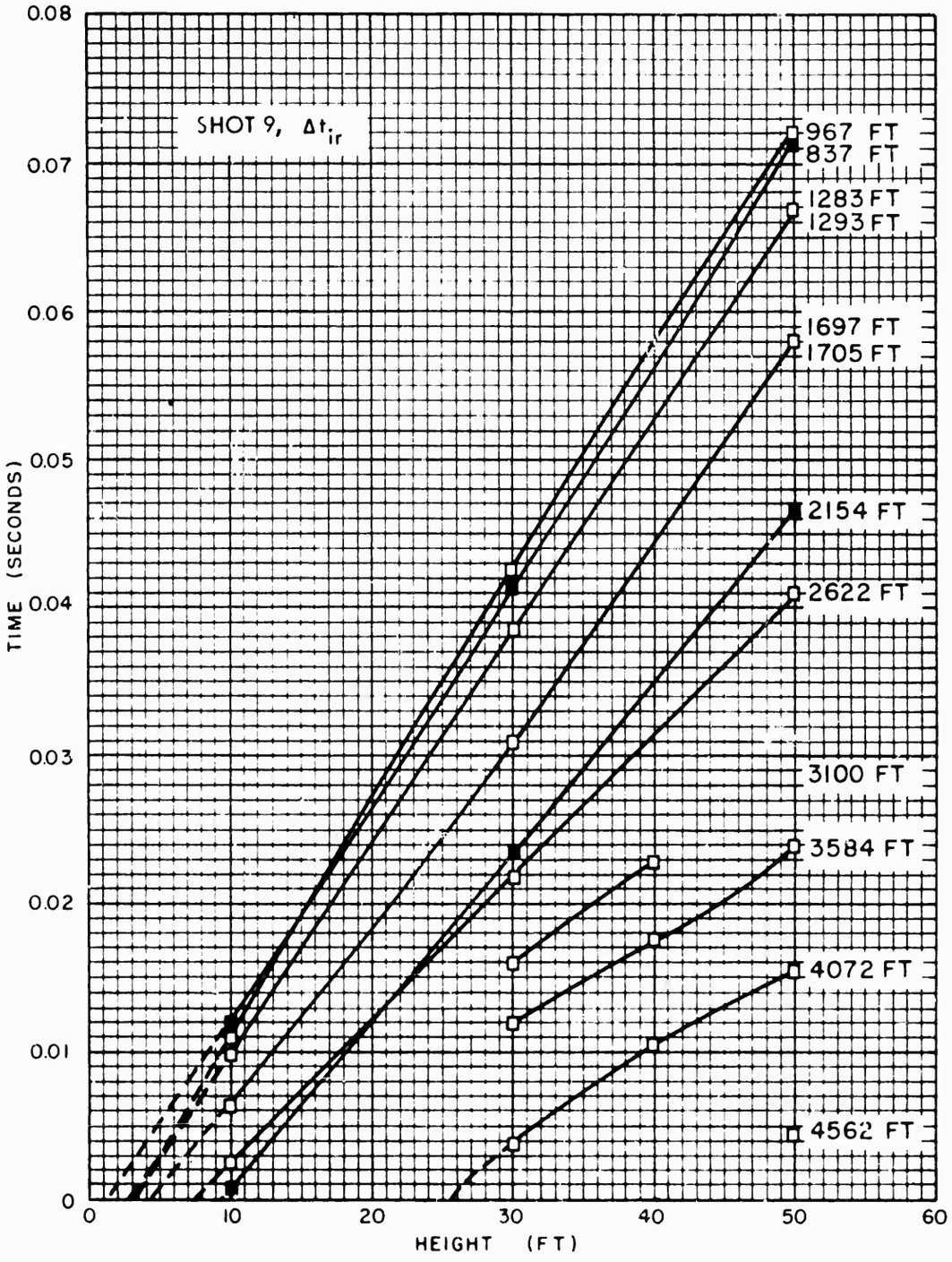

Fig. 5.17 Duration of Incident Air Pressure vs Height, Shot 9

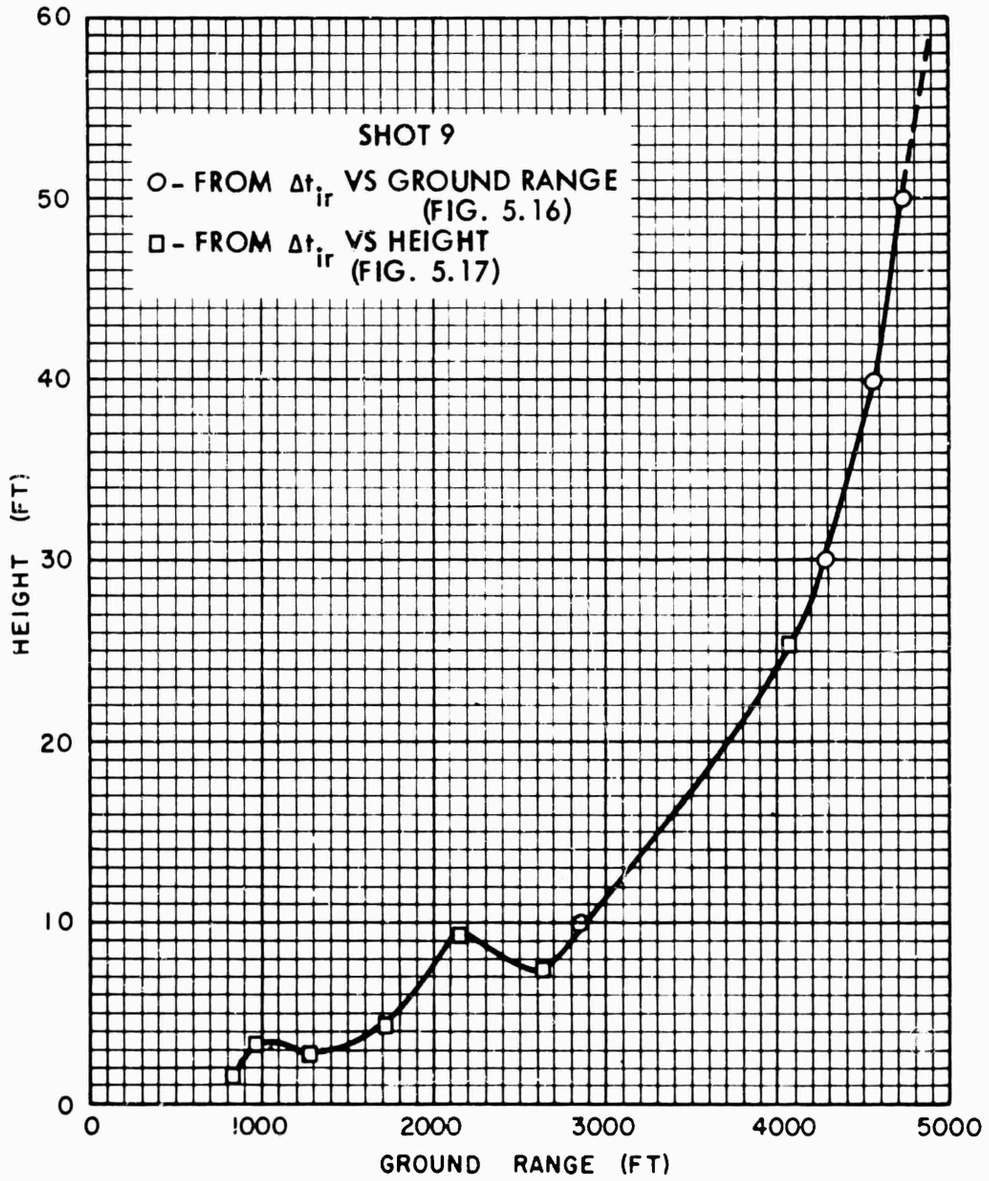

Fig. 5.18 As-Read Triple Point Trajectory, Shot 9

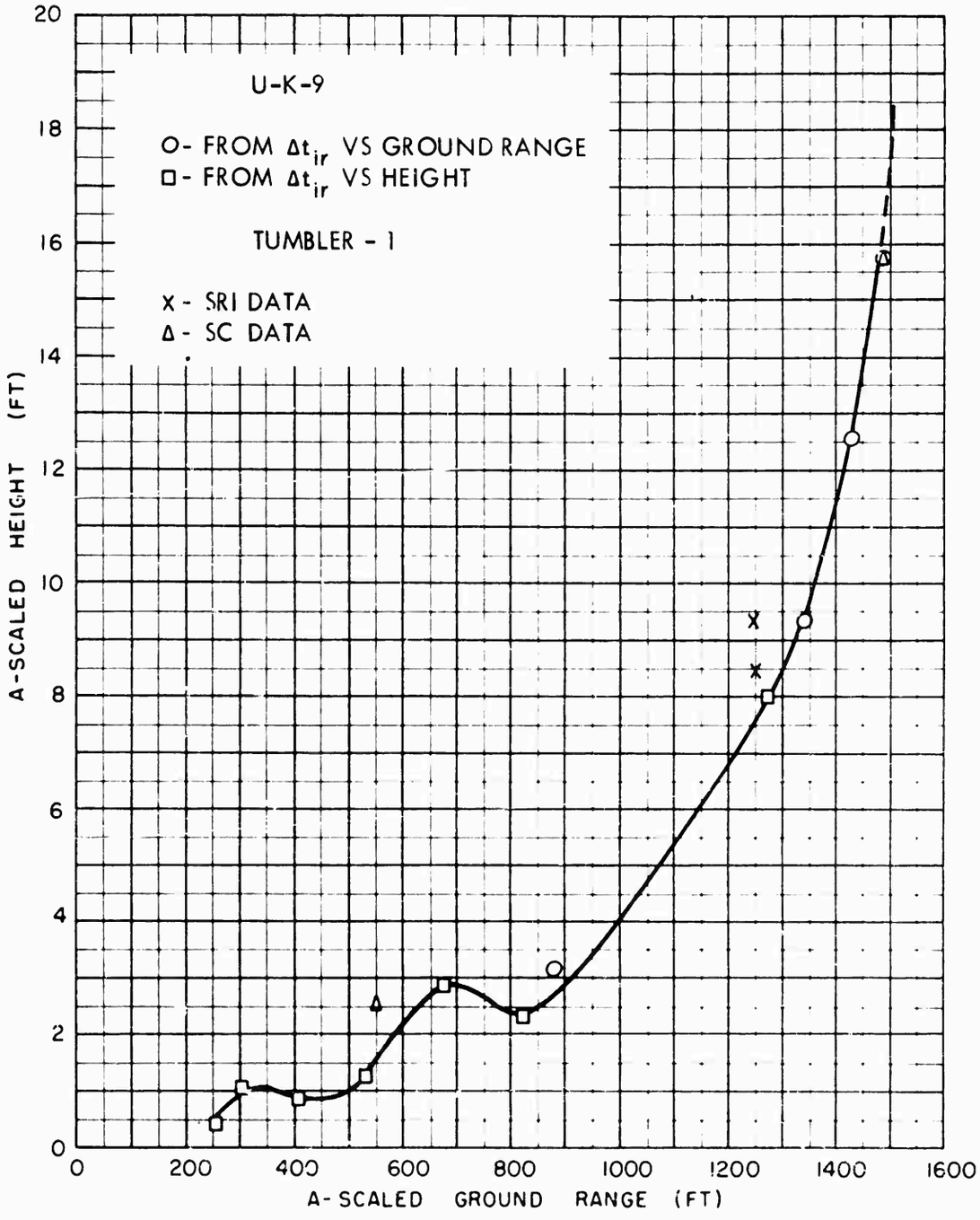

Fig. 5.19 A-Scaled Triple Point Trajectory, Shot 9, Compared to TUMBLER Shot 1

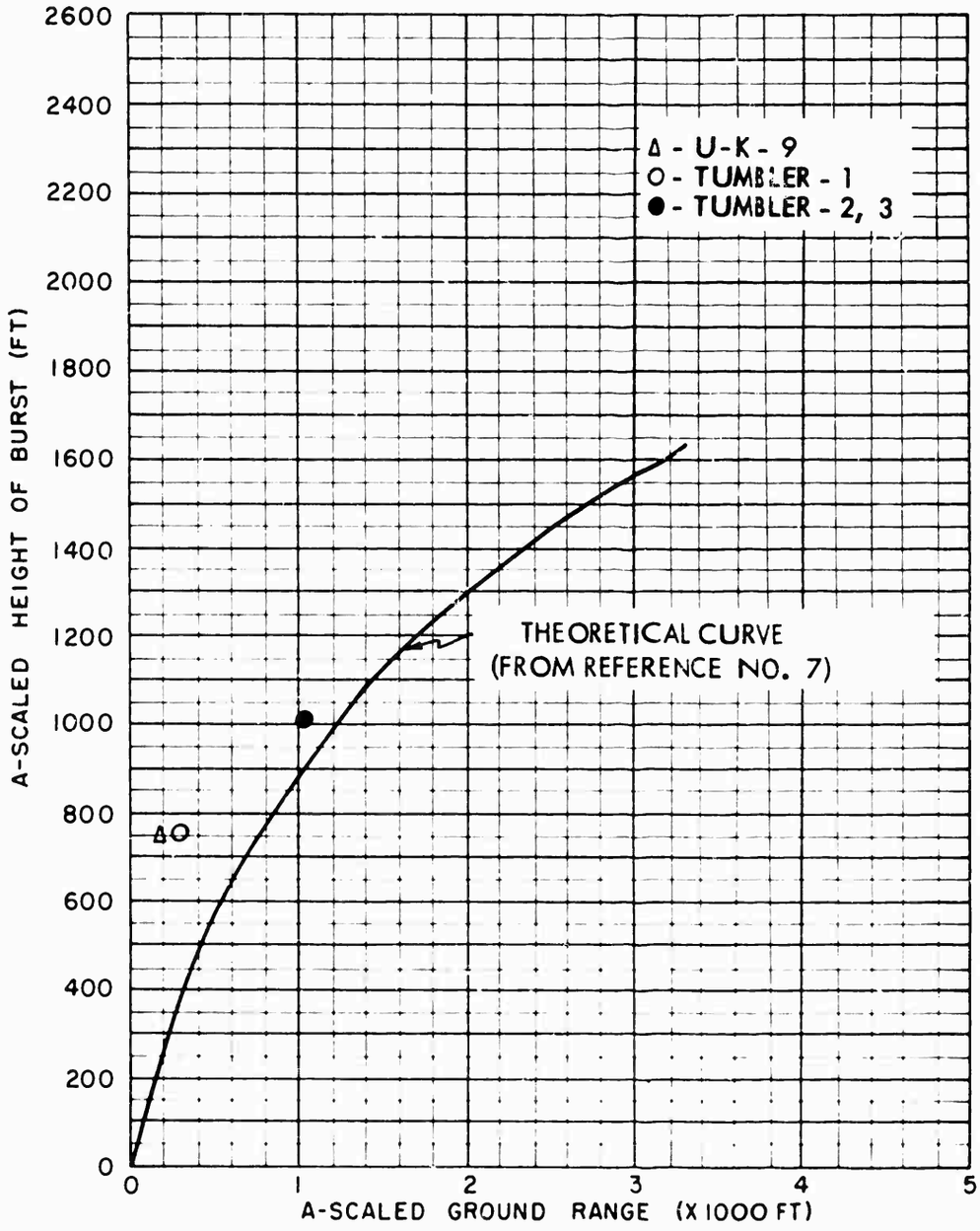

Fig. 5.20 Theoretical Curve for Onset of Mach Reflection with Experimental Points

and refracted waves would explain the inflections in the pressure-distance curves.

TUMBLER Shot 1 A-scaled Mach stem data are shown in Fig. 5.19. These data indicate a behavior similar to that observed on Shot 9; the hump occurs at an A-scaled ground range of about 800 ft. The ground range at which thermal-Mach reflection began on TUMBLER Shot 1 is shown on Fig. 5.20 and this point agrees well with the Shot 9 point on the same figure. This scaling between the two shots is confirmed in this respect. (See Section 5.2.1). In Fig. 5.20, the point for TUMBLER Shots 2 and 3 corresponds more closely with the theoretical curve, as might be expected from the greater burst height.

5.4.2 Wave Front Orientation

In order to follow more closely the behavior of the Mach reflection, studies were made of the times of arrival of the incident, reflected, and Mach fronts at the various stations. The calculations can be described as follows:

1. The as-read arrival times are corrected for differences in location of surface and aboveground gages using the horizontal trace velocity at each gage station.

2. Using the corrected arrival times and the arrival at the surface gage as the station reference time, the Δt for each level is determined.

3. The Δt values for each level are multiplied by the horizontal velocity to get ΔR.

The results of these calculations for Shot 9 are shown in Table 5.7 and plotted in Figs. 5.21 and 5.22. The dashed lines indicate the geometric incident angle to the shot source at each station; however, the position of the dashed line is not meant to imply that the position of the free air incident shock is known at these times. A fairly complete picture of the wave front configurations at the various gage stations can be seen from these figures. The measured incident and reflected wave angles correspond closely with the geometric orientations. The slight deviations in angle at the close-in stations (214 and 215) of Fig. 5.21 can be attributed to a thermal layer producing refraction which results in curvilinear wave transmission. This figure snows that the Mach stem exhibits a change in orientation in the region of 1293 ft (Station 216) to 2622 ft (Station 202). This corresponds to the region in which the large hump in the stem height curve is observed (Fig. 5.18). In the first part of this region the lower part of the stem seems to travel faster than the upper, while between Stations 200 and 202 the upper part catches up to give a vertical stem orientation. It is interesting to note that the wave front configurations at Stations 217 and 200 are very similar to those to be expected in the early stages of the formation of a precursor. Somewhat similar variations in the shape and position of the Mach stem Y are observed after the formation of the Mach stem is well developed, at Stations 206 and 209, Fig. 5.22.

TABLE 5.7 - Wave Front Orientation, Shot 9

Stn. No.	Grnd. Range (ft)	Horiz. Velocity (fps)	Arr.Time 0' Level (sec)	Height	t_s(0'level)-t_a		ΔR	
					Incident (ms)	Reflected (ms)	Incident (ft)	Reflected (ft)
214	837	3700	1.1016	10	5.6	-6.4	21	-24
				30	18.1	-23.4	67	-87
				50	31.1	-40.4	115	-150
215	967	3300	1.1381*	10	5.1	- 5.9	17	-20
				30	18.1	-24.4	60	-81
				50	31.1	-40.9	103	-135
216	1293	2800	1.2413	10	3.7	- 6.3	10	-18
				30	17.8	-20.7	50	-58
				50	29.8	-37.2	83	-104
217	1705	2350	1.4038	10	1.4	- 5.1	3	-12
				30	13.8	-18.1	32	-43
				50	25.8	-32.2	60	-76
200	2154	2000	1.616	10	-2.	- 3.	-4	- 6
				30	10.	-13.5	20	-27
				50	20.	-26.5	40	-53
202	2622	1750	1.8759	10	0.9	- 1.6	2	- 3
				30	11.9	-10.1	21	-18
				50	21.9	-19.1	38	-33
204	3100	1600	2.1687	10	0.2	**	0.3	**
				30	8.7	- 6.8	14	-11
				40	14.2	- 8.8	23	-14
				50	NR	NR	NR	NR
206	3584	1500	2.4847	10	-2.3	**	-3.5	**
				30	5.7	- 5.3	9	- 8
				40	9.7	- 7.8	15	-12
				50	14.2	- 9.8	21	-15
208	4072	1400	2.8244	10	-0.1	**	-0.1	**
				30	3.4	- 0.6	4.8	- 0.8
				40	6.9	- 2.1	9.7	- 2.9
				50	9.9	- 5.6	13.9	- 7.8
209	4562	1370	3.1782	10	-1.8	**	-2.5	**
				40	0.2	**	0.3	**
				50	3.7	- 0.8	5.1	- 1.1
210	5055	1310	3.5463	10	1.3	**	1.7	**
				50	1.8	**	2.4	**
285	6539	1270	4.706	10	0.6	**	0.8	**
				35	0.6	**	0.8	**

NR - No record
* - Estimated value
** - Mach stem region

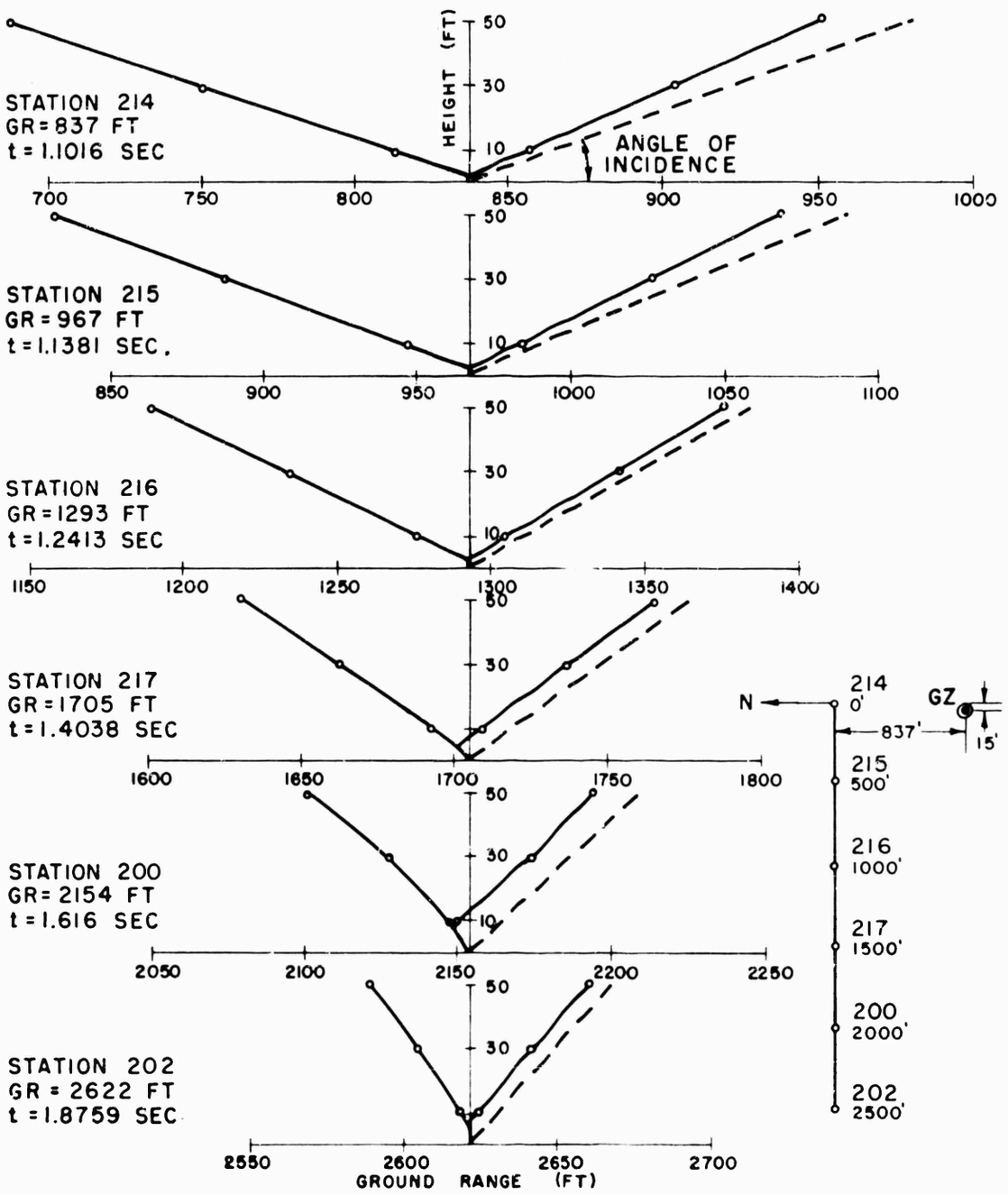

Fig. 5.21 Wave Front Orientation, Stations 214-202, Shot 9

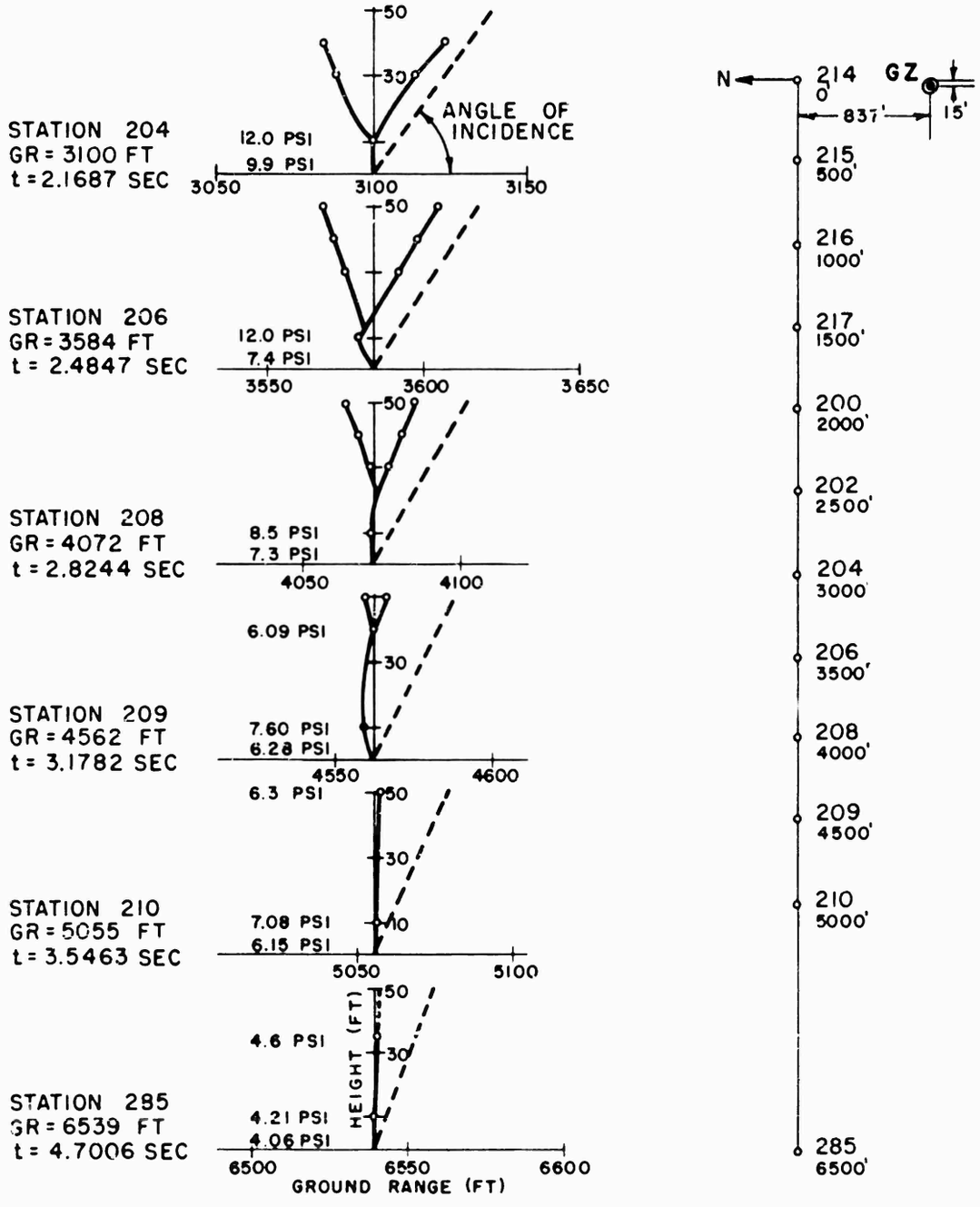

Fig. 5.22 Wave Front Orientation, Stations 204-285, Shot 9

TABLE 5.8 - Wave Front Orientation, Shot 10

Sta. No.	Grnd. Range (ft)	First Arrival 0' Level (sec)	Height	Precursor			Main Wave		
				Horiz. Velocity (fps)	Δt (ms)	ΔR (ft)	Horiz. Velocity (fps)	Δt (ms)	ΔR (ft)
216	925	0.1926	0	3800	0	0	2900	-59.4	-172
			10		- 2.2	- 8		CB	CB
			10A		- 3.2	- 12		CB	CB
			50		- 14.4	- 55		-47.9[a]	-139[a]
			50A		- 13.9	- 53			
217	1421	0.3518	0	2400	0	0	Irregular Wave form		
			10		- 7.5	- 18			
			30		- 14.7	- 35			
			50		- 23.7	- 57			
			10	2400	- 32.	- 77[b]			
			30		- 78.7	-189[b]			
			50		-120.	-288[b]			
200	1919	0.5966	0	1650	0	0	Irregular Wave form		
			10		- 8.4	- 14			
			30		- 20.9	- 34			
			50		- 33.9	- 56			
202	2418	0.9748	0	1250	0	0	1600	-66.8	-107
			10		- 4.2	- 5		-67.2	-108
			50		- 8.2	- 10		-60.2	- 96
204	2917	1.367	0				1430	0.0	0
			10					0.0	0
			30					0.0	0
			40					0.0	0
206	3417	1.744	0				1320	0.0	0
			30					0.0	0
			40					0.0	0
			50					0.0	0
208	3917	2.1305	0				1250	0.0	0
			10					0.0	0
			30					0.0	0
			40					0.0	0
			50					- 1.0	- 1.3
209	4416	3.525	0				1210	0.0	0
			10					- 1.0	- 1.2
			50					- 1.5	- 1.8
210	4916	2.927	0				1200	0.0	0
			50					- 1.0	- 1.2
285	6416	4.1725*	10				1190	0.0	0
			35					- 0.5	- 0.6

a - Values for incident wave. Reflected wave: Δt = -69.4 ms, ΔR = -201 ft
* - Estimated value
b - Secondary precursor shock

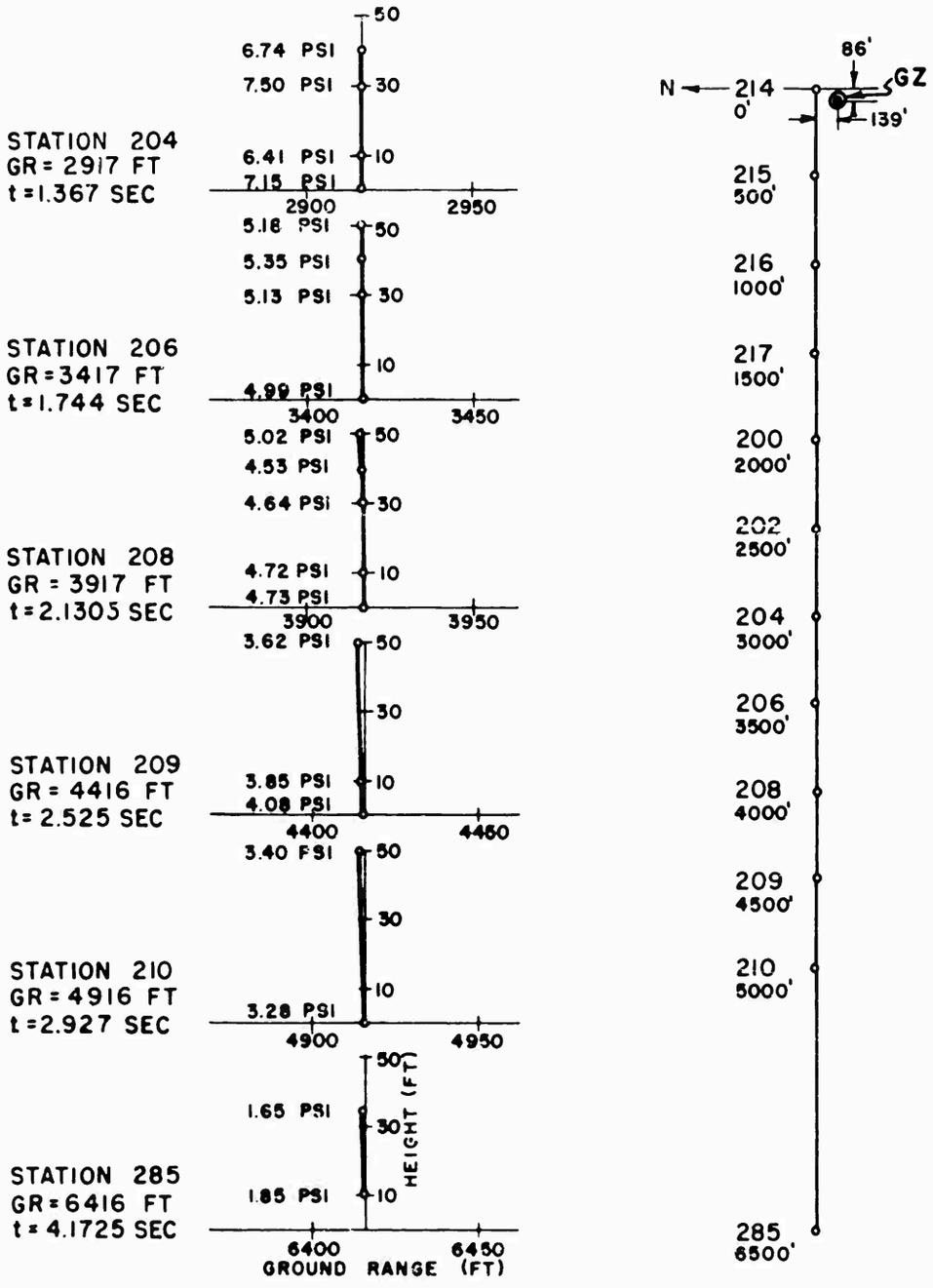

Fig. 5.23 Wave Front Orientation, Mach Stem Region, Shot 10

It has been observed in preceding sections of this report that, on Shot 9, certain inflections are apparent in the curves of pressure and Mach triple point height. The wave front orientation studies show incipient precursors, and the pressure-time wave forms (Fig. 4.7) show some distortion in this region. Similar inflections are to be seen on the data curves from TUMBLER Shot 1. These observations, taken in total, lead to the conclusion that thermal effects were present on these shots, probably in the form of a heated layer very near the ground surface.

For comparison, similar calculations of wave front orientation made for Shot 10 are shown in Table 5.8 and the results for the non-precursor region are plotted in Fig. 5.23. Here the Mach stem is essentially vertical at all stations.

5.5 PRECURSOR PHENOMENA

Some of the data obtained by this project, particularly from Shots 10 and 11, will be useful in supplementing the existing knowledge of precursor phenomena. From the air pressure time of arrival data on Shot 10, it is possible to obtain wave front orientations in the region of the precursor. The air pressure vs time records obtained on Shots 10 and 11 yield some valuable data on the general characteristics of the precursor wave and how this disturbance affects the main air blast wave. In addition, these UPSHOT-KNOTHOLE precursor records can be compared with those obtained from TUMBLER. Finally, on the basis of a measurement on Shot 11, the dynamic pressure as affected by a precursor wave will be discussed.

5.5.1 Wave Front Orientation

Wave front orientations were found for the precursor wave of Shot 10 in a manner similar to that described in Section 5.4.2 of this report. The results of these calculations are tabulated in Table 5.8 and shown in Fig. 5.24. The figure illustrates, at each gage station, the wave front orientation of the precursor wave.

Wave front orientations corresponding to the three stations closest to ground zero, F-216 (925 ft), F-217 (1421 ft), and F-200 (1919 ft), make the same angle with the ground surface. Referring to Section 1.3.2 and Fig. 1.3 of this report, it is noted that this angle corresponds to α_c, the critical angle for precursor formation. Measurement of the angle of the wave fronts yields a value of about 40 degrees with respect to the ground surface, a value which agrees well with that obtained from NOL shock photography data.[23] This result would indicate that the precursor wave on Shot 10 (burst height 524 ft) formed at about 440 ft ground range. This value is not inconsistent with observation, since the Station F-215 (430 ft ground range) air pressure record (see Fig. 4.9) exhibits a precursor pressure which precedes the main shock pressure wave by only 5 msec.

By the time the precursor wave arrived at Station F-202 (2418 ft ground range), a significant change in the wave front orientation had occurred. This is the last station at which a precursor was observed on Shot 10 and the orientation shows that the upper portions of the front were "catching up" with those near the ground, indicating that

the so-called thermal layer had almost if not entirely disappeared at this radius.

Figure 5.25 shows the comparison of precursor wave front orientations from TUMBLER Shot 4 and U-K Shot 10 (at A-scaled ground ranges).

The orientations in the vicinity of 350 ft (A-scaled) range show that the TUMBLER wave front makes a smaller included angle with the ground surface than does the Shot 10 precursor front. This result can be explained by either concluding that the precursor wave formed at a smaller A-scaled ground range on U-K Shot 10 or ascribing the difference in orientation angle to a more severe temperature gradient on TUMBLER Shot 4. Since the former explanation is contradicted by other analyses,[9] the temperature argument seems more plausible. Again referring to Fig. 5.25, the precursor wave front orientations for the two shots are similar in the 500 ft (A-scaled) range; however, near 730 ft, the indication is that, on a scaled basis, the TUMBLER Shot 4 precursor wave dissipated at a smaller ground range than did the same wave on Shot 10.

Because measurements were taken at only the surface and 10 ft levels on Shot 11, it is not possible to compute precursor wave front orientations that lend themselves to analysis.

5.5.2 Precursor Wave Characteristics

The heated layer theory of precursor formation and the remarks of the previous section point to the fact that the precursor wave follows a pattern of development and subsequent decay. One would expect the air pressures associated with the precursor to be highest at the ranges closest to ground zero; however, because of the time factors involved in development of the thermal layer, the durations and impulses of the precursor may not follow this same rule.

An insight into these characteristics can be gained from reference to Fig. 5.26. This figure shows the gage records obtained from the auxiliary gages on Shot 10 (surface level) and it illustrates some of the fine grain detail of the precursor wave characteristics. The records in the figure represent a variation of only 135 ft in slant range and the gage calibrations are similar enough to allow for visual comparisons. The general characteristics observed are as follows:

(1) The maximum air pressure associated with the precursor decreases with increasing ground range in about the same manner as the maximum air pressure of the main shock.

(2) The precursor pulse duration lengthens with increasing ground range, indicating that the transmitted wave front traveling in the thermal layer has a higher velocity than the main shock front (see Fig. 1.3); because of the cable breaks on records 16BA and 16BB, no pertinent comparison can be made to the durations of the main shock.

(3) As the precursor duration increases, the air pressure of the precursor wave decays to almost ambient pressure before the arrival of the main shock at the gage station.

(4) The rise time to the maximum pressure associated with the

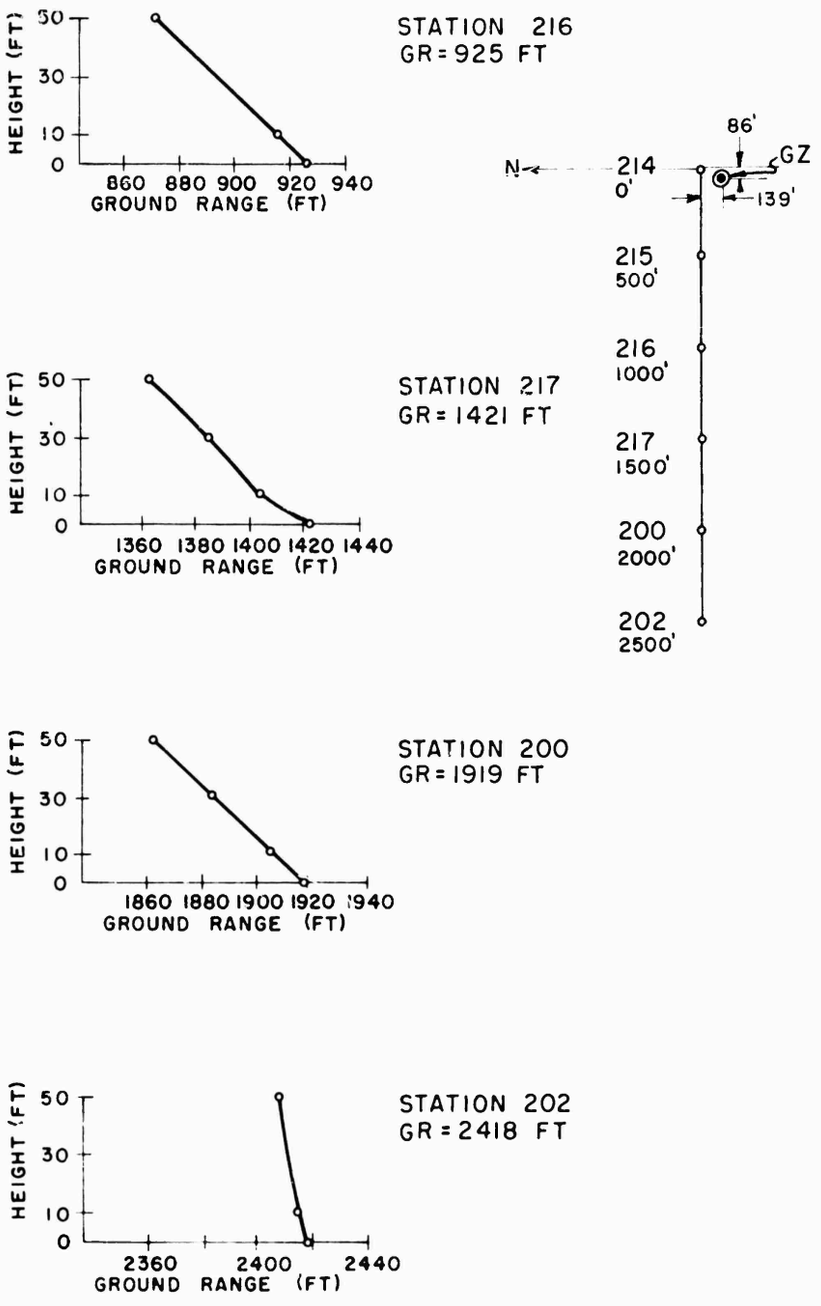

Fig. 5.24 Wave Front Orientation, Precursor Region, Shot 10

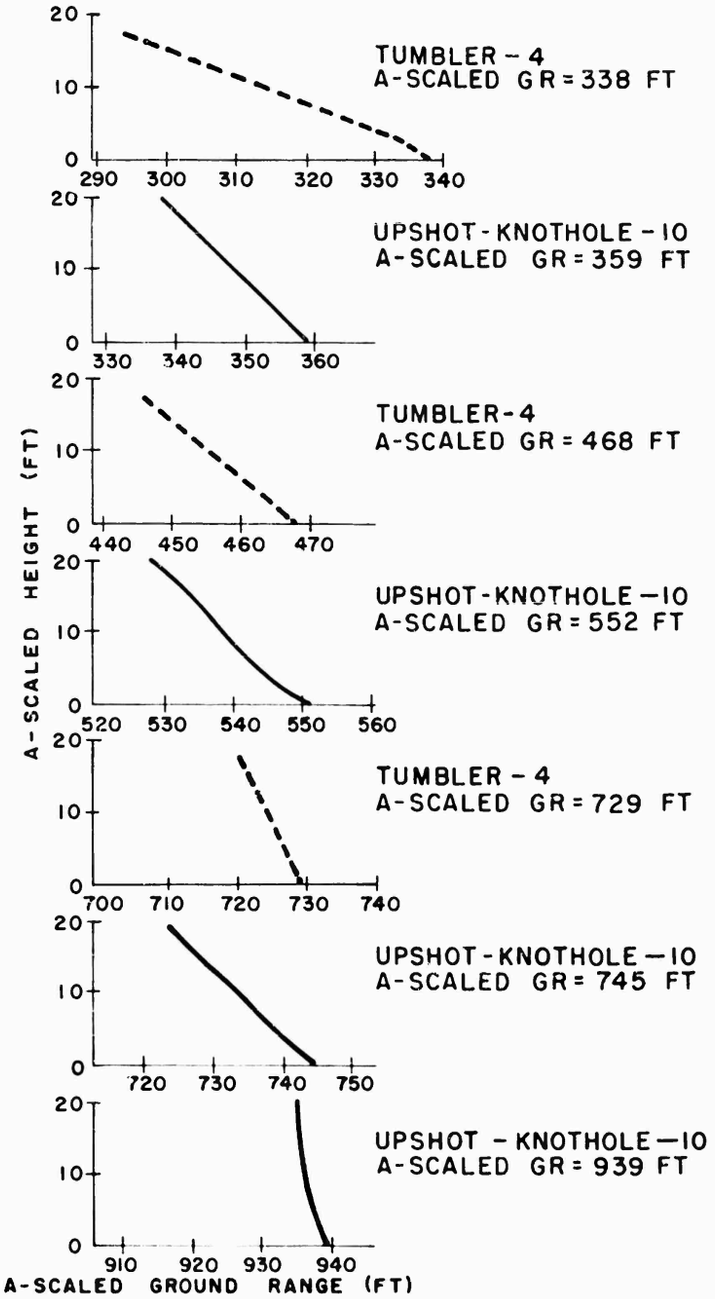

g. 5.25 Precursor Wave Front Orientation, Shot 10, Compared to TUMBLER Shot 4 (Note A-scaled Ground Range)

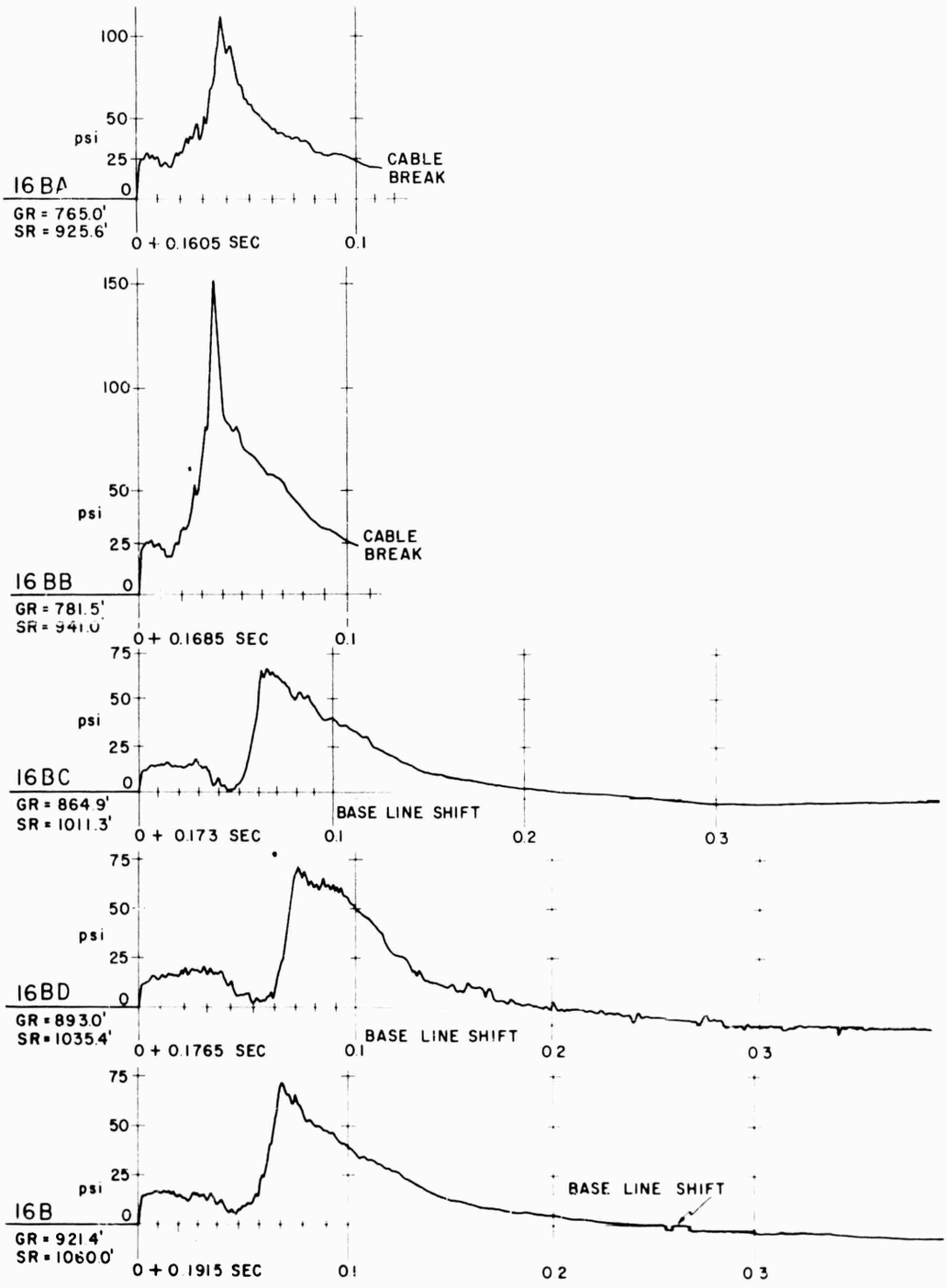

Fig. 5.26 Precursor Wave Forms, Shot 10

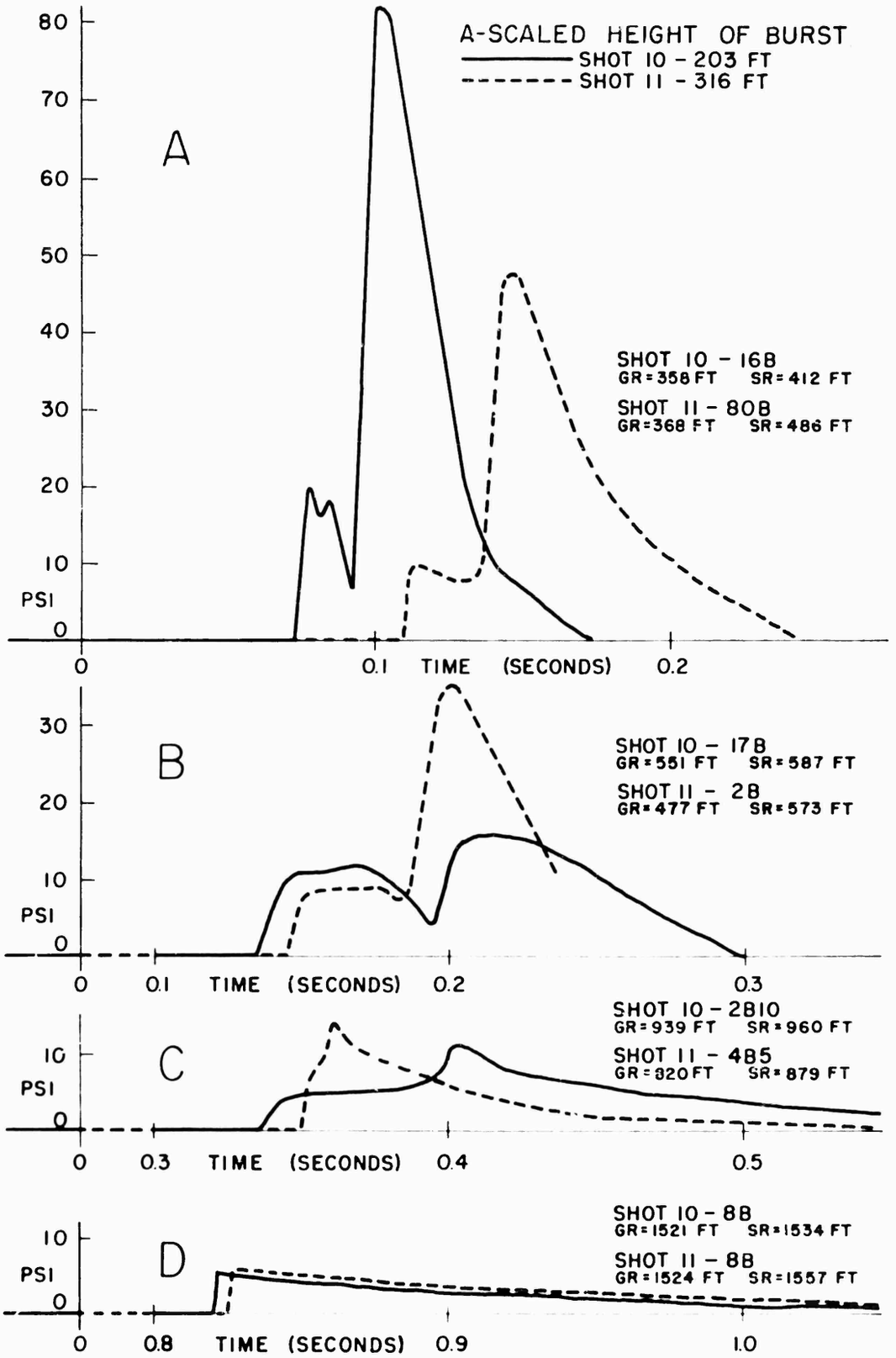

Fig. 5.27 A-Scaled Precursor Wave Forms, Shots 10 and 11

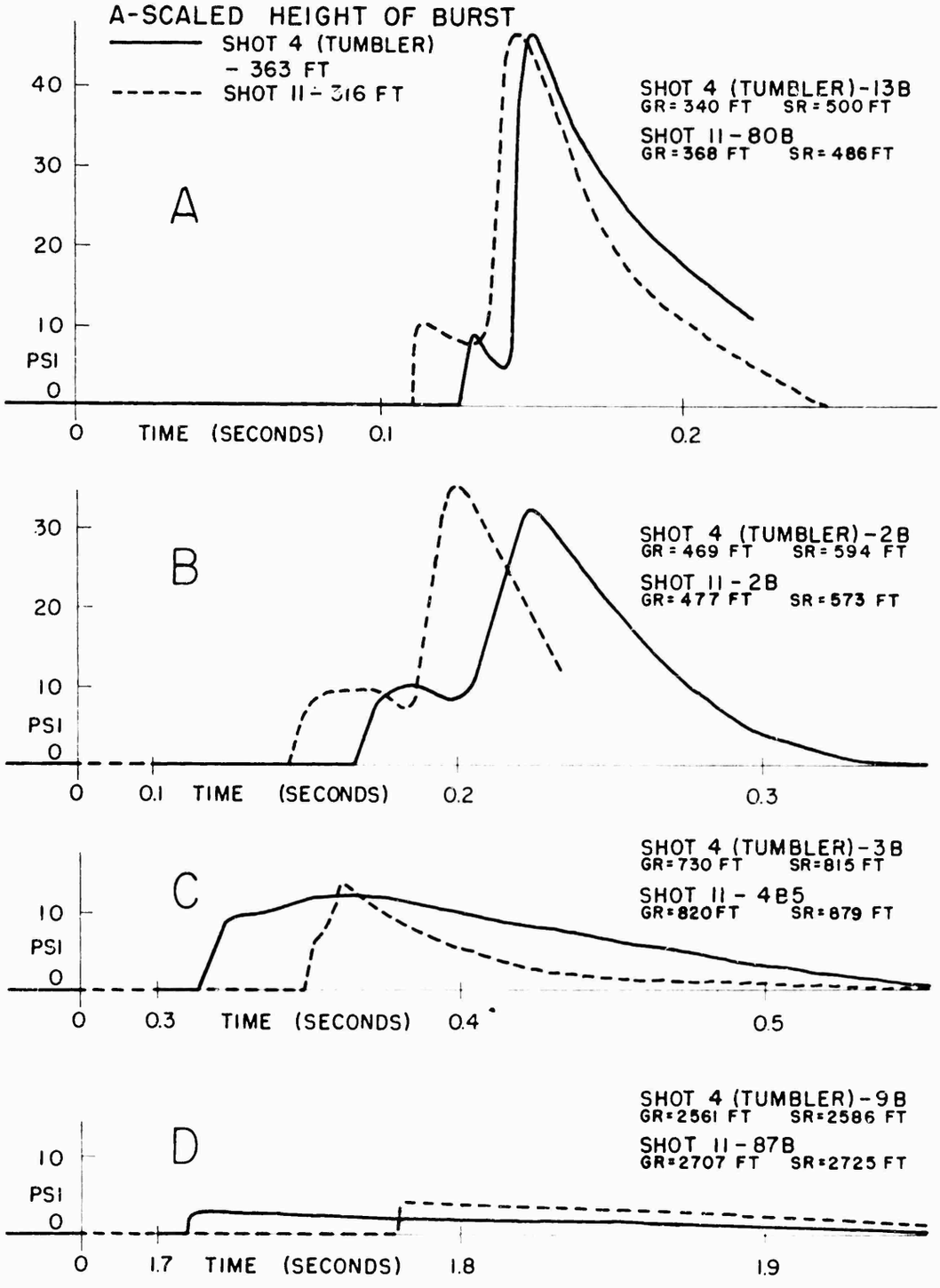

Fig. 5.28 A-Scaled Precursor Wave Forms, Shot 11, Compared to TUMBLER Shot 4

main shock is longer than for classic shock waves.

From the analysis of the previous sections concerning thermal phenomena, one might conclude that it is unlikely that the precursor wave obeys the same scaling laws as a normal undisturbed shock wave. There is actually little data available on how the precursor characteristics vary from shot to shot; however, some comparisons can be made between UPSHOT-KNOTHOLE and TUMBLER, as shown in Figs. 5.27 and 5.28.

Figure 5.27 shows the comparison of wave forms in the precursor region for U-K Shots 10 and 11. These wave forms have been replotted on A-scaled pressure and time coordinates. The scaled burst heights of these shots were quite different, 203 ft for Shot 10 (14.9 KT) and 316 ft for Shot 11 (60.8 KT). The wave forms in Part A of Fig. 5.27 are similar, but the difference in pressure magnitudes is probably due to the scaled burst height difference. Part B indicates that the Shot 11 precursor, although comparable to that on Shot 10, has not depressed the main shock pressure to the extent evident on the Shot 10 record. The Shot 11 precursor wave has almost disappeared on Part C of Fig. 5.27, whereas the Shot 10 wave is quite prominent. Part D shows a wave form comparison beyond the precursor regions; the similarity is obvious.

The comparison of precursor wave forms of TUMBLER Shot 4 and U-K Shot 11 is shown in Fig. 5.28. As in the previous figure, these records have been replotted to A-scaled coordinates. The scaled burst heights of these shots, however, were more comparable--363 ft for TUMBLER Shot 4 (19.6 KT) and 316 ft for U-K Shot 11 (60.8 KT). In Parts A and B of Fig. 5.28, [illegible]-scaled records from the two shots compare favorably both in form and magnitude. The Part C curves show that the TUMBLER Shot 4 record had a larger impulse associated with it; however, it should be noted that the Shot 11 data were taken almost 100 ft (A-scaled) farther out from ground zero. The pressure records at stations beyond the precursor region are shown in Part D.

5.5.3 Dynamic Pressure on Shot 11

The dynamic pressure associated with shock waves takes the form of a blast wind or impact pressure. The theory of dynamic pressures has as its basis the established hydrodynamic equations for shock waves.[24] The Rankine-Hugoniot relations lead to an expression for the dynamic pressure, q, given by

$$q = 1/2\ \rho u^2 = \frac{25}{14} \rho_o a_o^2 \left(\frac{y^2}{(7 + y)}\right), \quad (5.8)$$

where ρ is the air density, u is the particle (wind) speed, a_o is the velocity of sound in undisturbed air under ambient conditions, and y is the ratio of overpressure to ambient pressure.

It can be seen from this relation that if one considers overpressure the basic parameter, theoretical analysis can yield the variation of other parameters as a function of overpressure, and these results can be compared with the measurements. If the experimental data agree with theory, then further measurements of dynamic pressure would seem unwarranted since techniques for measuring static overpressure are

already well developed.

The results obtained on TUMBLER-SNAPPER[14] indicated that the above theoretical correlation between static and dynamic pressure may not hold in regions where the static air pressure exceeds 5 or 6 psi. In fact, even immediately behind the shock front, where one would expect the Rankine-Hugoniot equations to be reasonably valid, marked deviations from Equation 5.8 were evident. In view of these results, it was decided that more measurements of dynamic pressure should be made during UPSHOT-KNOTHOLE. This experimental investigation was primarily assigned to other projects, but when Shot 11 was scheduled late in the series, Project 1.1b was requested to make at least one such measurement.

On Shot 11, two gage channels were connected to a Pitot tube gage,[14] on loan from Sandia Corporation, designed to measure dynamic pressure. The purpose of this installation was to attempt to correlate a dynamic pressure measurement with a conventional side-on pressure measurement in the region of a precursor wave.

Figure 5.29 (from Table 5.9) shows a plot of the Rankine-Hugoniot relation between dynamic pressure (q) and static side-on pressure as measured by the Pitot gage; the curve is plotted to correspond to Shot 11 ambient conditions.

The records from the two q-gage channels are shown in Fig. 5.30, where 4B5 designates the static side-on overpressure record and 4Q5 is the dynamic pressure record.

The Pitot gage calibration factors were corrected for angle of yaw (ψ) and Mach number (M) on Shot 11. The magnitudes of these corrections were provided by the Sandia Corporation. The lower dashed line on the 4Q5 coordinates shows the dynamic pressure determined by using the plot of Fig. 5.29 in conjunction with the measured side-on pressure, 4B5. It is obvious that there is poor agreement between this q curve (from the graph) and the measured dynamic pressure record. In fact, the inferred curve appears to be about 40 per cent too low throughout.

As has been stated in Section 4.5 of this report, the existence of large thermal and dust effects shows evidence of depressing the maximum side-on air pressure measured near the ground surface. Since the thermal disturbances are known to have been appreciable on Shot 11, one may question the validity of accepting the 4B5 record as a measure of the Rankine-Hugoniot shock pressure. Instead, it is possible to estimate the approximate side-on pressure as a function of time under "normal" conditions, i.e., no thermal effects. The computation of the normal static pressure requires an estimate of the reflection factor and the incident free air pressure at the gage station in question (Station 204).

TABLE 5.9 Dynamic Pressure Calculations

ΔP (psi)	$1/2\rho u^2$ (psi)	q_c (psi)
1.0	0.0281	0.02812
2.0	0.111	0.1113
4.0	0.436	0.4404
6.0	0.958	0.9781
8.0	1.67	1.725
10.0	2.55	2.672
12.0	3.61	3.841

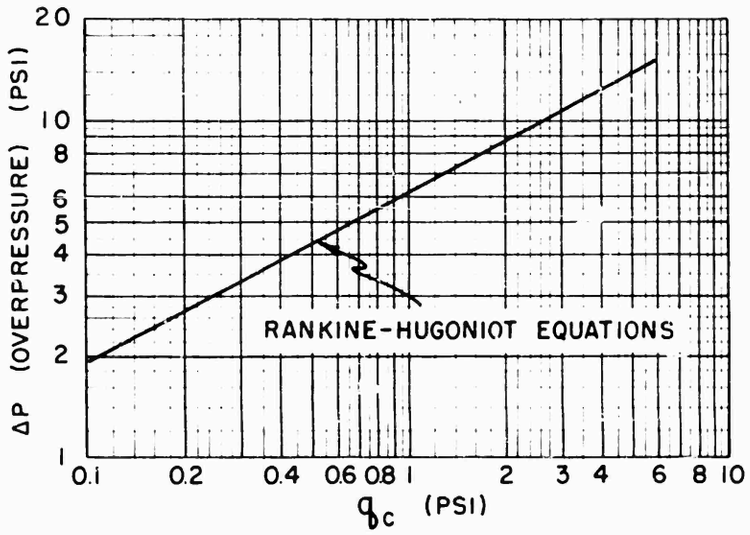

Fig. 5.29 Static Pressure vs Dynamic Pressure

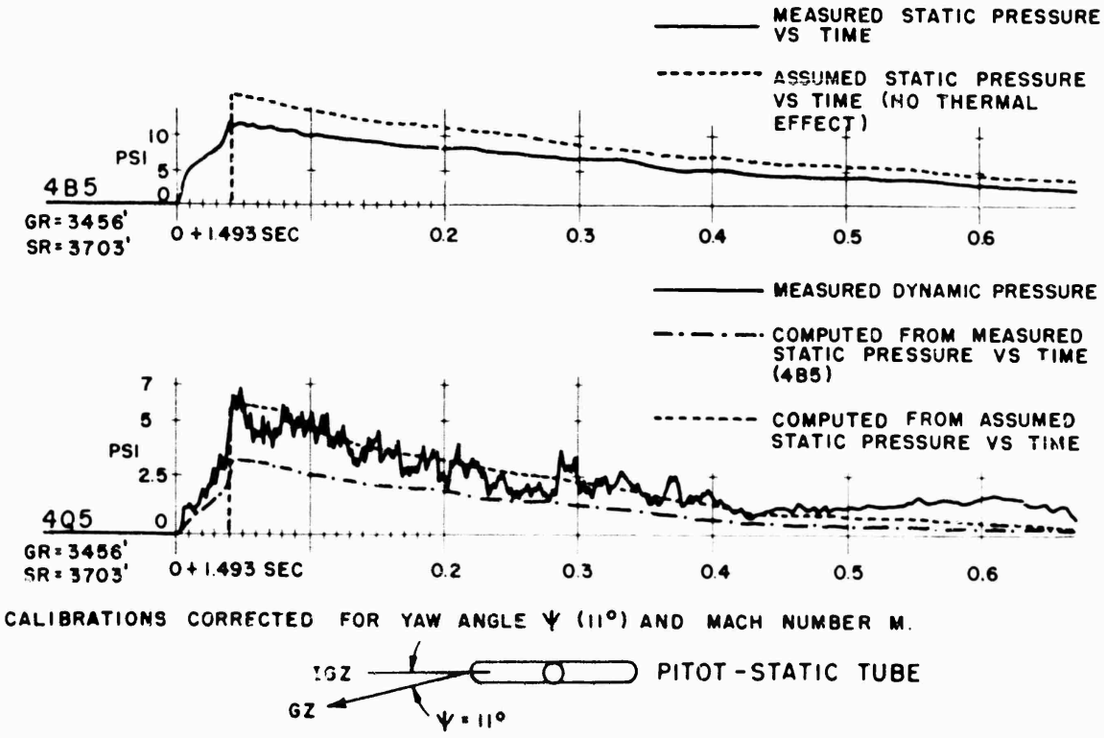

Fig. 5.30 Theoretical and Measured Dynamic Pressure vs Time, Shot 11, Station 204

Since the reflection factor is a function of shock strength, angle of incidence, and possibly type of terrain, it was thought best to look to data from previous tests for the estimate. Considering data from TUMBLER Shots 2 and 3, the value 2.3 was taken as the reflection factor at Station 204 (U-K Shot 11). The normal incident free air pressure was determined from the AFSWP free air curve.[7] The result of these calculations of normal static pressure yields the dotted curve on the 4B5 coordinates of Fig. 5.30. When this new static pressure vs time record is applied to the curve of Fig. 5.29, one obtains the dynamic pressure shown as a dotted line on the 4Q5 coordinates of Fig. 5.30. The general agreement with the measured dynamic pressure is evident. One must be cautious when basing conclusions upon such fragmentary data. However, it can be said that the Shot 11 dynamic pressure measurement yields a peak value which is significantly greater than would be computed using the measured side-on pressure and the classical Rankine-Hugoniot relations. In addition, the effect upon the dynamic pressure gage of large quantities of dust could have a profound influence upon any pertinent conclusions.

The single Shot 11 dynamic pressure measurement, as well as several similar measurements made on Shot 10,[15] points up the need for a new approach to the theoretical and physical concepts of dynamic pressure, particularly in regions of large thermal and/or dust effects.

5.6 HEIGHT OF BURST CONSIDERATIONS

A well-documented surface level height of burst chart is found in TM 23-200, Capabilities of Atomic Weapons[20] and is reproduced here in Fig. 5.31. This family of curves was drawn using all available data up to and including TUMBLER. The figure also shows points from U-K Shots 3, 4, 9, 10, and 11. These points were obtained from curves of Fig. 5.4 and are tabulated in Table 5.10. For completeness, surface level points for U-K Shot 1, reported by the Sandia Corporation[25] (Project 1.1c-1), are included.

TABLE 5.10 A-Scaled Height of Burst Data

Shot	A-Scaled Height of Burst (ft)	Pressure									
		50 psi	30 psi	20 psi	15 psi	10 psi	8 psi	6 psi	4 psi	3 psi	2 psi
		A-Scaled Ground Range									
1[25]	112.5	350	405	460	525	720 920	1110	1360	1800	2220	2940
10	203	420	495	570	620	735	1200	1445	1880	2240	2840
11	316	340*	465	560	625	1035	1230	1510	2035	2550	a
3	486	a	a	a	a	a	a	a	2300	2600	3200
9	764	a	240	425	615	1240	1480	1840	2440	2940	3720
4	2378	a	a	a	a	a	a	a	a	1400	2600

a - Not observed in instrumented region
* - Extrapolated

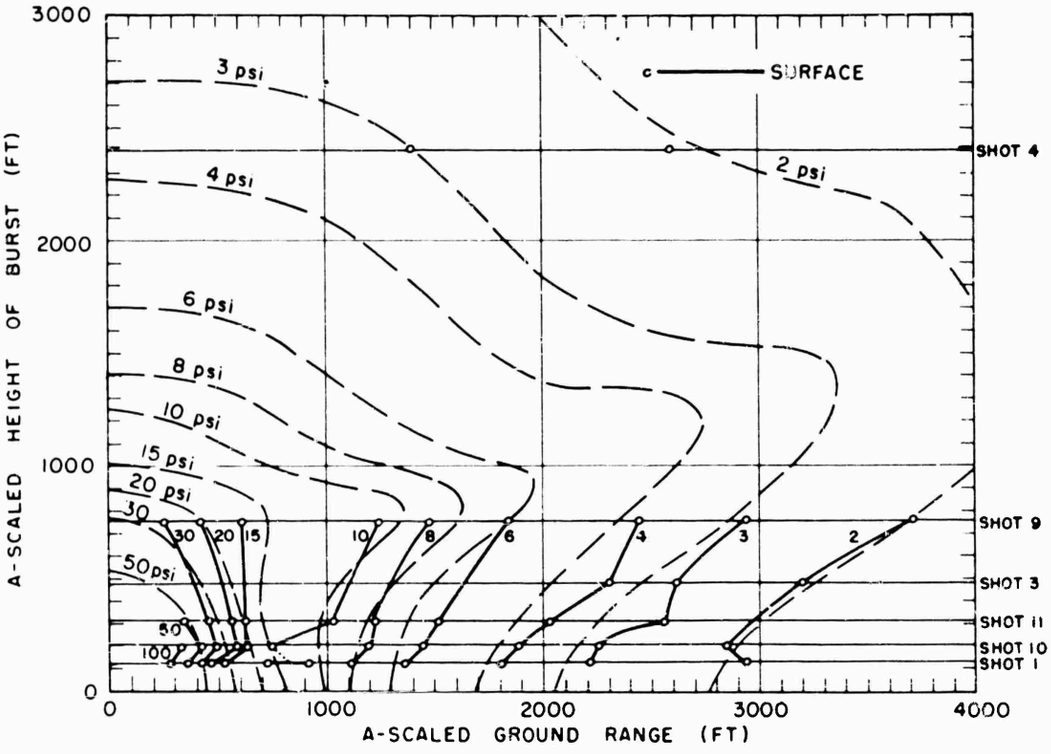

Fig. 5.31 Height of Burst Chart with UPSHOT-KNOTHOLE Data Points

With minor exceptions, these surface level data agree with the basic curves at A-scaled ground ranges of more than 1000 ft (A-scaled pressures less than 8 psi). In fact, Shot 4 data verify the extrapolation used for the extremely nigh burst heights. At higher pressures, however, some pronounced deviations appear.

In order to inspect more conveniently the nigh pressure portion of the height of burst chart, the curves of Fig. 5.32 are presented. These curves appear in Supplement No. 1 [26] to the TM 23-200 manual [20] in which account is taken of the condition of the target surface. This supplementary reference presents, for each pressure level, three curves designated as Good, Fair, and Poor, corresponding to good, fair, and poor surface reflection characteristics. The data from Table 5.10 also are plotted on Fig. 5.32.

For UPSHOT-KNOTHOLE Shot 9 (764 ft A-scaled burst height), the figure indicates agreement with the Fair and Good curves in the range of available data (6-30 psi). In the case of Shot 11 (316 ft A-scaled burst height), the surface level peak pressure data fall between the

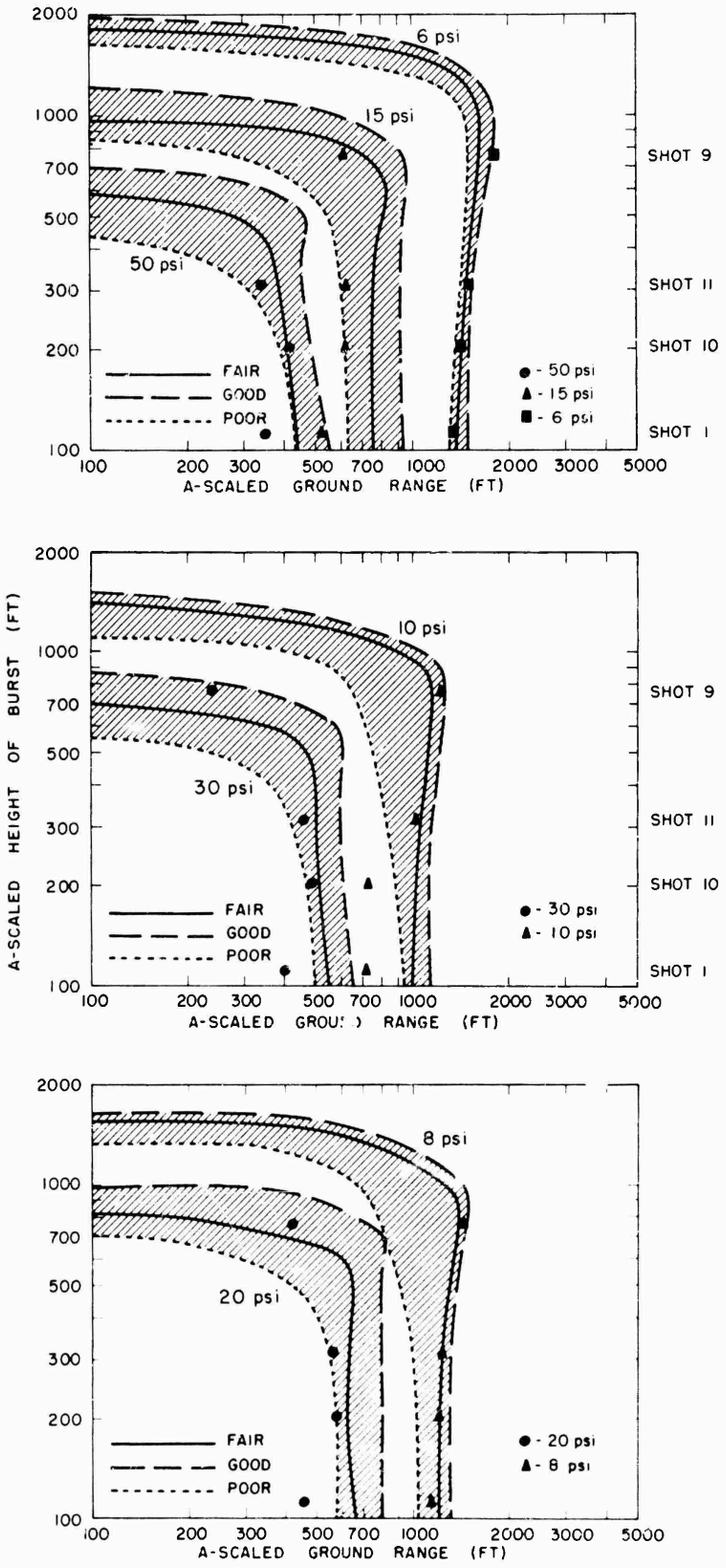

Fig. 5.32 Height of Burst Charts for Various Types of Reflecting Surfaces

Fair and Poor curves in the 10-50 psi region; however, agreement with the Fair and Good curves is evident for 8 psi and 6 psi, respectively. The Shot 10 burst height (A-scaled) was about 200 ft and the data plotted on Fig. 5.32 appear to agree well with the Fair curve for the 50 psi and 30 psi contours. For lower pressures (10-20 psi), however, the Shot 10 points favor the Poor curves. In fact, the 10 psi data point falls far outside the shaded portion corresponding to the 10 psi peak pressure level. The 6 psi and 8 psi points for Shot 10 agree well with the Fair curves of the figure.

Although the measurements were made by another agency, a few comments on the UPSHOT-KNOTHOLE Shot 1 (112 ft burst height) results shown in Fig. 5.32 are in order. In the pressure range 10-50 psi, the data points appear at significantly low A-scaled ground ranges; in other words, for this shot, the reflecting surface behaved as a very poor one indeed. The "double" data point for 10 psi is due to an inflection in the peak pressure vs distance curve at this pressure value, which defines an increment of ground range over which the peak pressure was essentially the same. The Shot 1 data corresponding to 6 and 8 psi agree well with the Fair curves of the figure.

In summary, it can be said that for A-scaled burst heights above about 300 ft the agreement with the Fair curves is reasonable in the 6-50 psi pressure range. Below 300 ft A-scaled burst heights, the tendency is toward agreement with the Fair and Poor curves. However, Shot 1 data present an interesting anomaly in the 10-50 psi region, where abnormal depressions of surface level peak pressure are evident. If the values for zero burst height (based on the JANGLE surface shot data[27]) are to be retained, an "elbow" in the curves for 15-50 psi must be introduced (see Fig. 5.31) near the 100 ft A-scaled height. Nevertheless, without more extensive data in this low burst height region, one should be cautious about substantially altering the TM 23-200 height of burst chart.

5.7 SECONDARY SHOCKS

Secondary shocks, or blips, in the negative pressure phase are observed on the pressure records of Shots 3, 9, 10, and 11. On Shot 11 records, additional shocks are observed in the positive phase; these shocks disappear at large ground ranges. On Shot 9, a very careful examination of gage records indicates an extremely minute secondary shock arrival at Stations 217 (4.257 sec), 200 (4.51 sec), 204 (5.169 sec), and 208 (5.939 sec); the A-scaled arrival times are 1.320, 1.398, 1.602, and 1.841 sec respectively. The pressure was so small that the displacement of the record trace was about one thickness of the trace.

On TUMBLER, calculations based on arrival times indicated that the source of these secondary shocks was at or slightly above the burst point. It was suggested that the main shock after reflection from the ground back up to the fireball was sufficiently refracted by the temperature inversion of the fireball to return to earth.[3]

The location of the source of the blips can be estimated from the U-K data by a comparison of the wave front orientation with the angle of incidence. In Fig. 5.33 the available data from Shots 9 and 10 are plotted. The solid line indicates the wave front orientation as

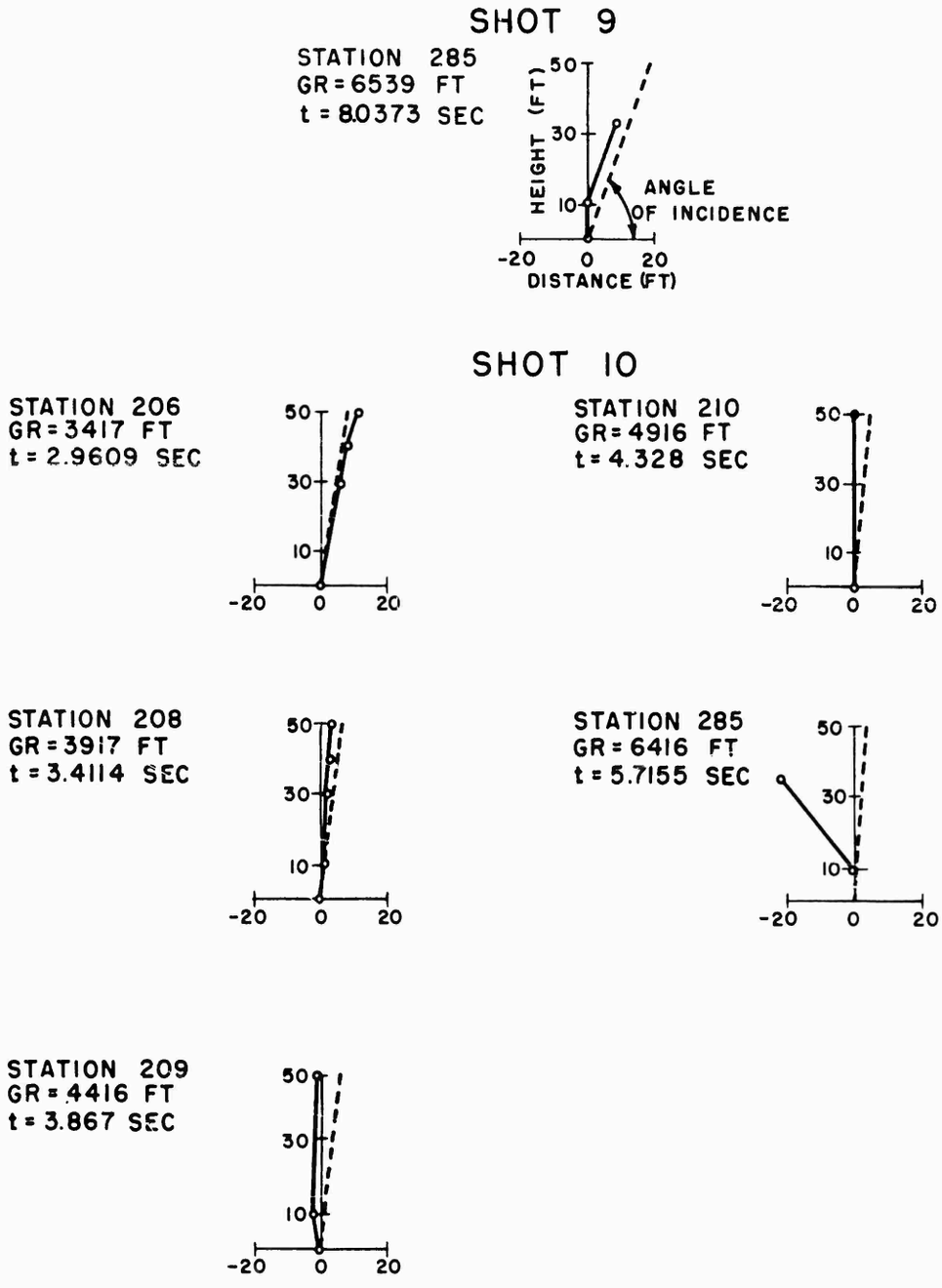

Fig. 5.33 Wave Front Orientation of Secondary Shock, Shots 9 and 10

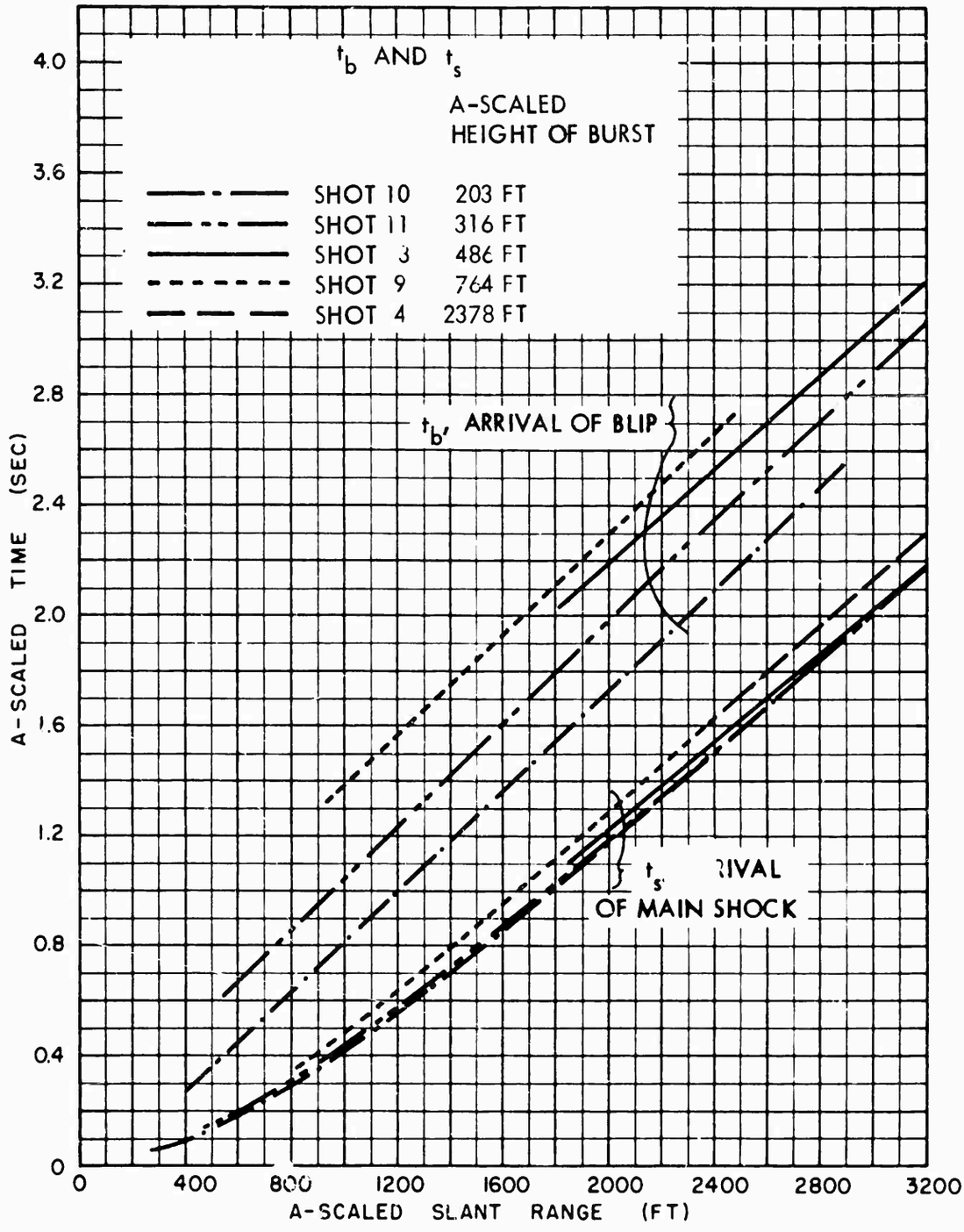

Fig. 5.34 A-Scaled Arrival Times vs Slant Range, Secondary Shocks (blips), All Shots

computed from arrival time differences (see Section 5.4.2); the dotted line shows the angle of incidence. The relation of the two is consistent with the assumption that the source is near the burst point.

If the secondary blips are caused by shock reflection from the ground followed by refraction by a fireball, it should be true that shots with a large height of burst will show a relatively late blip arrival. This fact is borne out by reference to Fig. 5.34 which shows the A-scaled blip arrival time plotted against A-scaled slant range for all shots.

No blips were observed on Shot 4 (scaled burst height 2378 ft) out to the end of the records at 15 sec (5.7 sec A-scaled). Examination of the following 5 or 10 sec at the time the oscillograph records were developed showed no apparent shocks, although it is possible that tiny blips such as those at the stations close to ground zero on Shot 9 might have been present but unobserved. It is possible that a blip existed but arrived later than 15 sec; it is also possible that no blip was formed. By the time the reflected shock returned to the fireball, the inversion layer created by the fireball might have been so dispersed that the angle of refraction was not great enough to return the shock to earth.

5.8 EARTH ACCELERATION AND PARTICLE VELOCITY

In Section 1.3.3 the process of transmitting energy from the air blast to the earth has been considered on a qualitative basis. In Section 4.3.6 the gage records of acceleration were presented and discussed and data taken from these gage records are presented in Tables 4.23 and 4.24. In this section we shall discuss the general behavior of these functions and any meanings to be derived therefrom.

5.8.1 Time of Arrival Curves

Figure 5.35 shows the time of arrival curves for Shots 9 and 10. A generalized form of these curves was shown in Fig. 1.7. The main body of each of these curves follows implicitly the air shock arrivals at the respective stations. At a point where the horizontal component of air shock velocity falls below the near-surface seismic velocity the transmitted wave begins to outrun the main shock arrival. On subsequent gages an early arrival can be detected progressively further ahead of the main shock arrival caused by air blast. These arrivals were very weak, however, and it was impossible to discern the exact time of the first arrival on many of the gage records. On TUMBLER Shot 1,[10] where the acceleration instrumentation was much more complete, this phenomenon was well documented, and velocity of departure was observed to be 1900 fps. Since these two shots (Shots 9 and 10) were on the same blast line as TUMBLER Shot 1, this velocity (dashed lines) has been inserted in Fig. 5.35. It will be seen that they fit the earliest observed points very well. The relative amplitude of the earth-transmitted wave as compared with the air-induced shock was in all cases very small and may be considered to be negligible from any effects standpoint.

5.8.2 Slap Acceleration

On TUMBLER, Project 1.7, it was observed that a definite correlation could be established between incident air pressure and maximum vertical acceleration measured at a 5 ft depth. On Project 1.1b all vertical accelerometers were located at 1 ft burial depth. Figure 5.36 shows maximum negative vertical slap accelerations plotted against peak air pressure for U-K Shots 9 and 10. These data are listed in Tables 4.23 and 4.24. For comparison, the curve from TUMBLER Shot 1 is also shown on the figure. The data from Shot 9 indicate slap accelerations three or four times greater than those measured on TUMBLER Shot 1 and the scatter of data points is considerably greater. The Shot 10 maximum vertical slap accelerations plotted on Fig. 5.36 are quite erratic. The results near 5 and 15 psi are comparable with those of Shot 9; however, near 8 psi the accelerations are much lower. In general all the U-K data points are above those represented by the TUMBLER Shot 1 curve, which is to be expected in view of the difference in gage depth. The scatter of the data is such that no meaningful figure for a relationship between air pressure and peak acceleration can be derived. The definite indication, however, that the acceleration to be expected from a given air shock pressure is considerably greater at 1 ft than at 5 ft is not contrary to previous experimental investigations of other phenomena. It is accepted that the attenuation of maximum peak pressure in the earth from an air blast of considerable duration would be expected to be very small, but the rise time of this pressure would be expected to increase with depth due to energy absorption in the earth. Any correspondence between earth stress measurements and acceleration measurements should be concerned with the derivative of the former with respect to time or with the integral of the latter.

5.8.3 Slap Particle Velocity

Earth particle velocities as a function of time on Shots 9 and 10 were determined by integration of the earth acceleration vs time recordings. The maximum values of earth particle velocities (V_s) appear in Tables 4.23 and 4.24 and representative curves of particle velocity vs time are shown in Figs. 5.37 and 5.38. These curves will be seen to be simpler in wave form than the acceleration records and to have durations more nearly resembling that of the air blast wave.

The values for maximum vertical earth particle velocities on Shots 9 and 10 are plotted against maximum air pressure in Fig. 5.39. Also shown on this figure is the maximum velocity curve from TUMBLER Shot 1.

In previous explosion tests, a question has arisen as to the validity of acceleration records due to the rather low maximum frequency response of instrumentation used. On Project 1.1b, for the vertical accelerometers only, an attempt was made to raise the frequency response characteristics of the instrumentation to avoid this question. Table 5.11 shows the comparison between the natural frequencies of the gages and galvanometers used and the maximum observed frequencies of the record. It is evident that in all the vertical measurements the maximum

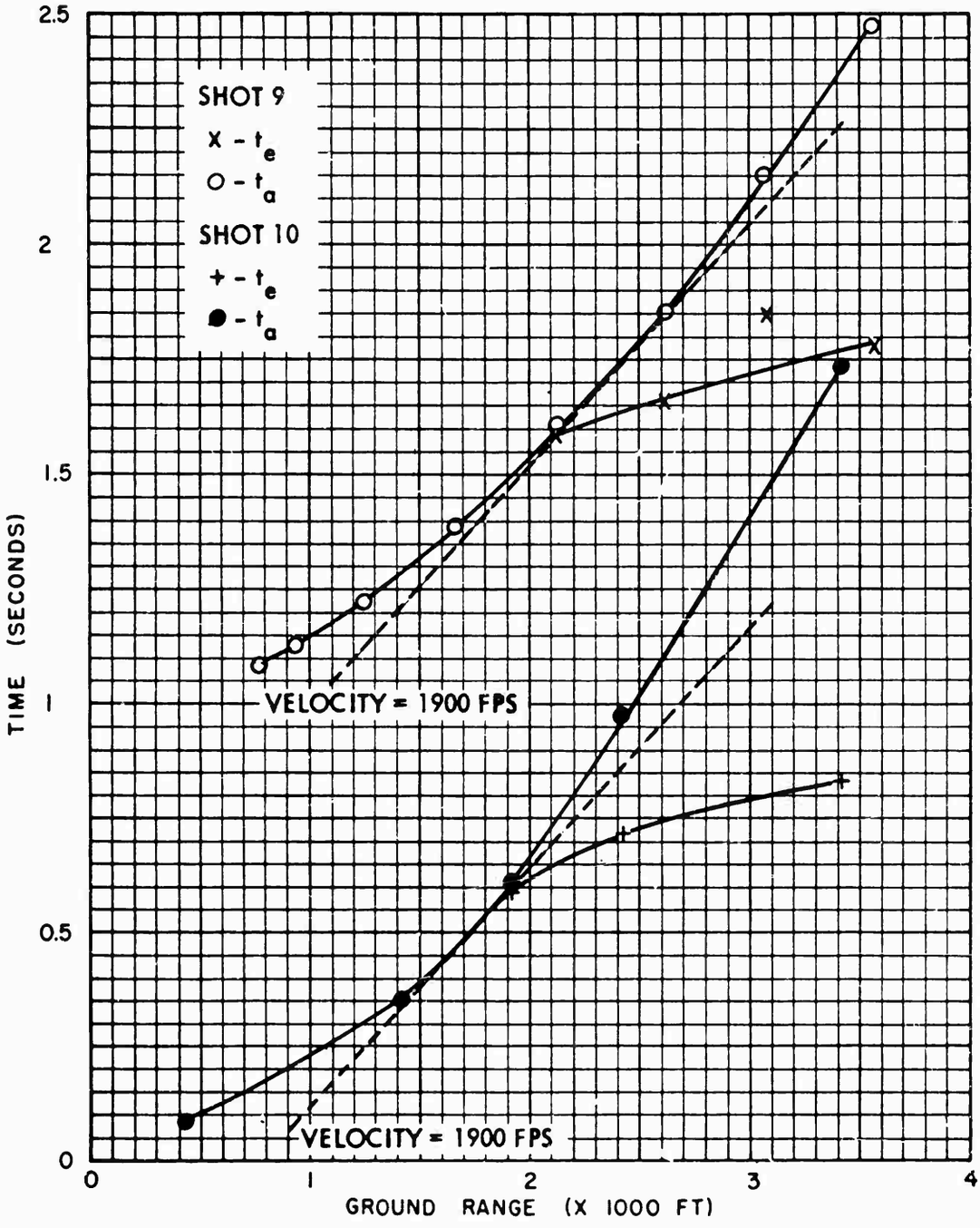

Fig. 5.35 Arrival Times of Earth Acceleration, Shots 9 and 10

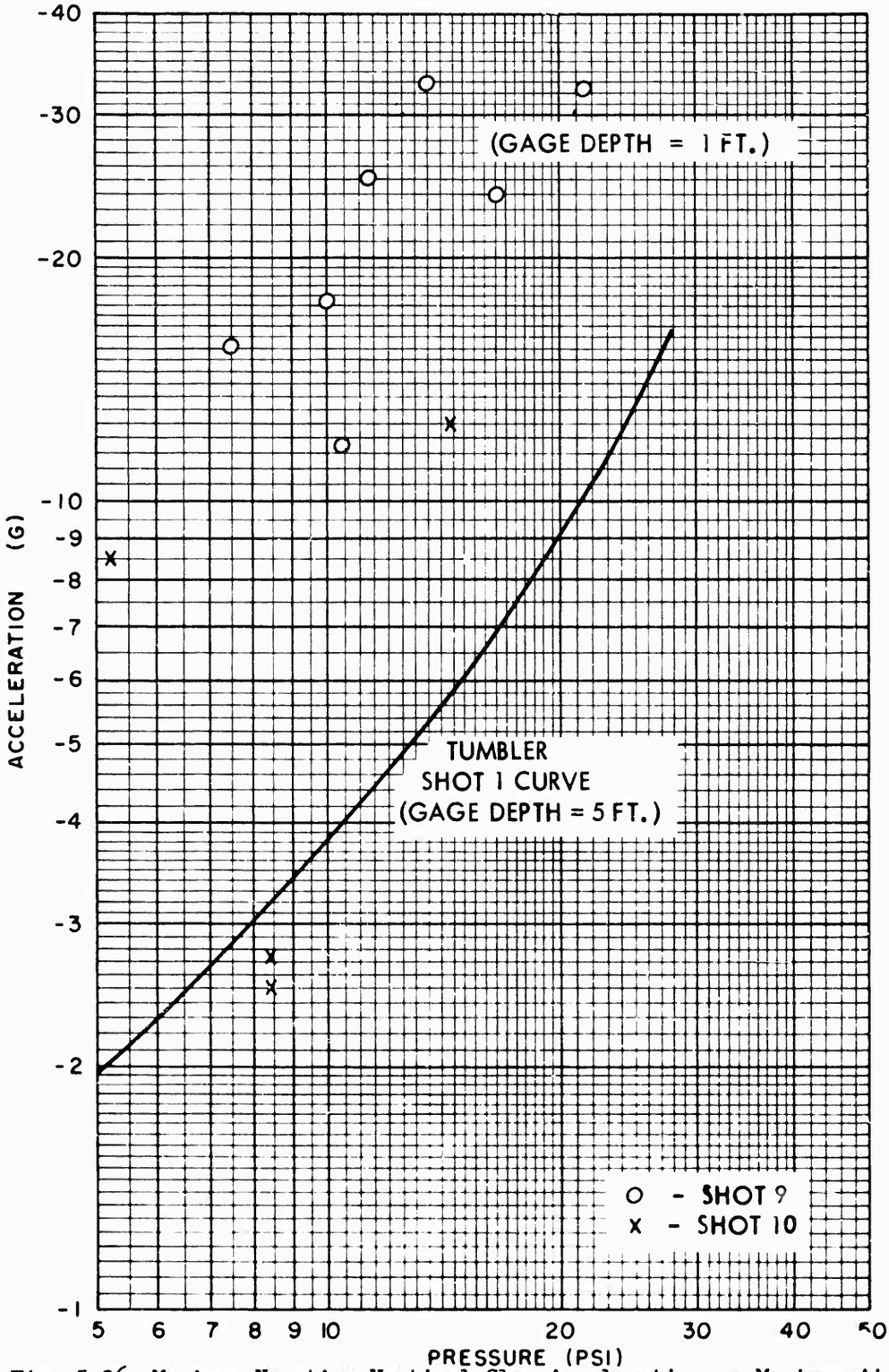

Fig. 5.36 Maximum Negative Vertical Slap Acceleration vs Maximum Air Pressure, Shots 9 and 10, Compared to TUMBLER Shot 1

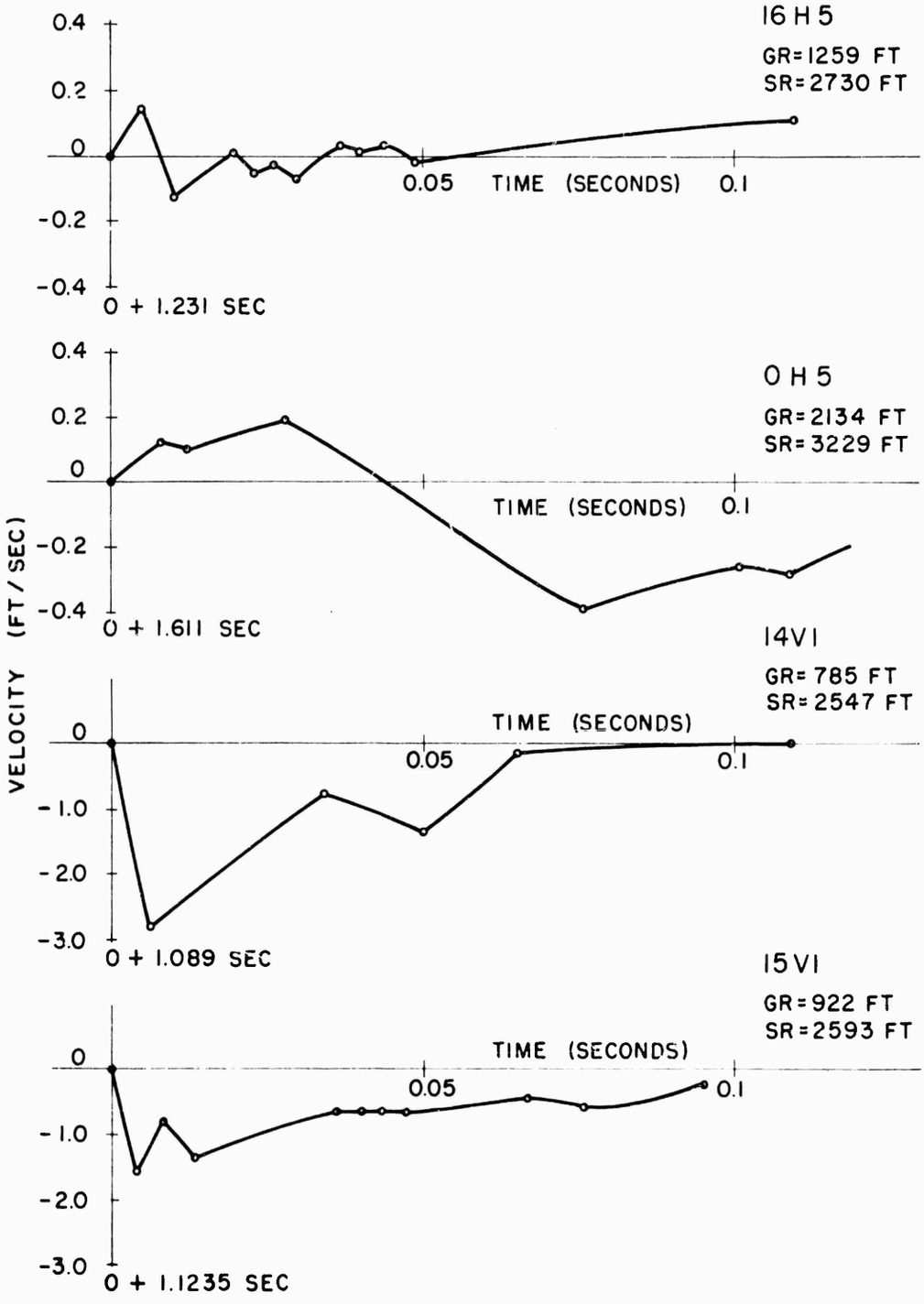

Fig. 5.37 Representative Curves, Earth Particle Velocity vs Time, Shot 9

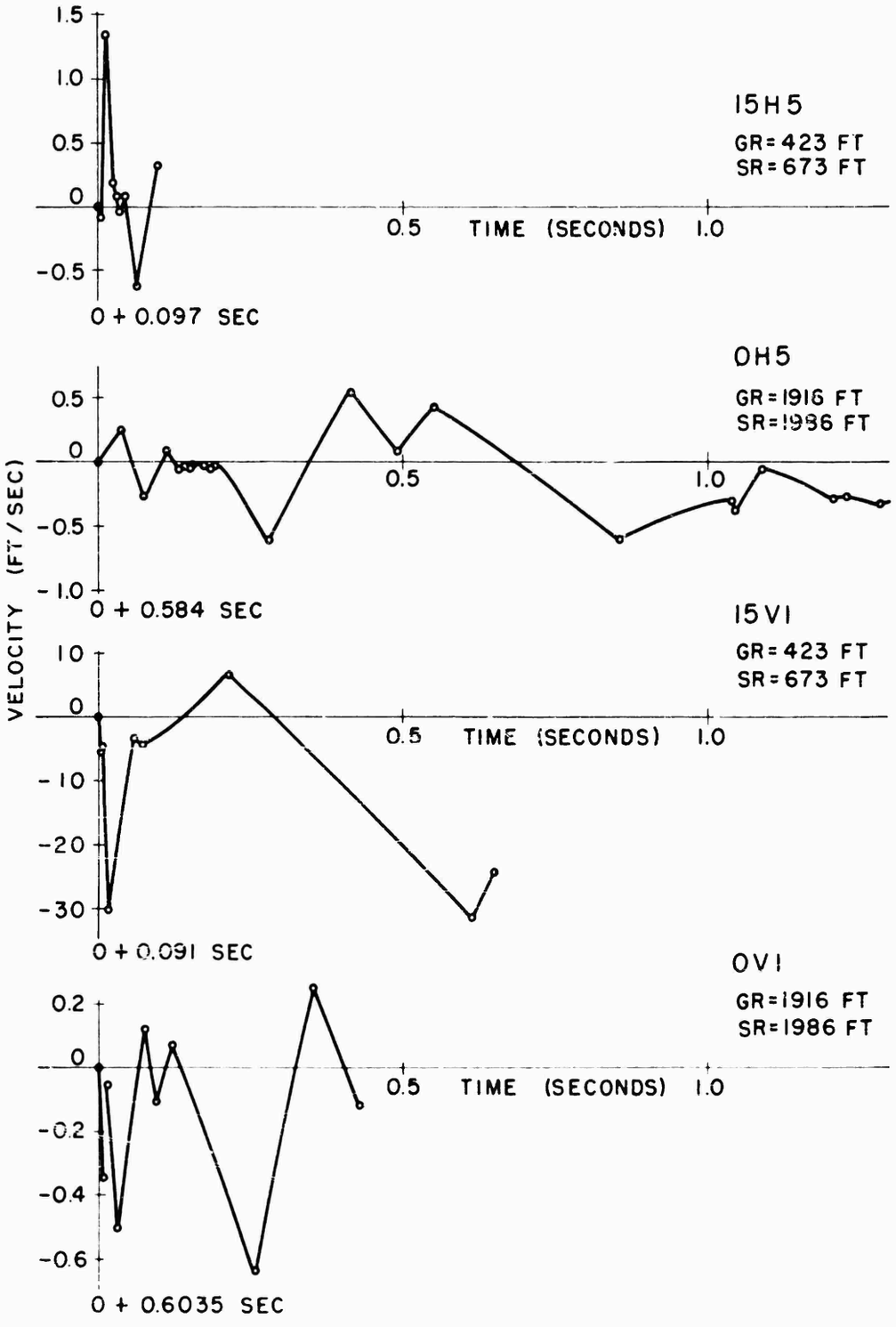

Fig. 5.38 Representative Curves, Earth Particle Velocity vs Time, Shot 10

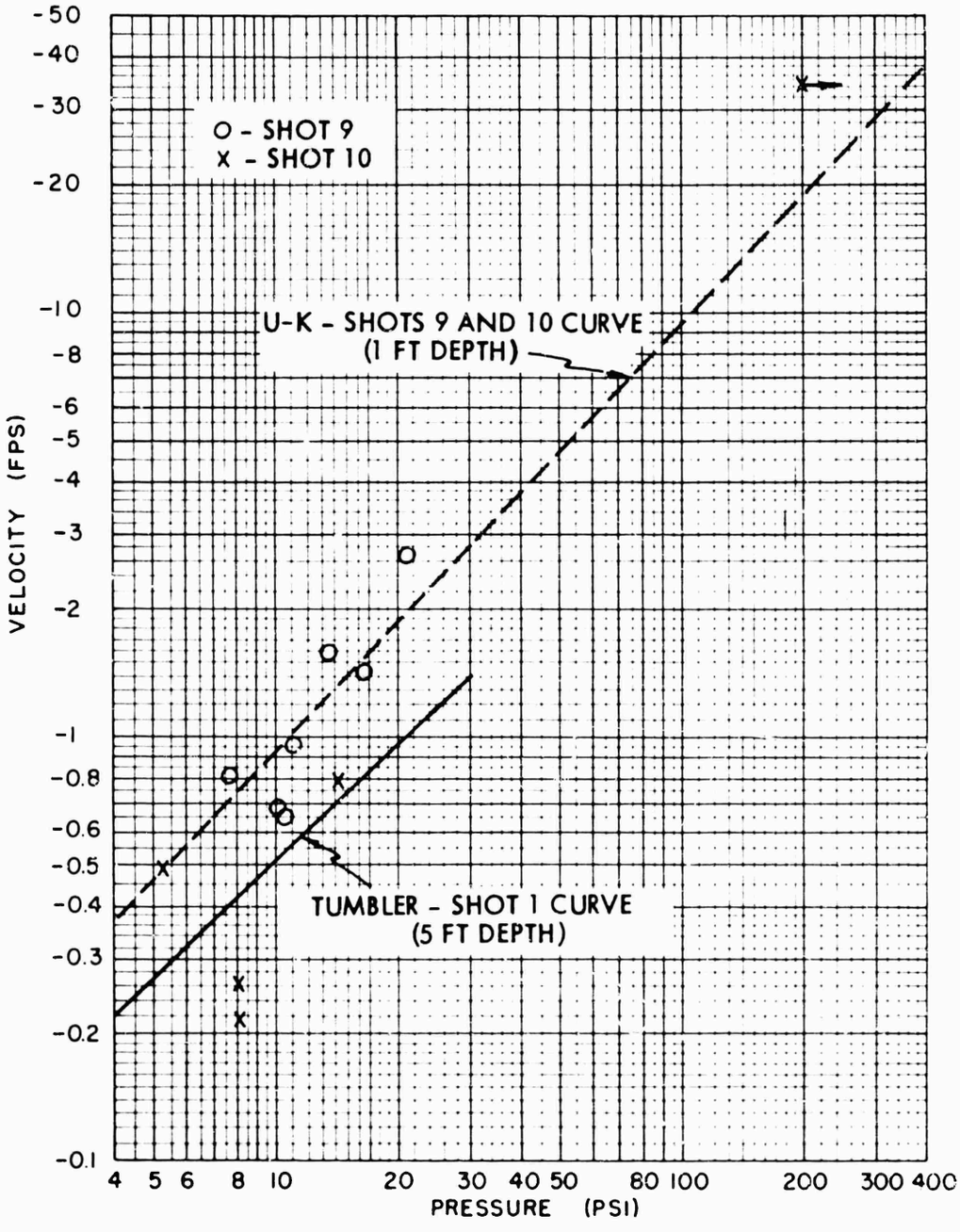

Fig. 5.39 Negative Vertical Slap Particle Velocity vs Maximum Air Pressure, Shots 9 and 10, Compared to TUMBLER Shot 1

TABLE 5.11 - Accelerometer Frequency Response

Gage	Undamped Natural Freq. (cps)		Maximum Recorded Frequency (cps)	
	Gage	Galv.	Shot 9	Shot 10
14V1	450	460	100	*
15V1	450	460	200	150
16V1	450	460	140	NR
17V1	450	460	200	150
0V1	450	460	250	150
2V1	450	460	250	100
4V1	450	460	160	NR
6V1	450	460	200	160
15H5	190	300	100	100
16H5	190	300	100	100
0H5	85	300	70	50
2H5	85	300	90	50
4H5	85	300	80	NR
6H5	85	300	90	90

* - Gage not connected for Shot 10
NR - No record obtained

frequency which was recorded by the gage was well below the undamped natural frequency of the gage. It is concluded that no frequency response correction is required for these records. In the case of the horizontal gages, particularly at the greater ground ranges, this condition does not exist, but no conclusions have been drawn from these records.

CHAPTER 6

CONCLUSIONS AND RECOMMENDATIONS

6.1 SUMMARY OF CONCLUSIONS

6.1.1 Air Blast Scaling

On the basis of the comparisons of A-scaled pressures, durations, and impulses, the total air blast phenomena of U-K Shot 9 and TUMBLER Shot 1 scaled very well, with the exception of some phenomena at intermediate ground ranges where differences in thermal disturbances appear to have caused relatively minor differences in performance. The yield ratio for these two shots was about 26:1 and both were detonated over the same surface at an A-scaled burst height of 750 ft.

6.1.2 Regular Reflections

The data regarding regular reflections are meager on this project. The indications from Shots 4 and 9 do not confirm previous observations (TUMBLER) that the measured values of reflected pressure were greater than those calculated from classical theory. On Shot 4 the check with calculated values is good, whereas on Shot 9 the measured values at intermediate ground ranges tend to be lower than the calculated values, which may be attributable to thermal effects.

6.1.3 Mach Reflection

The data permit a reliable description of the path of the Mach triple point for Shot 9 at levels below 50 ft. There is definite indication that the theoretical analysis of the triple point trajectory near ground surface is not applicable for this intermediate height of burst. Thermal effects are such that Mach reflection appears to begin at very short ground ranges and the rise of the triple point shows two plateaus below the 10 ft level. In these regions the Mach stem orientation deviates considerably from the vertical, resembling a rudimentary precursor. Such effects cannot be expected to scale in the conventional manner. After the Mach stem is well developed, variations of the stem orientation from vertical are observed but these appear to bear no relationship to the pressure gradient in the stem, and are attributable

to local disturbances.

6.1.4 Precursor Effects

Precursor phenomena were observed in detail on Shots 10 and 11. In comparison with TUMBLER Shot 4, these effects were more pronounced, particularly on Shot 10. This is in accord with the inverse relationship of thermal phenomena to scaled height of burst. Previous observations of the depression of maximum measured surface air pressures in the precursor region were confirmed. There is some evidence that this depression does not apply to dynamic pressures.

Precursor lead times of over 60 msec were observed and orientations of the precursor wave front corresponding approximately with those observed by photography were constructed for Shot 10 from arrival time data. These precursor wave front orientations seem to confirm the heated-layer theory of precursor formation.

6.1.5 Height of Burst

Additional points for a composite height of burst chart were obtained for a number of scaled burst heights. Correspondence with previous data is good in the low pressure region but the new data indicate modification of existing height of burst charts in pressure regions between 10 and 50 psi for low heights of burst. The reflection effectiveness (including thermal and dust effects) of the target surface seems to be a function of both peak pressure and height of burst. The UPSHOT-KNOTHOLE Shot 1 data present an anomaly in the 10-50 psi region where abnormal depressions of surface level peak pressure are observed.

6.1.6 Dynamic Pressures

A single measurement of dynamic pressures on Shot 11 demonstrates that the dynamic pressure as measured by a Pitot gage does not bear the relationship to side-on pressure derived from the Rankine-Hugoniot equations, when measurements are made in the precursor region. The UPSHOT-KNOTHOLE Shot 11 dynamic pressure measurement yields a peak value which is significantly greater than would be computed using the measured side-on pressure and the classical Rankine-Hugoniot relations.

6.1.7 Earth Acceleration and Particle Velocity

Few definitive data were obtained on earth acceleration phenomena on this project, the scatter of data for measurements at 1 ft burial depth allowing no precise conclusions. There is indication that an analytic relationship holds between peak vertical particle velocity and peak air pressure near the ground surface.

6.2 RECOMMENDATIONS

6.2.1 Usefulness of Data

The information obtained relative to the height of burst chart

appears to be reliable enough so that with certain qualifications it may be used for comparison and correlation with other tests for further documenting of the height of burst charts. The depressed surface level pressures from lower heights of burst in the precursor region are sufficiently consistent to indicate the necessity for more data and a possible modification of existing curves in this region. The verification of existing curves within regions other than the one mentioned above may be taken as an indication that further modification in these regions is not necessary.

The information obtained regarding Mach reflection has been combined with data from other tests and indicates that at intermediate heights of burst theoretical predictions of the Mach stem height should be modified to show an earlier formation of the stem or its equivalent insofar as diffraction around structures is concerned.

Precursor data obtained on this project were essentially descriptive rather than quantitative, but in connection with other observations they should be useful in further analysis of the mechanism of formation and results of the precursor effects.

Pressure-distance curves observed on the various shots were intended for, and should be useful to, other projects in establishing free-field conditions under which observations were made.

6.2.2 Recommendations for Further Studies

It is apparent that the major field of uncertainty in the prediction of air blast phenomena involves the region of thermally disturbed blast waves. Future experimental studies should be concentrated in these regions, particularly with reference to observations designed to establish the relationships between static and dynamic pressures under these conditions. This should include efforts to isolate the effects of dust loading on the dynamic pressure.

Dependent on the importance attached to extreme heights of burst, further analytical and experimental data are required for precise prediction of free air pressures at very high altitudes.

As an adjunct to other studies, further experimental data should be obtained to establish the reliability of prediction of early Mach stem formation phenomena.

It is recommended that further study of air blast-induced underground effects be directed toward target diffraction and response studies rather than toward free-earth phenomenology.

APPENDIX A

GAGE RECORDS

Reductions (about 1:3) of tracings of the interesting portion of all usable gage records comprise this Appendix. Features such as lengths of positive and negative phases, peak negative pressures, and secondary shocks do not appear in these reductions. These aspects of the pressure-time functions are relatively well-benaved, and pressure and times associated with them appear in the Tables.

The records are arranged first by shot, then by ground range for each vertical level (surface level first). Auxiliary records (twin baffles, backup gages, etc.) are introduced into the main sequence following the primary gage record.

Each record is provided with suitable time and pressure coordinates. The times indicated refer to zero time of the shot. Labeling comprises shot number, gage code symbol, ground range, slant range, and other information as required. The gage code symbol system appears in Section 3.2.4.

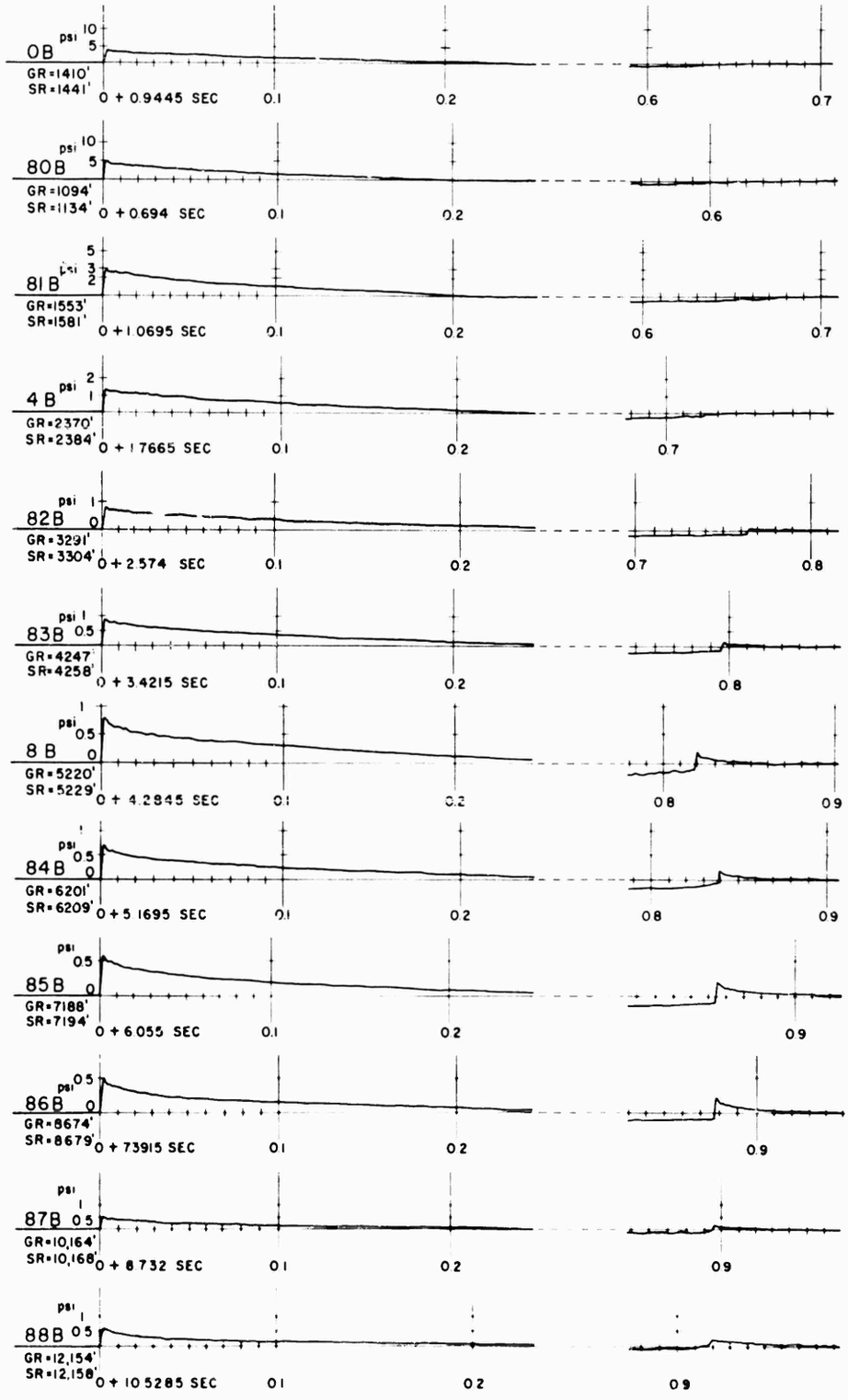

Fig. A.1 Gage Record Tracings, Shot 3, Surface Level

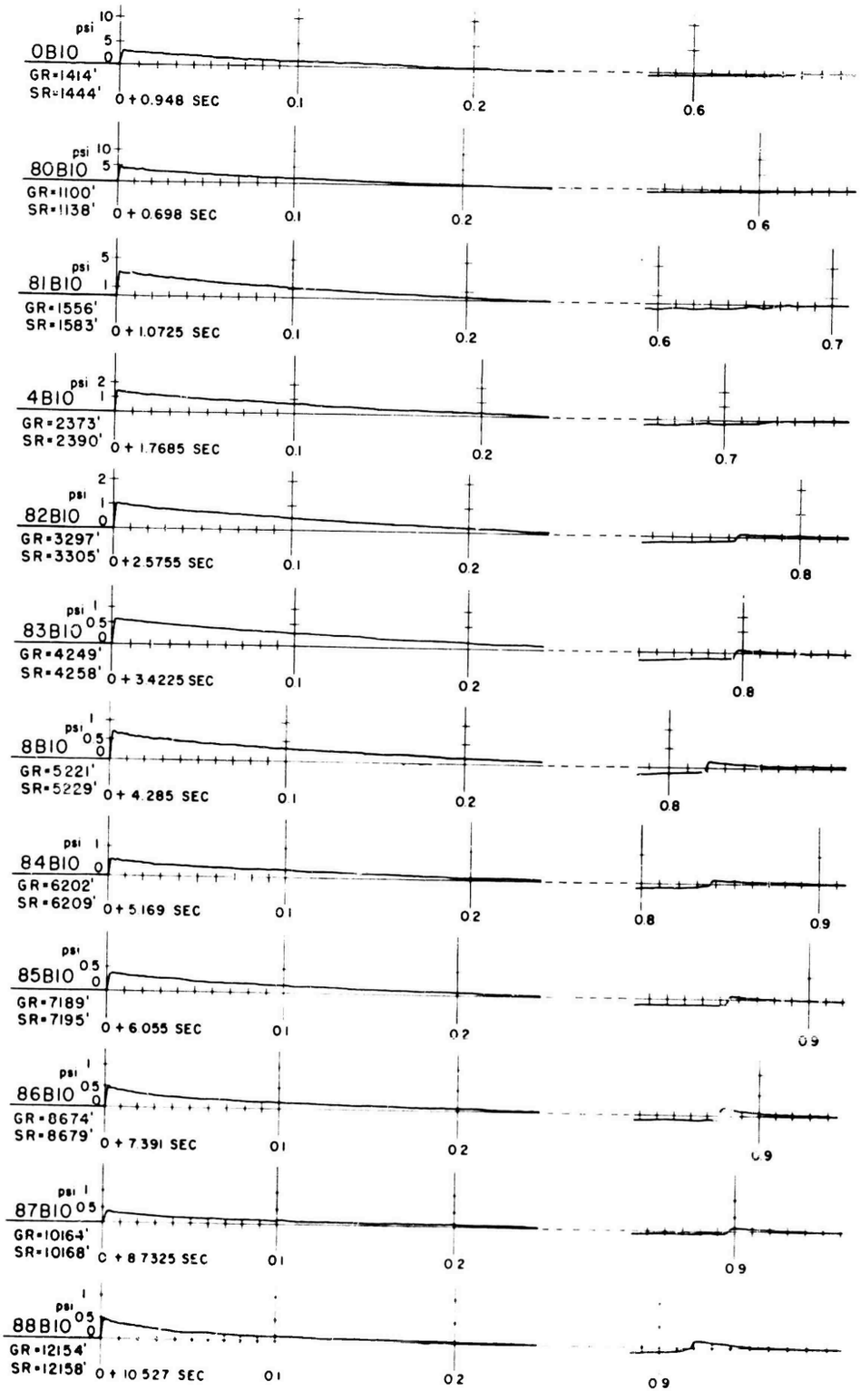

Fig. A.2 Gage Record Tracings, Shot 3, 10 Ft Level

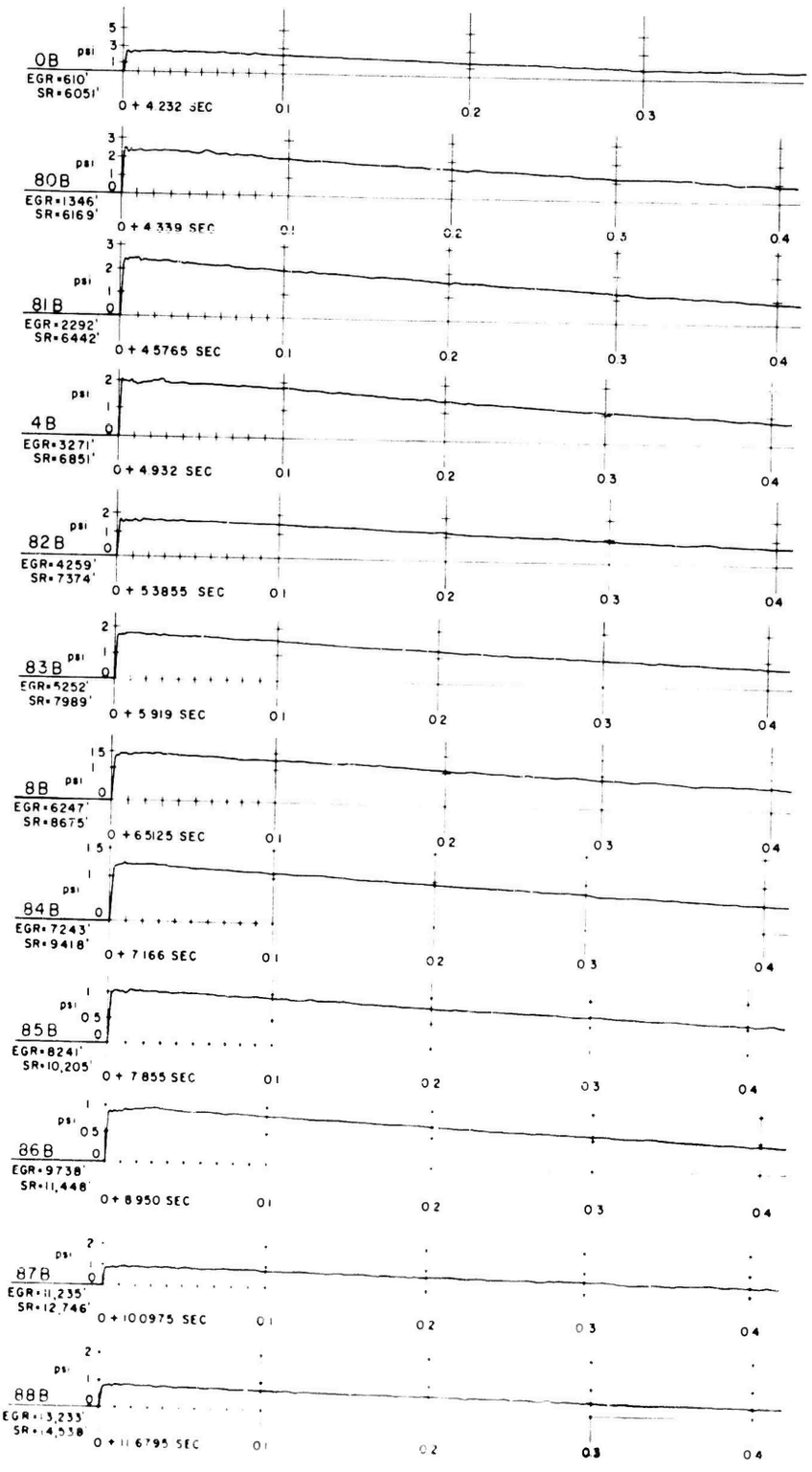

Fig. A.3 Gage Record Tracings, Shot 4, Surface Level

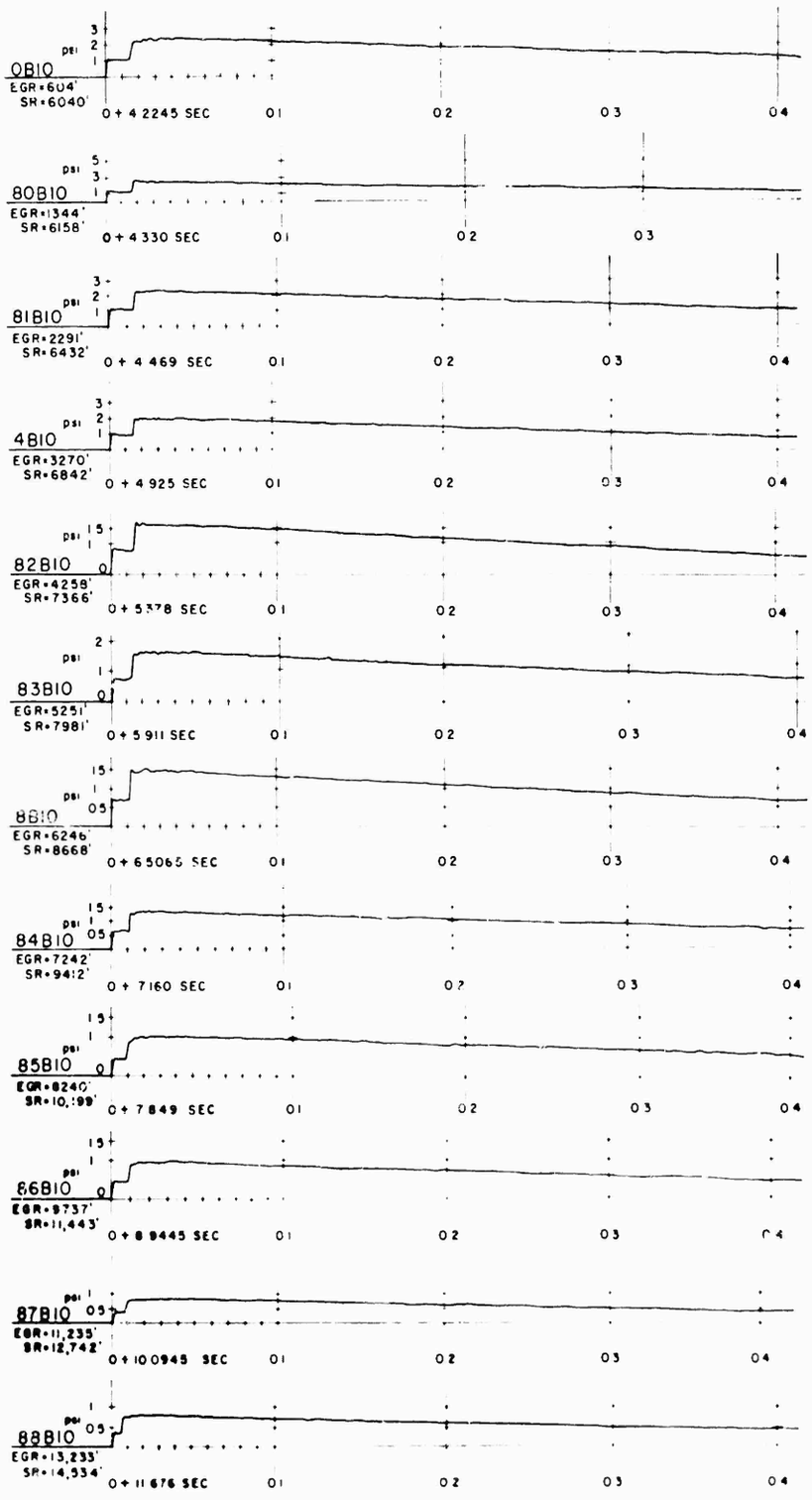

Fig. A.4 Gage Record Tracings, Shot 4, 10 Ft Level

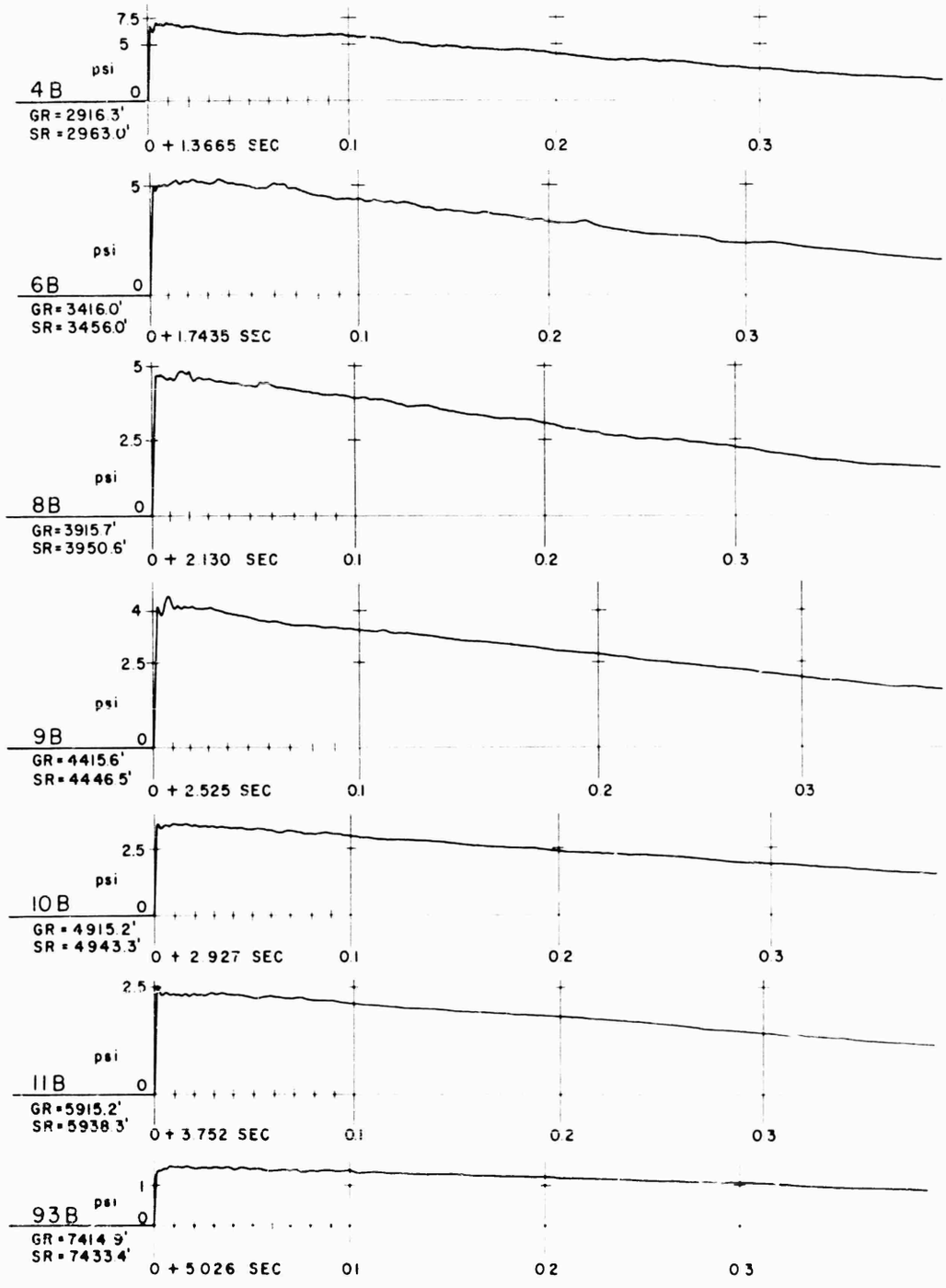

Fig. A.5 Gage Record Tracings, Shot 9, Surface Level

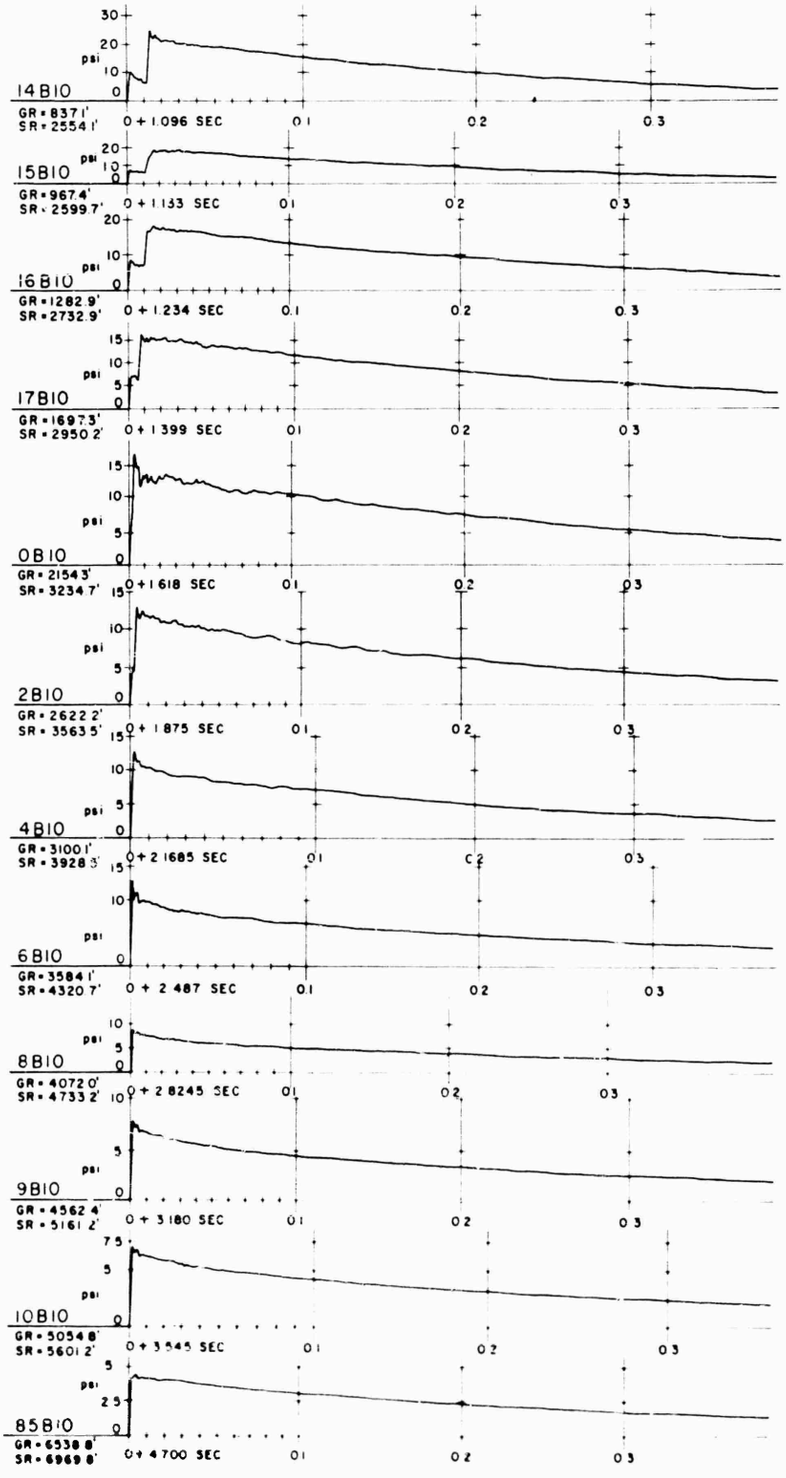

Fig. A.6 Gage Record Tracings, Shot 9, 10 Ft Level

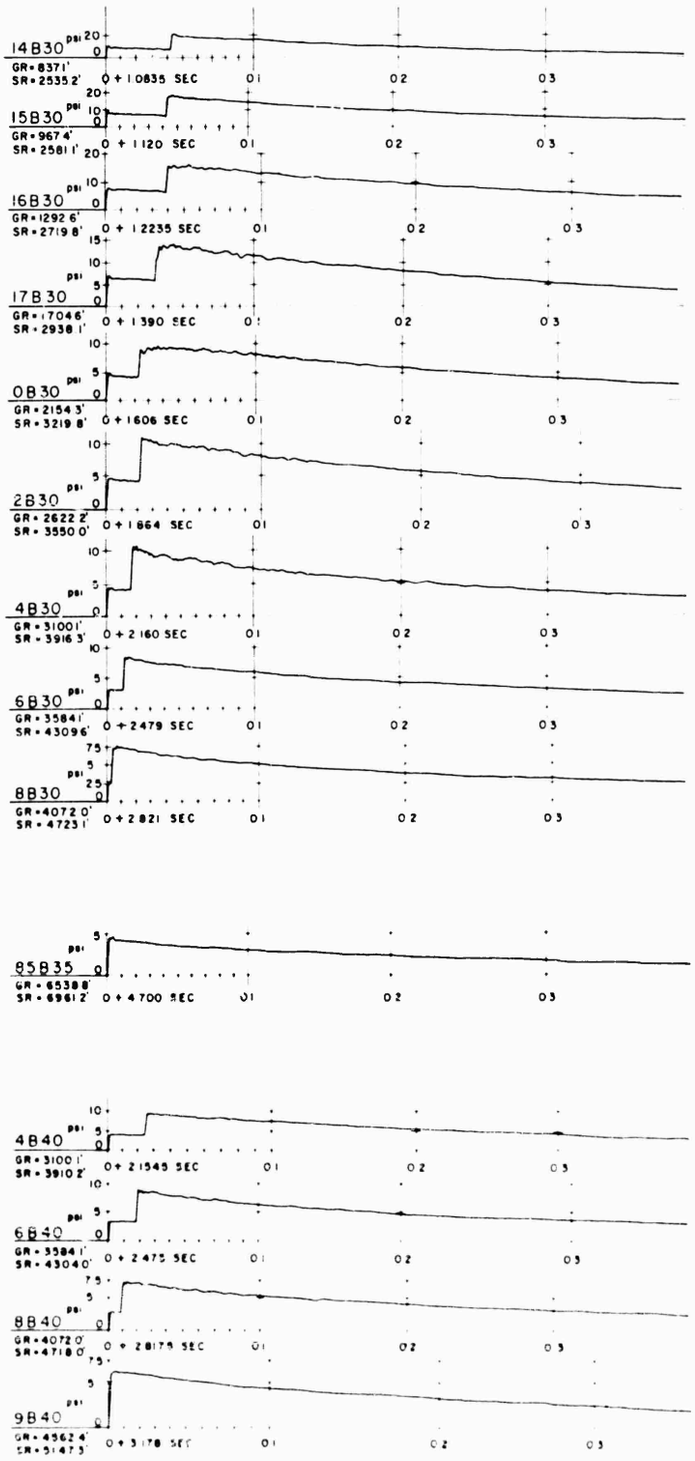

Fig. A.7 Gage Record Tracings, Shot 9, 30 and 40 Ft Levels

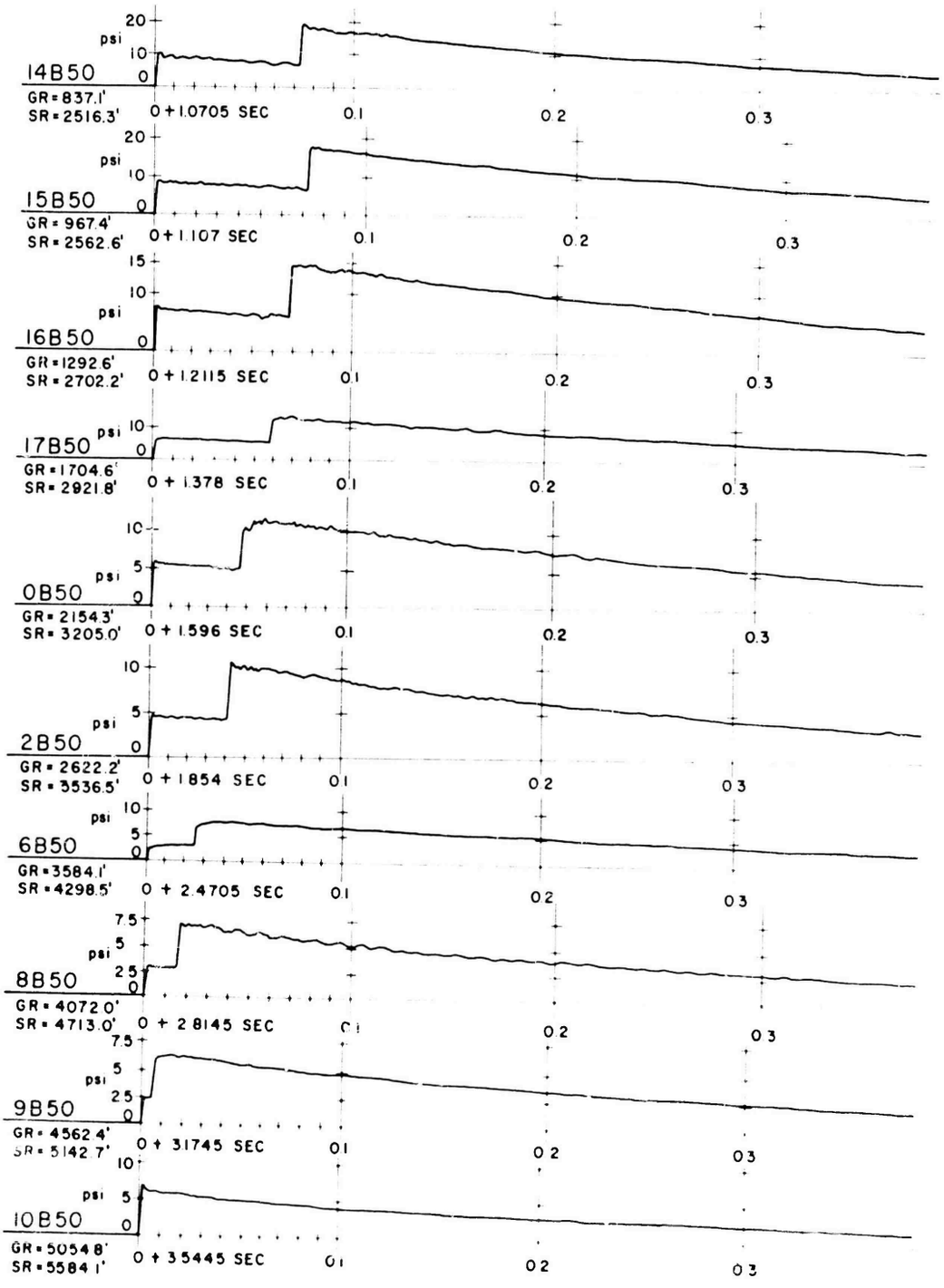

Fig. A.8 Gage Record Tracings, Shot 9, 50 Ft Level

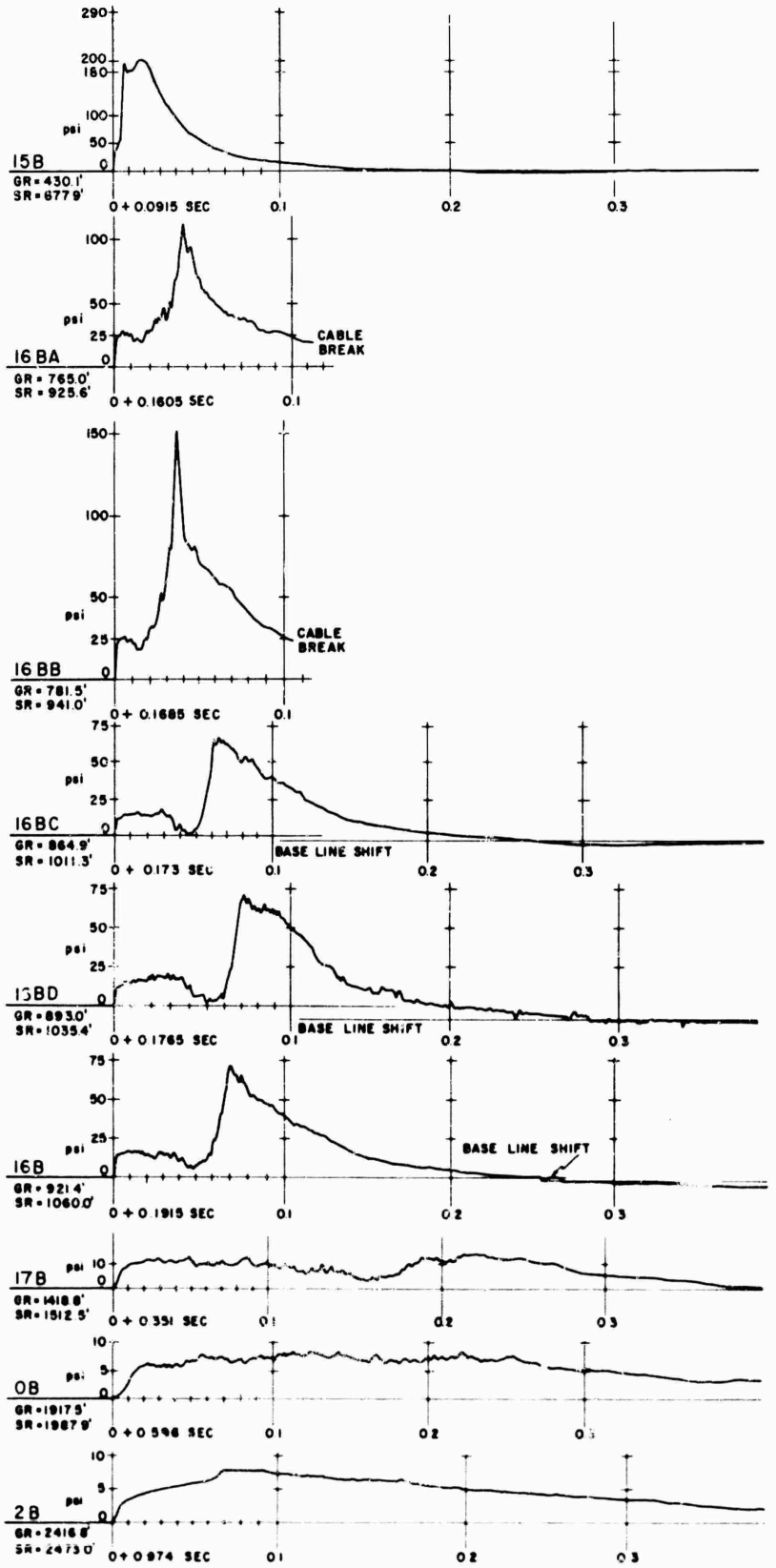

Fig. A.9 Gage Record Tracings, Shot 10, Surface Level, Gages 15B through 2B

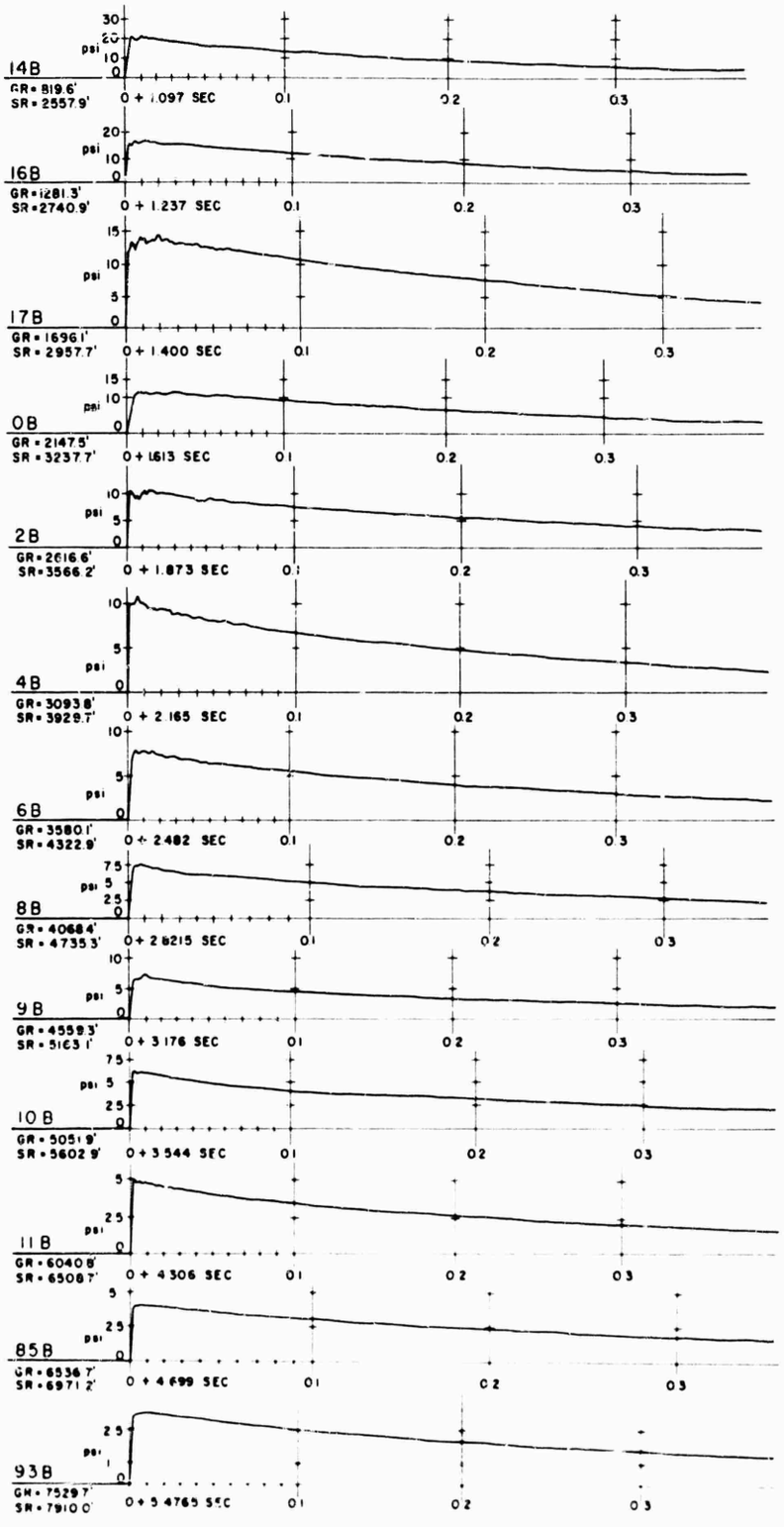

Fig. A.10 Gage Record Tracings, Shot 10, Surface Level, Gages 4B through 93B

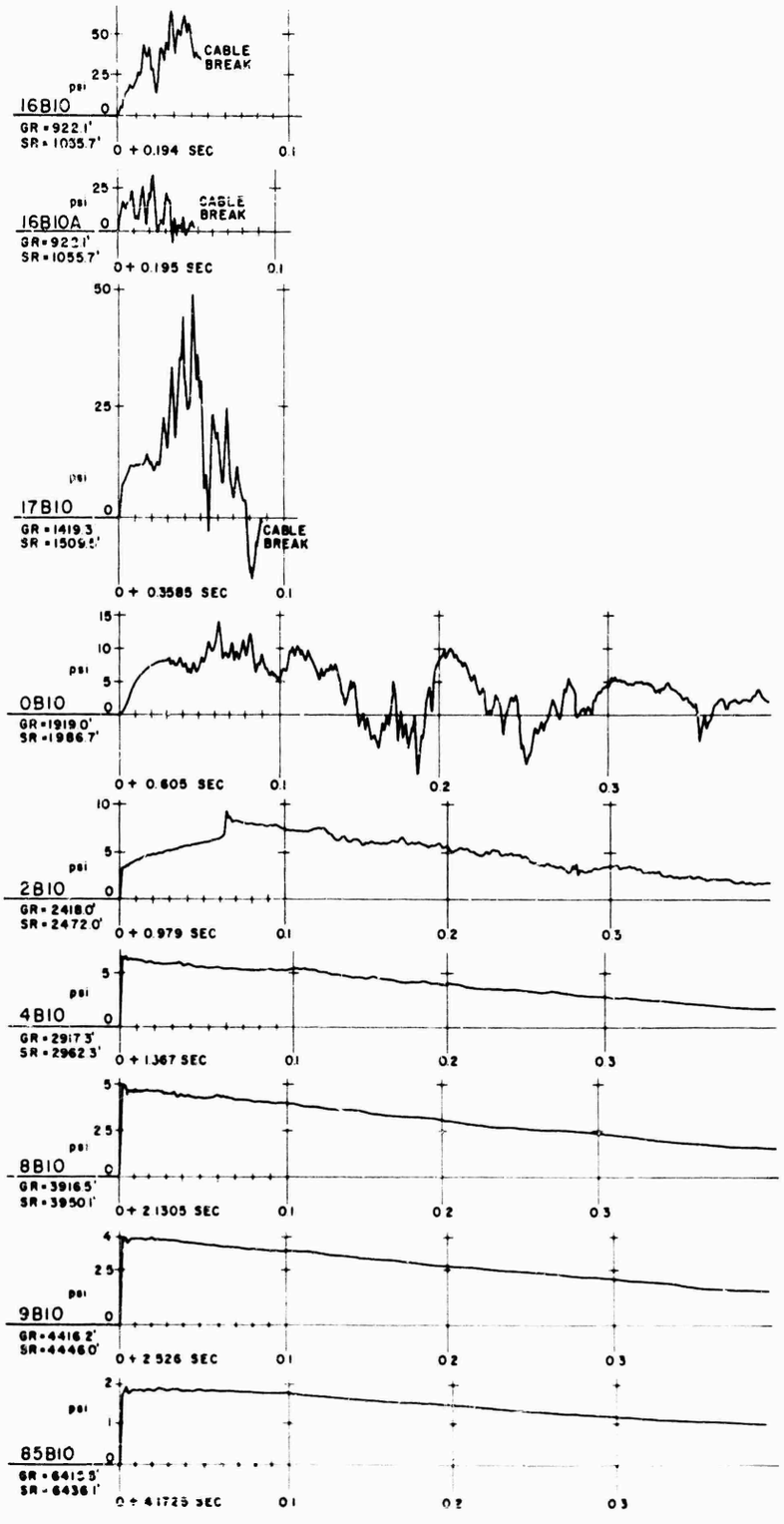

Fig. A.11 Gage Record Tracings, Shot 10, 10 Ft Level

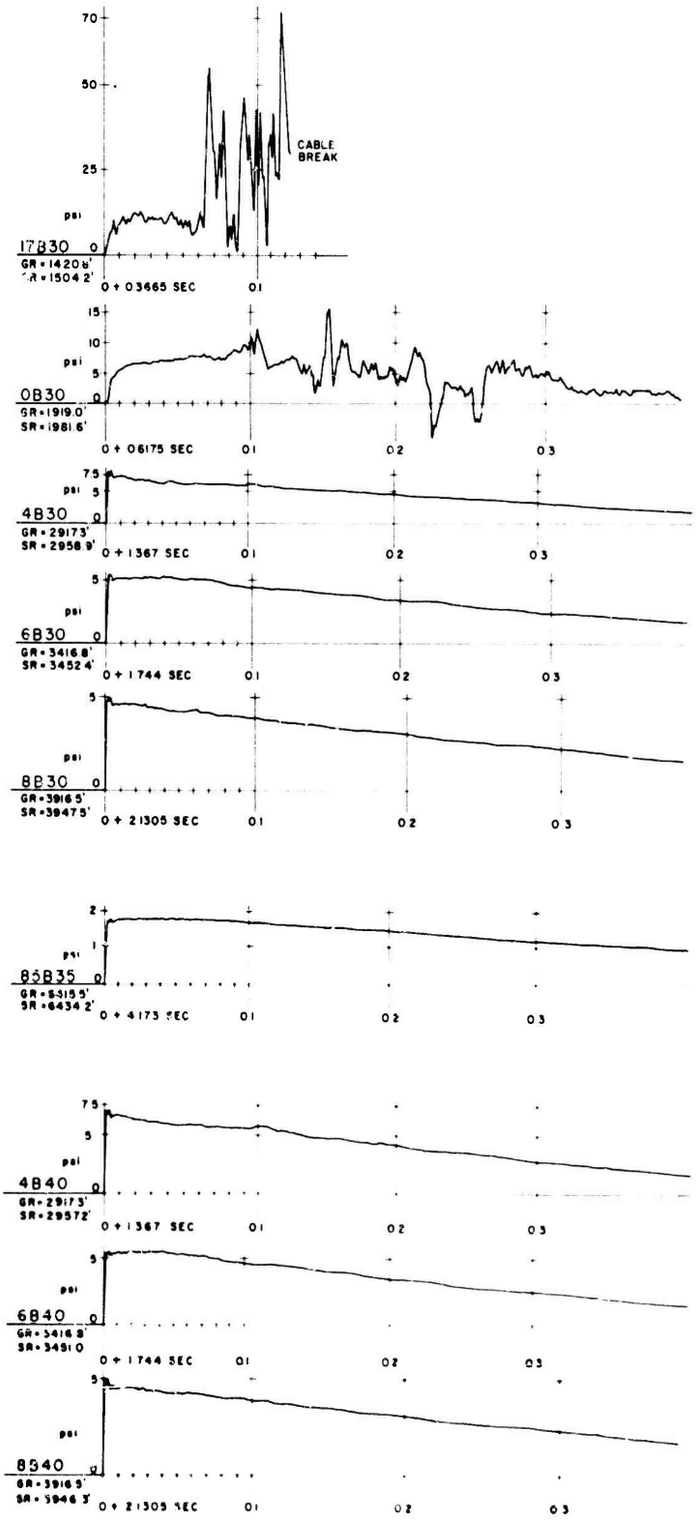

Fig. A.12 Gage Record Tracings, Shot 10, 30 and 40 Ft Levels

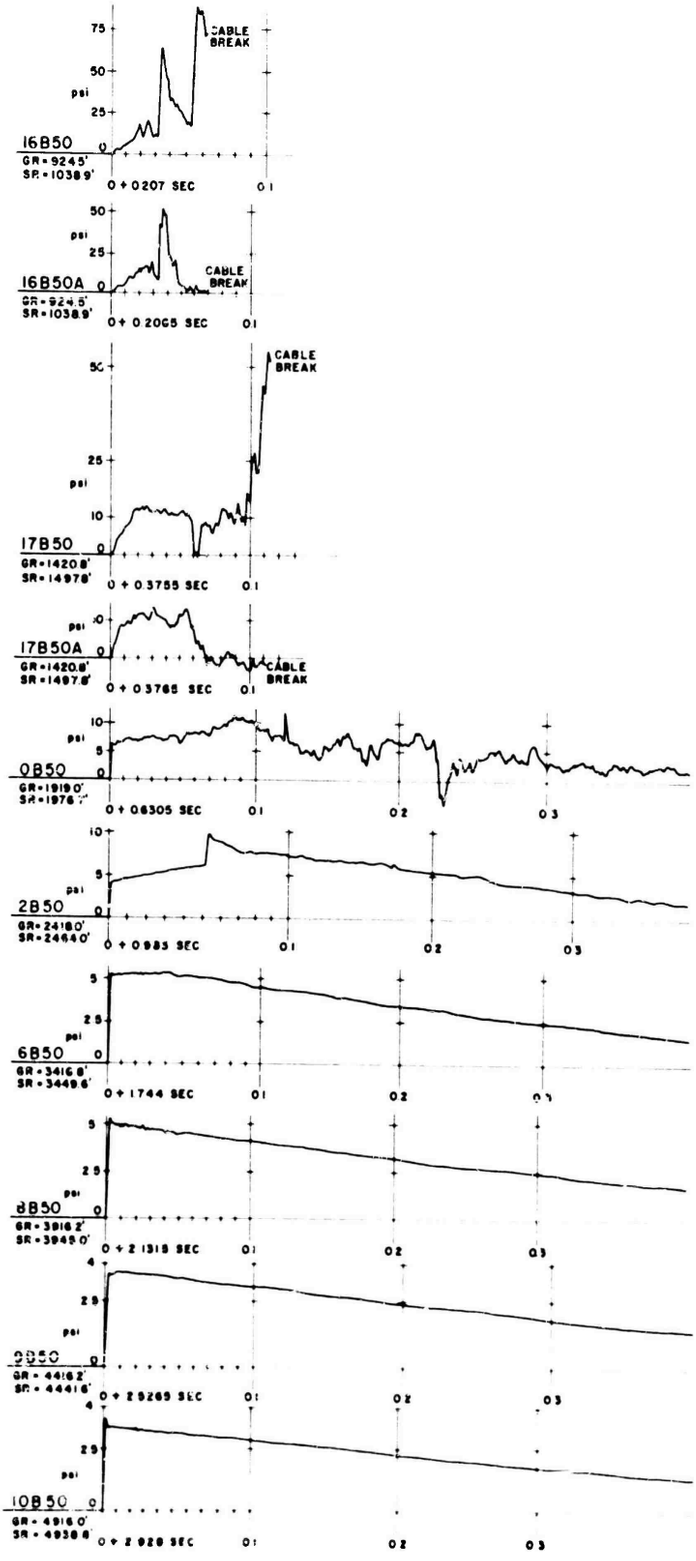

Fig. A.13 Gage Record Tracings, Shot 10, 50 Ft Level

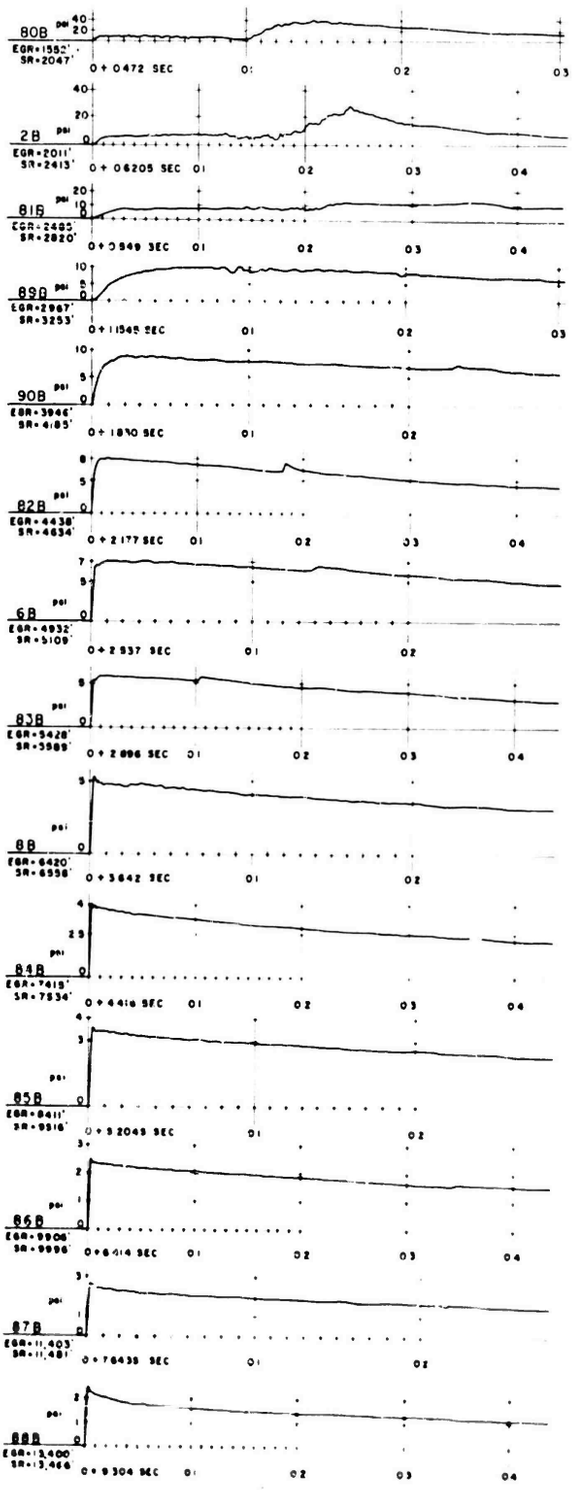

Fig. A.14 Gage Record Tracings, Shot 11, Surface Level

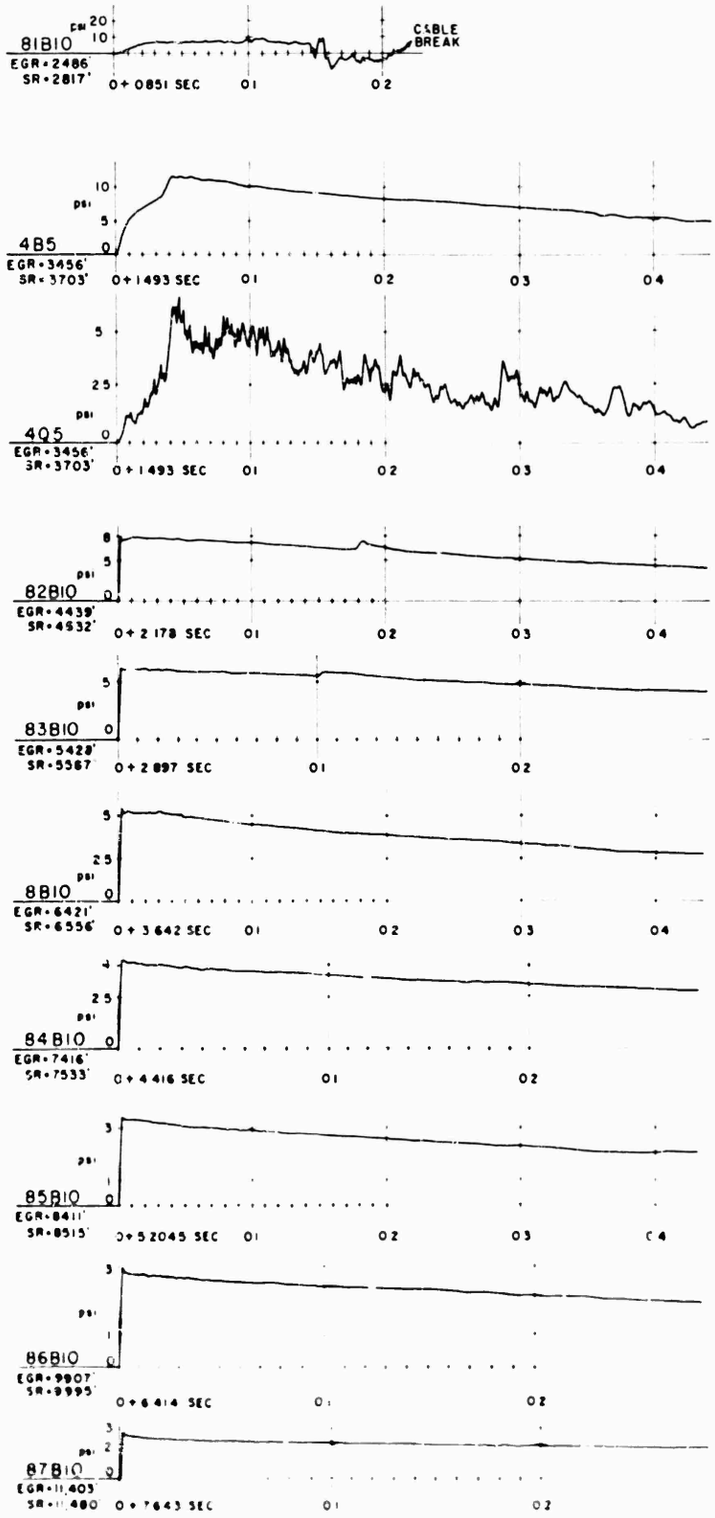

Fig. A.15 Gage Record Tracings, Shot 11, 10 Ft Level

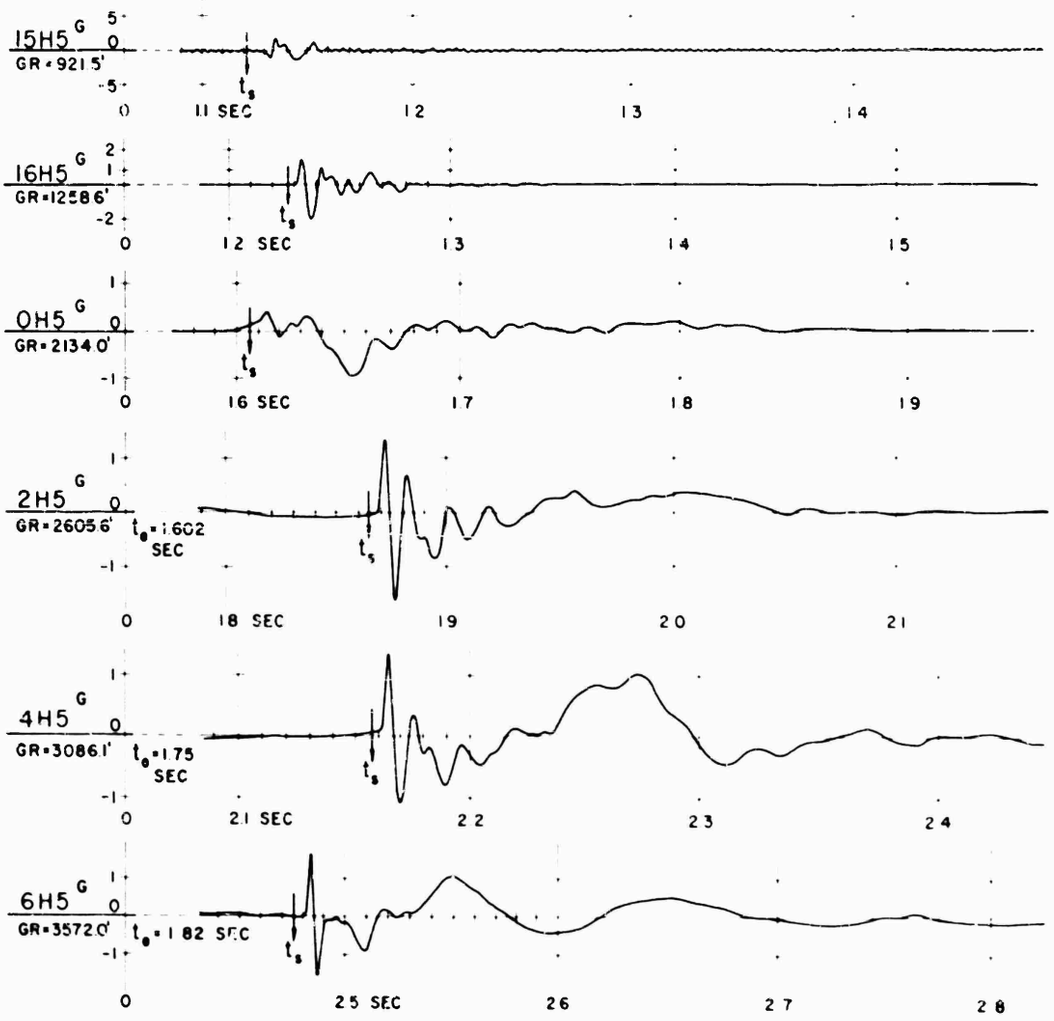

Fig. A.16 Acceleration Gage Record Tracings, Shot 9, horizontal

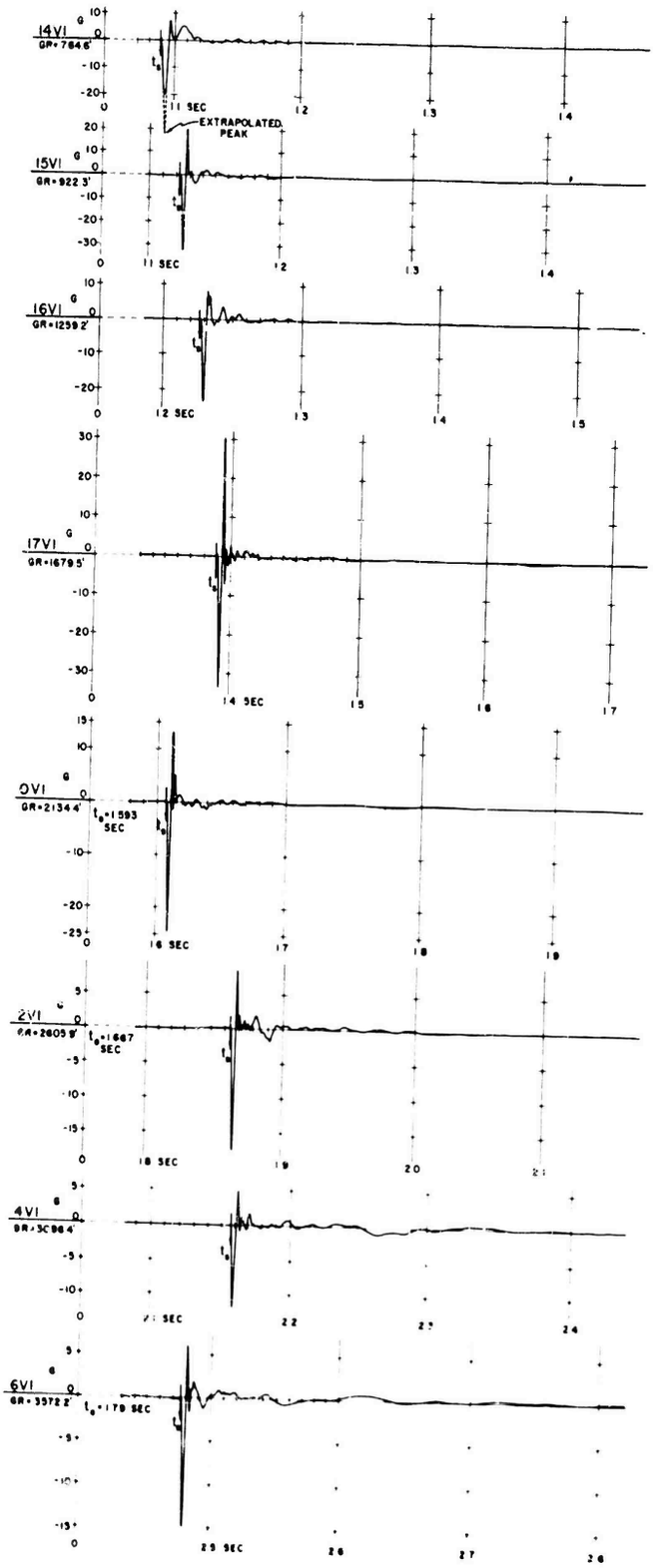

Fig. A.17 Acceleration Gage Record Tracings, Shot 9, Vertical

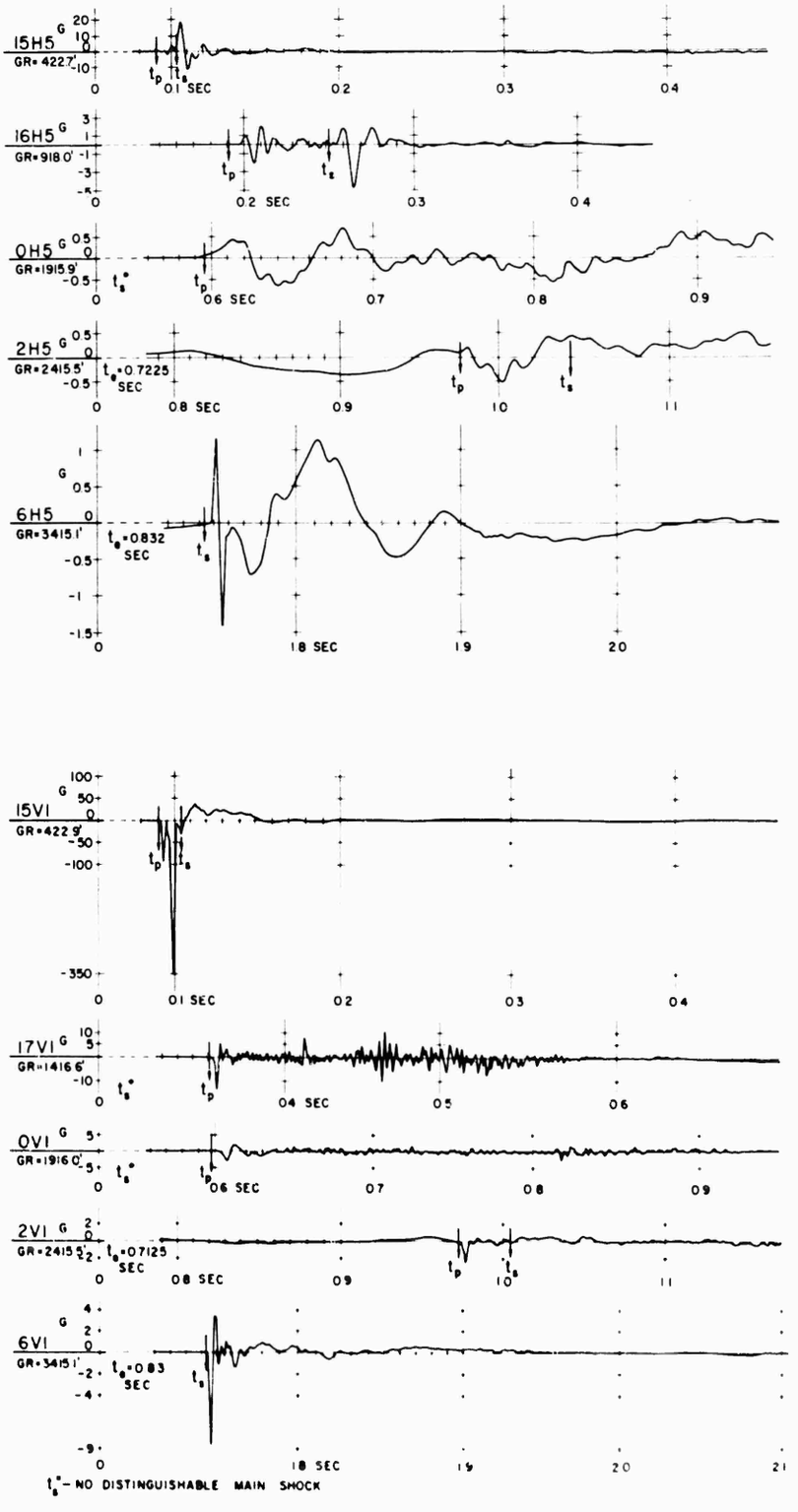

Fig. A.18 Acceleration Gage Record Tracings, Shot 10

APPENDIX B

EXPERIMENTAL RECORDING TESTS

In conjunction with Project 1.1b of Operation UPSHOT-KNOTHOLE a limited experimental project was undertaken to evaluate certain instrumentation and techniques for the recording and reproduction of explosion test data on magnetic tape. This instrument evaluation plan was undertaken with the understanding that it was to be secondary to the main project, and that it might be necessary to eliminate portions of this experiment in order to meet the schedule of the main test.

B.1 BACKGROUND AND HISTORY

The basic advantages of magnetic recording over direct oscillograph recording are:

(1) The possibility of electrical normalizing of records.

The vertical scale may be adjusted as desired in reproducing records; the time scale may be adjusted as desired, if an adjustment of the final recorder speed is provided. It is not evident how non-linearity of gage circuits may be compensated for in playback, but this compensation is probably possible.

(2) The possibility of electrical filtering of signals.

This may include differentiation, integration, or frequency discrimination to improve signal-to-noise ratio. In the case of acceleration records, it is possible and probable that electrical integration to obtain particle velocity would be of considerable value.

(3) The possibility of electrical combination of signals.

This may include addition, subtraction, or other mixing techniques. In the case of structural

tests, the combination of several gage records to obtain an average pressure has already been used, but would be much more readily controlled in playback of magnetically recorded data.

(4) The elimination of the necessity for radiation shielding of field instruments.

This feature has been given much attention in the past; however, it is now considered a secondary feature since the practicability of the use of photographic paper for nuclear tests has been proven.

Due to the characteristics of magnetic recording equipment and tape, it is assumed that such recording must involve the use of a frequency modulated or phase modulated carrier system. Direct recording or amplitude modulation of a carrier recorded on a tape suffers uncontrollable distortion due to the variable characteristics of the tape. The three such systems in use at present are:

(1) Phase modulation. The output of the transducer is connected in quadrature with a portion of the fixed carrier which supplies the transducer. The resultant phase modulated signal is recorded on the tape along with the fixed carrier or some signal which bears a fixed relationship to this carrier. Playback is accomplished by means of a phase sensitive detector which may consist of a "gated" multi-vibrator or a similar circuit.

(2) Frequency modulation. This is accomplished by feeding the signal voltage derived from the transducer into a reactance modulator or similar modulator which frequency-modulates a locally supplied carrier. Playback is accomplished by means of a discriminator circuit or pulse counting demodulator.

(3) The transducer as a fundamental part of a local oscillator. The changes in reactance or resistance of the transducer due to the signal are made to cause corresponding changes in frequency of this local oscillator. Playback is accomplished in the same manner as in (2).

Each of the three above systems was used by various agencies in UPSHOT-KNOTHOLE.

In essence, the first two systems transmit the signal from the transducer to the terminal equipment as an amplitude modulated signal. The conversion equipment is, therefore, subjected to and can be sensitive to any electrical noises picked up by the transmission cables, which may be of considerable length in a test of this type. The third system, by making the local oscillator essentially a portion of the transducer, avoids this handicap and should, therefore, present an improvement in signal-to-noise ratio.

One of the most important sources of noise in magnetic recording and reproducing is tape speed variations. These speed variations may occur in the recording or in the reproduction, either as overall capstan

speed variations or as flutter of the tape. These variations may also be due to uneven stretching of the tape between recording and reproduction. Experience has shown this to be a very important source of noise in tests of this type where the tape is subjected to severe changes in humidity and temperature between and during recording and playback. The phase modulation system, (1) above, is not directly subject to noise due to such changes, but an analysis will show that it is not entirely free from such disturbances.

The FM-local oscillator system, (3) above, offers certain incidental advantages over direct oscillograph recording. Primarily, the system permits the use of longer, cheaper cables. With the local oscillator near the gage, the length of the cable to the recorder becomes relatively unimportant and its electrical characteristics need not be as good as those required by AM systems. In addition, the system permits the use of a single cable for several channels by frequency separation of the channels. This feature is not considered to be as important as it was at one time.

In view of the several advantages offered by the third system, it was concluded that a further exploration of techniques in its use would be desirable. This experimental instrument "sub-project" was set up for this purpose.

B.2 EXPERIMENT PLAN

B.2.1 Instrumentation

In confining the planning to the use of a local oscillator near the gage to generate a frequency modulated carrier, certain criteria were set up:

(1) Although the local oscillator is to be considered a portion of the gage, it appeared desirable that a separation of at least 60 ft between the two would allow best use under the conditions of this test. This would permit the location of the oscillator near the base of a 50 ft tower with the gage at the top of the tower.

(2) The local oscillator should be designed for a minimum of power drain and for a maximum of resistance to shock.

(3) The output of the oscillator should be moderately high in order to overcome transmission losses and noises in the transmission line.

(4) The frequency deviation for rated gage signal should be as high as is consistent with other design factors.

(5) A standard frequency should be recorded on the same tape as are the signal channels in order to provide a timing standard for playback.

Although one of the purposes of the experiment was to investigage playback techniques, work schedules were such that little attention was given to the playback equipment in the early stages of the experiment plan. The attitude was taken that once gage records were obtained, time would permit investigation of playback techniques after the completion of the field phase of UPSHOT-KNOTHOLE.

The basic recording equipment obtained and used on this test consisted of an Ampex Model 306 7-channel tape recorder equipped with seven recording and seven playback heads. Since the capstan motor drive of such a recorder requires an accurate 60-cycle power supply for best results and since the power supply during recording was expected to be supplied from batteries, a fork amplifier (Ampex Model 375) was used which furnished sufficient 60-cycle, 120-volt output to drive the capstan motor. Other portions of the recorder were driven directly from 24-volt DC to 120-volt (nominal 60 cps) AC converters. Simple recording amplifiers were built which required an input of approximately 50 millivolts or more of carrier frequency to supply sufficient output power to saturate the recording heads.

Since the Wiancko variable-reluctance transducer is very widely used by many agencies in explosion tests, it was given prime consideration as the transducer for these experiments. It was considered very desirable to retain the fundamental balanced feature of this transducer; by so doing, the insensitivity of the air pressure gages to acceleration and shock was retained. In addition, such an approach allowed the use of existing gages interchangeably between the basic direct recording system and the magnetic recording system. It was found that Wiancko Engineering Company had developed an oscillator (Type 9-1002) for this purpose. This company supplied two such oscillators on a loan basis for this experiment. The circuit details of these oscillators were not disclosed, but their general characteristics met in a reasonable manner the criteria decided upon. The power supply requirements were moderate, the output relatively high, and the frequency deviation at full gage rating was approximately 10 per cent.

Two other oscillators were designed and built at the Stanford Research Institute (SRI) laboratories. The first of these, "SRI-A," consisted of an oscillator incorporating an "all-pass LC network" as the phase shifting device and separate gage amplifier supplying the carrier to the gage at the oscillator frequency. The output of the gage was fed in quadrature with the oscillator feedback voltage to the grid of the oscillator tube. An unbalance of the gage, due to the presence of a signal, resulted in a phase shift of the feedback voltage which in turn resulted in a change of oscillator frequency to compensate for this phase shift. Variations of this LC network circuit were experimented with, including the use of an RC network as a phase shifting element in the basic oscillator, but the circuit described was the most acceptable found in the time available. The second circuit, "SRI-B," was built in the simplest way which could be devised. It consisted of

a single-tube oscillator using the reflected total reactance of the gage itself as the frequency determining element. Since this reactance does not change with signal, the frequency shift with signal was obtained by feeding the gage output in quadrature with the normal feedback voltage in a fashion similar to that in the SRI-A circuit. Both of the above circuits, as built, failed to meet the original criteria in that the plate current drain was higher than desirable (about 40 milliamperes at 180 volts). The SRI-B circuit gave the greatest frequency deviation of any of the systems used, but left something to be desired in the linearity of frequency shift with signal. In addition to the four channels described above, two channels using the Vibrotron gage (Byron Jackson and Company) were connected. This gage, using a vibrating wire as the frequency determining element approaches in theory the ideal system for frequency modulation recording more nearly than other systems, since the frequency determining element is an inherent part of the gage itself. Although the manufacturer specifies a short cable between the Vibrotron gage and the controlling amplifier, it was found that its operation, under laboratory conditions, was entirely satisfactory with 60 feet of connecting cable.

B.2.2 Gage Layout

In order to obtain results which would provide direct comparison of gage records, it was decided that all six gage channels involved in this portion of the experiment should be subjected as nearly as possible to the same blast pressures and that there should be provided a standard gage channel at the same nominal radius from ground zero. Accordingly, these gages were installed at Station F-209 for Shots 9 and 10 (see Fig. B.1). Due to the presence of other instrumentation it was necessary to displace these gages slightly in a direction counterclockwise from the main gage tower. However, this displacement was not sufficient to cause any noticeable change in the pressure level, even under the conditions of Shot 9 where the true ground zero was considerably displaced from instrument ground zero. The local oscillators were mounted near the gage array, all six oscillators being shock-mounted in a single box. A wooden lid, plus a few inches of dirt, covered the box and protected it from blast. Batteries supplying the power to the oscillators were mounted in a second box adjacent to the first. In order to compare the performance of the Wiancko oscillators and the Vibrotron oscillators using long and short cables, one of each of these channels was connected to its gage through the shortest cable possible, while the other was connected through a cable of 60 ft length. Since the two SRI channels had been tested with 150 ft cables, they were connected with this length of cable. In all cases, except the two shortest, the surplus cable was folded in the connecting trenches and covered with earth.

Relay circuits were provided so that the battery supply to each oscillator could be turned on from the central recording station. Each gage oscillator was connected to the central recording station by a separate three-conductor cable, but only two conductors were used in all cables other than the one which also carried the relay signals. The circuitry, as designed, required that the transmission lines be unbalanced, that is, that one side of each transmission line be grounded.

DRAWING NOT TO SCALE

Fig. B.1 Location of Experimental Gages

It was intended that this grounding take place at the recording shelter. However, during installation of the gages it came to light that the Vibrotron gage was so built that one terminal was irremovably connected to the case of the gage. In the time available it was impossible to correct completely for this situation, with the result that the grounding system used was not optimum and gave rise to certain circulating currents. The only visible result of this improper grounding was that of a greater cross-feed between channels than had been expected. This was particularly true in the case of the Vibrotron channels. Time did not permit the operation of a dynamic test on these channels during installation, but an inspection of the wave form of the carrier plus cross-feed led to the conclusion (which later proved invalid) that the cross-feed would not cause serious effects.

At the recording station, the signal from each gage oscillator was fed through the recording amplifier to the individual recording heads. A 10,000 cps signal from a Hewlett-Packard Model 100 D Low Frequency Standard was fed to the seventh recording head. Provisions were incorporated for applying power to the recording amplifier and gage oscillators at a time of minus 15 minutes and for starting the recording tape at a time of minus 15 seconds. Calibration was performed on each gage by applying a known pressure to the gage and recording a short burst on the recording tape. Three or four values of pressure were recorded for each gage.

On Shot 9 the recording tape speed used was 30 inches per second. On Shot 10 the recording speed used was 60 inches per second.

B.3 PLAYBACK

The basic playback equipment consisted of seven channels of Ampex Model 306 playback amplifiers with their associated power supply equipment. Since most of the channels used a carrier frequency of approximately 10,000 cps and since the Model 306 playback amplifier was basically designed for approximately 28,000 cps a minor modification was made on four of these channels, increasing the pulse length by the change in capacity of one condenser.

This playback amplifier is of the type known as a pulse counting demodulator. The output from the recording head is amplified through three stages of cascade vacuum tube amplifiers, each stage being followed by a biased clipper. The resultant output, a square wave whose amplitude is primarily determined by the bias of the last clipper, is differentiated to form pulses. The pulses are amplified and rectified, and the rectified output is filtered to produce an output dependent upon the frequency of the input signal. The output of the demodulator is linear with respect to frequency within the operating range of the system. A balancing voltage is provided which allows the DC output to be adjusted to zero for the center carrier frequency.

When the records obtained from Shots 9 and 10 were played back through these amplifiers into a 300 cycle galvanometer recording on a William Miller recording oscillograph, the following results were immediately evident:

1. On both tests there was definite evidence of a slow speed

variation occurring at approximately the time that the blast wave arrived at the recording shelter. Since the recording shelter was approximately 1000 ft closer to ground zero than the gages themselves, this disturbance ended before the arrival of the blast wave at the gages.

2. On both shots each channel showed a sharp small deflection at zero time which provided a very satisfactory zero time reference. This deflection was due to the induction signal and the effect of this signal was, if anything, smaller than that observed on the direct oscillograph recording system.

3. On Shot 9, approximately 500 msec after the arrival of the blast wave, serious noise started on all channels. This noise might be attributed to microphonics of the gage oscillator except that it was also observed on the 10,000 cps standard frequency channel whose source was at the recording shelter.

4. On both tests the results from the two Vibrotron channels were entirely unsatisfactory. The noise level was so high that the signal was imperceptible. This noise appeared to result at least partly from cross-feed of the carriers of the other channels due to the grounding situation described above, but may have been also due to interference from other sources. An examination of the recording head output on the cathode-ray oscilloscope, showed a barely recognizable carrier at approximately 21,000 cps, but a very wide spectrum of noise obscured this carrier.

5. On both tests the two SRI channels produced records which were reasonably satisfactory. The long period noise described in 3. above was evident on both channels and certain shorter period noises were also present. The result was a certain increase in probable error over the direct recording record.

6. The two Wiancko channels show the same noises as are evident on the two SRI channels plus a small amount of relatively steady moderate frequency disturbance which is attributed to cross-feed.

Since one of the major purposes of this experiment was the investigation of certain techniques in playback for improvement of signal-to-noise ratio, these techniques were now initiated. The 10,000 cps crystal-controlled channel was fed through a demodulator similar to those used for the playback of the signal channels. Ideally, the output of this 10,000 cycle channel should be a steady DC signal which could be balanced to zero with the balancing control; in practice, this was not the case. Noises due either to speed variations in recording or playback or to tape stretch appeared on the output of this channel. For instance, the long period shift occurring at the time of blast arrival at the recording shelter was equally evident on this channel and on all other recording channels. Other shorter period noises were also evident. The simple cure for these noises on the recording channels was almost obvious. The output of a signal channel was connected in series opposition to the output of the 10,000 cycle reference channel,

after demodulation. By suitable adjustment of attenuators, a balance could be achieved, with the result that a very wide change of tape speed produced no signal output from the combined channels. Any noise from this source, therefore, would appear on both channels, and as a consequence would be eliminated from the combined output.

The correction method described above gave excellent results. It resulted in improvement of at least 20 db in signal-to-noise ratio on the SRI-A and SRI-B channels with a lesser improvement on the Wiancko channels since noises of other types were present. In practice, a slightly different arrangement appeared desirable since the arrangement described did not permit the simultaneous recording of the uncorrected signal and the corrected signal. This was true because a galvanometer connected across the signal channel output only received a certain amount of correction from the reference channel and the reference channel correspondingly received a certain amount of cross-feed from the signal channel. This difficulty was readily overcome by feeding each (the signal channel and the reference channel) into one of the two grids of a balanced cathode-follower DC amplifier through a suitable potentiometer. The combined recording galvanometer was connected between the cathodes of the two tubes. The individual recording galvanometers were connected directly to the individual channels through suitable attenuators. This arrangement avoided the cross-feed described above. To complete the playback system, a portion of the 10,000 cps signal was picked up after the amplifier stages in the 10,000 cps playback channel and was fed to a portion of the divider system from the Hewlett-Packard frequency standard. This nominal 10 kilocycle frequency was substituted for the controlled 10 kilocycle frequency of the frequency standard and was subdivided to 1000 cycles and 100 cycles. This combined 1000 cycles and 100 cycles was fed to a timing galvanometer. Although, due to any speed variation which might take place, these standard outputs were not exactly their nominal frequencies, they did represent, on the final record, time intervals which were exactly their normal period at the time of recording. They were used, therefore, for the counting of time on the final records. On each of the final records, then, four channels were recorded: a timing channel, the output of the reference oscillator channel, the uncorrected signal output, and the corrected signal output. Portions of some of these records are shown in Figs. B.2, B.3, and B.4.

B.4 LATER TESTS

Since no results were obtained from the two Vibrotron channels on Shots 9 and 10, a later opportunity was taken to conduct field tests of these instruments. During a series of tests using HE charges, at Camp Cooke, California (Project MOLE), these two channels were installed in a manner similar to that described in B.2. The gages were installed at the earth's surface 60 ft from a 256 pound TNT charge and adjacent to a standard Wiancko gage, normally recorded. Since playback tests had indicated that effects of tape speed variations could be minimized, the special fork amplifier was omitted, and the Ampex recorder was operated directly from an Onan engine-driven generator which also powered the remainder of the equipment.

Satisfactory results were obtained, and the final records are

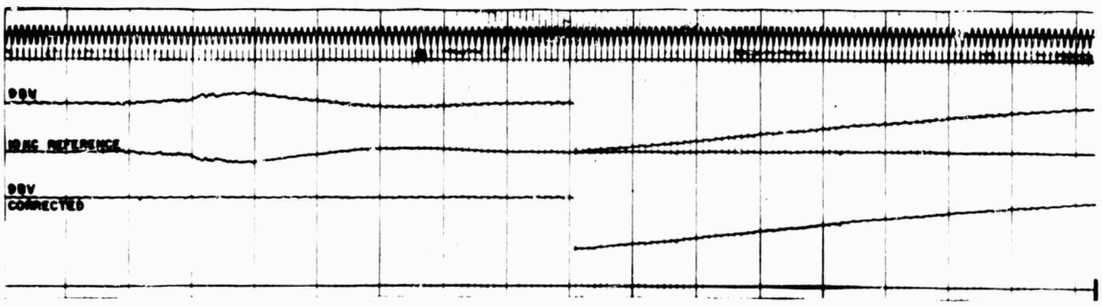

Fig. B.2 Channel 9BV, SRI B Oscillator, Shot 10

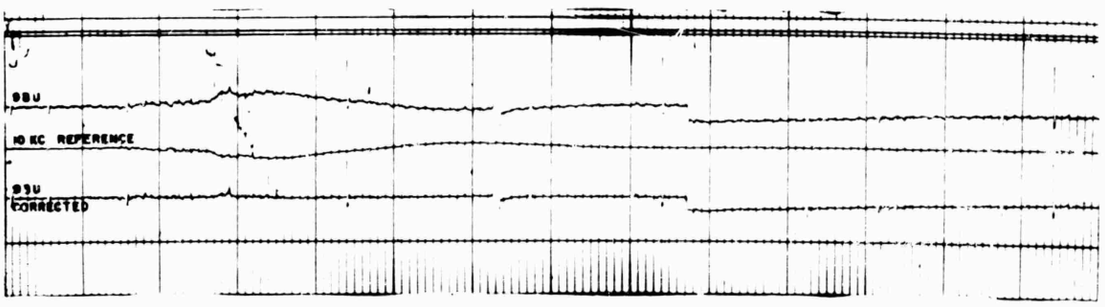

Fig. B.3 Channel 9BU, SRI A Oscillator, Shot 10

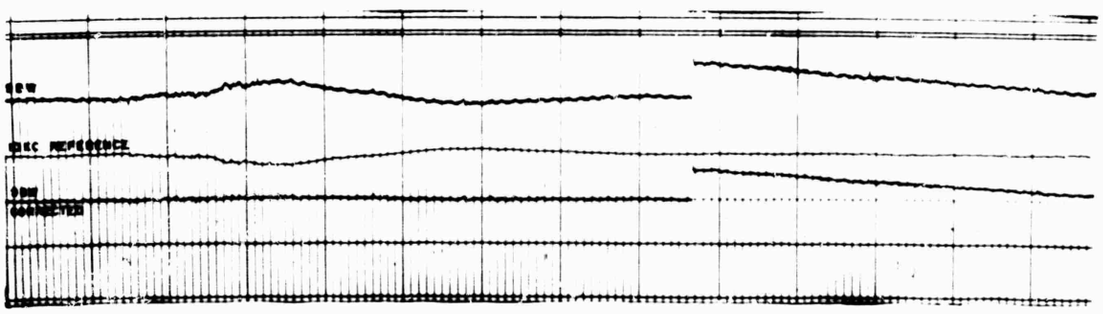

Fig. B.4 Channel 9BW, Wiancko 9-1002 Oscillator, Shot 10

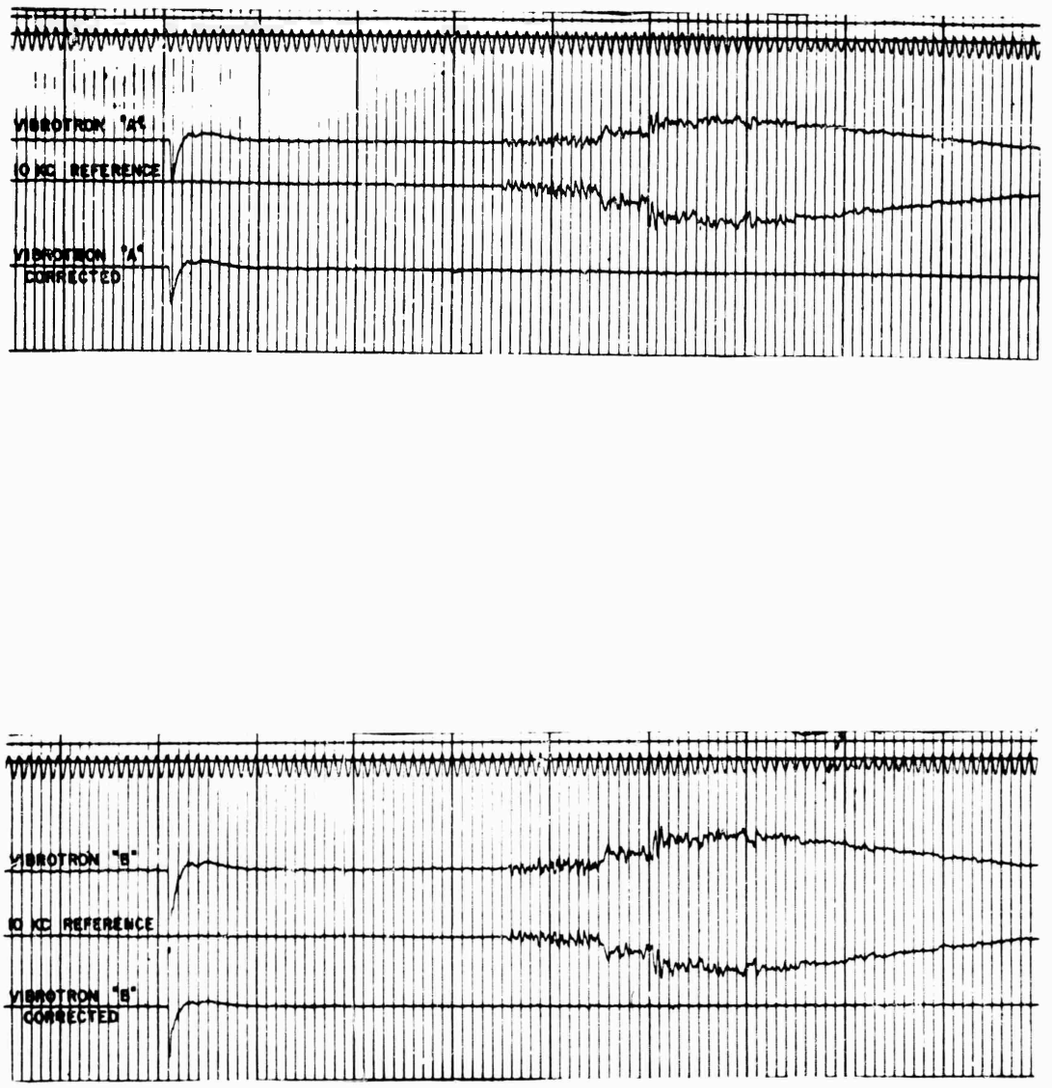

Fig. B.5 Vibrotron Channels, 250 Pounds HE

shown in Fig. B.5.

B.5 RECORD ANALYSIS

The final records were analyzed only to an extent sufficient to allow evaluation of the quality of the results. The calibration deflections, recorded at the same instrument settings used for the final records, were read and converted to a calibration curve. This curve was applied to the gage records to obtain values of peak pressure and pressure at later times. These values were compared with corresponding readings from the standard gages.

B.6 RESULTS AND OBSERVATIONS

In evaluating the results of these experiments, three separate portions of the equipment should be considered: (1) the transducer, including the local oscillator; (2) the recording equipment; (3) the playback instrumentation and techniques.

B.6.1 Transducers

The four channels using Wiancko gages as the primary transducer gave records which, as might be expected, resembled very closely those recorded directly from Wiancko gages, except that the signal-to-noise ratio was poorer. This ratio was best on channel 9BV (SRI-B oscillator) which had the greatest frequency deviation (Fig. B.2). Certain steady-state noise on channels 9BW and 9BX (Wiancko 9-1002 oscillators) may be attributable to the use of undesirable carrier frequency ratios. Other noises on these records were similar to those on channel 9BU (SRI-A oscillator) shown in Fig. B.3.

The record analysis shows pressure values from channel 9BV which deviate over 15 per cent from those obtained from the reference gage, whereas the others check within 5 per cent or better. It is concluded that this oscillator is less stable than is required for satisfactory operation.

The records from the two Vibrotron channels, shown in Fig. B.5, differ markedly from each other in damping characteristics and rise time. Figure B.5A shows a slow rise time and over-damped characteristics, B.5B a relatively fast rise but severe overshoot and later ringing. Indications, partly verified by discussions with the manufacturer, are that little attention is paid to the damping of these gages in their design and manufacture. They were designed for semisteady-state use.

B.6.2 Recording Equipment

On all records, there are noises introduced by the recording equipment. The most pronounced of these is a speed change at the time that the shock strikes the recorder. This is observed in Figs. B.2, B.3, and B.4 about 700 msec before the gage signal arrival, even though the recorder was mounted in a buried concrete shelter. In Fig. B.5, this is seen about 350 msec after the gage signal arrival, since in this case the recorder was more remote than the gage. The speed change was

more severe in this latter case, since the recorder was mounted in a truck which was directly exposed to the blast wave.

This disturbance is attributed to the mounting used for the capstan drive motor. During operation, the motor and its drive wheel are held against the capstan drive disc by a solenoid. The force applied by this solenoid is estimated to be somewhat less than the mass of the motor, so that a negative acceleration of less than 1 G can separate the contact, permitting the tape drive capstan to change speed temporarily. In addition to the above shortcoming, the open construction of the Ampex recorder makes it better suited to studio use than to field use.

B.6.3 Playback

The playback equipment operated as expected. The technique used to reduce the effects of speed variations is considered to be successful. Its operation is most apparent in Fig. B.5, where the large amplitude noise of wide frequency content which is caused by the recorder trouble described in B.6.2 is almost completely eliminated. It must be observed that this cancellation, adjusted for steady-state carrier conditions, becomes less complete during signal excursions. The ratio of remaining noise to the original noise is approximately proportional to the signal frequency deviation ratio. Since the signal frequency deviation ratio seldom exceeds 10 per cent, this represents a minimum reduction of this type of noise of 20 db under maximum signal conditions.

B.7 CONCLUSIONS

The following conclusions are considered justified:

1. None of the transducer-oscillator systems tested are entirely satisfactory. A modification of the SRI-B type or of the Wiancko 9-1002 type is probably most promising, pending a completely new gage design.

2. The Ampex recorder requires some redesign for completely satisfactory field use.

3. The playback technique described is considered to be a real improvement. In fact, its use may permit a considerable simplification of recorder construction without loss of record quality.

BIBLIOGRAPHY

1. F. B. Porzel and F. Reines, Height of Burst for Atomic Bombs, Los Alamos Scientific Laboratory, LA-743R, Series B, 3 August 1949. SECRET, RESTRICTED DATA

2. H. K. Gilbert and R. Q. Wilson, Operation BUSTER - Final Report, Armed Forces Special Weapons Project, Report WT-412, July 1952. SECRET SECURITY INFORMATION, RESTRICTED DATA

3. V. Salmon, Air Pressure vs Time, Stanford Research Institute, Operation TUMBLER Project 1.2, Report WT-512, February 1953. SECRET SECURITY INFORMATION, RESTRICTED DATA

4. J. von Neumann and F. Reines, The Mach Effect and the Height of Burst, Los Alamos Scientific Laboratory, Los Alamos Technical Series LA-1021, Volume 7, Chapter 10, 13 August 1947. SECRET, CIRCULATION LIMITED

5. W. Bleakney et al., Interaction of a Shock Wave With a Thermal Boundary Layer, Princeton University, 11 January 1952. CONFIDENTIAL SECURITY INFORMATION

6. R. R. Halverson, The Effect of Air Burst on the Blast from Bombs and Small Charges, Part II, The Analysis of Experimental Results, Underwater Explosives Research Laboratory, OSRD Report 4899, 1945. UNCLASSIFIED

7. H. Scoville, Jr., et al., Operation TUMBLER - Final Summary Report, Armed Forces Special Weapons Project, Report WT-514, May 1953. SECRET SECURITY INFORMATION, RESTRICTED DATA

8. J. J. Bates, J. A. Carter, and T. I. Monahan, Thermal and Optical Characteristics of Nevada Sand, U. S. Naval Materials Laboratory, Report NML 5046-3, Part 19, June 1952. CONFIDENTIAL SECURITY INFORMATION

9. F. H. Shelton, The Precursor - Its Formation, Prediction and Effects, Sandia Corporation, July 27, 1953. SECRET, RESTRICTED DATA

10. V. Salmon and S. R. Hornig, Earth Acceleration vs Time and Distance, Stanford Research Institute, Operation TUMBLER Project 1.7, Report WT-517, February 1953. CONFIDENTIAL SECURITY INFORMATION, RESTRICTED DATA

11. E. B. Doll and V. Salmon, Scaled HE Tests - Operation JANGLE, Stanford Research Institute, Operation JANGLE Project 1(9)-1, Report WT-377, December 1952. SECRET SECURITY INFORMATION, RESTRICTED DATA

12. E. B. Doll and V. Salmon, Ground Acceleration, Ground and Air Pressures for Underground Test, Stanford Research Institute, Operation JANGLE Project 1(9)a, Report WT-380, April 1952. SECRET SECURITY INFORMATION, RESTRICTED DATA

13. James D. Shreve, Jr., Orientation of Gauge Baffles in Overpressure Measurements, Sandia Corporation, 5111(68), September 1952. UNCLASSIFIED

14. T. B. Cook, Jr. and K. Kammermeyer, Sandia Laboratory Shock-Gauge Evaluation Tests, Sandia Corporation, Operation TUMBLER-SNAPPER Projects 19.1c and 19.1d, Report WT-505, 2 October 1952. CONFIDENTIAL SECURITY INFORMATION, RESTRICTED DATA

15. Carter D. Broyles, Dynamic Pressure vs Time and Supporting Air Blast Measurements, Sandia Corporation, Operation UPSHOT-KNOTHOLE Project 1.1d, Report WT-714. SECRET SECURITY INFORMATION, RESTRICTED DATA

16. Stanford Research Institute, Project DRAGON, Contract No. AF33(616)-226 1953, Wright Air Development Center.

17. N. A. Haskell and J. O. Vann, The Measurement of Free Air Atomic Blast Pressures, Air Force Cambridge Research Center, Operation JANGLE Project 1.3c, WT-325. SECRET SECURITY INFORMATION, RESTRICTED DATA

18. K. Fuchs, The Effect of Altitude, Los Alamos Scientific Laboratory, Los Alamos Technical Series LA-1021, Volume 7, Chapter 9, 13 August 1947. SECRET, CIRCULATION LIMITED

19. R. G. Sachs, The Dependence of Blast on Ambient Temperature and Pressure, Ballistic Research Laboratories, Report No. 466, May 1944. UNCLASSIFIED

20. Departments of the Army, Navy, and the Air Force, Capabilities of Atomic Weapons, TM 23-200, OPNAV Instruction 003400.1, AFOAT 385.2, Revised October 1952. SECRET SECURITY INFORMATION

21. J. G. Kirkwood and S. R. Brinkley, Jr., Theoretical Blast-Wave Curves for Cast TNT, Cornell University, OSRD Report 5481, 23 August 1945. UNCLASSIFIED

22. W. Bleakney and A. H. Taub, Interaction of Shock Waves, Rev. Mod. Phys. 21, 584 (October 1949). UNCLASSIFIED

23. W. E. Morris et al., Air Blast Measurements, Naval Ordnance Laboratory, Operation UPSHOT-KNOTHOLE Projects 1.1a and 1.2, Report WT-710. SECRET RESTRICTED DATA

24. R. Courant and K. O. Friedrichs, Supersonic Flow and Shock Waves, Interscience Publishers, Inc., New York, 1948. UNCLASSIFIED

25. James D. Shreve, Jr., Air Shock Pressure-Time vs Distance for a Tower Shot, Sandia Corporation, Operation UPSHOT-KNOTHOLE Project 1.1c-1, Report WT-712. SECRET RESTRICTED DATA

26. Departments of the Army, Navy, and the Air Force, Capabilities of Atomic Weapons - Supplement No. 1, TM 23-200, OPNAV-P-36-00100, AFOAT 385.2, Supp 1, 8 February 1952. SECRET SECURITY INFORMATION

27. Summary Report, Weapon Effects Tests, Armed Forces Special Weapons Project, Operation JANGLE, Report WT-414, November 1952. SECRET SECURITY INFORMATION, RESTRICTED DATA

SUPPLEMENTARY

INFORMATION

Defense Nuclear Agency
6801 Telegraph Road
Alexandria, Virginia 22310-3398

TITL

11 March 1994

MEMORANDUM FOR DEFENSE TECHNICAL INFORMATION CENTER
ATTENTION: FDAB

SUBJECT: Declassification of WT-711

ERRATA - AD-373 321L

Reference AD-373321L.

The Defense Nuclear Agency Security Office has declassified the following technical report:

WT-711
Operation Upshot- Knothole, Nevada
Proving Grounds, March - June 1953,
Project 1.1b - Air Pressure and
Ground Shock Measurements.

The following distribution statement applies:

Distribution authorized to U.S. Government agencies only; test and evaluation. Other requests for this document shall be referred to the Defense Nuclear Agency, 6801 Telegraph Road, Alexandria, Virginia, 22310-3398.

151.2018

FOR THE DIRECTOR:

ERRATA

I Rubink

G. RUBINK
Chief, Technical Information

Defense Special Weapons Agency
6801 Telegraph Road
Alexandria, Virginia 22310-3398

OPSSI

MAY 8 1998

MEMORANDUM FOR DISTRIBUTION

SUBJECT: Declassification Review of Operation UPSHOT-KNOTHOLE Test Reports

The following 90 reports concerning the atmospheric nuclear tests conducted during Operation UPSHOT-KNOTHOLE in 1953 have been declassified and cleared for open publication/public release:

WT-702, WT-703, WT-705, WT-709 thru WT-711, WT-713 thru WT-719, WT-721 thru WT-742, WT-744 thru WT-746, WT-749 thru WT-755, WT-757 thru WT-761, WT-763, WT-764, WT-766 thru WT-781, WT-784 thru WT-787, WT-789, WT-790, WT-792 thru WT-796, WT-798, WT-801, WT-805, WT-808, WT-809, WT-811, WT-812,WT-814, WT-817, WT-820, and WT-822

An additional 6 WTs from UPSHOT-KNOTHOLE have been re-issued with deletions and are identified with an "EX" after the WT number. These reissued versions are unclassified and approved for open publication. They are:

WT-743, WT-747, WT-802, WT-810, WT-825, and WT-828

This memorandum supersedes the Defense Special Weapons Agency, OPSSI memorandum same subject dated June 11, 1997 and may be cited as the authority to declassify copies of any of the reports listed in the first paragraph above.

RITA M. METRO
Chief, Information Security

DISTRIBUTION
See Attached